5-12-2016 12:00 AM

Ground-Motion Prediction Equations for Central and Eastern North America, with Emphasis on Site Effects

Behzad Hassani, *The University of Western Ontario*

Supervisor: Dr. Gail M. Atkinson, *The University of Western Ontario*

A thesis submitted in partial fulfillment of the requirements for the Doctor of Philosophy degree in Geophysics

Abstract

The works presented in this thesis are aimed at understanding and modeling earthquake ground motions in central and eastern North America (CENA), with an emphasis on the modeling of site effects. A number of approaches are taken, beginning with analysing of the observed ground-motion amplitudes with respect to a ground-motion prediction equation model (GMPE) of a well recorded region (California) (referenced empirical approach). In this work, we show that the ground-motion amplitudes of CENA earthquakes are very similar to the equivalent California values of Boore et al. (2014; BSSA14) at close distances, at low to moderate frequencies. At regional distances and at high frequencies the ground-motion amplitudes are larger in CENA than for the BSSA14 reference model, presumably due to lower attenuation and higher stress for CENA events relative to those in active tectonic regions.

Next, a modeling approach is taken to develop a simulation-guided generic GMPE model for southern Ontario, examining regional site effects. Then, in a collaborative study with colleagues, we use the regional model in a technique that inverts ShakeMaps parameters (e.g. response spectra at selected frequencies) to estimate moment magnitude and stress parameter in near-real-time, for earthquakes of small to moderate earthquake (**M** ~3 to 6).

Finally, we explore site response more deeply, building on the empirical findings of the ground-motion modeling work. We examine the applicability of the site fundamental frequency (f_{peak}) as a descriptive variable for site response in CENA. We introduce a new f_{peak}-based proxy measure for V_{S30} (time-averaged shear-wave velocity in the upper 30 m) for sites in CENA; this is useful because V_{S30} is a standard site response parameter for building code and other applications. We also examine the applicability of the Next-Generation-West2 V_{S30}-based site effects model (Seyhan and Stewart, 2014; SS14) for the recording stations in CENA. We develop a new f_{peak}-based model for site amplification in CENA to address inadequacies in the V_{S30}-based site effects model, and show that use of the new model reduced ground-motion prediction variability by a significant amount.

Keywords

Ground-motion prediction equations, ShakeMap parameters, moment magnitude, stress parameter, site fundamental frequency, site effects, sigma

Co-Authorship Statement

The materials present in Chapters 2, 3, 4 and 5 have been previously published or submitted for publication to the peer-reviewed journals of *Seismological Research letters* and *Bulletin of Seismological Society of America*. This thesis contains only the original results of research conducted by the candidate under supervision of his mentor. The original contributions are summarized as follows:

Compilation and data processing of ground-motion time series for selected earthquakes in southern Ontario; Compilation of seismological parameters as well as peak ground motions and response spectral amplitudes from NGA-East flatfile for the study events in Chapters 2, 3, and 4; Determination of H/V spectral ratios for sites in CENA; Determination of site fundamental frequency (f_{peak}) form the H/V spectral ratios for sites in CENA; Lay out an algorithm for near real-time determination of moment magnitude and stress parameter; Determination of a calibrated regional GMPE model for southern Ontario; Determination of a regional stress model and attenuation model for southern Ontario; Calculation of event-specific GMPEs for southern Ontario; Regression analysis and statistical analysis of residuals; Showing the inadequacy of western-based site effects model for sites in CENA; Determination of f_{peak}-based site effects model for CENA.

Dr. Gail M. Atkinson is the co-author in all five articles presented in this thesis (Chapters 2, 3,4 and 5).

The co-authors of Chapter 3 are Dr. Karen Assatourians, Dr. Emrah Yenier, and Arpit Singh, who provided great discussions and valuable comments.

Acknowledgments

I would like to express my sincere gratitude to my supervisor Professor. Gail Atkinson for her continuous support, guidance and encouragement during my PhD study. She has guided me with her insightful knowledge, helped me in every step of the way to become more knowledgeable, and kindly shared her expertise with me.

I would like to extend my appreciation to my advisor committee members Dr. Kristy Tiampo and Dr. Robert Shcherbakov for following my progress and providing useful suggestions. I would like to express my sincere thanks to my external examiners Dr. Christine Goulet and Dr. Tim Newson for their useful comments which led to significant improvements in this thesis.

I would like to thank my labmates for their useful discussions and suggestions during my study. In particular, I would like to thank Dr. Karen Assatourians, Dr. Hadi Ghofrani, and Dr. Emrah Yenier who generously have spent their time to help me.

I would like to express my gratitude to my master thesis supervisors Dr. Hamid Zafarani and Dr. Jamshid Farjoodi who made me interested in engineering seismology and encouraged me to continue my studies.

Last but not the least, I would like to thank my parents and my brother Farhad for their constant support and endless love throughout my study and my life in general.

Table of Contents

List of Tables

List of Figures

List of Appendices

List of frequently-used symbols and acronyms

B/C	B/C boundary between NEHRP site classes
CENA	Central and Eastern North America
$\Delta\sigma$	Stress parameter
ε	Within-event error term (intra-event error term)
ENA	Eastern North America
η	Between-event error term (inter-event error term)
f_{peak}	Peak frequency obtained form horizontal to vertical spectral ratios
GMPE	Ground-motion prediction equation
H/V	Horizontal to vertical spectral ratio (in this study response spectra)
κ_0	Near surface diminution term
M	Moment magnitude
NEHRP	National Earthquake Hazards Reduction Program
NGA	Next Generation Attenuation
NGA-East	Next Generation Attenuation Relationship for the Central and Eastern North American Region
NGA-West	Next Generation Attenuation Relationship for shallow crustal earthquakes in active tectonic regions (original project)
NGA-West2	Next Generation Attenuation Relationship for shallow crustal earthquakes in active tectonic regions (phase 2 of NGA-West project)
PGA	Peak ground acceleration

PGV	Peak ground velocity
φ	Within-event variability (Intra-event variability)
φ_{S2S}	Site-to-site variability
φ_{SS}	Within-site variability (single-station variability)
PSA	Pseudo-spectral acceleration (5% damping)
Q	Quality factor
R_{epi}	Epicentral distance
R_{hyp}, R_{hypo}	Hypocentral distance
R_{jb}	Joyner-Boore distance: closest distance to horizontal projection of fault trace
R_{cd}, D_{rup}	Rupture distance: closest distance to the fault trace
Sigma (σ)	total variability of a ground-motion prediction equation
SOSN	Southern Ontario seismic network
τ	Between-event variability (inter-event variability)
V_{S30}	Time-averaged shear-wave velocity in top 30 meters of geomaterial
WNA	Western North America

Chapter 1

1 Introduction

Ground-motion prediction equations (GMPEs) are a key component in seismic hazard analysis. GMPEs predict the expected median ground-motion amplitudes by using source, path and site terms to describe how ground-motion amplitudes scale with magnitude, distance and site conditions. The generic functional form for a GMPE model can be expressed as (Boore et al., 2014):

$$\ln Y = F_{Source} + F_{Path} + F_{Site} + F_{Var} , \quad (1.1)$$

where $\ln Y$ is the natural logarithm of the predicted ground-motion parameter, such as 5% damped pseudo-spectral acceleration (PSA) or peak ground amplitudes (e.g. peak ground velocity [PGV], and peak ground acceleration [PGA]); F_{Source} is the source functional form, which explains how ground-motion amplitudes scale with magnitude and fault mechanism; F_{Path} accounts for the path effects on the ground-motion amplitudes, which usually includes geometrical spreading and anelastic attenuation terms; F_{Site} accounts for the site effects including the near surface geology and topography on the ground-motion amplitudes, and F_{Var} accounts for the variability of ground-motion amplitudes.

The most common approach to develop GMPE models in data-rich regions like western North America (WNA) is to use the observed ground-motion amplitudes and derive an appropriate function to match the observed data (empirical method). An example of the modern empirical GMPE models is the well-known Next Generation Attenuation GMPEs set (NGA-West1 and NGA-West2; Bozorgnia et al., 2014), developed for shallow crustal earthquakes in active tectonic regions. The empirical method has been successfully implemented in data-rich regions as the number of observed data are sufficient to derive reliable empirical functions.

The common regression approach that is usually implemented for empirical GMPE development is the mixed effects regression of residuals introduced by Abrahamson and

Youngs (1992). For mixed effects regression, the error terms are partitioned into two parts which are between-event and within-event terms:

$$\ln Y_{ij} = f(M_i, R_{ij}, \theta) + \eta_i + \varepsilon_{ij}\ , \qquad (1.2)$$

where Y_{ij} is a ground-motion parameter from event *i* at station *j*, $f(M_i, R_{ij}, \theta)$ is the selected functional form for our GMPE model, M_i is the moment magnitude of event *i*, R_{ij} is the distance between event *i* and station *j*, and θ is a vector of model parameters. η_i is the between-event term (inter-event term) for event *i*, which is the random effects for event *i*, and ε_{ij} is the within-event term (intra-event term) which is the error term from event *i* at station *j*. η_i and ε_{ij} are assumed to be independent and have normal distributions with standard deviation of τ and φ, and the total variability (σ) of the GMPE model can be expressed as $\sigma = \sqrt{\tau^2 + \varphi^2}$. Abrahamson and Youngs (1992) proposed an iterative algorithm to maximize the likelihood of Equation (1.3) and find the model parameters values (θ) as well as the error terms and their corresponding variabilities. In this approach, we first estimate the model parameters using a fixed effects regression (assuming $\eta_i = 0$). Then using the determined model parameters, we estimate σ^2 and τ^2 by maximizing the likelihood of Equation (1.2) (Equation 3 in Abrahamson and Youngs, 1992). In the next step, using the determined values for model parameters and error variabilities we estimate random event terms (η_i) (Equation 10 in Abrahamson and Youngs, 1992). Using the values of the random event terms, we estimate the model parameters again after removing the random event terms (e.g. $\ln Y_{ij} - \eta_i$). We iterate these steps until we have maximized the likelihood of Equation (1.2).

For stable tectonic regions like central and eastern North America (CENA), with a low rate of seismicity, the empirical method of determining the model parameters may not be robust. Although CENA data are relatively plentiful for small-to-moderate events, especially at regional distances, they are too sparse in the magnitude-distance range of engineering interest to allow direct regression of ground-motion amplitude data to determine reliable empirical GMPEs. The most common approach to develop GMPEs in stable tectonic regions is using the simulation-based method which relies on a seismological model to model source, path and site terms (Atkinson and Boore, 1995;

Toro et al., 1997; Atkinson, 2004). For this approach the input parameters for the selected seismological model are usually calibrated based on the observed ground-motion amplitudes from small-to-moderate magnitude events, mostly recorded at regional distances, and then the model is used to predict the expected amplitudes over a wide range of magnitudes and distances.

The most important component of the simulation-based models is the model used to specify the spectrum of the ground-motion. Typically the Fourier acceleration spectrum of the ground-motion, $Y(f)$, at an effective distance R can be modeled with an ω^2shape, in which ω is the angular frequency can be written as (Brune, 1970; 1971; Boore, 2003):

$$Y(f) = CM_0G(R)(2\pi f^2)/[1 + (f/f_0)^2]A(f)\exp(-\pi f\kappa_0)\exp(-\pi fR/Q\beta), \qquad (1.3)$$

where $M_0$is the seismic moment that controls the low frequency content of the spectrum, β is the shear-wave velocity in the vicity of the source, and f_0 is the corner frequency which can be written as $f_0 = 4.906 \times 10^6\beta(\Delta\sigma/M_0)^{1/3}$. $\Delta\sigma$ is the stress parameter, which is a modeling variable that controls the high frequency content of the spectrum. The constant C can be written as $C = \Re_{\theta\phi}FV/(4\pi\rho\beta^3)$ in which $\Re_{\theta\phi}$is the radiation pattern (on average 0.55 for shear waves), F is the free-surface effect (2.0), V is the partition onto two horizontal components (0.71), and ρ is the density (e.g. 2.8 gr/cm^3) (Boore, 1983; 2003). $G(R)$ is the geometrical spreading function. At close distances (R < 50 km), decay of direct-wave amplitudes in a layered crust controls the geometrical spreading effect (e.g. $1/R^{1.3}$.), and at regional distances (R > 50 km) reflections and refractions from Moho and a transition to surface-wave spreading control the geometrical spreading (e.g. $1/R^{0.5}$) (e.g. Atkinson, 2004). The term $\exp(-\pi fR/Q\beta)$ is the anelastic attenuation effect, which is a function of distance and frequency; it explains the decay of seismic waves amplitudes due to inelastic attenuation or internal friction during wave propagation. The quality factor $Q\ (f)$ is an inverse measure of effective anelastic attenuation. The kappa effect, given by $\exp(-\pi f\kappa_0)$, is a low-pass filter to account for near-surface attenuation that produces rapid spectral decay at high frequencies (Anderson and Hough, 1984). Finally, $A(f)$ is the amplification from the source to the surface, which is controlled by the near-surface geology.

Another common approach to come up with a GMPE model in stable tectonic regions is the hybrid empirical method in which the GMPEs for a target region (data-poor regions like CENA) are derived from GMPEs of a host region (data-rich regions like WNA) by applying an adjustment factor (Campbell, 2003; Pezeshk et al., 2011). The adjustment factors are defined as the ratio of the simulated ground-motion amplitudes for the target region divided by the simulated ground-motion amplitudes for the host region.

The third approach which has been developed for CENA is the referenced empirical approach (Atkinson, 2008; Atkinson and Boore, 2011; Hassani and Atkinson, 2015) which is similar to the hybrid empirical method, but the adjustment factors are determined based on the ratio of the observed empirical ground-motion amplitudes in the target region to the predicted ground-motion amplitudes in the host region. The main assumption of this method is that the magnitude scaling and the overall near-source behavior of ground motions are the same in the host and the target regions, although the overall ground-motion levels at the source might be different (if the source parameters differ), and the attenuation might be different.

Another method that is recently proposed is the generic GMPE approach by Yenier and Atkinson (2015). The generic GMPE approach is a robust simulation-based method in which the functional form is parameterized using the fundamental source (magnitude [**M**] and stress parameter [$\Delta\sigma$]) and attenuation parameters (geometrical spreading and anelastic attenuation) based on their isolated effects determined from ground-motion simulations. The utility of this approach is that once the generic GMPE is defined, we can use it to relate observed motions to **M** and $\Delta\sigma$ without the need to repeat simulations. This facilitates inversion of the GMPE to obtain the underlying source and attenuation parameters directly from response spectra (PSA) observations.

One of the most important issues in developing accurate and GMPEs is the effective use of limited regional site information in developing a site effects model. Amplitudes of ground motions can be amplified significantly as they propagate through a soft soil layer (Borcherdt, 1970; Anderson et al., 1986; Shearer and Orcutt, 1987). In modern GMPE models, site effects are usually characterized by a set of simplified parameters (often only

one) that characterize the overall near-surface state. Common site parameters include site fundamental frequency (f_{peak}) (e.g. Zhao et al., 2006) and V_{S30} (e.g. Boore et al., 2014). V_{S30} is currently the most prevalent site parameter in GMPE models, especially in North America. Well-known examples of the recent GMPEs which use V_{S30} as the explanatory variable for site effects is the NGA-West2 GMPE models (Bozorgnia et al., 2014), and also recently published Next-Generation-East (NGA-East) GMPE models developed as part of the NGA-East project (Goulet et al., 2015) for shallow crustal earthquakes in CENA. While the use of V_{S30} as an effective predictive variable for site effects has been well-documented for WNA (e.g Abrahamson et al., 2014; Boore et al., 2014; Campbell and Bozorgnia, 2014; Chiou and Youngs, 2014; Idriss, 2014), it is not clear if such models apply to sites in CENA. The approach was originally developed based on empirical observations that show how the amplification of ground motion behaves in California (Borcherdt, 1994), where alluvial soils transition gradually to rock as depth increases, generally without any clear interface between soil and rock. CENA has been tectonically stable over the last several hundred million years, resulting in competent crustal conditions that are generally characterized by high velocities and low attenuation. There are many regions in which post-glacial soils, which may be shallow or deep, overlie a much harder glaciated bedrock surface, providing a sharp impedance contrast and setting up the conditions for strong amplification at the fundamental frequency of the site.

1.1 Purpose of study

The purpose of this study is to develop ground-motion models for central and eastern North America (CENA) with emphasis on the site effects term. We first develop a referenced empirical GMPE model for CENA. The update to this approach is timely because the NGA-West2 GMPEs for shallow crustal earthquakes in active tectonic regions enable a significant improvement in the implementation of this method. Here we use the NGA-East database and we consider both natural and potentially induced earthquakes (flagged in the NGAEast flatfile) in our analysis. Therefore, we do not discriminate between induced and natural events in this study.

We then turn our attention to simulation-based models of ground motion. We derive a well-calibrated regional GMPE model that can be used to determine moment magnitude (**M**) and stress parameter ($\Delta\sigma$) in near real-time, in the immediate aftermath of a small to moderate earthquake (**M** ~3 to 6) in southern Ontario, from ShakeMap ground motion parameters (5%-damped pseudo spectral acceleration [PSA] at 1 Hz, 0.33 Hz, 10 Hz and/or peak ground acceleration [PGA]).

Next, we turn our attention to an improved modeling of site response in GMPEs. We show the applicability of the site fundamental frequency (f_{peak}) measured from the horizontal–to-vertical spectral ratios (H/V) of recorded ground motion (or ambient noise) as an effective site indicator for site response in CENA. f_{peak} may be used as a V_{S30} proxy to significantly reduce its estimation uncertainty in comparison to other proxies such as topographic slope (Wald and Allen, 2007). By modeling empirically-derived site terms as a function of f_{peak}, we propose a new f_{peak} -based site amplification model for sites in CENA. The new model reduces the variability of ground-motion estimates in CENA, which is an important result for seismic hazard studies.

1.2 Organization of thesis

The thesis is presented in six chapters. The first chapter provides background information regarding ground-motion prediction equations (GMPEs) and site effects models used in CENA. The second chapter presents a GMPE using the referenced empirical approach for CENA (Hassani and Atkinson, 2015). Chapter 3 lays out an approach for near real-time estimation of moment magnitude (**M**) and stress-parameter ($\Delta\sigma$) using the observed regional ground-motion amplitudes, and examines the approach for the southern Ontario seismic network (Atkinson et al., 2015). Chapter 4 discusses the applicability of site fundamental frequency (f_{peak}) as a site effects indicator in CENA, and the use of f_{peak} as a V_{S30} proxy (Hassani and Atkinson, 2016a). We also explore the applicability of the NGA-West2 site effects model for sites in CENA (Hassani and Atkinson, 2016b). Finally in chapter 5, an f_{peak} -based site effects model for CENA is proposed for different reference site conditions (Hassani and Atkinson, 2016c).

1.3 References

Abrahamson, N.A., and R.R. Youngs (1992). A stable Algorithm for regression analysis using the random effects model, *Bull. Seismol. Soc. Am*. **82**, 505-510.

Abrahamson, N.A., W.J. Silva, and R. Kamai (2014). Summary of the ASK14 ground motion relation for active crustal regions, *Earthq. Spectra*. **30**, 1025-1055.

Anderson, J.G., P. Bodin, J.N. Brune, J. Prince, S.K. Singh, R. Quaas, and M. Onate (1986). Strong ground motion from the Michoacan, Mexico, earthquake, *Science*. **233**, 1043-1049.

Atkinson, G.M. (2004). Empirical attenuation of ground-motion spectral amplitudes in southeastern Canada and the northeastern United States, *Bull. Seismol. Soc. Am*. **94**, 1079-1095.

Atkinson, G.M. (2008). Ground-motion prediction equations for eastern north America from a referenced empirical approach: implications for epistemic uncertainty, *Bull. Seismol. Soc. Am*. **98**, 1304-1318.

Atkinson, G.M., and D.M. Boore (1995). Ground-motion relations for eastern North America, *Bull. Seismol. Soc. Am*. **85**, 17-30.

Atkinson, G.M., and D.M. Boore (2011). Modifications to existing ground-motion prediction equations in light of new data, *Bull. Seismol. Soc. Am*. **101**, 1121-1135.

Atkinson, G.M., B. Hassani, A. Singh, E. Yenier, and K. Assatourians (2015). Estimation of Moment Magnitude and Stress Parameter from ShakeMap Ground-Motion Parameters, *Bull. Seismol. Soc. Am.* **105,** 2572-2588.

Boore, D.M. (1983). Stochastic simulation of high-frequency ground motions based on seismological models of the radiated spectra, *Bull. Seismol. Soc. Am*. **73**, 1865-1894.

Boore, D.M. (2003). Simulation of ground motion using the stochastic method, *Pure and applied geophysics*. **160**, 635-676.

Boore, D.M., J.P. Stewart, E. Seyhan, and G.M. Atkinson (2014). NGA-West2 equations for predicting PGA, PGV, and 5% damped PSA for shallow crustal earthquakes, *Earthq. Spectra*. **30**, 1057-1085.

Borcherdt, R.D. (1970). Effects of local geology on ground motion near San Francisco Bay, Bull. *Seismol. Soc. Am*. **60**, 29-61.

Borcherdt, R.D. (1994). Estimates of site-dependent response spectra for design (methodology and justification), *Earthq. Spectra*. **10**, 617-653.

Bozorgnia, Y., N.A. Abrahamson, L.A. Atik, T.D. Ancheta, G.M. Atkinson, J.W. Baker, A. Baltay, D.M. Boore, K.W. Campbell, B.S.-J. Chiou, R. Darragh, S. Day, J. Donahue, R.W. Graves, N. Gregor, T. Hanks, I.M. Idriss, R. Kamai, T. Kishida, A.R. Kottke, S.A. Mahin, S. Rezaeian, B. Rowshandel, E. Seyhan, S. Shahi, T. Shantz, W. Silva, P. Spudich, J.P. Stewart, J. Watson-Lampery, K. Wooddell, and R. Youngs (2014). NGA-West2 research project, *Earthq. Spectra*. **30**, 973-987.

Brune, J.N. (1970). Tectonic stress and the spectra of seismic shear waves from earthquakes, *J. Geophys. Res*. **75**, 4997-5009.

Brune, J.N. (1971). Correction: Tectonic stress and the spectra of seismic shear waves, *J. Geophys. Res*. **76**, 5002.

Campbell, K.W. (2003). Prediction of strong ground motion using the hybrid empirical method and its use in the development of ground-motion (attenuation) relations in eastern North America, *Bull. Seismol. Soc. Am*. **93**, 1012-1033.

Campbell, K.W., and Y. Bozorgnia (2014). NGA-West2 ground motion model for the average horizontal components of PGA, PGV, and 5% damped linear acceleration response spectra, *Earthq. Spectra*. **30**, 1087-1115.

Chiou, B.S.-J., and R.R. Youngs (2014). Update of the Chiou and Youngs NGA model for the average horizontal component of peak ground motion and response spectra, *Earthq. Spectra*. **30**, 1117-1153.

Goulet, C.A., Y. Bozorgnia, and N.A. Abrahamson (2015). Introduction, in NGA-East: *Median Ground-Motion Models for the Central and Eastern North America Region*, Chap. 1, PEER Report No. 2015/04, Pacific Earthquake Engineering Research Center, Berkeley, CA, 1-10.

Hassani, B., and G.M. Atkinson (2015). Referenced Empirical Ground-Motion Model for Eastern North America, *Seism. Res. Lett*. **86**, 477-491.

Hassani, B., and G.M. Atkinson (2016a). Applicability of the site fundamental frequency as a V_{S30} proxy for Central and Eastern North America, *Bull. Seismol. Soc. Am.* **106,** 653-664.

Hassani, B., and G.M. Atkinson (2016b). Applicability of the NGA-West2 Site Effects Model for Central and Eastern North America, *Bull. Seismol. Soc. Am.* **106,** In press.

Hassani, B., and G.M. Atkinson (2016c). Site Effects Model for Central and Eastern North America Based on Peak Frequency, *Bull. Seismol. Soc. Am.* Submitted.

Idriss, I. (2014). An NGA-West2 empirical model for estimating the horizontal spectral values generated by shallow crustal earthquakes, *Earthq. Spectra*. **30**, 1155-1177.

Pezeshk, S., A. Zandieh, and B. Tavakoli (2011). Hybrid empirical ground-motion prediction equations for eastern North America using NGA models and updated seismological parameters, Bull. *Seismol. Soc. Am*. **101**, 1859-1870.

Shearer, P.M., and J.A. Orcutt (1987). Surface and near-surface effects on seismic waves theory and borehole seismometer results, Bull. *Seismol. Soc. Am*. **77**, 1168-1196.

Toro, G.R., N.A. Abrahamson, and J.F. Schneider (1997). Model of strong ground motions from earthquakes in central and eastern North America: best estimates and uncertainties, *Seism. Res. Lett*. **68**, 41-57.

Wald, D.J., and T.I. Allen (2007). Topographic slope as a proxy for seismic site conditions and amplification, *Bull. Seismol. Soc. Am*. **97**, 1379-1395.

Yenier, E., and G.M. Atkinson (2015). Regionally adjustable generic ground-motion prediction equation based on equivalent point-source simulations: Application to central and eastern North America, *Bull. Seismol. Soc. Am*. **105**, 1989-2009.

Zhao, J.X., J. Zhang, A. Asano, Y. Ohno, T. Oouchi, T. Takahashi, H. Ogawa, K. Irikura, H.K. Thio, P.G. Somerville, and others (2006). Attenuation relations of strong ground motion in Japan using site classification based on predominant period, *Bull. Seismol. Soc. Am*. **96**, 898-913.

Chapter 2

2 Referenced empirical ground-motion model for eastern North America[1]

In this chapter, we update ground-motion prediction equations (GMPEs) for eastern North America using the referenced empirical approach (Atkinson, 2008). The update is timely because the Next Generation Attenuation-West2 GMPEs for shallow crustal earthquakes in active tectonic regions enable a significant improvement in the implementation of this model, relative to previous work. The updated referenced empirical GMPE model can have significant implications for seismic-hazard evaluations of sites in CENA, specifically to account for epistemic uncertainty in seismic-hazard applications.

2.1 Introduction

Ground-motion prediction equations (GMPEs) are simple functions that describe ground-motion amplitudes as a function of magnitude, distance and site condition, and which are a key element in seismic hazard modeling. The common approach to develop GMPEs in data-rich regions is to empirically correlate the observed ground-motion amplitudes to predictive variables that represent source, path and site terms using a suitable functional form. An example of recent empirical GMPEs is the Pacific Earthquake Engineering Research–Next Generation Attenuation (PEER–NGA West) equations, which have been developed for shallow crustal earthquakes in active tectonic regions (Power et al., 2008; Bozorgnia et al., 2014). The second generation of the NGA equations was recently published as part of the NGA-West2 project, as described by Bozorgnia et al. (2014) and references contained therein. The NGA-West2 equations facilitate a fresh look at GMPEs for ENA. This is because the NGA-West2 equations are much more robust for small-to-moderate magnitude events than previous empirical GMPEs, enabling meaningful comparisons between eastern and western events in the magnitude range for which ENA

[1] A version of this chapter has been published. Hassani, B., and G.M. Atkinson (2015). Referenced Empirical Ground-Motion Model for Eastern North America, *Seism. Res. Lett.* **86,** 477-491.

data are plentiful. Note that although ENA data are relatively plentiful for small-to-moderate events, especially at regional distances, they are too sparse in the magnitude-distance range of engineering interest to allow direct regression of ground-motion amplitude data to determine robust empirical GMPEs.

In general, three different approaches have been proposed to develop GMPEs in ENA. The most widely-used approach is the stochastic simulation-based method, in which a seismological model is used to model source, path, and site effects (e.g. Atkinson and Boore, 1995, 2006, 2011; Toro et al., 1997; Silva et al., 2002). Simulation-based GMPEs usually rely on a simple seismological model in which the underlying source, path and site parameters are determined from small-to-moderate magnitude events, then used to model expected motions over a wider range of magnitudes and distances. Another popular approach is the hybrid empirical method (Campbell, 2003; Tavakoli and Pezeshk, 2005; Pezeshk et al., 2011). In this method, GMPEs from host regions (active regions with robust empirical GMPEs) are adjusted to produce GMPE models for target regions (regions with poor ground-motion databases). This method also makes use of stochastic simulations: specifically, the adjustment factors are defined as the ratio of the simulated ground-motion amplitudes for the target region divided by the simulated ground-motion amplitudes for the host region. A third method for development of GMPEs in data-poor regions is the referenced empirical method (Atkinson, 2008). In this method, sparse observational data are compared to an empirical GMPE model from a data-rich region (Atkinson, 2008; Atkinson, 2010; Atkinson and Boore, 2011; Atkinson and Motazedian, 2013). This method is similar in concept to the hybrid empirical method. The difference is that the adjustment factors are purely empirical, estimated using the ratio of the observed regional ground motions in the target region to the predicted values for the host region.

In both the hybrid empirical method and the referenced empirical method, we anchor our predictions to experience from data-rich regions. This approach is fundamentally robust, particularly in light of the growing body of evidence that regional differences in ground motions may not be as significant as once believed (e.g. Douglas, 2004; Bommer et al., 2007; Atkinson and Morrison, 2009). The general similarity in ground motions between

regions lends weight to the concepts implicit in such approaches. These concepts are that the magnitude scaling and overall near-source behavior should be the same in the host and the target regions, with regional differences being attributed to differences in fundamental source and attenuation parameters.

In this study, we use the referenced empirical method to develop a GMPE model for ENA, relative to the reference model of Boore et al. (2014; denoted BSSA14) which was developed as part of the NGA-West2 Project (Bozorgnia et al., 2014). Any of the NGA-West2 equations could be used with relatively similar results, because the method is essentially a calibration of the GMPE to the database. The BSSA14 GMPE is especially convenient as all of its necessary input parameters are available for the ENA database. Moreover, it is well constrained at low magnitudes (**M**>3.5) and large distances $R \leq 400$ km, making comparisons to ENA data robust.

We could have developed a referenced empirical GMPE for each of the NGA-West2 equations, to include some measure of epistemic uncertainty due to the choice of the reference equation. However, this would represent only a partial source of epistemic uncertainty in the resulting GMPEs. The relative magnitude of this uncertainty can be judged by the comparisons given by Gregor et al. (2014) between the NGA-West2 models. We believe that other sources of epistemic uncertainty, especially those arising from limitations in the ENA database, are more important. Therefore, we choose to restrict the focus of this work, and do not aim to characterize epistemic uncertainty here. Rather, this work presents one approach that can be used, alongside other approaches, in a broader evaluation of epistemic uncertainty.

The referenced empirical method has been previously used to develop GMPE models in ENA. Atkinson (2008) developed a referenced GMPE model (A08) for ENA based on the first generation of NGA GMPE equations (Boore and Atkinson, 2008; denoted BA08), which was updated by Atkinson and Boore (2011) (with the updated model being denoted A08'). In this study, we make a major improvement on A08' by using a reference GMPE that is dramatically improved for small-to-moderate magnitudes, enabling a much more robust GMPE to be developed for ENA. Moreover, we show that the approach is in

demonstrable agreement with predictions that would be made using the hybrid empirical approach for ENA, using recent validated equivalent point-source models for both the host and target regions. Thus we 'close the loop' between the referenced empirical and hybrid empirical methods.

2.2 The ground-motion database for ENA

Our target region is ENA, defined here as North America east of 105° W longitude. The ENA database of this study is compiled from several different resources (see Section 2.7). Figure 2.1 is a map of recording stations and events used in this study. The ENA database consists of two separate regions, the central United States (designated Central), and southeastern Canada and northeastern United states (designated East). The regions differ in that data from the Central region is recorded predominantly on soil sites, while that from the East region is recorded predominantly on rock sites. We removed recorded ground motions in the Gulf Coast region (Figure 2.1) from our database, because of significantly deep sediments in this region which cause considerably different attenuation behavior (EPRI, 2004).

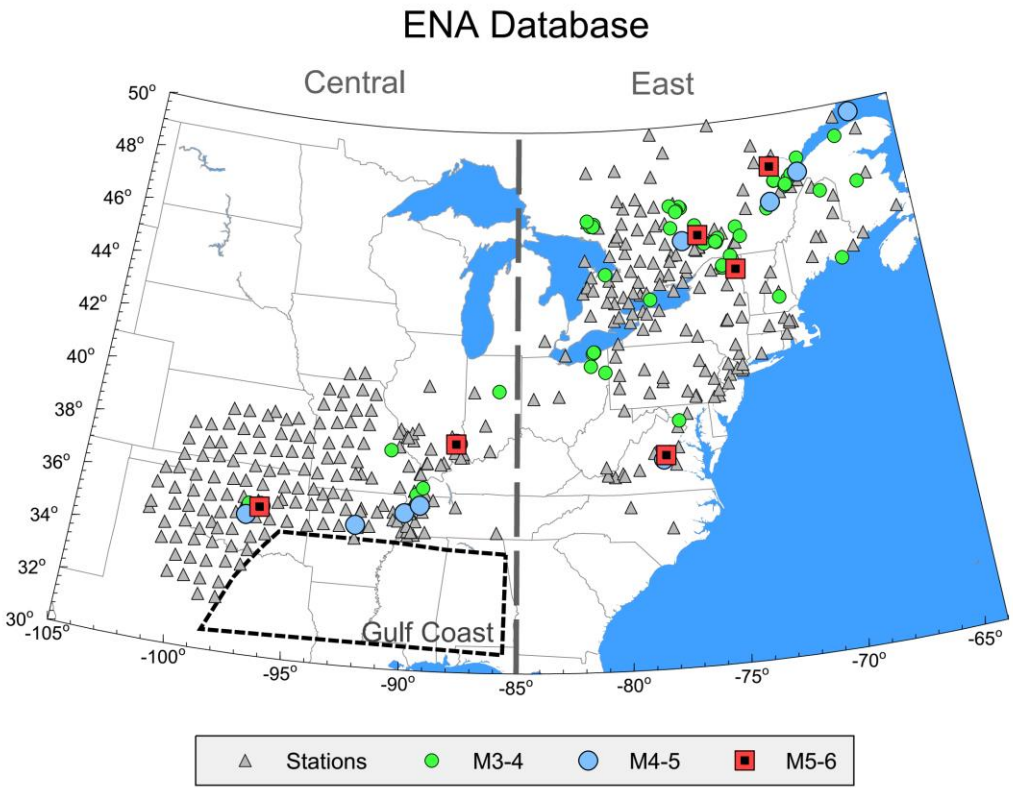

Figure 2.1: Geographic distribution of study events and stations.

The database of this study consists of peak ground-motion amplitudes (peak ground acceleration [PGA], peak ground velocity [PGV]) and response spectra (5%-damped pseudo-acceleration [PSA]) at frequencies from 0.1 to 20 Hz for horizontal components of ground motions; we use rotation-angle-independent geometric average of horizontal ground-motion amplitudes (RotD50) (Boore, 2010) if available, and geometric mean of the two horizontal components if the RotD50 is not available (see Section 2.7). We use instrument-corrected response spectra and ground-motion amplitudes whenever available, and process time histories to calculate these ground-motion parameters when it is needed. The processing of the waveforms involved baseline correction, windowing, tapering, digital filtering, removing instrumental response, and obtaining response spectra and Fourier spectra at defined frequencies band, as described by Assatourians and Atkinson (2010). We retain data only for those frequencies with a signal-to-noise ratio greater than 2. Moreover, we use only events with at least five records, and having moment magnitude (**M**) greater than three. The moment magnitudes of the events are either

known (see Section 2.7) or can be reliably estimated (within 0.2 units) from the PSA amplitude at 1 Hz as described by Atkinson and Babaie Mahani (2013).

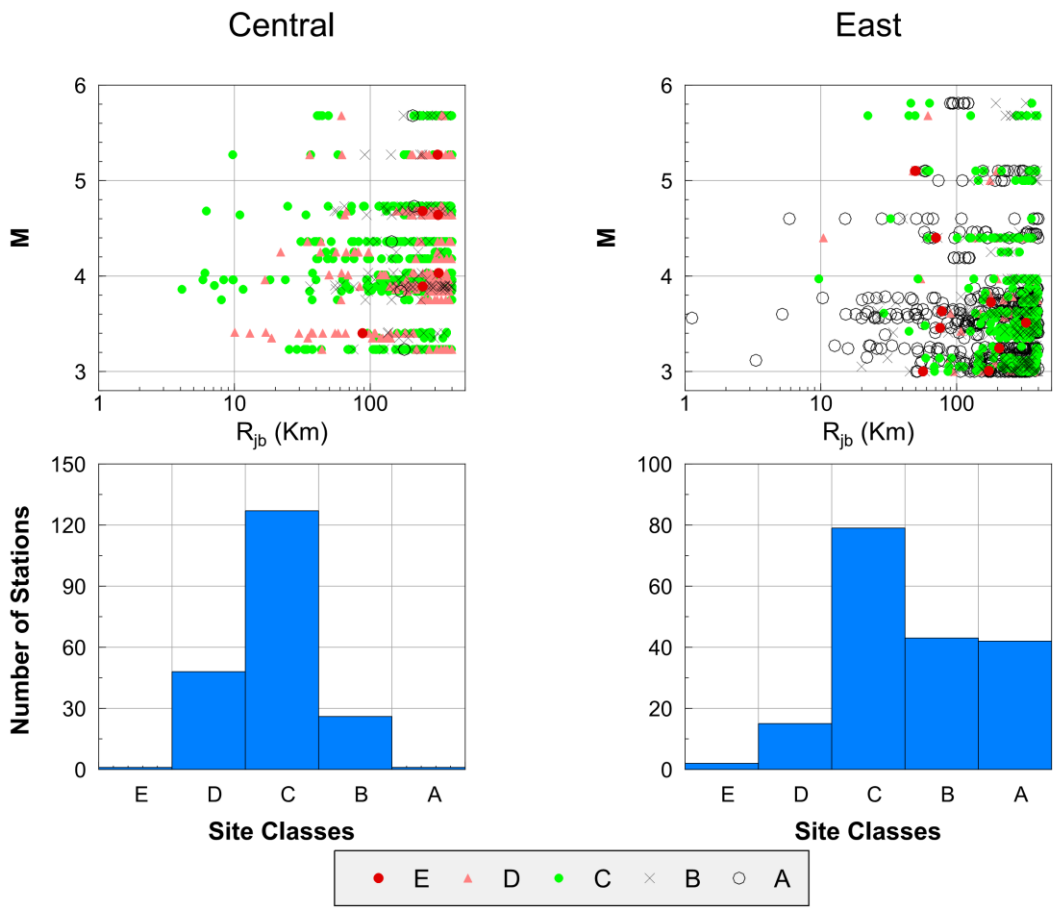

Figure 2.2: Top: Magnitude-distance distribution of the database, by NEHRP site classes; Bottom: Histogram of number of stations in each site class.

The ENA database consists of events with **M** ≤ 5.8 with relatively few observations at close distances (R≤ 50 km). Therefore, for the ENA database we can assume that the closest distance to the surface projection of the rupture (R_{jb}) is approximately equal to the epicentral distance (R_{epi}), and that the closest distance to the rupture surface (R_{cd}) is equal to hypocentral distance (R_{hyp}). We consider records with $R_{epi} \leq 400$ km, to be consistent with NGA-West2 database (Boore et al., 2014). To consider site amplification effects following the format of the reference BSSA14 GMPEs, we characterize each site according to its time-averaged shear wave velocity in the upper 30m (V_{S30}). V_{S30} information is extracted from the updated NGA-East database (see Section 2.7).

According to the NGA-East database, V_{S30} values are either measured or estimated using two to five different proxies. The weighted average of these proxies provides more reliable estimate of V_{S30} comparing to the values obtained by a single proxy (e.g. such as the topographic slope method of Wald and Allen, 2007). Figure 2.2 shows the magnitude-distance distribution of the database, distinguishing between different site classes based on their NEHRP (National Earthquake Hazards Reduction Program) site classification. Here, the histogram of number of sites in each site class is also shown for both regions (Note: NEHRP site classifications are based on V_{S30} value, where $V_{S30}\leq$180 m/sec considered as site class E, 180 $<V_{S30}\leq$ 360 m/sec considered as site class D, 360 $<V_{S30}\leq$ 760 m/sec considered as site class C, 760 $<V_{S30}\leq$ 1500 m/sec considered as site class B, and V_{S30} > 1500 m/sec considered as site class A).

2.3 Referenced empirical method

The idea behind the referenced empirical approach is to adjust well-calibrated empirical GMPEs from a data-rich region (host region) to match the observed data in a target region. Applying this method, we can make the best use of both region-specific empirical ground-motion data and global experience from better-instrumented regions. The main assumption of this method is that the magnitude scaling and overall near-source behavior of ground motions are the same in the host and target regions, although the overall ground-motion levels at the source might be different (if the source parameters differ), and the attenuation might be different. Under these conditions, if we can establish the regional differences at moderate magnitudes, we can extend them to larger magnitudes. To proceed, we compute the residuals, defined as the difference (in log units) between the observed ground-motion parameters from the target region and the predicted ground-motion parameters of the host region GMPEs. Adjustment factors are defined to model the observed residual trends. The adjustment factors can modify the overall level of the reference GMPEs frequency-by-frequency, and possibly change their shape as a function of distance, in order to match the regional data. Adjustments to the overall level can accommodate regional variations in stress parameter and event type, while adjustments to the distance coefficients can accommodate regional variation of attenuation parameters,

including any differences in anelastic attenuation or geometrical spreading (Atkinson, 2008; Atkinson, 2010; Atkinson and Motazedian, 2013).

The key inputs to construct referenced empirical GMPEs are regional ground-motion data from the target region and a set of reference GMPEs from the host region. The ground-motion database of this study is the ENA database as discussed in the previous section (horizontal components), while the reference GMPE is BSSA14 (Boore et al., 2014). Input parameters for BSSA14 are **M**, R_{jb}, V_{S30}, and source mechanism (assumed as unspecified). The outputs of BSSA14 are RotD50 (Boore, 2010) of horizontal ground-motion amplitudes (PGA, PGV) and PSA at the defined frequency range (0.1 to 20 Hz), which is approximately the geometric mean of two randomly-oriented horizontal components.

The residuals (in log units) are computed for each record as the log (base10) of the ratio of the observed ENA horizontal ground motions to those predicted by BSSA14 reference model (i.e. log (residual)= log (observed ENA amplitude/ predicted amplitude from BSSA14)). Figure 2.3 shows the residuals for Central and East regions at two selected frequencies (1 and 5 Hz) versus distance (R_{jb}), along with the function used to model the residuals (described in the following). Inspection of Figure 2.3 reveals that the averages of the residuals (filled squares) are positive in all distance bins, except at very close distances. This implies relatively higher ground-motion amplitudes in ENA in comparison to those in active regions, although at short distances ($R \leq 50$ km) the differences in amplitudes do not appear to be significant (at $f \leq 5$ Hz). There is an increasing residual trend at distances >50 km, which is increasingly important, especially at high frequencies. The residual trends observed here agree with our general expectations, considering the slower attenuation of ENA motions at regional distances (Atkinson, 2004). At distances ≤ 50 km, the differences between ENA amplitudes and the predictions of BSSA14 model are not significant, at least at 1 and 5 Hz.

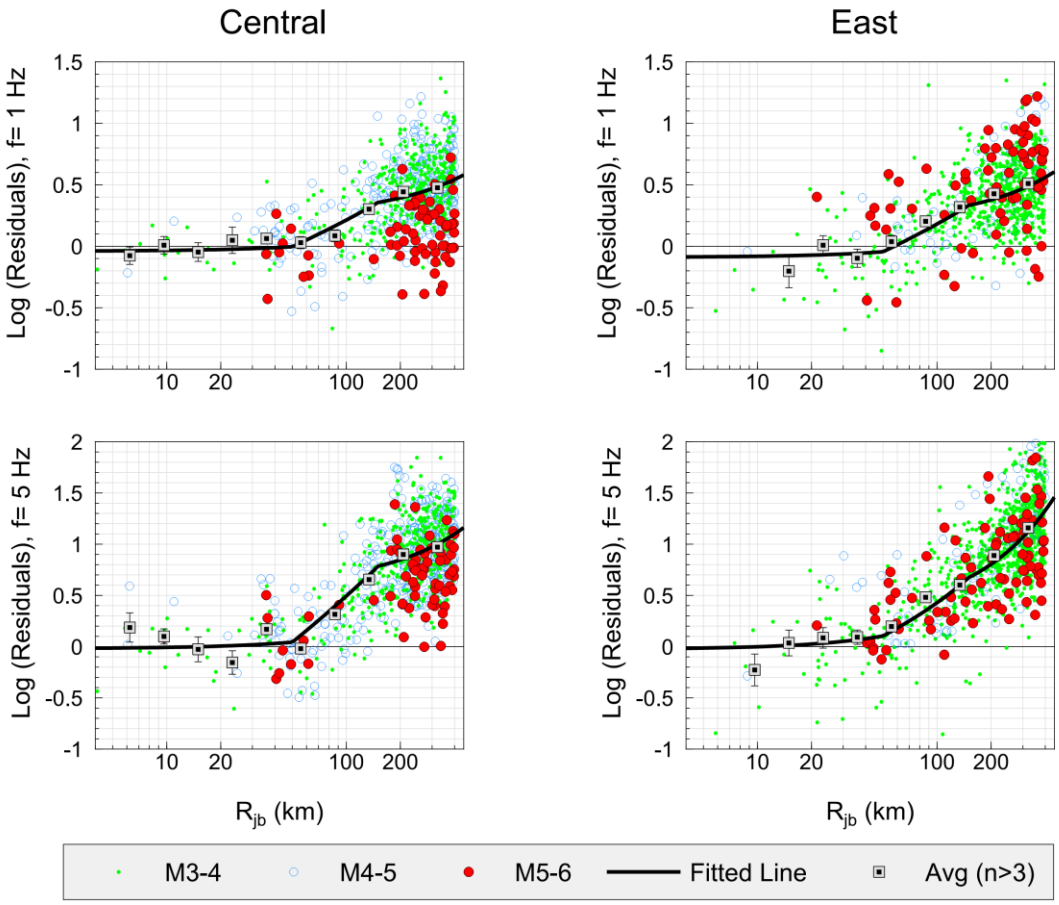

Figure 2.3: Residuals in Central and East regions compared to BSSA14 reference GMPE in log_{10} units for PSA at 1 and 5 Hz frequencies. The residuals are coded by magnitude. Filled squares show mean residuals in equally log-spaced distance bins with their corresponding standard error, and solid lines show the fit line to residuals (Equation 2.1).

The residual trends in the Central region are very similar to the equivalent values in the East region, which suggests similar ground-motion amplitudes for both regions. This agrees with a previous conclusion by Babaie Mahani and Atkinson (2012), and with expectations based on modeling studies by EPRI (2004). Therefore, in order to develop more robust adjustment factors, the residuals for the East and Central regions are combined.

Figure 2.4 shows the residuals at four selected frequencies (0.5, 1, 5 and 10 Hz) for the whole ENA database. Here, the residual trends are defined as:

$$\log\left(F_{ENA}(f)\right)_{ij} = C_1(f) + C_2(f)\left(R_{jb}\right)_{ij} + C_3(f)\max\left(0, \log\left(\min\left(\left(R_{jb}\right)_{ij}, 150\right)/50\right)\right) + \eta(f)_i + \varepsilon(f)_{ij}, \quad (2.1)$$

where $\log(F_{ENA}(f))_{ij}$ is the residual estimated for recording *j* in event *i* as a function of frequency, $C_1(f)$ adjusts the overall level of BSSA14 reference GMPEs, $C_2(f)$ is a factor to model regional differences in anelastic attenuation, $C_3(f)$ is a factor to adjust the shape of the reference GMPEs (as a function of distance) to match the observed ground motion attenuation shape in ENA in the transition zone from direct wave to Lg-spreading ($50 \leq R < 150$ km) and beyond, η_i is the random event term for event *i*, and ε_{ij} represents the within-event residual for recording *j* in event *i*. Event terms have zero mean and standard deviation of τ ($\log_{10}$ units), while within-event errors have zero mean and standard deviation of φ ($\log_{10}$ units).

The adopted functional form of Equation (2.1) produces a relatively flat attenuation zone between 50 and 150 km, which is consistent with proposed tri-linear ENA empirical models (e.g. Atkinson and Mereu, 1992; Atkinson, 2004). This functional form offers advantages in fitting the observed residuals over alternative bilinear forms, which are also commonly used (e.g. Boatwright and Seekins, 2011; Atkinson and Boore, 2011). The transition zone models the effect of reflections and refractions off the Moho discontinuity, which disrupts amplitude decay in the distance range from 50 to 200 km (e.g. Burger et al., 1987).

To solve Equation 2.1, we applied a mixed effects regression of residuals according to Abrahamson and Youngs (1992). An iterative regression was performed to maximize the likelihood of the model (Equation 3 in Abrahamson and Youngs, 1992) and estimate the adjustment factor coefficients ($C_1(f), C_2(f)\ and\ C_3(f)$), as well as the variability parameters (η_i, ε_{ij}, τ and φ). The total standard deviation σ is obtained as:

$$\sigma = \sqrt{\tau^2 + \varphi^2}. \quad (2.2)$$

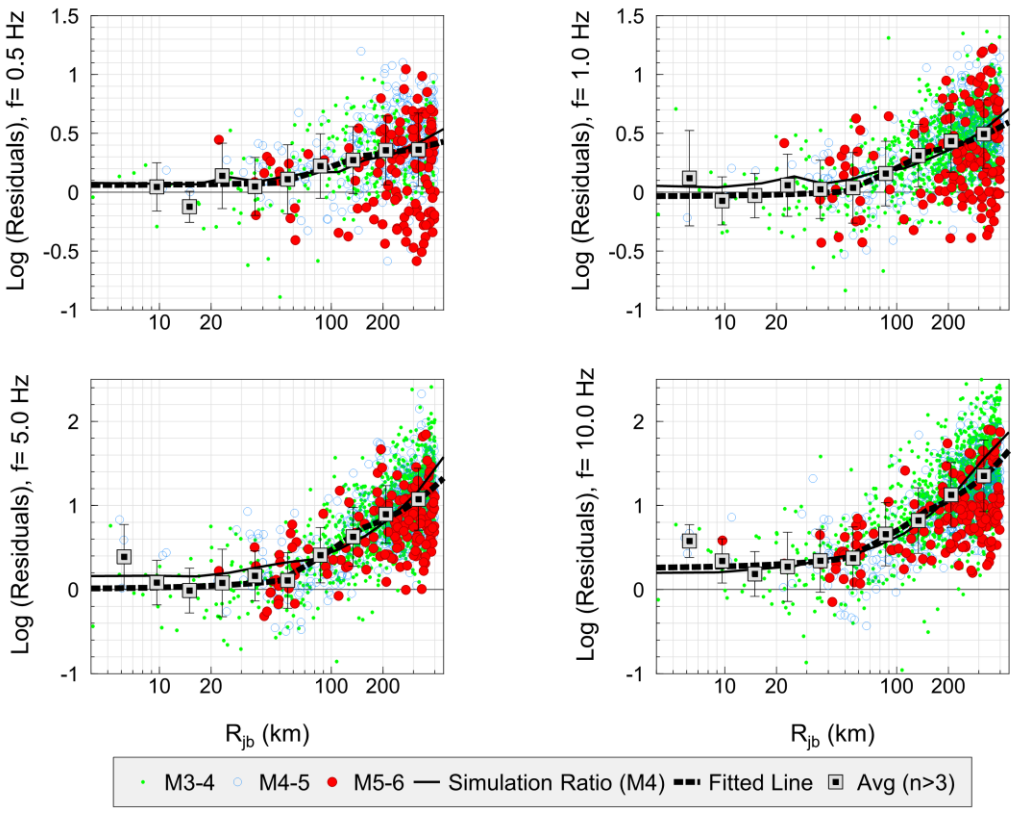

Figure 2.4: Residuals for the whole ENA database compared to BSSA14 reference GMPE in $\log_{10}$ units for PSA at 0.5, 1, 5 and 10 Hz frequencies. The residuals are coded by magnitude. Filled squares show mean residuals in equally log-spaced distance bins with their corresponding standard deviations, and dashed lines show the fit line to Equation 2.1. Solid lines shows the ratio obtained from proposed seismological models for ENA and WNA (predicted ground-motion parameter using ENA seismological model / predicted ground-motion parameter using WNA seismological model)

Table 2.1 shows the estimated coefficients for PGA, PGV and PSA at 0.1 to 20 Hz frequencies, as well as the between-event standard deviation (τ), within-event standard deviation (φ), and total standard deviation (σ). The referenced empirical GMPE for ENA is given by:

$$Y'_{ENA} = F_{ENA} Y_{BSSA14}, \qquad (2.3)$$

Table 2.1: Values of adjustment factor coefficients and variability parameters (in $\log_{10}$ units) of Equations 2.1 and 2.2.

Frequency (Hz)	C_1	C_2	C_3	σ (ENA)	ϕ	τ
PGV	0.166	0.0007	0.73	0.33	0.28	0.18
PGA	0.384	0.0017	0.63	0.41	0.30	0.27
0.10	0.065	0.0006	0.22	0.25	0.21	0.14
0.13	0.029	0.0006	0.27	0.28	0.21	0.19
0.16	0.010	0.0006	0.27	0.29	0.22	0.20
0.20	0.025	0.0006	0.22	0.29	0.22	0.18
0.25	0.052	0.0006	0.21	0.28	0.23	0.17
0.32	0.067	0.0005	0.27	0.28	0.23	0.16
0.40	0.061	0.0004	0.36	0.28	0.23	0.16
0.50	0.041	0.0004	0.44	0.28	0.24	0.15
0.63	0.020	0.0005	0.48	0.29	0.24	0.15
0.79	-0.009	0.0006	0.50	0.28	0.25	0.14
1.00	-0.043	0.0009	0.54	0.28	0.25	0.13
1.26	-0.067	0.0011	0.57	0.28	0.25	0.12
1.58	-0.077	0.0013	0.59	0.29	0.26	0.13
2.00	-0.068	0.0014	0.63	0.30	0.27	0.14
2.51	-0.053	0.0015	0.71	0.31	0.28	0.14
3.16	-0.036	0.0016	0.80	0.33	0.29	0.15
3.98	-0.016	0.0018	0.86	0.34	0.29	0.17
5.01	0.014	0.0020	0.89	0.35	0.30	0.18
6.31	0.074	0.0021	0.88	0.36	0.30	0.20
7.94	0.158	0.0022	0.81	0.38	0.30	0.22
10.00	0.264	0.0023	0.71	0.40	0.31	0.25
12.59	0.370	0.0024	0.61	0.42	0.32	0.28
15.85	0.439	0.0023	0.52	0.45	0.33	0.30
≥19.95	0.472	0.0022	0.44	0.47	0.36	0.32

where Y'_{ENA} is the predicted ground-motion parameter value (PGA, PGV and PSA) in ENA and Y_{BSSA14} is the predicted amplitude of the BSSA14 reference GMPEs. This equation should not be used at distances greater than 400 km, as it is unconstrained. If the GMPE is to be extended beyond 400 km, a maximum value of 400 km should be used in defining the adjustment factor.

In Table 2.1, the quoted total standard deviation of the residuals is very large (0.29 to 0.40 $\log_{10}$ units). This is due to a variety of factors including the combination of a wide range of regions and site classes; and the use of a wide range of magnitudes and distances, particularly including many data of **M** < 4. It has been shown that smaller-magnitude data have larger variability, and also that the use of larger distances increases variability (e.g. Boore et al., 2014, and Campbell and Bozorgnia, 2014). By contrast, Atkinson (2013) obtained relatively low ground-motion variability when considering a more tightly-constrained ENA database. To obtain more representative estimates of variability for the range of engineering interest, we compute the geomean residual for events of **M** ≥ 4 recorded at distances < 70 km. The calculated variability parameters corresponding to the confined magnitude and distance ranges are smaller at some frequencies in comparison to the values obtained from the whole ENA dataset; however the difference is not that significant. This may be because of the paucity of the data is the range of engineering interest in the ENA database. Therefore, the same value of variability parameters is suggested for all of the magnitude and distance ranges.

As we discussed earlier, the referenced empirical approach is similar in concept to the hybrid empirical method of Campbell (2003). Therefore, if we calculate the expected residual trends using calibrated simulation-based models in both regions, we expect to predict similar trends to those that we observed empirically. To test whether this is so, we use an equivalent point-source stochastic model that has recently been calibrated for applications in both western North America (WNA) and ENA (Atkinson et al., 2014). The model uses the equivalent point-source approach of Yenier and Atkinson (2014), with a bilinear attenuation model in both regions, characterized by geometric spreading of $R^{-1.3}$ at $R \leq 50$ km (where R is a generic distance measure, typically hypocentral distance), with $R^{-0.5}$ beyond, with typical regional Q models. The average stress parameter is a factor of two higher in ENA in comparison to WNA. For both regions, we neglect the effects of crustal and site amplification, as we are calculating only the ratio between two models, so these factors approximately cancel each other under the assumption that they are similar. Simulations are generated over a range of magnitudes and distances using the SMSIM algorithm of Boore (2003) in the time domain, with the simulation parameters as given in Table 2.2. The predicted residual trends based on the

hybrid empirical approach are determined from the log of the ratio of the simulated motions in ENA to the corresponding simulated motions in WNA.

Table 2.2: Seismological Parameters Used in the WNA and ENA Stochastic Models for a reference rock site (Atkinson et al., 2014)

Parameter	Western North America (WNA)	Eastern North America
Source spectrum	Brune ω-square, point source (Brune, 1970, 1971)	Brune ω-square, point source (Brune, 1970,
Stress parameter, $\Delta\sigma$ (bar)	300	600
Geometric attenuation	$R^{-1.3}$; R<50 $R^{-0.5}$; R≥50	$R^{-1.3}$; R<50 $R^{-0.5}$; R≥50
Source duration, T_S (Sec)	$1/f_0$	$1/f_0$
Path duration, T_p (Sec)	$0.05R$	$0.05R$
Path attenuation, Q	$170\, f^{0.45}$ (minimum Q=100)	$525\, f^{0.45}$
Shear velocity, β_S (km/sec)	3.7	3.7
Density, ρ_S (g/cc)	2.8	2.8
Site attenuation, κ_0 (sec)	0.02	0.02
Site amplification	no crustal or site amplifications are applied	no crustal or site amplifications are applied

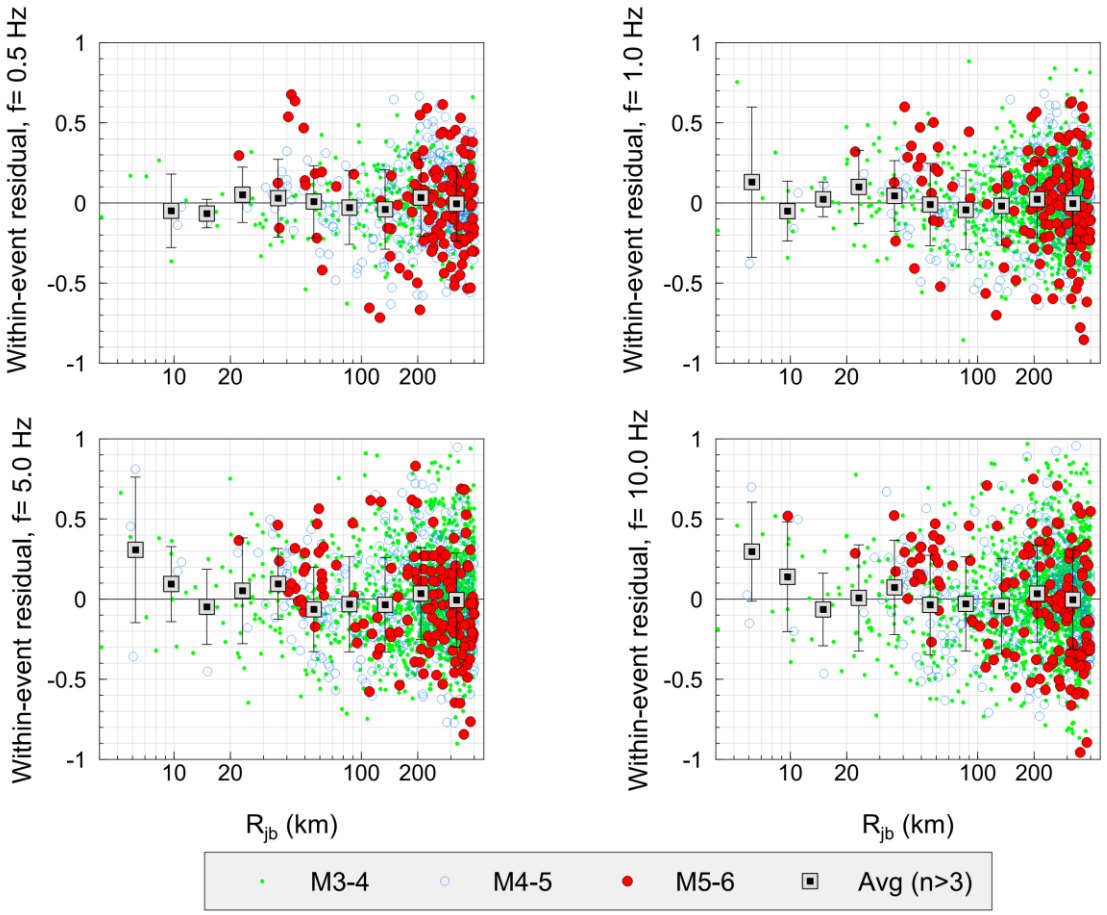

Figure 2.5: Within-event residuals ε ($\log_{10}$ units) for the whole ENA database for PSA at 0.5, 1, 5 and 10 Hz. The residuals are coded by magnitude. Filled squares show mean residuals in equally log-spaced distance bins with their corresponding standard deviations.

In Figure 2.4, we compare the referenced empirical residuals to those predicted by the hybrid empirical approach for the ENA vs. WNA simulation models for **M** = 4, assuming a focal depth of 10 km in both regions, and assuming that $R_{epi} = R_{jb}$. The trend lines obtained from the referenced empirical approach follow the predictions of the hybrid empirical method well overall (within 0.1 log units). Some differences are seen at near-source distances ($R \leq 50$ km) for low to moderate frequencies ($f \leq 5$ Hz), for which the hybrid-empirical approach would suggest relatively higher ground-motion amplitudes than would the referenced empirical method. However, it should be noted that the ENA database is sparse at close distances, hindering robust conclusions regarding ground-

motion amplitudes at near-source distances. Moreover, we have not included consideration of any regional difference in the 'calibration constant' required to center the model predictions for the dataset (see Atkinson et al., 2014). The offset between the referenced empirical and hybrid empirical lines on Figure 2.4 could be interpreted as an estimate of the difference in this calibration constant between the east and the west (ie. about 0.1 log units).

Figure 2.5 shows the within-event residuals at four sample frequencies obtained from Equation 2.1. The residuals do not show any apparent distance or magnitude dependency, and the overall behavior of the residuals at all frequencies is satisfactory. This demonstrates that the model works well in matching the observed ENA ground-motion data.

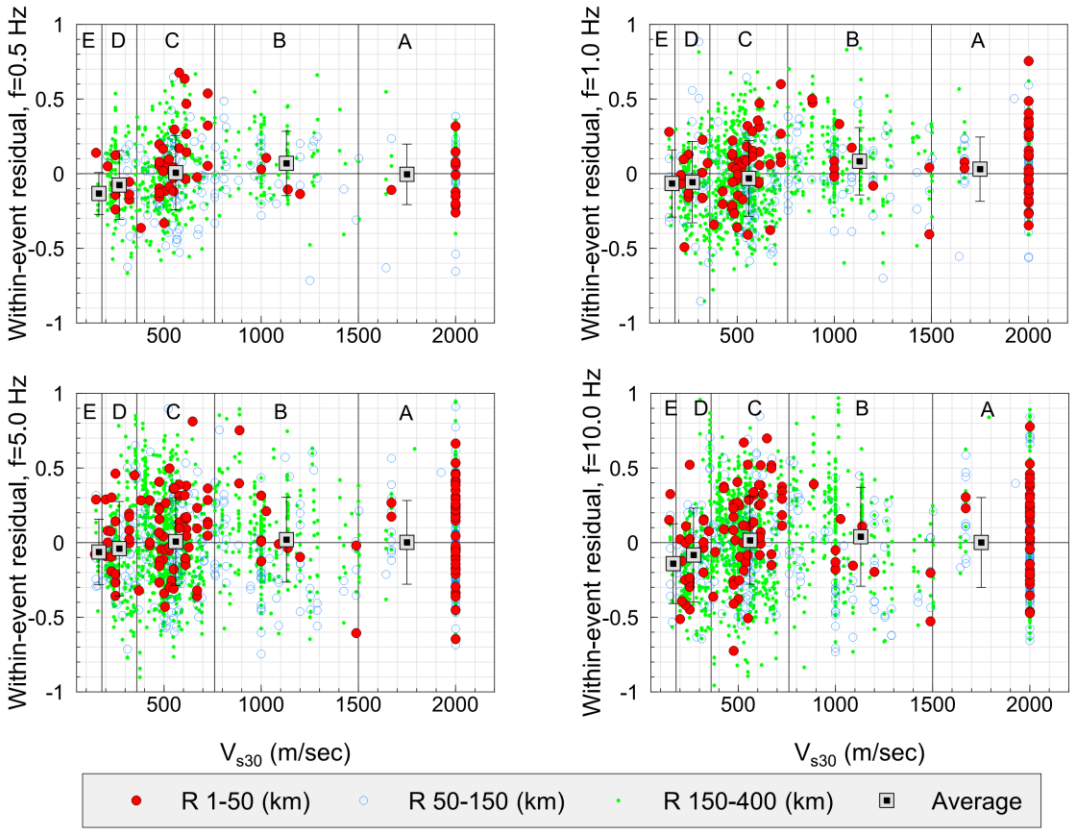

Figure 2.6: Within-event residuals ε ($\log_{10}$ units) for ENA as a function of V_{S30} of the stations. The residuals are coded by distance. Filled squares show mean residuals in NEHRP site classes with their corresponding standard deviations.

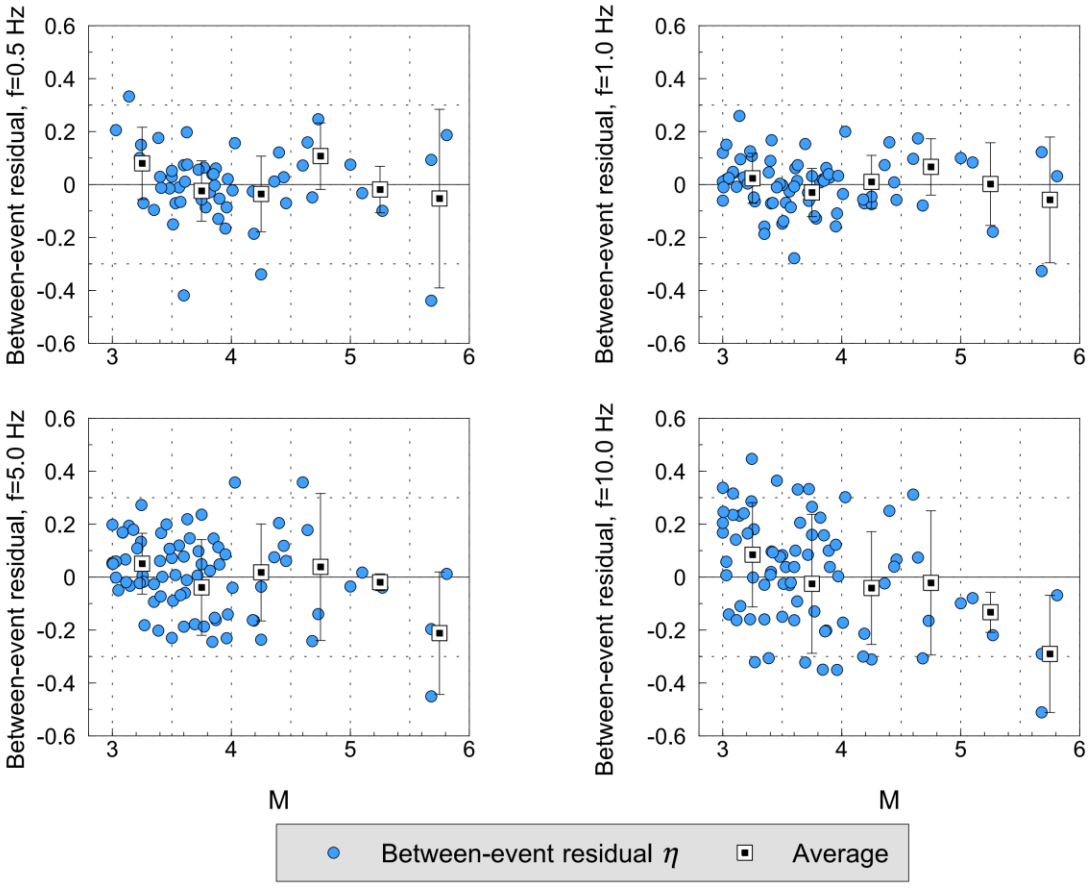

Figure 2.7: Between-event residuals η ($\log_{10}$ units)for ENA events as a function of magnitude. Filled squares show mean residuals in 0.5 magnitude bins with their corresponding standard deviations.

It is interesting to investigate the behavior of the within-event residuals in terms of the site conditions, to see how successfully the site correction factors of BSSA14, which are implicitly included in the GMPE, have removed the overall site effects. Figure 2.6 shows the within-event residuals as a function of V_{S30} for PSA at four sample frequencies. The general behavior of the residuals at all frequencies is acceptable. However, we note a small tendency to lower average residuals (overprediction of ENA amplitudes by ~0.1 log units) at softer sites (D and E sites) at lower frequencies. This may be because the western GMPEs that form the reference level are influenced to a greater extent at longer periods by deep sedimentary section effects, including basin effects. Moreover, it should be noted that the proposed site amplification model of BSSA14 was obtained based on sites in active tectonic regions, although there might be regional site response variations

within these regions as discussed in Boore et al. (2014). However, there is little available information regarding expected differences in site response between ENA and the active regions considered in NGA-West2; inspection of the residuals shows no apparent trend corresponding to V_{S30} that we might attribute to such factors.

In Figure 2.7, the between-event residuals η are plotted as function of magnitude. The within-event residuals do not show any apparent magnitude dependency, and the overall behavior of the residuals at all frequencies is satisfactory. However, there is a tendency to lower average residuals (overprediction of amplitudes by ~0.2 log units) for $\mathbf{M} > 5$. This is attributable mainly to the events that are located in Central region, near the boundaries of the Gulf coast region (Figure 2.1 and 2.2), where the stations are not symmetrically distributed around the events. Moreover, the database for $\mathbf{M} > 5$ is too sparse to define any magnitude trends in a robust way. Therefore, we assume no magnitude dependence for the residuals in the proposed GMPE model. We note that we might expect a stress-drop effect on the adjustment factors, which could be significant for larger events at some frequencies, due to regional differences in stress parameter between ENA and WNA. The difference in corner frequency between ENA and WNA (for the same magnitude) should theoretically result in regional variability in magnitude scaling between the corner frequencies. One could calculate the expected effect using the available simulation-based model in ENA and WNA, which is essentially what the hybrid-empirical model (Campbell, 2003) does. However, we did not observe any noticeable magnitude trends based on the available data, and thus under the referenced-empirical philosophy we did not include any such effect. This unmodeled effect is a source of epistemic uncertainty in the referenced-empirical GMPE, the importance of which can be assessed by comparison of its predictions to those of hybrid-empirical model predictions.

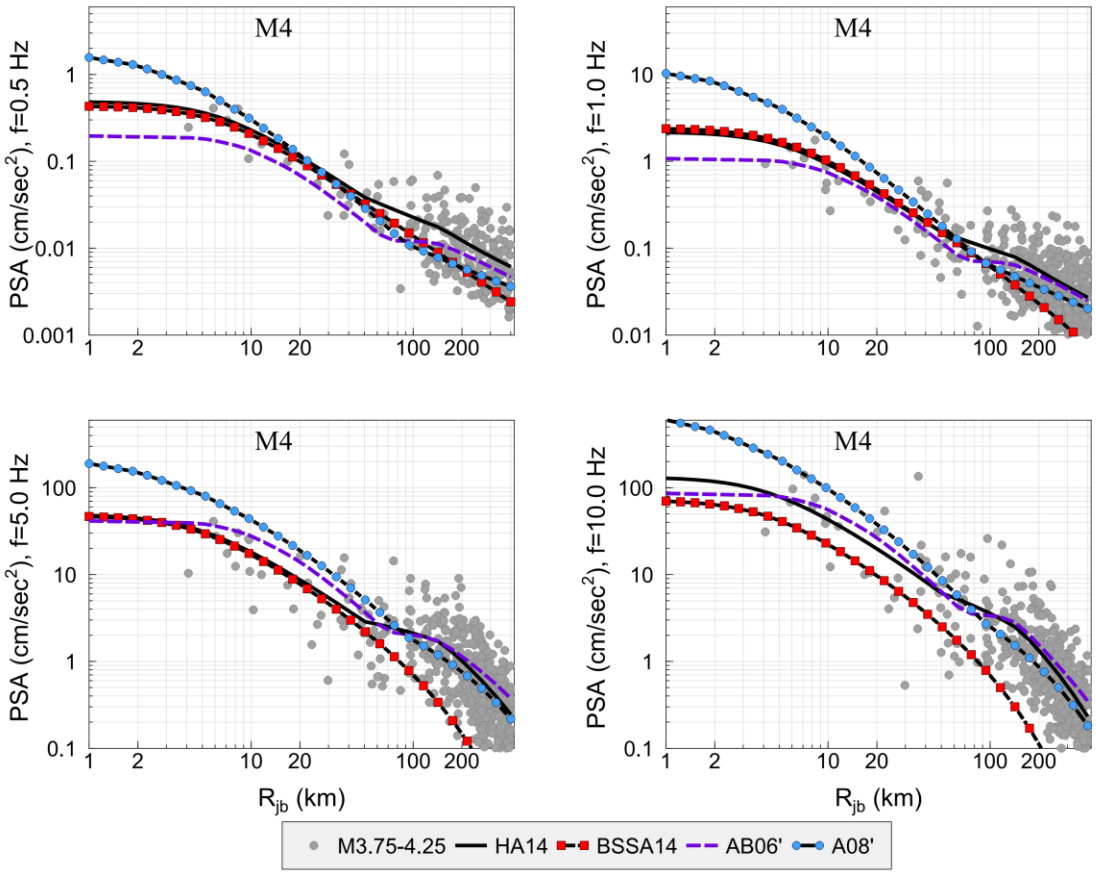

Figure 2.8: Proposed ENA referenced empirical GMPEs (HA14) for M4 assuming an unspecified focal mechanism and B/C site condition, compared to the observed data in ENA corrected for B/C site condition. Reference GMPEs of BSSA14, simulation-based GMPEs of AB06', and former referenced empirical GMPE of A08' are also shown for M4.

In Figures 2.8 and 2.9, we display the performance of the proposed referenced empirical GMPE model of this study (denoted as HA14) against the observed ENA data. The observed data are all adjusted to equivalent amplitudes for B/C site condition (V_{S30}=760 m/sec) using the site amplification model of BSSA14. We plot the GMPEs as a function of distance for **M**4 and **M**5 for an unspecified source mechanism and B/C site condition. GMPEs are plotted for the proposed referenced empirical model for ENA, the BSSA14 reference model, the stochastic simulation-based GMPE of Atkinson and Boore (2011, denoted AB06′), and the former ENA referenced empirical model of Atkinson and Boore (2011, denoted AB08′). The proposed referenced empirical GMPE model for ENA matches the observed regional data at all distances, as we would expect from its

definition. It is interesting and important to note that at close distances ($R \leq 50$ km), for $f \leq 5$ Hz, the referenced empirical model predicts the same level of ground-motion amplitudes as does the BSSA14 model, implying that differences between ENA and WNA motions are only important at high frequencies (all distances) and at regional distances (all frequencies). These trends are presumably due to the lower attenuation rate of ENA motions at regional distances, and to the effects of higher stress parameter in ENA (e.g. Atkinson and Boore, 2014). Comparison between the HA14 model and the referenced empirical model of A08' shows that at $R \leq 50$ km the A08' model predicts higher ground-motion amplitudes at all frequencies, which is more obvious for **M**4. This is likely because the previous generation of the NGA models were not originally developed for small magnitude events, and do not model their amplitudes as well as the newer models. Comparing the referenced empirical model of this study with the simulation-based model of AB06' reveals that both models are similar in shape, although they predict different amplitudes - especially at close distances ($R \leq 50$ km), where there are not enough data to constrain the prediction models.

In Figure 2.10, we compare the proposed referenced empirical GMPE of this study with the BSSA14 reference model, the AB06' simulation-based GMPE, and the former referenced empirical GMPE of A08' for a large-magnitude event (**M**7, unspecified source mechanism, and B/C site condition) at four sample frequencies. As Equation 2.1 implies, there is no magnitude dependency for the adjustment factors. Therefore, the comparison between HA14 and BSSA14 models reveals the same features as discussed in Figures 2.8 and 2.9. Comparison of the HA14 and the A08' models shows that both of the models predict similar ground-motion amplitudes at $R \leq 50$ km and $f > 5$ Hz. However the HA14 model predicts higher ground-motion amplitudes at $f \leq 5$ Hz and $R < 50$ km. Comparison of the HA14 and the AB06' models shows that the HA14 model predicts smaller ground-motion amplitudes especially at $R \leq 20$ km. This suggests that near-distance saturation effects are stronger in the BSSA14 empirical equations than in the stochastic simulations employed by AB06'. However, at $f \geq 5$ Hz and $R > 50$ km, the referenced empirical model suggests higher ground-motion amplitudes in comparison to the AB06' model. This difference is a factor of two at $R > 200$ km, which could have significant implications for seismic hazard evaluations in some cases. As there are no direct ground-

motion observations to justify this difference, it should be considered a source of epistemic uncertainty in seismic hazard applications.

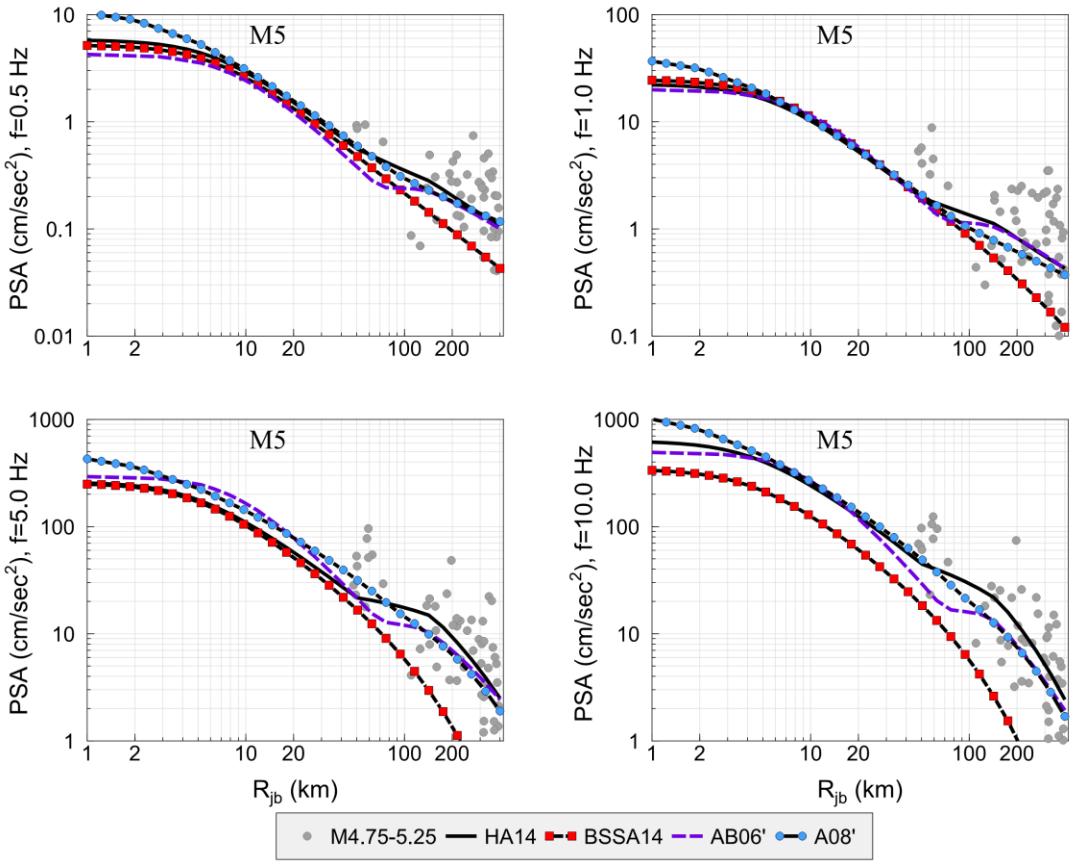

Figure 2.9: Proposed ENA referenced empirical GMPEs (HA14) for M5 assuming an unspecified focal mechanism and B/C site condition, compared to the observed data in ENA corrected for B/C site condition. Reference GMPEs of BSSA14, simulation-based GMPEs of AB06', and former referenced empirical GMPE of A08' are also shown for M5.

In Figure 2.11, the predicted response spectra of a **M**5 and a **M**7 event at R_{jb} = 10 km and R_{jb} = 100 km (unspecified source mechanism, and B/C site condition) are plotted for the proposed referenced empirical GMPE of this study, to illustrate the overall frequency behavior of the model. Response-spectra of BSSA14, AB06' and A08' are also plotted for the same magnitudes and distances. The differences between the HA14 and BSSA14 response spectra are as already discussed, based on the adjustment factors obtained in Equation 2.1. Comparison between the HA14 and AB06' and A08' response spectra shows that all of them present similar ground-motion amplitudes at R_{jb} = 10 for **M**5 and

M7. However, HA14 predicts higher ground-motion amplitudes at R_{jb} = 100 km, reflecting trends seen in regional seismographic data.

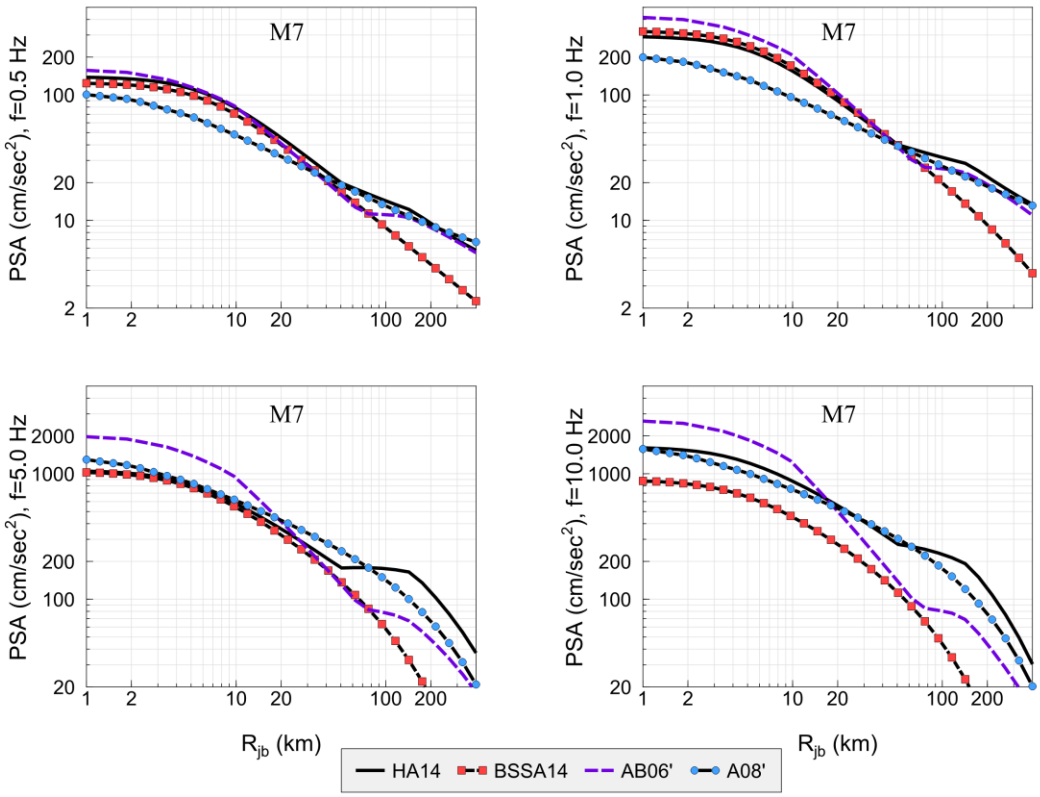

Figure 2.10: Proposed ENA referenced empirical GMPEs (HA14) for M7 assuming an unspecified focal mechanism and B/C site condition compared to the Reference GMPEs of BSSA14, the simulation-based GMPEs of AB06', and the former referenced empirical GMPE of A08' for the same magnitude.

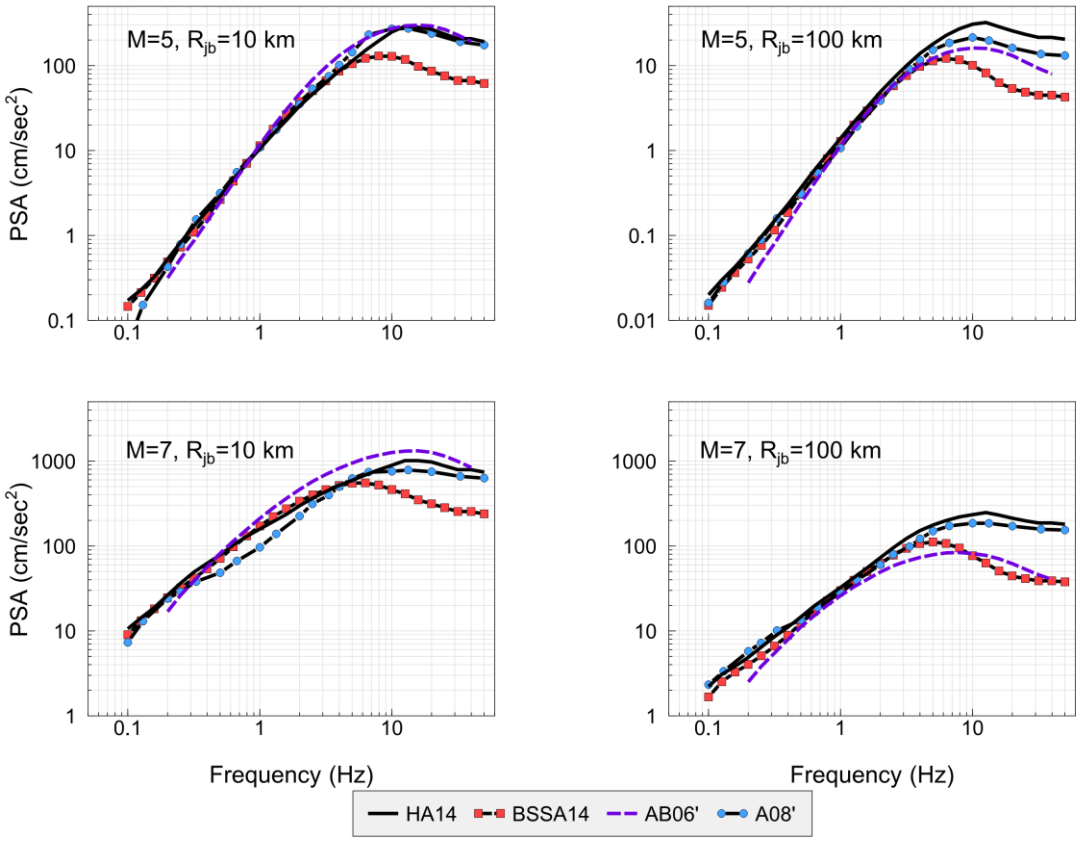

Figure 2.11: Response spectra of M5and M7at R_{jb}=10 km and R_{jb}=100 km for the proposed ENA referenced empirical GMPEs (HA14) for unspecified focal mechanism and B/C site condition compared to the Reference GMPEs of BSSA14,the simulation-based GMPEs of AB06', and the former referenced empirical GMPE of A08' for the same magnitude.

We also provide ground-motion predictions for very hard rock site condition (V_{S30} = 3000 m/s). Atkinson (2012) derived site factors that allow amplitude conversion between sites with V_{S30} = 760 m/s and $V_{S30} \geq$ 2000 m/s, using the predictions of Atkinson and Boore (2006). The site factors are given independent of distance, except for very high frequencies and PGA (Table 2.3). For $f \geq$ 40 Hz, the site factor is given as a function of R_{epi}. We convert ground-motion predictions for V_{S30} = 760 m/s to the equivalent motions for V_{S30} = 3000 m/s based on the site factors of Atkinson (2012). Here, we assume that the amplitude difference between sites with $V_{S30} \geq$ 2000 m/s and V_{S30} = 3000 m/s is small enough to neglect. We use R_{jb}-R_{epi} distance conversion method described in Atkinson (2012) to evaluate site factors for $f \geq$ 40 Hz and PGA. To switch from V_{S30} = 760 m/sec to

V_{S30} = 3000 m/sec site condition, the values provided in Table 2.3 should be subtracted from predicted ground-motion parameters ($\log_{10}$ base) for V_{S30} = 760 m/sec.

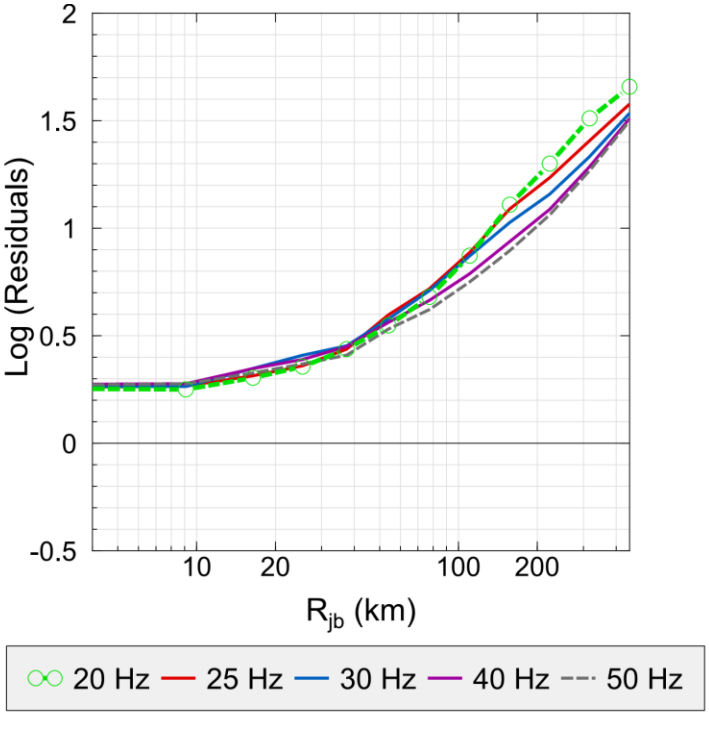

Figure 2.12: Residual trends obtained from proposed seismological models for ENA and WNA (predicted ground-motion parameter using ENA seismological model / predicted ground-motion parameter using WNA seismological model) as a function of distance at 20 Hz, 25 Hz, 30 Hz, 40 Hz, and 50 Hz for a sample event with M = 4.

To extend the proposed GMPE model for higher frequencies (>20 Hz) where number of reliable data reduces significantly, it is not rational to use the empirical data to develop adjustment factor. Therefore, we investigate the residual trends obtained from simulation-based models of Atkinson et al. [2014] (predicted ground-motion parameter using ENA seismological model / predicted ground-motion parameter using WNA seismological model) at higher frequencies for a sample event with **M** = 4 in Figure 2.12. Here, we plotted the residual trends at five different frequencies, namely 20 Hz, 25 Hz, 30 Hz, 40 Hz, and 50 Hz. As we observe here, the estimated residual trend at 20 Hz is a good approximation for higher frequencies (≥ 20 Hz). Although, it may slightly overestimates the predicted ground-motion parameters at very high frequencies. Therefore, for $f \geq 20$ Hz we suggest to use the adjustment factors obtained at 20 Hz.

Table 2.3: Site conversion factors from Atkinson (2012).

f (Hz)	$\log(Y_{ENA}[V_{S30}=760\ m/s]) - \log(Y_{ENA}[V_{S30}=3000\ m/s])$
PGV	0.09
PGA	$-0.3 + 0.15\log(R_{epi})$
≤ 0.2	0.06
0.5	0.09
1.0	0.11
2.0	0.14
3.0	0.14
5.0	0.12
10.0	0.03
20.0	-0.1
≥ 40	$-0.3 + 0.15\log(R_{epi})$

2.4 Conclusion

The proposed referenced empirical GMPEs for ENA are in agreement with regional ground-motion data to a distance of 400 km, while being constrained to follow the overall scaling behavior of ground motion that is observed for larger events in active tectonic regions. The referenced empirical model of this study suggests that ground-motion amplitudes in ENA are similar to those predicted by the BSSA14 reference equations at distances smaller than 50 km at frequencies ≤ 5 Hz. At higher frequencies and larger distances, ENA ground-motion amplitudes are significantly higher than predicted by the BSSA14 model, reflecting higher stress parameter and lesser attenuation in ENA relative to active tectonic regions.

2.5 Data and Resources

Corrected ground-motion parameters (PGA, PGV, PSA) for events in the central U.S. were obtained from the NGA-East database as provided by the NGA-East project (www.peer.berkeley.edu, last accessed Oct. 2014) which provides 5%-damped RotD50 response spectrum of horizontal ground motions; we used a pre-publication version of the database made available to project participants by C. Goulet (pers. Comm.). Many of the event data for the East region were obtained from the Engineering Seismology Toolbox website which provides 3-component processed ground-motion parameters

(www.seismotoolbox.ca, last accessed December 2013). For recent unprocessed data from Canadian stations, horizontal velocity waveforms were obtained from the Automatic Data Request Manager Facility (AutoDRM of the Geological Survey of Canada (autodrm@seismo.nrcan.gc.ca, last contacted December 2013). For unprocessed data of U.S. stations, including data from the U.S Transportable Array (TA) stations in southern Ontario, horizontal velocity waveforms were obtained from the IRIS AutoDRM (breq_fast@iris.washington.edu, last contacted December 2013). V_{S30} information for U.S stations was extracted from the updated NGA-East database. Moment magnitude information was extracted from the same resources as the ground-motion database if available, and obtained from the following references if needed: 1) Global Centroid Moment Tensor project (www.globalcmt.org; last accessed December 2013), 2) USGS earthquake catalogue (www.earthquake.usgs.gov; last accessed December 2013), 3) regional moment Tensor solution by R. B. Herrmann (http://www.eas.slu.edu/eqc/eqcmt.html; last accessed December 2013). We used MATLAB (www.mathworks.com) for regression of the ground-motion amplitudes and CoPlot (www. cohort.com) for making the figures.

2.6 Acknowledgements

This work was financially supported by the Natural Sciences and Engineering Research Council of Canada and the NGA-East Project. We thank Chris Cramer and the NGA-East project for sharing updated versions of ground-motion databases. We are grateful to Dave Boore and an anonymous reviewer for thorough and constructive reviews that led to an improved document.

2.7 References

Abrahamson, N., and R. Youngs (1992). A stable Algorithm for regression analysis using the random effects model, *Bulletin of the Seismological Society of America* **82**, 505–510.

Assatourians, K., and G. Atkinson (2010). Database of processed time series and response spectra data for Canada: An example application to study of 2005 MN5.4 Riviere du Loup, Quebec, earthquake. *Seismological Research Letters* **81**, 1013–1031.

Atkinson, G. (2004). Empirical attenuation of ground-motion spectral amplitudes in southeastern Canada and the northeastern United States. *Bulletin of the Seismological Society of America* **94**, 1079–1095.

Atkinson, G. (2008). Ground-motion prediction equations for eastern North America from a referenced empirical approach: Implications for epistemic uncertainty. *Bulletin of the Seismological Society of America* **98**, 1304–1318.

Atkinson, G. (2010). Ground-motion prediction equations for Hawaii from a referenced empirical approach. *Bulletin of the Seismological Society of America* **101**, 1304–1318.

Atkinson, G. M. (2012). White paper on proposed ground-motion prediction equations (GMPEs) for 2015 national seismic hazard maps, http://www.seismotoolbox.ca/GMPEtables2012/r12_GMPEs9b.pdf (last accessed in January 2015).

Atkinson, G. (2013). Empirical evaluation of aleatory and epistemic uncertainty in eastern ground motions. *Seismological Research Letters* **84**, 130-138.

Atkinson, G., and A. Babaie Mahani (2013). Estimation of moment magnitude from ground motions at regional distances. *Bulletin of the Seismological Society of America* **103**, 107-116.

Atkinson, G., and D. Boore (1995). New ground motion relations for eastern North America. *Bulletin of the Seismological Society of America* **85**, 17–30.

Atkinson, G., and D. Boore (2006). Ground motion prediction equations for earthquakes in eastern North America. *Bulletin of the Seismological Society of America* **96**, 2181–2205.

Atkinson, G., and D. Boore (2011). Modifications to existing ground-motion prediction equations in light of new data. *Bulletin of the Seismological Society of America* **101**, 1121–1135.

Atkinson, G., and D. Boore (2014). The attenuation of Fourier amplitudes for rock sites in eastern North America. *Bulletin of the Seismological Society of America* **104**, 513-528.

Atkinson, G., and R. Mereu (1992). The shape of ground motion attenuation curves in southeastern Canada. *Bulletin of the Seismological Society of America* **82**, 2014–2031.

Atkinson, G., and D. Motazedian (2013). Ground-motion amplitudes for earthquakes in Puerto Rico. *Bulletin of the Seismological Society of America* **103**, 1846–1859.

Atkinson, G., and W. Silva (2000). Stochastic modeling of California ground motions. *Bulletin of the Seismological Society of America* **90**, 255–274.

Atkinson, G., D. Greig, and E. Yenier (2104). Estimation of moment magnitude (M) for small events (M<4) on local networks. *Seismological Research Letters* **85**, 1116-1124.

Babaie Mahani, A., and G. Atkinson (2012). Evaluation of functional forms for attenuation of small-to-moderate-earthquake response spectral amplitudes in North America. *Bulletin of the Seismological Society of America* **102**, 2714–2726.

Bommer, J., P. Stafford, J. Alarcon, and S. Akkar (2007). The influence of magnitude range on empirical ground-motion prediction. *Bulletin of the Seismological Society of America* **97**, 2152–2170.

Boatwright, J., and L. Seekins (2011). Regional spectral analysis of three moderate earthquakes in northeastern North America. *Bulletin of the Seismological Society of America* **101**, 1,769–1,782.

Boore, D. (2010). Orientation-independent, non geometric-mean measures of seismic intensity from two horizontal components of motion, *Bulletin of the Seismological Society of America* **100**, 1830–1835.

Boore, B., J. Stewart, E. Seyhan, and G. Atkinson (2014). NGA-West 2 Equations for Predicting PGA, PGV, and 5%-Damped PSA for Shallow Crustal Earthquakes. *Earthquake Spectra* **30**, 1057-1085.

Bozorgnia, Y., N. Abrahamson, L. Al Atik, T. Ancheta, G. Atkinson, J. Baker, A. Baltay, D. Boore, K. Campbell, B. Chiou, R. Darragh, S. Day, J. Donahue, R. Graves, N. Gregor, T. Hanks, I. Idriss, R. Kamai, T. Kishida, A. Kottke, S. Mahin, S. Rezaeian, B. Rowshandel, E. Seyhan, S. Shahi, T. Shantz, W. Silva, P. Spudich, J. Stewart, J. Watson-Lamprey, K. Wooddell, and R. Youngs (2014). NGA-West2 Research Project. *Earthquake Spectra* **30**, 973-987.

Brune, J. (1970). Tectonic stress and the spectra of seismic shear waves, *Journal of Geophysical Research* **75**, 4997–5009.

Brune, J. (1971). Correction: Tectonic stress and the spectra of seismic shear waves, *Journal of Geophysical Research* **76**, 5002.

Burger, R., P. Somerville, J. Barker, R. Herrmann, and D. Helmberger (1987). The effect of crustal structure on strong ground motion attenuation relations in eastern North America. *Bulletin of the Seismological Society of America*. **77**, 420–439.

Campbell, K. (2003). Prediction of strong ground motion using the hybrid empirical method and its use in the development of ground motion (attenuation) relations in eastern North America. *Bulletin of the Seismological Society of America* **93**, 1012–1033.

Campbell K., Y. Bozorgnia (2014). NGA-West2 Ground Motion Model for the Average Horizontal Components of PGA, PGV, and 5% Damped Linear Acceleration Response Spectra. *Earthquake Spectra* **30**, 1087-1115.

Douglas, J. (2004). An investigation of analysis of variance as a tool for exploring regional differences in strong ground motions. *Journal of Seismology* **8**, 484–496.

EPRI (2004). "CEUS Ground Motion Project Final Report," EPRI, Palo Alto, CA: 2004. 1009684.

Motazedian, D., and G. M. Atkinson (2005). Stochastic finite-faults modeling based on a dynamic corner frequency. *Bulletin of the Seismological Society of America* **95**, 995–1010.

Pezeshk, S., A. Zandieh, and B. Tavakoli (2011). Hybrid empirical groundmotion prediction equations for eastern North America using NGA models and updated seismological parameters. *Bulletin of the Seismological Society of America* **101**, 1859–1870.

Power, M., B. Chiou, N. Abrahamson, Y. Bozorgnia, T. Shantz, and C. Roblee (2008). An overview of the NGA project. *Earthquake Spectra* **24**, 3–21.

Silva, W. J., N. J. Gregor, and R. Darragh (2002). *Development of regional hard rock attenuation relations for central and eastern North America*, Technical Report, Pacific Engineering and Analysis, El Cerrito, CA.

Tavakoli, B., and S. Pezeshk (2005). Empirical-stochastic ground-motion prediction for eastern North America. *Bulletin of the Seismological Society of America* **95**, 2283–2296.

Toro, G., N. Abrahamson, and J. Schneider (1997). Model of strong ground motions from earthquakes in central and eastern North America: best estimates and uncertainties. *Seismological Research Letters* **68**, 41–57.

Wald, D. J., and T. I. Allen (2007). Topographic slope as a proxy for seismic site conditions and amplification, *Bulletin of the Seismological Society of America* **97**, 1379–1395.

Yenier, E., and G.M. Atkinson (2014). Equivalent point-source modeling of moderate-to-large magnitude earthquakes and associated ground-motion saturation effects, Bull. Seismol. Soc. Am. 104, 1458-1478.

Chapter 3

3 Estimation of moment magnitude and stress parameter from ShakeMap ground-motion parameters[2]

In this chapter, we describe an efficient method to determine moment magnitude and stress parameter in near-real-time, in the immediate aftermath of a small-to-moderate earthquake (**M**~3–6), from ShakeMap ground-motion parameters. The methodology is based on relating ShakeMap parameters to source and attenuation parameters within the context of a generic stochastic point-source model. The method is optimized for applications in regions with sparse networks and an example is provided for southern Ontario. We initially develop a simulation-guided generic ground-motion prediction equation (GMPE) model based on the available database in the region. We derive the applicable regional anelastic attenuation, stress parameter, and site amplification models. Then, using the estimated regional models, we show how to invert ShakeMaps parameters to estimate moment magnitude and stress parameter in near-real-time, to define an event-specific GMPE for an event that just happened. The event-specific GMPE can be used to provide robust, calibrated ShakeMaps that are fully consistent with ground-motion observations.

3.1 Introduction

For many applications in engineering seismology, it is useful to characterize events in terms of their moment magnitude (**M**) and stress parameter ($\Delta\sigma$). This two-parameter representation provides a fairly-comprehensive summary of the source parameters of the event, in the context of the simple ω^2 Brune model (Brune, 1970, 1971; Boore, 2003). As shown in Figure 3.1, **M** controls near-source spectral amplitudes at low frequencies, while $\Delta\sigma$ controls those amplitudes at high frequencies. Note that at high frequencies there is a trade-off between $\Delta\sigma$ and the near-surface attenuation parameter (κ_0) (Anderson

[2] A version of this chapter has been published. Atkinson, G.M., B. Hassani, A. Singh, E. Yenier, and K. Assatourians (2015). Estimation of Moment Magnitude and Stress Parameter from ShakeMap Ground-Motion Parameters, *Bull. Seismol. Soc. Am.* **105,** 2572-2588.

and Hough, 1984), so that these parameters should be considered coupled in ground-motion modeling.

The definition of near-source spectral content is a key component in the development of ground-motion prediction equations (GMPEs). Moreover, as we will show in this work, it greatly facilitates the development of robust and reliable near-real-time ShakeMaps. Real-time ShakeMaps, showing the intensity of shaking over the region and/or at specific sites of interest, have become a valuable tool for real-time hazard and risk management worldwide (Wald et al., 1999; Earle et al., 2009). Because of the popularity of these tools, calculation of ShakeMap ground-motion parameters has become routine on many standard seismological platforms. The ShakeMap parameters include peak ground acceleration (PGA) and velocity (PGV), and the 5% damped pseudo-spectral acceleration response (PSA) at selected frequencies, typically 0.33 Hz, 1 Hz, 3.33 Hz, and 10 Hz. It should be noted that there are some differences in practice as to which parameters are calculated and/or reported. For example, some agencies use the maximum of two horizontal components while others use the geometric mean of horizontal components. Some report the vertical component while others do not. Moreover the 10 Hz PSA is reported in only some applications. We argue herein that the 10 Hz PSA is very valuable in characterizing small-to-moderate events, which are often important in regions of low seismicity, so we would advocate for including it among standard ShakeMap parameters.

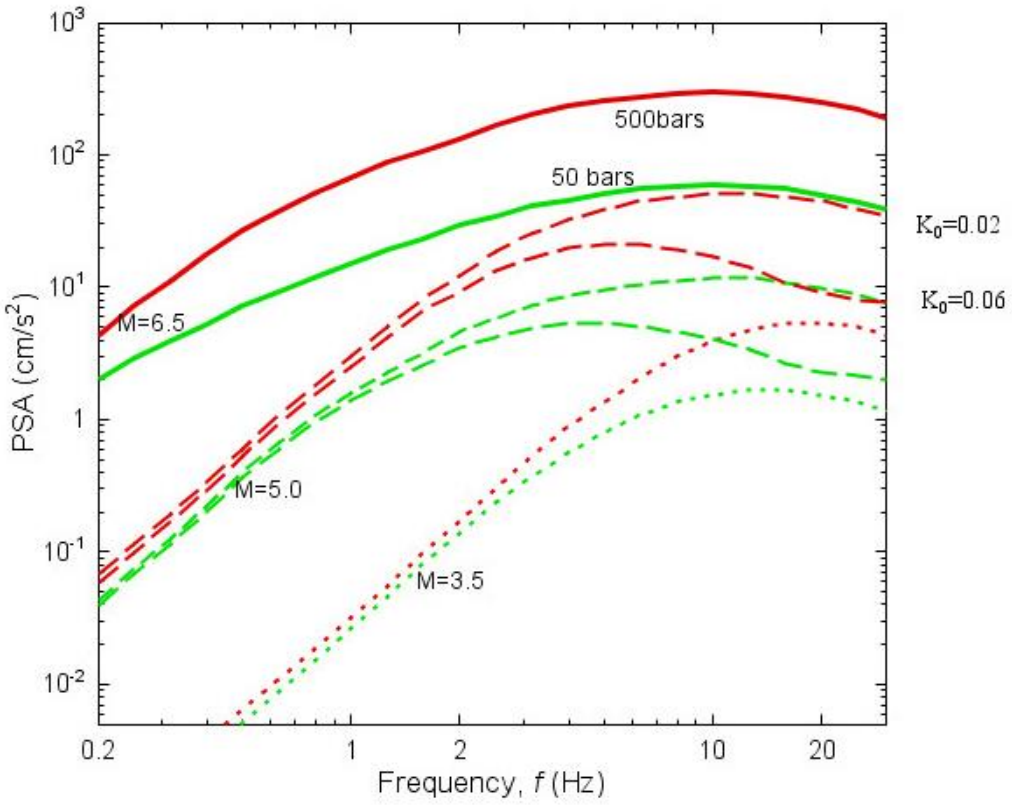

Figure 3.1: Illustration of the effect of source parameters on response spectral amplitudes for M=3.5, 5.0, 6.5 events with Δσ=50 (darker lines) and 500(lighter lines) bars, for κ0 =0.02. Influence of κ0 is illustrated by also plotting curves for κ0=0.06 at M5 (lower dashed curves for M5). PSA amplitudes simulated using SMSIM (Boore, 2005).

For GMPE and ShakeMap applications in regions of low to moderate seismicity, such as central and eastern North America (CENA), ground-motion estimates are required for the small to moderate events that happen fairly often (i.e. ~ once a year). Such events may not be damaging, in most cases, but rapid information on the amplitudes of shaking is required to inform the public and government or regulatory officials as appropriate. Moreover, we need to be able to demonstrate that ShakeMaps and GMPEs are reliable for the small-to-moderate events that happen regularly, in order to provide confidence in their performance potential in the event of larger earthquakes. Small events are an excellent calibration and testing ground for ShakeMaps and GMPEs.

In this chapter, we lay out a methodology to determine **M** and $\Delta\sigma$ from ShakeMap ground-motion parameters (PSA at 1 Hz or 0.33 Hz, PGA or PSA at 10 Hz), and demonstrate its use in southern Ontario. The methodology is suitable for use in the immediate aftermath of a small to moderate earthquake (**M**~3 to 6), occurring in a region having a sparse network. Its utility is that it enables the robust definition of a calibrated event-specific GMPE in real-time, which can then be used to produce reliable ShakeMaps that are tuned to the event that just happened, at both low and high frequencies. Such ShakeMaps are more accurate than those based on average regional GMPEs, as they are self-calibrating, and inherently remove the inter-event component of variability; these benefits are realized across a broad range of frequencies.

The methodology is based on relating observed ShakeMap parameters for a specific event to the basic source and attenuation parameters that comprise a generic stochastic point-source model. These event parameters, in concert with the underlying stochastic model equations, are the calibration elements that enable real-time construction of an event-specific GMPE that faithfully reproduces the observed amplitudes across the region. Moreover, the model provides a basic physical interpretation of the motions in terms of its source parameters (**M** and $\Delta\sigma$). We show that the proposed approach is well-suited to the development of real-time interactive ground-motion maps for events of **M** 3 to 6 in southern Ontario.

3.2 Methodology

The essential ground-motion information that is used to produce real-time maps of earthquake shaking is selected ShakeMap (Wald et al., 1999) parameters. Here we focus on the use of the 1 Hz and 10 Hz PSA, though we also discuss alternative formulations using the 0.33 Hz PSA (useful if the calculated **M**>4) or the PGA (useful if the 10 Hz PSA is unavailable). The ShakeMap ground-motion parameters are routinely calculated on many standard seismological platforms. Here, we calculate them using the processing procedures of the ICORRECT algorithm as described by Assatourians and Atkinson (2010); note that we refer to this processing algorithm as QCORRECT (a quick version of our instrument-correction algorithm), as it has been streamlined for fast operations, largely by calculating fewer response spectral ordinates, and outputting fewer

intermediate products. Briefly, the QCORRECT algorithm reads the raw velocity time series output by the seismographic stations, windows the portion containing the event, applies suitable low-cut and high-cut filters and removes the instrument response in the frequency domain, then calculates response spectra from the instrument-corrected accelerograms.

To estimate **M** and $\Delta\sigma$ from the observed PSA values, we relate these source parameters to the predictions of an equivalent point-source stochastic model that has been optimized for the attenuation and site response attributes of the region, as described by Yenier and Atkinson (2015a,b). Yenier and Atkinson used time-domain simulations obtained from the SMSIM algorithm of Boore (2003, 2005) to develop a robust simulation-based generic GMPE. They developed a functional form for the simulation-based GMPE that decouples the effects of the basic source and attenuation parameters on peak ground motions and response spectra. The utility of this approach is that once the generic GMPE is defined, we can use it to relate observed motions to **M** and $\Delta\sigma$ without the need to repeat simulations. This facilitates inversion of the GMPE to obtain the underlying source and attenuation parameters directly from response spectra observations. We define the generic GMPE as a linear combination of source, path and site terms that are easily separated, following Yenier and Atkinson (2015b):

$$\ln Y = F_E + F_Z + F_\gamma + F_S + C \,, \tag{3.1}$$

where ln$Y$ is the natural logarithm of a ground-motion intensity measure, such as the PSA at a selected frequency. F_E, F_Z, F_γ and F_S represent functions for earthquake source, geometrical spreading, anelastic attenuation and site effects, respectively. The C term is an empirical calibration factor that accounts for the residual differences between simulations and empirical data. The source function (F_E) describes the effects of magnitude and stress parameter on ground-motion amplitudes. Within this function we have decoupled the effects of magnitude and stress parameter on amplitudes, as:

$$F_E = F_M + F_{\Delta\sigma}, \tag{3.2}$$

where F_M represents the magnitude effect on ground-motion amplitudes that would be observed at the source, if there were no near-distance-saturation effects. It is defined for a reference stress ($\Delta\sigma$), κ_0 parameter, and site condition; the use of a reference stress shifts the effects of stress parameter into a separate term ($F_{\Delta\sigma}$), simplifying inversion procedures. We choose $\Delta\sigma$ = 100 bars and κ_0 = 0.025 s as the reference modeling parameters for convenience, because these parameters are the standard values found for earthquakes in California by previous similar inversion studies (Yenier and Atkinson, 2015a). The use of this standard model simplifies GMPE development by allowing previous simulation results to be used, without the need to repeat the derivation of the magnitude-scaling term for the GMPE. However, any other reference model could also be used as a starting point. It is the sum of the reference model and adjustment term that controls the resulting ground motions, so a different reference model would simply result in a different adjustment term, while preserving the sum of the effects. $F_{\Delta\sigma}$ represents the stress adjustment factor that is needed when $\Delta\sigma$ is different than 100 bars. This term will be significant in stable continental regions such as southern Ontario, because the stress parameter is expected to be greater than that for California. For example, Yenier and Atkinson (2015b) find that the stress parameter in CENA is greater than that in California by a factor of three on average.

The F_M term is defined as a function of moment magnitude (**M**), using a hinged-quadratic function that is borrowed from empirical GMPEs for California (e.g. Boore et al., 2014):

$$F_M = \begin{cases} e_0 + e_1(\mathbf{M} - \mathbf{M}_\mathrm{h}) + e_2(\mathbf{M} - \mathbf{M}_\mathrm{h})^2 & \mathbf{M} \le \mathbf{M}_\mathrm{h} \\ e_0 + e_3(\mathbf{M} - \mathbf{M}_\mathrm{h}) & \mathbf{M} > \mathbf{M}_\mathrm{h} \end{cases} \quad (3.3)$$

, where the hinge magnitude, $\mathbf{M}_\mathrm{h}$, and model coefficients, e_0 to e_3, are frequency-dependent coefficients. The value of these coefficients, as determined from the simulations performed by Yenier and Atkinson (2015b), are given in Table A.1 (Appendix A) for the ShakeMap parameters. The stress adjustment term is defined as:

$$F_{\Delta\sigma} = e_{\Delta\sigma}\ln(\Delta\sigma/100), \quad (3.4)$$

where $e_{\Delta\sigma}$ describes the rate of the ground-motion scaling with $\Delta\sigma$. Equation (3.4) describes the relationship between stress parameter and response spectral amplitudes, facilitating the determination of $\Delta\sigma$ from PSA observations, once **M** has been estimated. The values of $e_{\Delta\sigma}$ as determined from the simulations have a variability in magnitude and frequency that is rather complicated, and the shape of the function differs depending on whether one is upscaling or downscaling the stress parameter. Yenier and Atkinson (2015b) found that the shape was best described by a polynomial:

$$e_{\Delta\sigma} = \begin{cases} s_0 + s_1\mathrm{M} + s_2\mathrm{M}^2 + s_3\mathrm{M}^3 + s_4\mathrm{M}^4 & \Delta\sigma \leq 100 \text{ bar} \\ s_5 + s_6\mathrm{M} + s_7\mathrm{M}^2 + s_8\mathrm{M}^3 + s_9\mathrm{M}^4 & \Delta\sigma > 100 \text{ bar} \end{cases} \quad (3.5)$$

, where s_0 to s_9 are frequency-dependent coefficients, reproduced from Yenier and Atkinson (2015b) in Table A.2 (Appendix A) for the ShakeMap parameters.

Geometrical spreading effects are modeled using an equivalent point-source distance metric:

$$R = \sqrt{{D_{rup}}^2 + h^2}\ , \quad (3.6)$$

where D_{rup} is the closest distance from the site to the fault-rupture surface and h is a pseudo-depth term that accounts for distance saturation effects. The pseudo-depth term is adopted from inversion results for active regions (Yenier and Atkinson, 2015a), for which there are sufficient data to constrain such effects:

$$h = 10^{\,-0.405\,+\,0.235\mathrm{M}}, \quad (3.7)$$

For small to moderate events we may assume that D_{rup} is equivalent to the hypocentral distance (D_{hypo}). The geometrical spreading function (F_Z) is:

$$F_Z = \ln(Z) + (b_3 + b_4\mathrm{M})\ln\left(R/R_{ref}\right), \quad (3.8)$$

where Z represents the geometrical attenuation of Fourier amplitudes, while the multiplicative component, (b_3 + b_4**M**) ln(R/R_{ref}), accounts for the change in the apparent

attenuation that occurs when ground motions are modeled in the response spectral domain rather than the Fourier domain. The frequency-dependent coefficients b_3 and b_4 are given in Table A.1 (adopted from Yenier and Atkinson, 2015a). R_{ref} is the reference effective distance, given as $R_{ref} = \sqrt{1 + h^2}$. Z is a hinged bilinear model that provides for a transition from direct-wave spreading to surface-wave spreading of reflected and refracted waves:

$$Z = \begin{cases} R^{b_1} & R \leq R_t \\ {R_t}^{b_1}(R/R_t)^{b_2} & R > R_t \end{cases} \quad (3.9)$$

, where R_t represents the transition distance (=50 km), and b_1 (=-1.3) and b_2 (=-0.5) are the geometrical attenuation rates of Fourier amplitudes at $R \leq R_t$ and $R > R_t$, respectively.

The anelastic attenuation function (F_γ) is given as:

$$F_\gamma = \gamma D_{rup}, \quad (3.10)$$

where γ is a frequency-dependent anelastic attenuation coefficient, whose value is given for CENA and for California in Table A.3. These coefficient values were determined in two previous studies (Yenier and Atkinson, 2015a,b) by inversion of the Next Generation Attenuation-East (NGA-East), and the Next Generation Attenuation-West 2 (NGA-West 2) databases, respectively (see Section 3.6). Note that for our example application for southern Ontario, described in the next section, we refine the anelastic attenuation (as well as the calibration constant, C) to better represent the observed attenuation rates in our specific region of interest. This is a key attribute of the overall methodology behind our generic GMPE development philosophy: most of the magnitude and distance scaling terms are fixed by previous detailed simulation studies, while a select few parameters – specifically the anelastic attenuation and calibration constant – are fine-tuned for the region of interest. In other words, we calibrate a well-behaved and validated generic model for a specific region of interest; the calibration can be accomplished using limited data on amplitude levels and attenuation.

The site effects (F_S) are given relative to a reference site condition, such as NEHRP (National Earthquake Hazards Reduction Program) B/C boundary site condition (travel-time weighted average shear-wave velocity over the top 30 m, V_{S30} , =760m/s). A number of approaches could be used to determine F_S at each site. The simplest of such approaches is to assume that the site response is negligible on the vertical component. In this case, we could use the vertical-component motions as a proxy for the unamplified horizontal-component motions, and assume that $F_S = 0$. Another alternative is to use a standard empirical site response model, such as that of Boore et al. (2014), to estimate F_S based on the V_{S30} value of the site. The approach used in this study, which uses regression to determine site terms directly from the observations, is described in the next section.

We can readily re-arrange the terms of the generic GMPE as described in the foregoing to solve for the values of **M** and $\Delta\sigma$ that best describe the ground-motion observations of an individual event. Note that we require knowledge of the event location so that the distance to each station can be estimated. The procedure to calculate the event-specific values of **M** and $\Delta\sigma$ is as follows:

1) For each observation, subtract the estimated or assumed site response term from the recorded ShakeMap ground-motion parameters to obtain the equivalent values that would be recorded on the reference site condition.

2) Use 1 Hz PSA data to obtain an estimate of **M** from each station, and take the average value over all stations. For events of **M** $\leq$ 4, 1 Hz amplitudes are not sensitive to $\Delta\sigma$, and thus a regional $\Delta\sigma$ value can be used to estimate **M** for most earthquakes that occur in the region. We use Equation (3.1) for 1 Hz PSA to find an estimate of **M** for each station. For larger magnitude events (**M** > 4) one should use 0.33 Hz PSA, because 1 Hz PSA becomes sensitive to $\Delta\sigma$ (Note: 1Hz is preferred for smaller events due to noise considerations).

3) Using the estimated average value of **M**, calculate the stress parameter ($\Delta\sigma$) from the high-frequency ShakeMap parameters. We calculate $\Delta\sigma$ for each recording and find the average $\Delta\sigma$ over all stations that recorded the event (using a geometric mean). The

preferred ShakeMap parameters for this purpose are 10 Hz PSA and PGA, as discussed in the next section.

4) At this point, we have a reasonable estimate of the event-specific value of **M** and $\Delta\sigma$. If refinement is desired, we could iterate steps 2 and 3, using the estimated value of $\Delta\sigma$ to refine the estimate of **M** (step 2), then recalculating $\Delta\sigma$ (Step 3). This should not be necessary for events of $\mathbf{M} \leq 5$.

The event-specific GMPE is completely defined for the event by substituting the applicable values of **M** and $\Delta\sigma$ into the generic form for the region; it can then be used to compute the response spectrum of the event at any distance for the reference site condition. This is useful in estimating the ground motions at sites of interest across the region for ShakeMap and related applications, and in preliminary interpretations of the event's source parameters. The use of the event-specific GMPE ensures that the predictions are calibrated to match the observations from that event on average. Moreover, the ground motions are readily understandable in terms of a simple and widely-used seismological model. In the next step we discuss the applicability of this approach for the southern Ontario seismic network (SOSN).

3.3 Application to southern Ontario

The Southern Ontario Seismic Network (SOSN) is operated by the University of Western Ontario (Department of Earth Sciences) for Ontario Power Generation and Bruce Power, providing rapid ground-motion information at the sites of Ontario's nuclear power facilities (SOSN, 2015). The SOSN is a real-time network that currently comprises 25 broad-band three component seismic stations; it has been in operation since 1991 (Mereu et al., 2002).

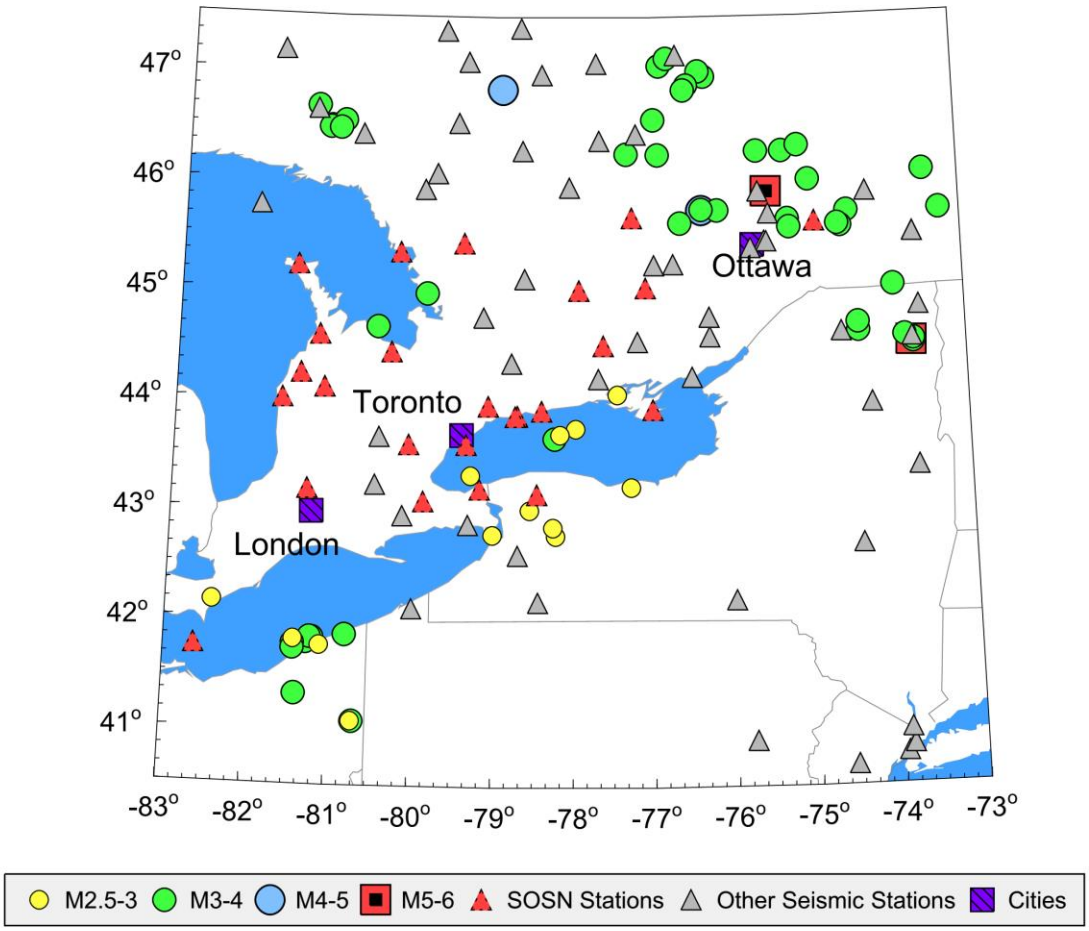

Figure 3.2: Geographic distribution of study events and stations.

The database of this study is extracted from a larger set of data developed by Hassani and Atkinson (2015) for CENA (see Section 3.6) and is shown in Figure 3.2. In summary, the processing of the waveforms involved baseline correction, windowing, tapering, digital filtering, removing instrumental response, and obtaining response spectra and Fourier spectra at defined frequencies band, as described by Assatourians and Atkinson (2010). We retain data only for those frequencies with a signal-to-noise ratio greater than 2. We use only events having moment magnitude (**M**) greater than 2.5 that were recorded on at least three stations with $D_{rup} \leq 600$ km; we use only those stations that recorded at least three such events. The final database consists of 1205 horizontal ground-motion parameter sets (PGA, PGV and PSA at 0.1 to 20 Hz) from 62 events and 84 stations (including the 25 SOSN and other regional stations). We use rotation-angle-independent

geometric average of horizontal ground-motion amplitudes (RotD50) (Boore, 2010) from the data that we retained from the NGA-East database, and the geometric mean of the two horizontal components for rest of the data that we used (see Section 3.6). Figure 3.3 shows the magnitude-distance distribution of the database, color-coded for different NEHRP site classes. Note that the largest event in the southern Ontario database has **M**5.1, and we have few observations at close distances (≤ 50 km). Therefore, for the SOSN database we can assume that the rupture distance (D_{rup}) is equivalent to the hypocentral distance (D_{hypo}).

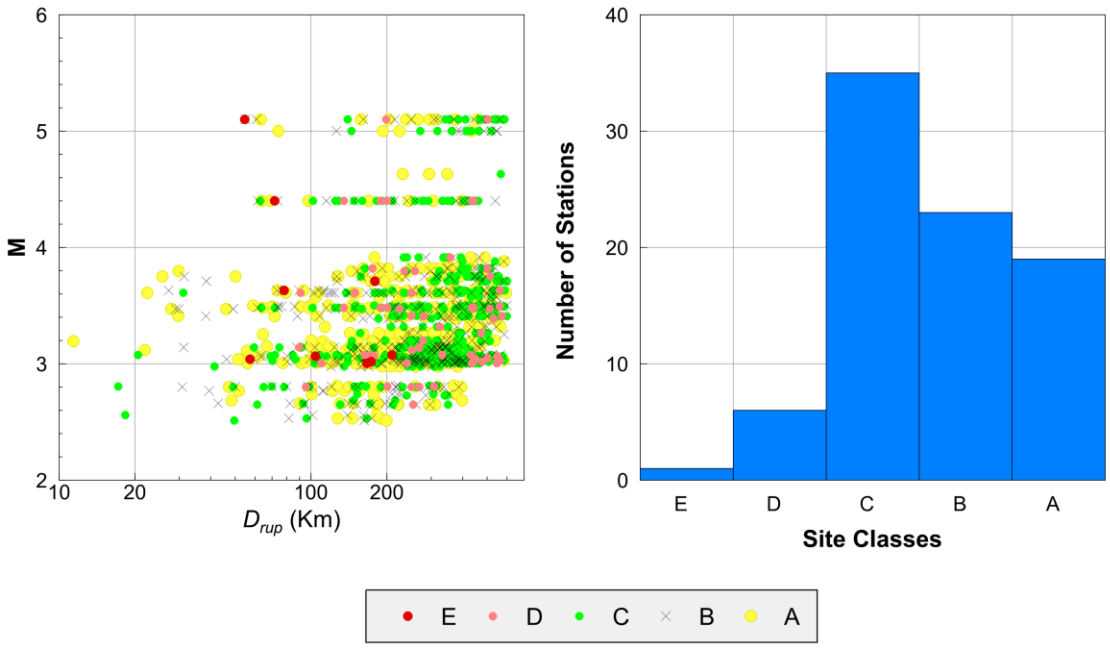

Figure 3.3: Left: Magnitude-distance distribution of the database, by NEHRP site class; Right: Histogram of number of stations in each site class.

In the formulation of the generic GMPE, the source function ($F_E = F_M + F_{\Delta\sigma}$) and the geometrical spreading function (F_Z) are obtained from the simulated ground-motion parameters of the reference model developed by Yenier and Atkinson (2015a) using the NGA-West 2 database (Bozorgnia et al., 2014). We assume that the magnitude scaling function in the study region is the same as that in the reference model. This assumption is consistent with the body of evidence that general scaling characteristics of ground motions are consistent across regions (e.g. Douglas, 2004; Atkinson and Morrison, 2009).

We also assume that the geometrical spreading function is the same as the reference model. This geometrical spreading function, which is a bilinear model with rate of attenuation of b_1=-1.3 at close distances (R < 50 km), is consistent with regional attenuation models proposed for CENA (e.g. Atkinson, 2004; Atkinson and Boore, 2014). After removing the assumed magnitude scaling and geometrical spreading functions from the observed ground-motion parameters, we can rewrite Equation (3.1) as:

$$\ln Y_{ij} - F_{M,i} - F_{Z,ij} = E_i + \gamma_{SOSN} D_{rup,ij} + F_{S,j} \tag{3.11}$$

where Y_{ij} represents the observed horizontal ground-motion parameter for event i and station j. $F_{M,i}$ and $F_{Z,ij}$ are the magnitude scaling function (Equation 3.3) calculated for the known **M** and $D_{rup,ij}$. The E_i term is the event term, which includes both stress parameter adjustment factor ($F_{\Delta\sigma}$, Equation 3.4) and the regional calibration factor (C). γ_{SOSN} and $F_{S,j}$ are the regional anelastic attenuation and site amplification relative to the reference site condition (B/C site condition) for station j, respectively.

We solve Equation (3.11) for the unknown terms (γ_{SOSN}, $F_{S,j}$ and E_i) using the generalized inversion scheme proposed by (Andrews, 1986) for PGV, PGA, and PSA at 17 equally log-spaced frequencies in the frequency range of 0.5 to 20 Hz. Note that we don't use PSA at frequencies lower than 0.5 Hz, because of the very few reliable observations at lower frequencies for small-to-moderate events.

To remove the trade-off between the source and the site terms, we need to assume a reference site condition with known site amplification. Here we assume that the reference site condition is the hard-rock site condition that is typical of seismograph sites in eastern Canada (Atkinson, 2004); this corresponds to hard-rock sites with V_{S30} ~ 2000 m/s. We note that this differs from the reference site condition for the simulation-based model of Yenier and Atkinson (2015a) for a broader region covering all of CENA, which was the B/C site condition (V_{S30} ~ 760 m/s). In total we have 17 hard-rock reference stations in the southern Ontario database. We constrain the inversion by specifying that the average site amplification at each frequency, averaged over the 17 reference sites, equals zero (in

ln units). Therefore, the GMPE model will be calibrated for an average site condition of hard rock, and the remaining site terms will be relative to the hard rock site condition.

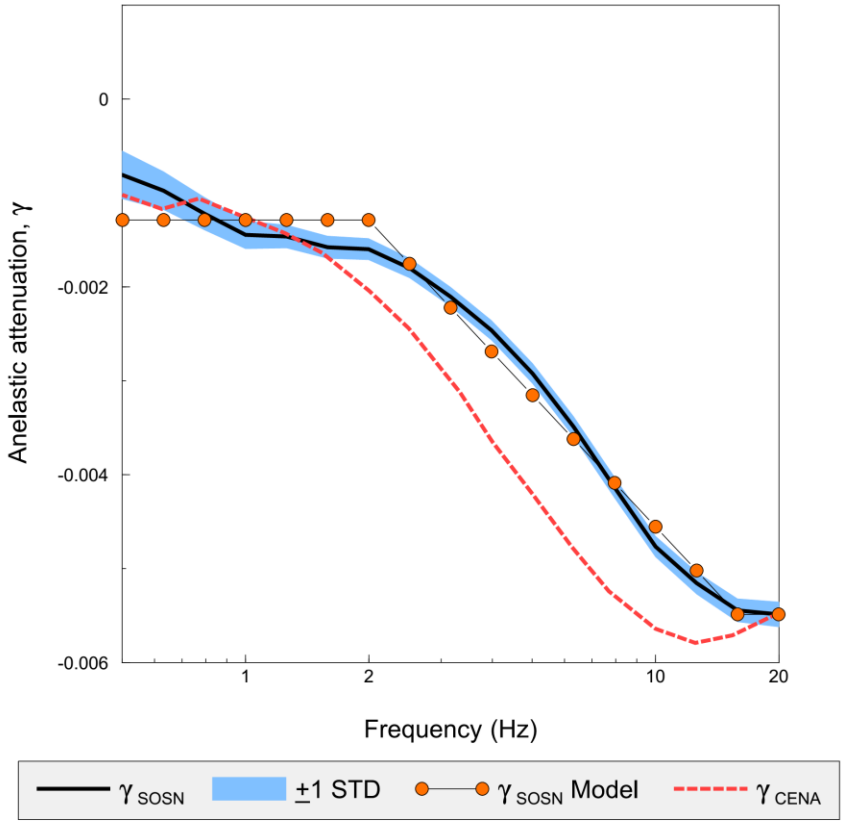

Figure 3.4: Anelastic attenuation (γ) for southern Ontario and its standard deviation (thick black line with shading). Solid line with circles shows the proposed anelastic attenuation model for southern Ontario (Equation 3.12); dashed line represents the anelastic attenuation for CENA (Yenier and Atkinson, 2015b).

The first output of the inversion is the regional anelastic attenuation term (γ_{SOSN}) which is shown in Figure 3.4 and tabulated for the ShakeMap parameters in Table 3.1. It can be modeled as a trilinear function:

$$\gamma_{SOSN} = \begin{cases} -0.0013 & f \leq 2.0\ Hz \\ -0.002 \times \ln(f) + 0.0001 & 2.0 < f \leq 15.8\ Hz \\ -0.0055 & f > 15.8\ Hz \end{cases} \quad (3.12)$$

. The anelastic attenuation in southern Ontario is slower than that obtained for CENA as a whole (Yenier and Atkinson, 2015b). This result is consistent with other regional attenuation model developed for the this area (e.g. Atkinson 2004; Atkinson and Boore 2014).

Table 3.1: Anelastic attenuation, calibration factor, and variability parameters for ShakeMap parameters, obtained from southern Ontario database. The stated value of C_{SOSN} gives ln Y in cm/s for PGV, in g for PGA and PSA. Note that conversion from units of g to cm/s^2 can be made by subtracting 6.888 ln units from the value of C_{SOSN}.

Frequency (Hz)	γ_{SOSN}	C_{SOSN} (ln units)	σ (ln units)	τ (ln units)	φ (ln units)
PGV	-0.0029	-0.74	0.51	0.38	0.35
PGA	-0.0049	-0.38	0.58	0.42	0.40
0.33 Hz	-0.0013	-0.25	0.52	0.34	0.39
1.00 Hz	-0.0013	-0.77	0.50	0.34	0.37
03.33 Hz	-0.0023	-0.98	0.50	0.38	0.32
10.00 Hz	-0.0046	-0.60	0.57	0.45	0.34

The second output of the generalized inversion is the site amplification term ($F_{S,j}$) relative to the assumed reference site condition (V_{S30} ~ 2000 m/s) for each of the individual stations (84 sites). The determined site amplifications can be used in the first step of **M** and $\Delta\sigma$ estimation to remove the site effects and level all of the records to the same reference site condition. Here we only use the site amplifications for the SOSN stations (25 stations), as given in Table 3.2 for the selected ShakeMap parameters. It should be noted that three of the SOSN sites are borehole stations, namely BASO, BWLO and BMRO, and three of the stations are considered as reference sites (hard rock), which are DELO, KLBO and PLVO. We note that although we have used an inversion to find the site terms in this study, another alternative is to specify the site terms based on some combination of geological and seismological information (e.g. Braganza et al., 2015).

Table 3.2: Site amplification term (F_S) for SOSN stations for selected ShakeMap parameters.

				Site Amplification (ln units)					
Station	**Lat˚**	**Long˚**	**V_{S30} (m/s)**	**PGV**	**PGA**	**0.33 Hz**	**1.0 Hz**	**3.33 Hz**	**10 Hz**
ACTO	44.51	-73.70	966	0.79	0.87	0.56	0.53	0.82	1.19
ALFO	47.01	-76.36	1000	-0.30	-0.30	-0.11	-0.33	-0.12	-0.53
BANO	46.96	-76.29	1000	0.70	1.01	0.18	0.07	0.08	0.91
BASO	46.88	-76.52	500	0.18	-0.24	0.23	0.22	0.51	-0.34
BMRO	46.26	-77.31	500	-0.13	-0.62	0.44	0.44	0.12	-0.79
BRCO	46.96	-76.29	311.5	1.33	1.03	0.99	1.02	1.31	1.11
BUKO	42.79	-79.00	1000	0.06	0.19	0.12	0.13	-0.03	0.29
BWLO	46.88	-76.52	500	-0.05	-0.36	0.24	0.39	0.07	-0.40
CLWO	46.01	-74.95	500	1.05	1.29	0.70	1.04	1.33	0.63
DELO	46.96	-76.29	2000	-0.09	-0.06	0.16	0.02	0.03	-0.12
DRCO	41.09	-80.68	500	0.44	0.81	0.66	0.28	0.18	1.21
DRWO	43.71	-78.17	500	1.39	1.33	0.94	0.98	1.67	1.43
ELFO	43.33	-79.28	451	1.18	1.16	0.95	0.81	1.58	1.26
KLBO	47.01	-76.36	2000	-0.16	-0.22	-0.04	0.24	-0.12	-0.13
MEDO	42.79	-79.00	500	0.37	0.83	0.59	0.22	0.18	0.06
PECO	46.96	-76.29	1000	0.01	0.00	-0.16	0.07	0.07	0.00
PEMO	44.62	-74.37	591	0.41	1.05	-0.02	-0.08	0.18	0.21
PKRO	44.51	-73.70	403	1.34	0.95	0.96	1.22	1.41	1.23
PLIO	41.84	-81.19	2000	-0.14	0.13	-0.01	-0.16	-0.38	-0.03
PLVO	42.79	-79.00	2000	0.08	0.47	-0.07	-0.07	-0.06	0.06
STCO	44.51	-73.70	415	0.97	0.72	0.38	0.41	1.35	0.84
TOBO	47.01	-76.36	1000	0.05	0.31	0.51	0.26	0.05	-0.30
TORO	43.67	-78.23	303	1.15	1.15	1.53	2.70	1.07	1.08
TYNO	44.51	-73.70	404	1.22	0.96	0.65	0.58	1.67	1.19
WLVO	44.51	-73.70	1137	0.30	0.53	-0.01	0.04	0.10	0.44

The last output of the inversion is the source term for each of the individual events (E_i). The E_i term includes both the event-specific stress adjustment factor and the regional calibration factor. A common approach to determine the stress parameter from the E_i term is to match the amplitudes at high frequencies for the known moment magnitude. However, this approach leads to a non-unique $\Delta\sigma$ value due to the trade-off between earthquake source and geometric spreading rate (Boore et al., 2010; Yenier and Atkinson, 2014). Moreover, the resulting $\Delta\sigma$ has little effect at low frequencies and thus cannot properly calibrate the response spectral amplitudes at low frequencies (Yenier and Atkinson, 2015a,b). A preferred approach, which breaks the trade-off between $\Delta\sigma$ and geometric spreading, is to find the $\Delta\sigma$ value that matches the shape of the response spectrum for the known moment (Yenier and Atkinson, 2015a, b). This approach is equivalent to finding the corner frequency of the observed spectrum, and ensures that the calibrated model is consistent over a wide frequency range. In this study, we match the shape of the source term over the frequency range from 2 to 20 Hz (using higher frequencies to avoid low-frequency noise effects).

We generalize the resulting values as a stress parameter model ($\Delta\sigma_{SOSN}$), in which the stress parameter shows an increasing trend with depth (d) and magnitude (**M**):

$$\ln\Delta\sigma_{SOSN} = 6.10 + \min[0,0.37(d - 7.5)] + \min[0,1.12(\boldsymbol{M} - 3.5)] \qquad (3.13)$$

. We caution that this model is simply a convenient way to summarize the average trends seen in the stress parameters of the study events, as shown in Figures 3.5 and 3.6. An overall misfit between empirical and predicted spectral shapes maps into the stress parameter as the cube of the misfit due to the relationship between corner frequency and stress. This results in a large scatter of determined $\Delta\sigma$ values. Therefore, we do not attribute a high level of significance to the coefficients. On average, the stress parameter shows an increasing trend with focal depth, up to d = 7.5 km, and after that it remains relatively constant (≈ 300 bars), as shown in Figure 3.5. Figure 3.6 shows the estimated $\Delta\sigma$ values as a function of moment magnitude (**M**), along with the stress model for d = 5 and 10 km. Up to **M**3.5, an increasing trend is observed for the mean estimated stress parameter, while for **M** > 3.5 the stress appears to be relatively constant (≈ 450 bar).

These results are consistent with those of Yenier and Atkinson (2015b) for CENA. Figure 3.7 shows the residuals of the stress model as a function of depth and magnitude. The overall behavior of the residuals is satisfactory and the mean residuals attain values around zero; as noted previously, however, the stress model should be viewed with caution given the sparse data and the scatter of values.

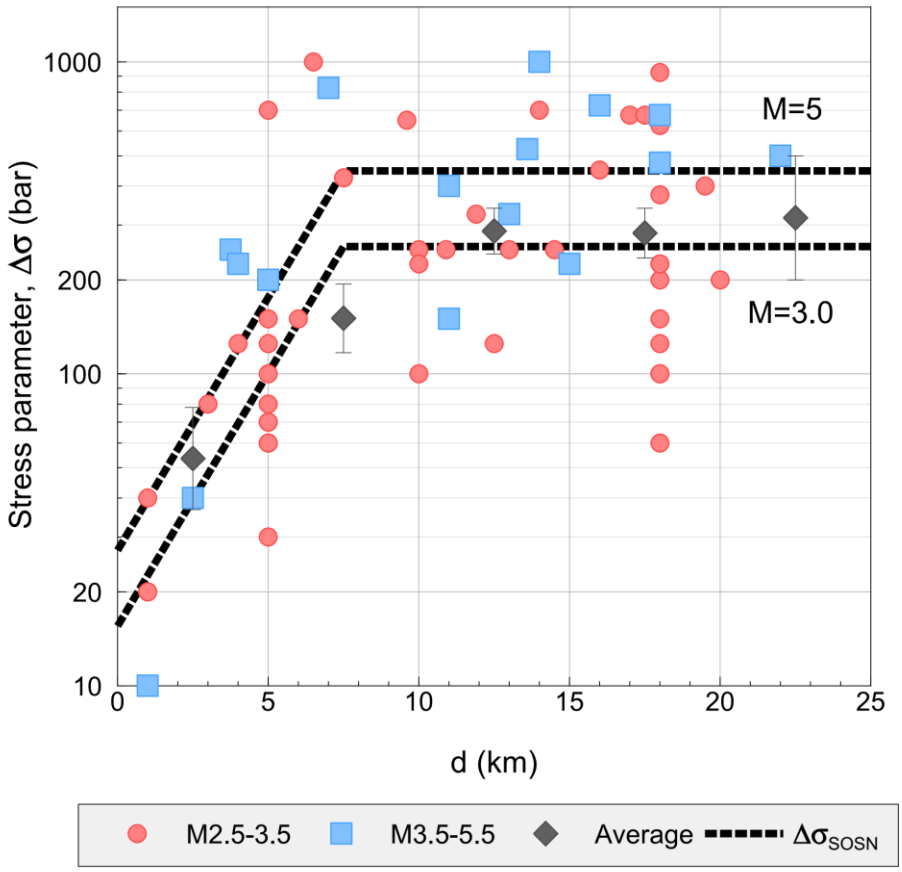

Figure 3.5: Event-specific stress parameters ($\Delta\sigma$) determined for southern Ontario events shown as function of depth (d), classified for different magnitude bins. Diamonds show the average stress parameters at equally-spaced distance bins and their corresponding standard errors. Dashed lines show the proposed stress parameter model ($\Delta\sigma_{SOSN}$; Equation 3.13) for M3 and M5.

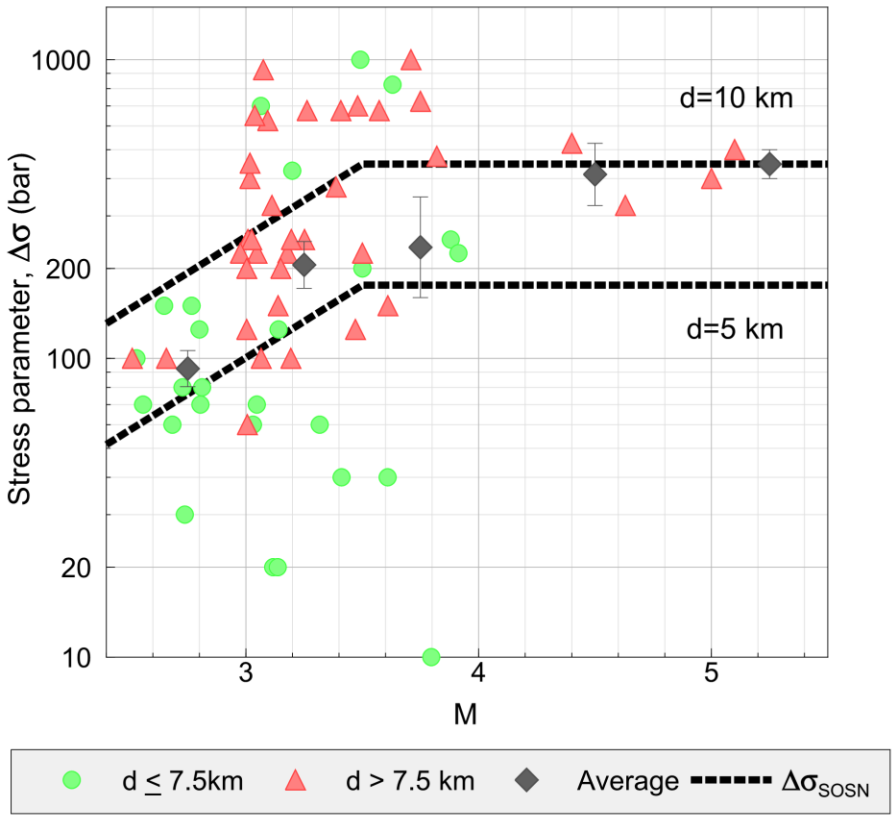

Figure 3.6: Event-specific stress parameters ($\Delta\sigma$) determined for southern Ontario events shown as function of magnitude (M), classified for different depth bins. Diamonds show the average of stress parameters in equally-spaced magnitude bins and their corresponding standard errors. Dashed lines shows the proposed stress parameter model ($\Delta\sigma_{SOSN}$ Model; Equation 3.13) for d = 5 and 10 km.

After removing the stress parameter adjustment factor ($F_{\Delta\sigma}$) using the proposed stress model ($\Delta\sigma_{SOSN}$), we can determine the regional calibration factor (C). The calibration factor compensates for the average difference between the observed ground-motion parameters and the simulated amplitudes. This difference can be attributed to a combination of factors not included in the simplified version of reality that is captured by the simulations (Yenier and Atkinson, 2015a). By removing the estimated terms form Equation (3.11) we have:

$$\ln Y_{ij} - \left(F_{M,i} + F_{Z,ij}\right) - F_{\Delta\sigma,\,SOSN} - \gamma_{SOSN} D_{rup,ij} - F_{S,j} = C_{SOSN} + \eta_i + \varepsilon_{ij}, \qquad (3.14)$$

where C_{SOSN} is the regional calibration factor, η_i is the between-event error, and ε_{ij} is the within-event error. Here, we use a mixed effects regression of residuals according to Abrahamson and Youngs (1992) to solve this equation. We perform an iterative regression to maximize the likelihood of the model (Equation 3 in Abrahamson and Youngs, 1992) and estimate the regional calibration factor (C_{SOSN}), as well as the residual error of the observations with respect to the model, partitioned into its between-event and within-event components (η_i and ε_{ij}).

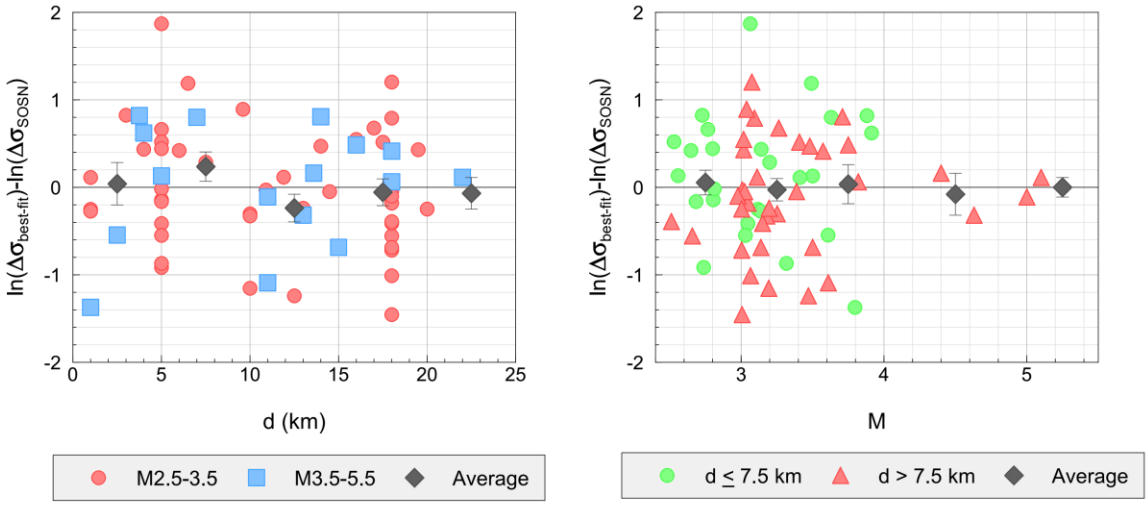

Figure 3.7: Residuals between the event-specific $\Delta\sigma$ values for southern Ontario events and the estimates of the proposed regional $\Delta\sigma_{SOSN}$ model (Equation 3.13) as a function of depth (left) and magnitude (right). Diamonds show the average of residuals in equally-spaced bins.

The regional calibration factor is tabulated in Table 3.1 for the ShakeMap parameters and also shown in Figure 3.8. The C_{SOSN} obtains almost a constant value at high frequencies (> 7.8 Hz), and shows an increasing trend at decreasing frequencies (< 2 Hz). The increasing trend observed at low frequencies may be due to inherent limitations of stochastic methods at low frequencies; specifically, stochastic methods do not model surface wave phases or coherent pulses well. The calibration factor can be modeled as a quadratic function constrained at low and high frequencies:

$$C_{SOSN} = \begin{cases} -0.25 & f \le 0.5\ Hz \\ +0.31\ [\ln(f)]^2 - 0.55\ \ln(\mathrm{f})\ - 0.77 & 0.5\ Hz < f \le 7.8\ Hz \\ -0.6 & f > 7.8\ Hz \end{cases} \quad (3.15)$$

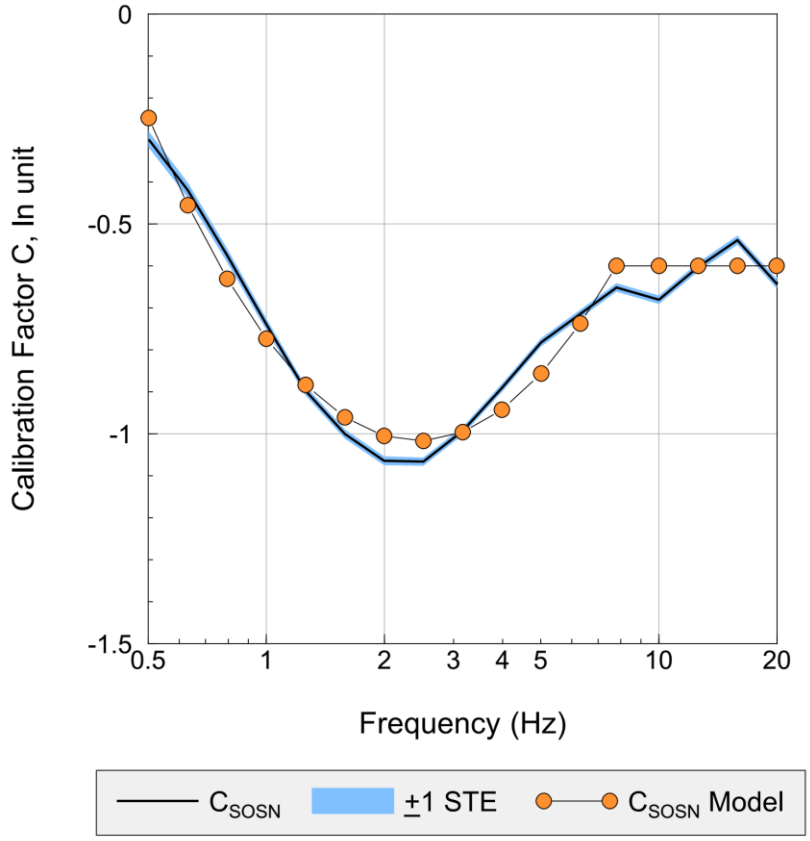

Figure 3.8: Calibration factor obtained for southern Ontario database (solid line; shading shows standard error). Solid line with circles shows the proposed calibration factor model.

. The error terms (η_i and ε_{ij}) are normally distributed (in ln units) and have standard deviations τ and φ, respectively. Thus the total standard deviation (σ) of Equation (3.14) can be written as:

$$\sigma = \sqrt{\tau^2 + \varphi^2}, \quad (3.16)$$

The value of σ is in the range of 0.50 to 0.58 ln units (see Table 3.1), which is smaller than values found in other studies (e.g. Hassani and Atkinson, 2015). This could be due to a variety of factors, such as use of a regionally-confined database (southern Ontario database) instead of using a much broader region like CENA. Another important factor is the way that we define site amplifications for the study sites. Here we obtain site amplifications relative to the assumed reference site condition (V_{S30} ~ 2000 m/s) by inverting the observed data, instead of by assuming V_{s30}-based empirical amplification function derived from studies in other regions (e.g. Boore et al., 2014). Atkinson (2013) obtained relatively low ground-motion variability when considering a tightly-constrained CENA database using only recorded ground motions on hard rock sites in Charlevoix seismic zone. This again suggests that we are able to reduce a large portion of GMPE uncertainties by using a regionally-constrained database, as well as using the records from the same site condition, or leveling them to the same reference site condition using an appropriate site amplification model for the region.

In Figure 3.9, the between-event residuals η are plotted as function of focal depth (d). The overall behavior of the residuals at all frequencies is satisfactory. The residuals do not show any apparent magnitude dependency. However, at 0.5 Hz for small magnitude events ($\mathbf{M} \leq 3.5$) there is a tendency to higher average residuals for shallow events, and also a tendency to lower average residuals for deeper events. This may be due to the fact that we have very few observations at 0.5 Hz for small magnitude events, which limits our ability to distinguish any magnitude or depth dependency. For ShakeMap applications, we note that we effectively compensate for the between-event term error by adjusting the main source parameters ($\mathbf{M}$ and $\Delta\sigma$) to match the observed ShakeMap parameters.

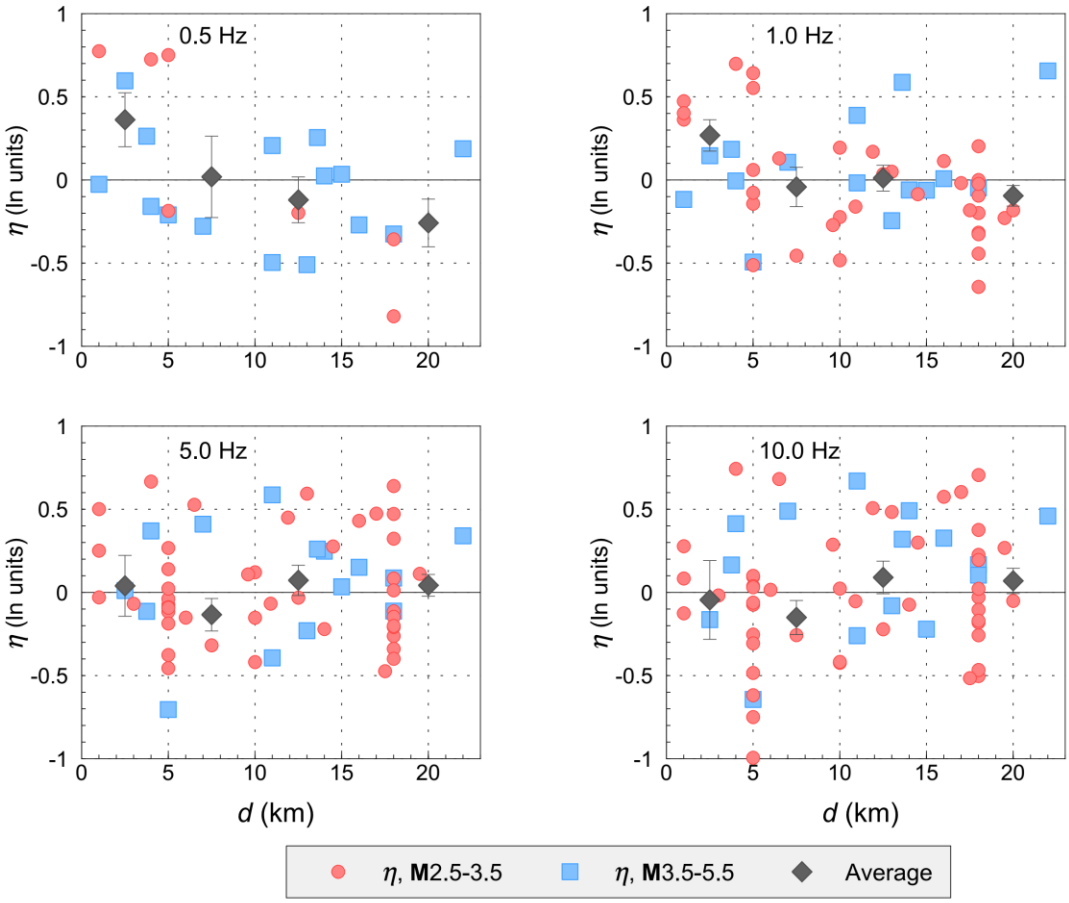

Figure 3.9: Between-event residuals (η) as a function of depth (d), for different magnitude ranges. Diamonds show the average residuals at equally-spaced depth bins and their standard errors.

Figure 3.10 shows the within-event residuals as function of distance. The residuals do not show any apparent distance or magnitude dependency, and the average residual values attain a zero value at all distance bins. This implies that the assumed geometrical spreading model and the estimated regional anelastic attenuation model work well in matching the observed ground-motion data. The only exception is at near distances (D_{rup} < 30 km) where the model overpredicts the sparse amplitude data on average by ~ 0.1 ln unit (about 10%).

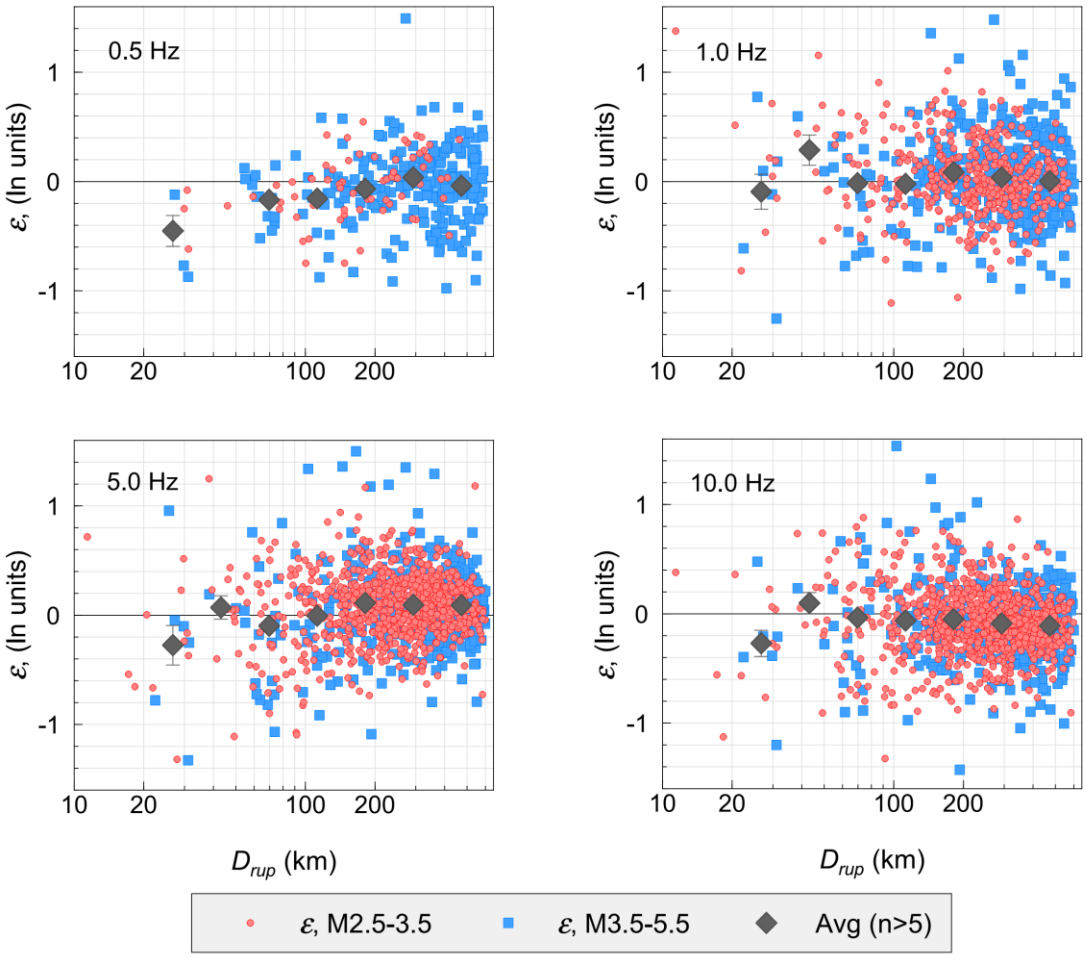

Figure 3.10: Within-event residuals (ε) as a function of distance, classified for different magnitude bins. Diamonds show the average residuals at equally log-spaced distance bins and their standard errors.

In Figure 3.11, the within-event residuals are plotted as a function of V_{S30} to investigate how well the site amplification effects have been removed. The average of the within-event residuals attains a near-zero value for all NEHRP site classes. This suggest that we are able to successfully remove the site effects and level the observed data to the assumed reference site condition (V_{S30} ~ 2000 m/s).

The final SOSN GMPE model can be written as:

$$\ln(Y) = F_M + F_Z + F_{\Delta\sigma,\,SOSN} + \gamma_{SOSN} D_{rup} + F_S + C_{SOSN}, \tag{3.17}$$

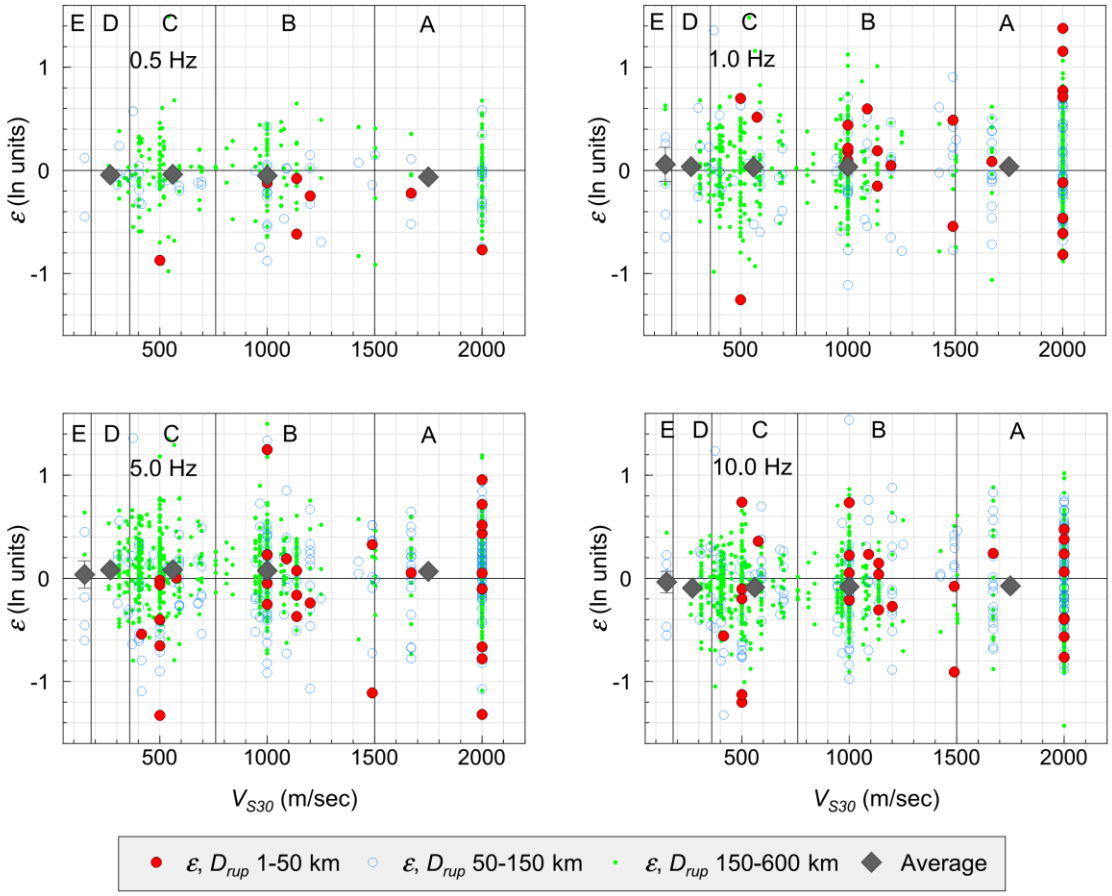

Figure 3.11: Within-event residuals (ε) as a function of V_{S30}, classified in distance bins. Diamonds show the average residuals at NEHRP site classes and their standard errors.

which includes the assumed magnitude scaling and geometrical spreading functions, and the derived models for the stress parameter, anelastic attenuation, site amplification, and calibration factor (respectively). Equation (3.17) can be used to predict median amplitudes of PGV (cm/s), PGA (g) and 5%-damped PSA (g) in southern Ontario, using the coefficient values in Tables A1 and A2, and in Table 3.1. Note that adjustment of PGA and PSA to units of cm/s^2 can be made by adjusting the constant, C_{SOSN} (see Table 3.1). In Figure 3.12, we show how the generic SOSN GMPE model (no event-specific parameters) compares with observed southern Ontario ground motions for events in three magnitude ranges (**M**3.3-3.7; 4.3-4.7; and 5.0-5.2). The observed data are all leveled to the reference site condition (V_{S30}~2000 m/s) by removing the site amplifications as

derived from Equation (3.11). We also plot the equivalent GMPEs of Yenier and Atkinson (2015b; noted as YA15) for CENA, corrected to the same site condition. The proposed SOSN GMPE model matches the observed regional data at all distances and magnitude bins, as would be expected. It shows similar ground-motion amplitudes as the YA15 model. This is consistent with previous studies which showed similarity of the observed ground-motion amplitudes between the central United States and southeastern Canada (e.g. Hassani and Atkinson, 2015). One noted difference is that the SOSN GMPE model predicts larger ground-motion amplitudes at distances $D_{rup} \geq 200$ km at high frequencies $f \geq 5$ Hz. This is due the slower anelastic attenuation obtained for southern Ontario in comparison with the YA15 model, which is more apparent at higher frequencies. Another notable difference is that the SOSN GMPE model predicts larger amplitudes at low frequencies (0.5 Hz). This reflects an observational difference that comes from calibration to the SOSN database, which is suggesting relatively higher amplitudes at lower frequencies, possibly due to surface wave effects in the region. However, we note that the sparse observational data at low frequencies ($f \leq 0.5$ Hz) hinder any robust conclusion.

Figure 3.13 shows the comparison between the SOSN and YA15 GMPE models, for southern Ontario and CENA, respectively, for **M**5 and **M**7.5 for the hard rock site condition ($V_{S30} \sim 2000$ m/s), to investigate how the models scale ground motions for larger magnitude events. The comparison between the SOSN GMPE and the YA15 models shows the same features seen in Figure 3.12, as the magnitude scaling (F_M) and geometrical spreading (F_Z) functions are the same in both models. The slower anelastic attenuation in southern Ontario results in larger ground-motion amplitudes at regional distances ($D_{rup} \geq 200$ km), which is more apparent at high frequencies ($f \geq 5$ Hz). At low frequencies (0.5 Hz) we observe a significant difference between the predictions of the models as noted above.

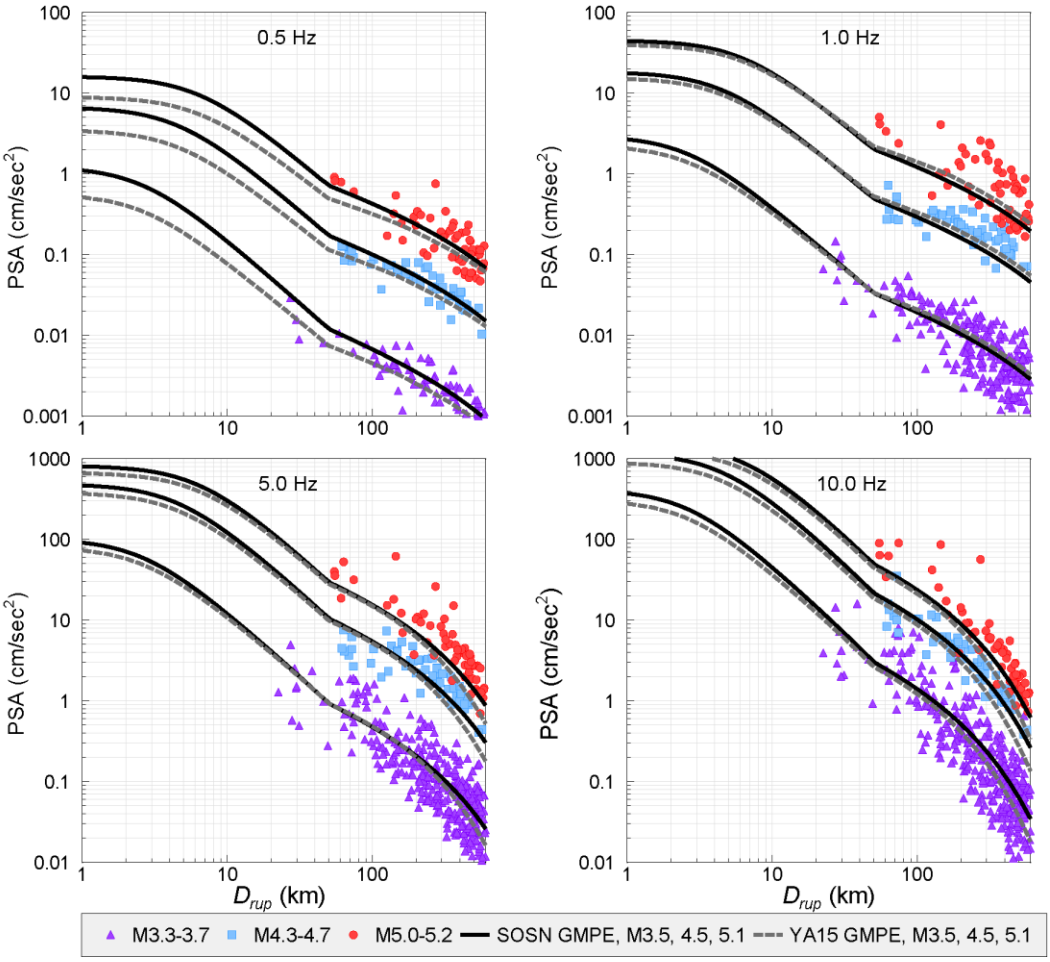

Figure 3.12: Proposed SOSN GMPE model for M3.5 (±0.2), 4.5(±0.2) and 5.1(±0.1) for hard rock site condition (V_{S30} ≈ 2000 m/s) compared with the southern Ontario observed data leveled to the assumed reference site condition. YA15 GMPE model (Yenier and Atkinson, 2015b) for the same site condition is also shown.

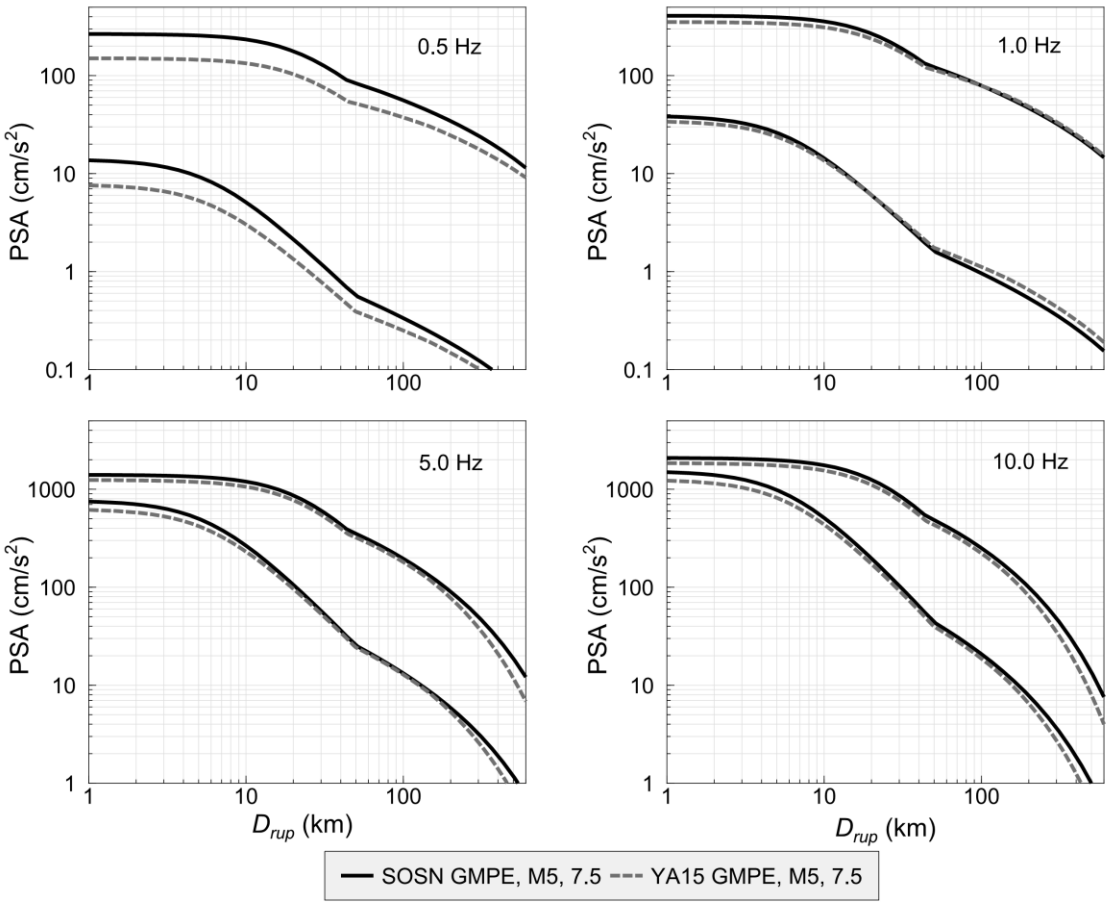

Figure 3.13: Comparison between SOSN and YA15 (Yenier and Atkinson, 2015b) GMPE models for M5 and 7.5 for hard rock site condition ($V_{S30} \approx$ 2000 m/s).

3.4 Real-time M and Δσ estimation for SOSN network

In this section, we use the regionally-adjusted SOSN GMPE (Equation 3.17) and the selected ShakeMap parameters to develop a simplified procedure for real-time moment magnitude and stress parameter estimation, and event-specific GMPE calibration. We make use of the GMPE given by Equation (3.17), but as described further below we re-arrange its form to facilitate robust determination of source parameters in real time. The rationale is that Equation (3.17) describes a forward model for ground motion, given magnitude and stress, whereas we seek to determine those source parameters from the recorded ground motions, and do so in a way that is quick and easily automated. We use the ShakeMap parameters from SOSN stations as these are the only stations accessible in

real-time. We consider events with at least three observed records on the SOSN seismic network at $D_{rup} \leq 600$ km, which includes 37 events.

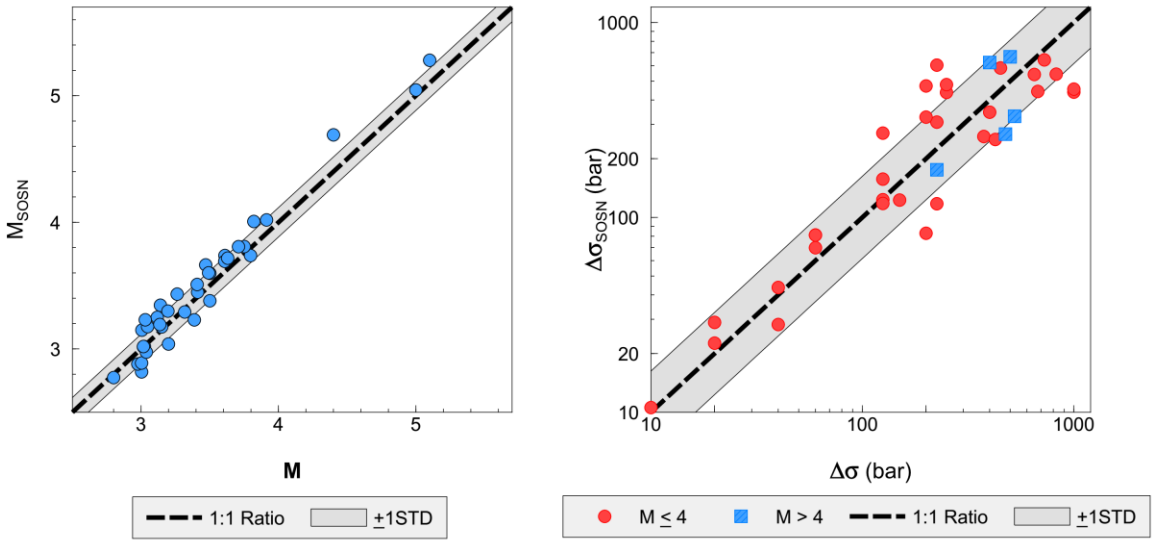

Figure 3.14: Left: Comparison between M and its estimated value from SOSN (M_{SOSN}) using low-frequency ShakeMap parameters. Right: Comparison between the shape-based estimate of stress parameter ($\Delta\sigma$) and the estimate using high-frequency ShakeMap parameters ($\Delta\sigma_{SOSN}$). Dashed line shows 1:1 ratio, and shaded area shows standard deviation.

We first remove the site effects from the observed SOSN ShakeMap parameters, and level the observed data to the reference site condition (V_{S30} ~ 2000 m/s), using the derived terms for SOSN stations as provided in Table 3.2. Note that in this study we only consider linear site effects because our motions are predominantly too weak to invoke non-linear response. If this approach were to be used for larger magnitude events (**M** > 6) for near-source soft soil stations, an empirical nonlinear site effects function could be implemented to remove nonlinear site effects (e.g. Boore et al. 2014)

For each event, we use PSA_{1Hz} observations (in cm/s^2 units) to estimate **M**. Because we want to determine both **M** and $\Delta\sigma$ from the ground motions in real-time, we seek to simplify the parameterization that we derived more rigorously in Equation (3.17). For the purposes of estimating **M,** we note that 1-Hz PSA should scale approximately as:

$$\ln(PSA_{1Hz}) = C_1\boldsymbol{M} + C_2 \ln(R) + C_3 D_{rup} + C_4, \quad (3.18)$$

This is the simplest of all GMPE forms that can be used to characterize observed spectral amplitudes across a broad range of distances (e.g. Atkinson, 2013). The form is particularly convenient because it can be rapidly and easily inverted. To linearize the source term of our generic GMPE ($F_E = F_M + F_Z$), we use Equations (3.2) to (3.4) to calculate F_E for magnitude values from 2.5 to 6 in 0.1 unit increments, assuming a value of $\Delta\sigma$ = 450 bars, which is the average regional stress parameter value for **M** >3.5 and d = 10 km (an assumed nominal focal depth). Recall that PSA at 1 Hz is not sensitive to stress, so the use of an average value for this calculation is sufficient. The slope of the calculated values of F_E versus **M** can be mapped into the C_1 term of Equation (3.18), while the intercept maps into the C_4 term. We fix the pseudo-depth at 0 so that $R \sim D_{rup} \sim D_{hypo}$; this assumption is also not critical because most observations are at regional distances. C_2 can be calculated from the distance-dependent part of the geometrical spreading function (Equation 3.8 and 3.9). Note that the magnitude-dependent part of the geometrical spreading function, which is also a function of distance, is mapped into C_1, while its constant portion is mapped into C_4. C_3 is the anelastic attenuation coefficient. The constant, C_4, includes the contributions noted above, plus the regional calibration factor from Equation (3.15). It is easy to verify that the simplified equation that we have derived provides a reasonable approximation to the values given by Equation (3.17) for PSA_{1Hz} for **M**3.5 to 6, for distances from 0 to 600 km. In summary, Equation (3.18) provides a convenient approximation to the GMPE model for 1-Hz amplitudes that simplifies **M** estimation: C_1 is a linearized magnitude scaling coefficient, C_2 is a simplified geometrical spreading coefficient, C_3 is the anelastic attenuation coefficient and C_4 is the constant of the equation (for PSA in cm/s^2). The coefficient values are given in Table 3.3 for 1 Hz and 0.33 Hz (in case we want to use 0.33 Hz data to estimate **M** for **M** > 4, as described further below).

We can readily invert Equation (3.18) to find **M** for each recorded value of PSA_{1Hz}:

$$\boldsymbol{M} = (\ln(PSA_{1Hz}) - C_2 \ln(R) - C_3 D_{rup} - C_4)/C_1, \quad (3.19)$$

We take the average value of **M** over all SOSN stations. Based on the study events, the typical standard deviation of the estimation of **M** for an event (station-to-station variability) is 0.1 magnitude units. We caution that if the average estimate of **M** is larger than 4, PSA at 0.33 Hz will provide a more accurate estimate of **M**, because motions at 1 Hz become sensitive to $\Delta\sigma$ as magnitude increases. The 0.33 Hz PSA remains insensitive to $\Delta\sigma$ effects at least for $\mathbf{M} \leq 6$. Therefore, if the **M** obtained from PSA_{1Hz} is larger than 4, we switch to PSA at 0.33 Hz and recalculate **M**. Having made an initial estimate of **M**, we can adjust the pseudo-depth (h), effective distance (R) and rupture distance (D_{rup}) values and recalculate **M** to refine its value slightly. (Note: If this approach is to be used for large magnitude events ($\mathbf{M} > 6$), we suggest not to linearize the source term, as the combination of the F_M and $F_{\Delta\sigma}$ terms gets more complicated. In this case, it would be better to implement a grid search to find **M** and $\Delta\sigma$ from PSA at 0.33 Hz using tabulated ground-motion prediction values).

Table 3.3: Coefficients of Equation (3.18) for 1 Hz and 0.33 Hz PSA, in units of cm/s^2.

Data range	C_1	C_2	C_3	C_4
1.00 Hz, R ≤ 50 km	2.50+0.03$ln(R)$	-1.60	-0.0013	-6.6
1.00 Hz, R > 50 km	2.50+0.03$ln(R)$	-0.80	-0.0013	-9.73
0.33 Hz, R ≤ 50 Km	2.38+0.07$ln(R)$	-1.81	-0.0013	-7.87
0.33 Hz, R > 50 km	2.38+0.07$ln(R)$	-1.01	-0.0013	-11.00

Figure 3.14 compares the estimated magnitude using the proposed procedure ($\mathbf{M}_{SOSN}$) with known values of **M**, as extracted from the southern Ontario database (see Section 3.6). It is acknowledged that for smaller events there is considerable overlap in the information used to determine the values of **M**, so they are not considered as independent estimates but rather as a check on the simplified procedure. The average of residuals between $\mathbf{M}_{SOSN}$ and **M** attains a near zero value with standard deviation of 0.1. This suggests that we are able to use low frequency ShakeMap parameters (1 Hz PSA for $\mathbf{M} \leq 4$ and 0.33 Hz PSA for $\mathbf{M} > 4$) as described in the foregoing to successfully estimate **M**, with a standard error of 0.1 units relative to other equivalent measures.

After finding **M**, we now wish to invert Equation (3.17) to estimate $\Delta\sigma$ using the high-frequency ShakeMap parameters. The preferred high-frequency ShakeMap parameter is 10 Hz PSA, although we could use PGA if the 10 Hz PSA values are not available. We rewrite Equation (3.17), for PSA_{10Hz},as:

$$F_{\Delta\sigma} = \ln(PSA_{10Hz}) - F_M - F_Z - \gamma_{SOSN} D_{rup} - C_{SOSN}\text{-}6.888, \quad (3.20)$$

where PSA_{10Hz} is the 10 Hz PSA in cm/s^2 (note subtraction of 6.888 ln units for conversion to cm/s^2). F_M and F_Z are the magnitude scaling and geometrical spreading functions, which can be easily calculated from Equations (3.3) and (3.8) respectively. γ_{SOSN} and C_{SOSN} are the regional anelastic attenuation and calibration factors, obtained from Table 3.1. By recalling from Equation (3.4) that $F_{\Delta\sigma} = e_{\Delta\sigma}\ln(\Delta\sigma/100)$, we can rewrite Equation (3.20) as:

$$\ln(\Delta\sigma) = (\ln(PSA_{10Hz}) - F_M - F_Z - \gamma_{SOSN} D_{rup} - C_{SOSN} - 6.888)/e_{\Delta\sigma} + \ln(100), \quad (3.21)$$

where $e_{\Delta\sigma}$ is calculated from **M** using Equation (3.5), knowing that for $\Delta\sigma$> 100 bars, $F_{\Delta\sigma}$ is positive, while for $\Delta\sigma \leq 100$ bars $F_{\Delta\sigma}$ is negative. Note that Equation (3.20) and (3.21) could also be written for PGA. We find $\Delta\sigma$ for each of the SOSN stations and confine the estimated value to $10 \leq \Delta\sigma \leq 1000$ bar to be consistent with the original format of the generic GMPE approach (Yenier and Atkinson 2015b). The average $\Delta\sigma$ value is obtained by taking the geomean of the $\Delta\sigma$ values from all SOSN stations.

Figure 3.14 compares the estimated stress parameter ($\Delta\sigma_{SOSN}$) using the high frequency ShakeMap parameters with the shape-based stress parameter obtained from the source terms of Equation (3.11). For this comparison, we used PGA for $\mathbf{M} \leq 4$ and 10 Hz PSA for $\mathbf{M} > 4$. The average of the residuals between $\Delta\sigma_{SOSN}$ and $\Delta\sigma$ attains a near-zero value with a standard deviation of 0.49 ln units. It confirms that we are able to use high frequency ShakeMap parameters to successfully estimate stress parameter, though there is significant scatter introduced by using a single ground-motion variable instead of the entire spectral shape.

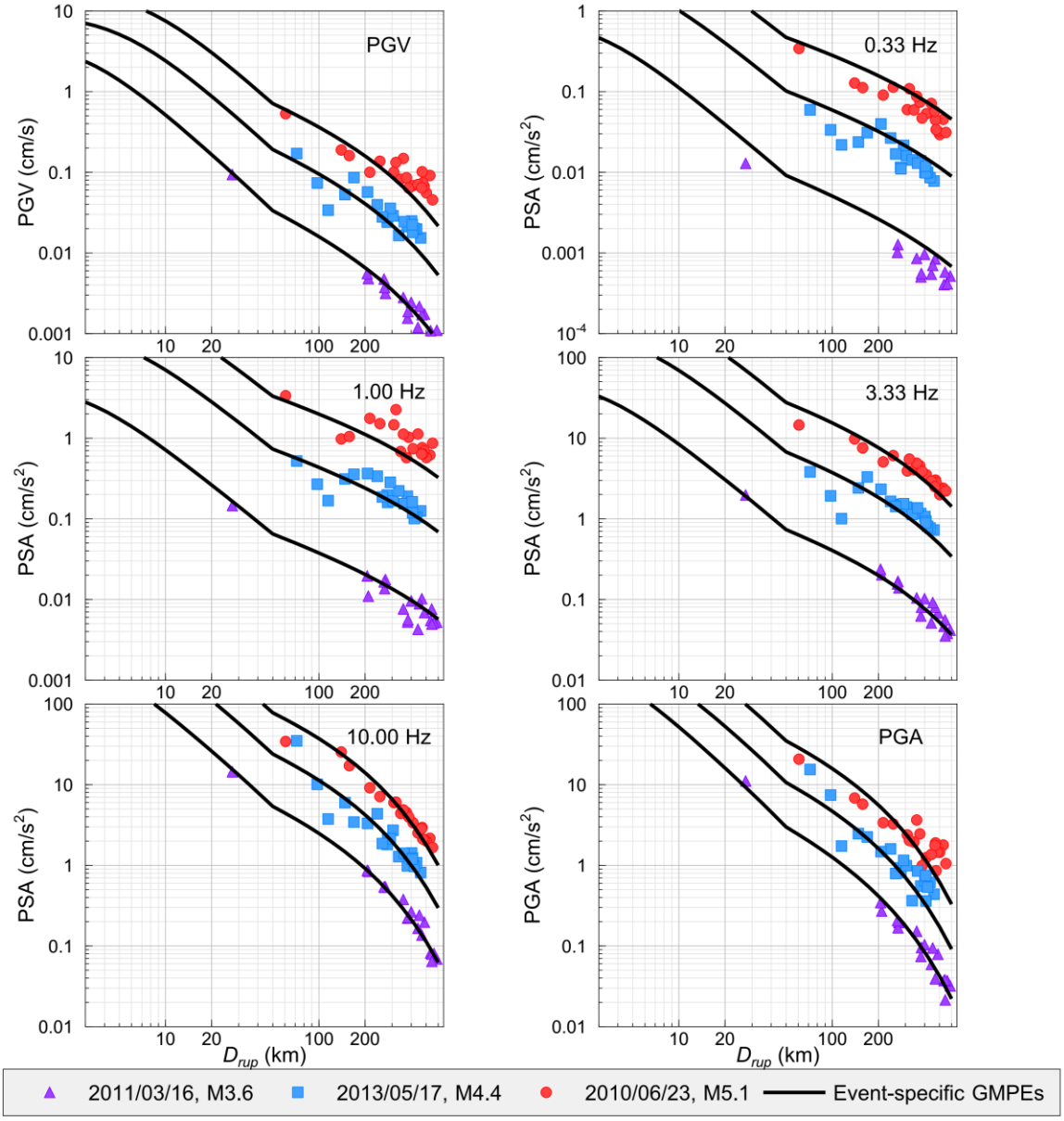

Figure 3.15: Comparison between the event-specific SOSN GMPEs and observed SOSN ShakeMap parameters adjusted for the reference site condition ($V_{S30} \approx 2000$ m/s) for three different events.

Using the estimated **M** (M_{SOSN}) and $\Delta\sigma$ ($\Delta\sigma_{SOSN}$) values, we can rapidly define event-specific GMPEs which are fully compatible with the observed data. This is done by using $\mathbf{M}_{SOSN}$ and $\Delta\sigma_{SOSN}$ in Equation (3.17), along with the regionally-adjusted attenuation and calibration factor. The resulting event-specific GMPE is developed for the reference site condition, and can be used with a regional site amplification map to produce real-time

ShakeMaps. In Figure 3.15, we display the performance of the event-specific GMPEs against the observed SOSN data for selected events: the 2010/06/23 Val-des-Bois **M**5.1, the 2011/03/16 **M**3.6, and the 2013/05/17 **M**4.4 earthquakes. The observed data are all adjusted to the equivalent amplitudes for the reference site condition (V_{S30} ~ 2000 m/s). The event-specific GMPEs closely follow the observed data at all distances for all ShakeMap parameters.

3.5 Conclusion

We can make reliable estimates of **M** and $\Delta\sigma$ in near-real-time using commonly-available ShakeMap parameters. These two source parameters are the essential input to an equivalent point-source stochastic model that can be optimized for the attenuation and site response attributes of a region of interest, allowing rapid event-specific GMPEs to be defined. The SOSN seismic network is used to show the application of this approach. In summary, we first used the southern Ontario database to derive a regionally-adjusted GMPE model, by deriving regional stress parameter, anelastic attenuation, calibration factor, and site amplification models from the observed data. This model can be used to define event-specific GMPEs in near-real-time by using the event estimates of **M** and $\Delta\sigma$. This same approach could readily be used for other seismic networks in different seismotectonic regions. It is particularly useful for applications where ShakeMaps are desired for small-to-moderate events in sparsely-instrumented regions.

3.6 Data and Resources

The ground-motion database of this study was extracted from the larger database used by Hassani and Atkinson (2015) for CENA. In summary, they utilized data from three different sources. The processed ground-motion parameters (PGA, PGV and PSA) were obtained either from the NGA-East database, which provides 5%-damped RotD50 response of horizontal ground motions (www.peer.berkeley.edu, last accessed October 2014), or were extracted from the Engineering Seismology Toolbox website which provides 3-component processed ground-motion parameters (www.seismotoolbox.ca, last accessed December 2013). Additional unprocessed data were obtained from the Automatic Data Request Manager Facility (AutoDRM of the Geological Survey of

Canada (autodrm@seismo.nrcan.gc.ca, last contacted December 2013). For unprocessed data of U.S. stations, including data from the U.S Transportable Array (TA) stations in southern Ontario, horizontal velocity waveforms were obtained from the IRIS AutoDRM (breq_fast@iris.washington.edu, last contacted December 2013). V_{S30} and moment magnitude information was also extracted from the database of Hassani and Atkinson (2015). We used MATLAB (www.mathworks.com, last accessed January 2015) for regression of the ground-motion amplitudes and CoPlot (www.cohort.com, last accessed January 2015) for making the figures. Information on the SOSN is available at www.gp.uwo.ca (last accessed January 2015). Time history simulations were made using the SMSIM program of Boore (2005).

3.7 Acknowledgments

This study was funded by the Natural Sciences and Engineering Research Council of Canada and by Ontario Power Generation. We thank Adrien Oth and an anonymous reviewer for valuable suggestions which improved the clarity of the manuscript.

3.8 References

Abrahamson, N. A., and R. R. Youngs. 1992. A stable algorithm for regression analysis using the random effects model, *Bull. Seismol. Soc. Am.* **82**, 505–510.

Anderson, J. G., and S. E. Hough. 1984. A model for the shape of the Fourier amplitude spectrum of acceleration at high frequencies, *Bull. Seismol. Soc. Am.* **74**, 1969–1993.

Andrews, D. J. 1986. Objective determination of source parameters and similarity of earthquakes of different size, *Earthq. source Mech.* :259–267.

Assatourians, K., and G. Atkinson. 2010. Database of processed time series and response spectra data for Canada: An example application to study of 2005 MN 5.4 Riviere du Loup, Quebec, earthquake, *Seismol. Res. Lett.* **81**, 1013–1031.

Atkinson, G. 2013. Empirical evaluation of aleatory and epistemic uncertainty in eastern ground motions, *Seismol. Res. Lett.* **84**, 130–138.

Atkinson, G. M. 2004. Empirical attenuation of ground-motion spectral amplitudes in southeastern Canada and the northeastern United States,. *Bull. Seismol. Soc. Am.* **94**, 1079–1095.

Atkinson, G. M., and D. M. Boore. 2014. The attenuation of Fourier amplitudes for rock sites in eastern North America, *Bull. Seismol. Soc. Am.* **104**, 513–528.

Atkinson, G. M., and M. Morrison. 2009. Observations on regional variability in ground-motion amplitudes for small-to-moderate earthquakes in North America, *Bull. Seismol. Soc. Am.* **99**, 2393–2409.

Boore, D. M. 2010. Orientation-independent, nongeometric-mean measures of seismic intensity from two horizontal components of motion, *Bull. Seismol. Soc. Am.* **100**, 1830–1835.

Boore, D. M. 2003. Simulation of ground motion using the stochastic method, *Pure Appl. Geophys.* **160**, 635–676.

Boore, D. M. 2005. SMSIMFortran programs for simulating ground motions from earthquakes: version 2.3. A revision of OFR 96--80-A, *US Geol. Surv. open-file Rep.*

Boore, D. M., K. W. Campbell, and G. M. Atkinson (2010). Determination of stress parameters for eight well-recorded earthquakes in eastern North America, *Bull. Seismol. Soc. Am.* **100**, 1632–1645.

Boore, D. M., J. P. Stewart, E. Seyhan, and G. M. Atkinson. 2014. NGA-West2 equations for predicting PGA, PGV, and 5% damped PSA for shallow crustal earthquakes, *Earthq. Spectra*. **30**, 1057–1085.

Bozorgnia, Y., N. A. Abrahamson, L. Al Atik, T. D. Ancheta, G. M. Atkinson, J. W. Baker, A. Baltay, et al. 2014. NGA-West2 research project, *Earthq. Spectra*. **30**, 973–987.

Braganza, S., H. Ghofrai and G.M Atkinson. A prileminiry model of site amplification for use in ground-motion modeling in southern Ontario. Presented in the AGU and CGU Joint Assembly, Montreal, Canada, May 2015, Abstract.

Brune, J. N. 1971. Correction: Tectonic stress and the spectra of seismic shear waves, *J. Geophys. Res.* **76**, 5002.

Brune, J. N. 1970. Tectonic stress and the spectra of seismic shear waves from earthquakes, *J. Geophys. Res.* **75**, 4997–5009.

Douglas, J. 2004. An investigation of analysis of variance as a tool for exploring regional differences in strong ground motions, *J. Seismol.* **8**, 485–496.

Earle, P. S., D. J. Wald, K. S. Jaiswal, T. I. Allen, M. G. Hearne, K. D. Marano, A. J. Hotovec, and J. M. Fee. 2009. *Prompt Assessment of Global Earthquakes for Response (PAGER): A system for rapidly determining the impact of earthquakes worldwide*, US Geological Survey.

Hassani, B., and G. M. Atkinson. 2015. Referenced Empirical Ground-Motion Model for Eastern North America, *Seismol. Res. Lett.* **86**, 477–491.

Mereu, R. F., H. W. Asmis, B. Dunn, J. Brunet, D. Eaton, S. Dineva, and A. Yapp. 2002. The Seismicity of the Western Lake Ontario Area: Results from the Southern Ontario Seismic Network (SOSN), 1992-2001, *Seismol. Res. Lett.* **73**, 534–551.

Wald, D. J., V. Quitoriano, T. H. Heaton, H. Kanamori, C. W. Scrivner, and C. B. Worden. 1999. TriNet ShakeMaps: Rapid generation of peak ground motion and

intensity maps for earthquakes in southern California. *Earthq. Spectra*. **15**, 537–555.

Yenier, E., and G. M. Atkinson. 2014. Equivalent point-source modeling of moderate- to-large magnitude earthquakes and associated ground-motion saturation effects. *Bull. Seismol. Soc. Am.* **104**, 1458–1478.

Yenier, E., and G. M. Atkinson. 2015a. An Equivalent Point-Source Model for Stochastic Simulation of Earthquake Ground Motions in California. *Bull. Seismol. Soc. Am.* **105**, 1435-1478.

Yenier, E., and G.M. Atkinson 2015b. Regionally adjustable generic ground-motion prediction equation based on equivalent point-source simulations: Application to central and eastern North America, *Bull. Seismol. Soc. Am.* **105,** 1989-2009.

Chapter 4

4 Fundamental Frequency as a descriptive variable for site response in central and eastern North America

In this chapter, we first introduce a new proxy measure for V_{S30} (time-averaged shear-wave velocity in the upper 30 m) for central and eastern North America (CENA). The new proxy is the site fundamental frequency (f_{peak}), measured from the horizontal-to vertical (H/V) spectral ratios of recorded ground motions. We correlate the measuredV_{S30} values at recording stations with the corresponding f_{peak} values to obtain a predictive relationship forV_{S30}. The uncertainty of theV_{S30} estimate using the f_{peak}-based model is small (0.14 $\log_{10}$ units) in comparison to that for the proxy-based methods (e.g., topographic slope and surface geology proxies) used in the Next Generation Attenuation-East (NGA-East) database (0.25 $\log_{10}$ units).

In the next step, we explore the applicability of the Next Generation Attenuation-West2 site-effects model (Seyhan and Stewart, 2014), which is aV_{S30}-based model, to sites in CENA, using the NGA-East ground-motion database. We determine residual site terms by comparing the observed CENA ground-motion amplitudes, adjusted to B/C site condition (V_{S30}= 760m/s) using the western site-effects model, to the corresponding predicted amplitudes of a CENA ground-motion prediction equation for B/C site condition (Yenier and Atkinson, 2015). Plotting the residual site terms versus their corresponding site fundamental frequencies (f_{peak}) reveals significant f_{peak}-dependent trends at all frequencies. Average residual site terms for CENA sites, after the western site amplifications have been removed, can be as large as 0.45 in $\log_{10}$ units (2.8 in nonlog units) around $f \approx f_{peak}$. The results of this study reveals the inadequacy of the western site-effects model to sites in CENA, demonstrate the importance of a well-calibrated regional site-effects model for CENA and the importance of f_{peak} as a site indicator.

4.1 Fundamental frequency as a V_{S30} proxy for central and eastern North America[3]

4.1.1 Introduction

One of the most important issues in developing accurate and useful ground-motion prediction equations (GMPEs) is the effective use of limited regional site information in developing a site effects model. Amplitudes of ground motions can be amplified significantly as they propagate through a soft soil layer (Borcherdt, 1970; Anderson et al., 1986; Shearer and Orcutt, 1987). There are two general approaches that are commonly used for determining site amplification. In the first approach site amplification is determined relative to a reference site condition by comparing ground motions at soil and reference sites. One variation of this method is to assume that the attenuation difference between two nearby soil and reference rock stations at sufficient distance from the source is negligible, and the corresponding spectral ratio would represent the relative soil site amplification (Borcherdt, 1970). Andrews (1986) recast the method into a generalized-inverse (GI) problem by simultaneously solving an equation parameterizing the ground-motion amplitudes for multiply-recorded events in terms of site effect, source term, and attenuation. In both of these approaches site amplification is obtained relative to a reference site condition. However, it is not always feasible to find a suitable reference site.

In the second approach, site amplification does not rely on a reference site. Nakamura (1989) first introduced the horizontal-to-vertical spectral ratio method (H/V) to determine site amplification using ambient noise. The main assumption of this method is that horizontal-component ground motions are amplified around the fundamental frequency of a site, while the vertical-component of ground motion does not experience significant amplification. Therefore, the H/V ratio provides a good estimate of the dominant frequency and corresponding amplification of the site. Although this method was first developed based on microtremor analysis, it was more widely developed and justified for

[3] A version of this section has been published. Hassani, B., and G.M. Atkinson (2016). Applicability of the site fundamental frequency as a V_{S30} proxy for Central and Eastern North America, *Bull. Seismol. Soc. Am.* **106,** 653-664.

strong ground-motion data in subsequent studies (Lermo and Chávez-García, 1993; Bonilla et al., 1997; Ghofrani et al., 2013). Moreover, Kawase et al. (2011), using the diffuse-field concept, showed that the H/V spectral ratio of the observed ground-motion is proportional to the one-dimensional transfer functions of S-wave motions relative to P-wave motions, implying that the H/V ratio may be inverted to obtain a velocity model from the bedrock to the surface.

It is generally accepted that the peak frequency obtained from the H/V method, obtained using either ambient noise or strong-ground-motion data is a robust estimate of the fundamental frequency of a soil layer (Lermo and Chávez-García, 1993; Field and Jacob, 1995; Bonilla et al., 1997; Konno and Ohmachi, 1998; Kawase et al., 2011; Ghofrani et al., 2013); moreover, this value can be closely correlated to alternative site parameters such as time-averaged shear-wave velocity in the upper 30 m (V_{S30}) (e.g. Ghofrani and Atkinson, 2014). However, it is also generally accepted that the H/V method tends to underestimate the amplitude of site amplification (Field and Jacob, 1995; Bonilla et al., 1997). This occurs because the vertical component may also have some amplification at the fundamental frequency, contrary to the underlying assumption of negligible amplification on the vertical component.

In modern empirical GMPE models, site effects are usually characterized by a set of simplified parameters (often only one) that characterize the overall near-surface state. Common site parameters include site fundamental frequency (f_{peak}) (e.g. Zhao et al., 2006b) and V_{S30} (e.g. Boore et al., 2014). V_{S30} is currently the most prevalent site parameter in GMPE models. An example of recent empirical GMPEs which use V_{S30} as the explanatory variable for site effects is the second generation Pacific Earthquake Engineering Research–Next Generation Attenuation-West (PEER–NGA-West2) equations set, which has been developed for shallow crustal earthquakes in active tectonic regions (Bozorgnia et al., 2014). Another example is the NGA GMPE models for central and eastern North America (CENA), developed as part of the NGA-East project (Goulet et al., 2015). In both the NGA-East and NGA-West2 GMPEs, V_{S30} was selected as the main input parameter to model the site effects. However, there is a significant difference between NGA-West2 and NGA-East in the number of measurement-based

V_{S30} values. While in the NGA-West2 database almost 50% of the recording stations have measured V_{S30} values (Seyhan et al., 2014), in the NGA-East database only 6% of the recording stations (84 out of 1379 stations) have measured V_{S30} values (Goulet et al., 2014). Therefore, most of the "preferred" V_{S30} values in the NGA-East database are derived from a weighted average of different proxy-based V_{S30} estimates; these proxies include topographic slope (Wald and Allen, 2007), terrain category (Yong et al., 2012), surface geology (Kottke et al., 2012), hybrid slope-geology (Thompson and Silva, 2013), and P-wave seismogram (Kim et al., 2015) proxies. For the measurement-based V_{S30} values the assumed uncertainty or dispersion (based-10 log standard deviation, σ_{logV}) in the estimation of V_{S30} is small, only 0.04. For the proxy-based V_{S30} values, the assigned uncertainty is derived from a weighted average of different proxies' uncertainty. For the NGA-East database, these values range from 0.20 to 0.25, whereas for the NGA-West2 database the proxies have somewhat lower uncertainty (0.15 to 0.20 $\log_{10}$ units) (Seyhan et al., 2014). The large uncertainty in the estimation of V_{S30} can translate into errors in the assumed site amplification and hence increased ground-motion variability for the NGA-East GMPE models, in comparison to the NGA-West2 models.

In this study, we use the NGA-East database to show that the site fundamental frequency (f_{peak}) is a more accurate V_{S30} proxy than the proxies used in the NGA-East database (e.g. topographic slope and surface geology proxies). We use the H/V spectral ratio approach to determine the fundamental frequencies of the recording stations and develop a relationship between V_{S30} and f_{peak}. The use of f_{peak} as a proxy for site response is particularly effective for sites in CENA, which tend to be characterized by large responses at dominant frequencies, which range from 1 Hz to 10 Hz, depending on the depth of the soil. The use of f_{peak} as a proxy for site response works well because in CENA the depth to bedrock, and hence f_{peak}, is the most diagnostic predictor of the expected site response. The uncertainty of the V_{S30} estimate using the f_{peak}-based model is significantly lower than that for the proxy-based methods used in the NGA-East database. The results of this study can be used to recalculate the V_{S30} values more accurately for stations with known f_{peak} values and potentially reduce the overall variability of the developed NGA-East GMPE models. However, the means of achieving greater variability reductions would be to measure f_{peak} at all recording stations (which could be

done using inexpensive microtremor surveys) and re-parameterize the site response accordingly.

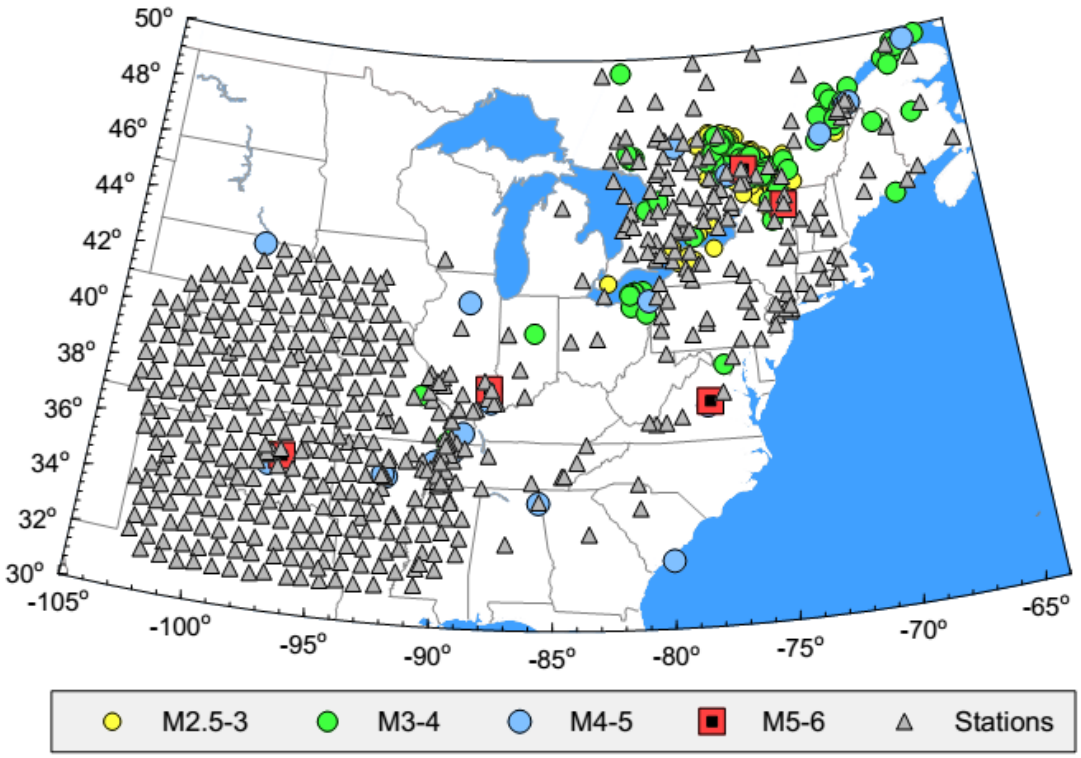

Figure 4.1: Geographic distribution of study events and stations.

4.1.2 Database

Figure 4.1 is a map of recording stations and events used in this study. Most of the ground-motion database was compiled from the NGA-East database, supplemented by some additional data from Ontario (see Section 4.1.7). The database consists of three-component peak ground-motion amplitudes (peak ground acceleration [PGA], peak ground velocity [PGV]) and response spectra (5% damped pseudoacceleration [PSA]) sampled at 28 equally log-spaced frequencies from 0.1 to 50 Hz. Most of the ground-motion data had been already processed as part of the NGA-East project (Goulet et al., 2014). For the remaining data, the processing of the waveforms involved baseline correction, windowing, tapering, digital filtering, removing instrumental response, and obtaining response spectra and Fourier spectra at defined frequencies band, as described by Assatourians and Atkinson (2010). We retain data only for those frequencies with a

signal-to-noise ratio greater than 2. We use records for events having moment magnitude (**M**) greater than 2.5, recorded on stations with hypocentral distance $R_{hypo} \leq 800$ km; we use only those stations that recorded at least three such events. The NGA-East databse includes 1379 stations. The selected database consists of 5783 three-component ground-motion parameter sets (PGA, PGV and PSA) from 225 events and 535 stations. Figure 4.2 shows the magnitude-distance distribution of the database, distinguished by NEHRP (National Earthquake Hazards Reduction Program) site class; it also shows a histogram of the number of stations for each of the NEHRP site classes. Most of the observed data are recordings from small to moderate magnitudes ($2.5 \leq \mathbf{M} \leq 4.5$) at regional distances ($100 \leq R_{hypo} \leq 800$ km).

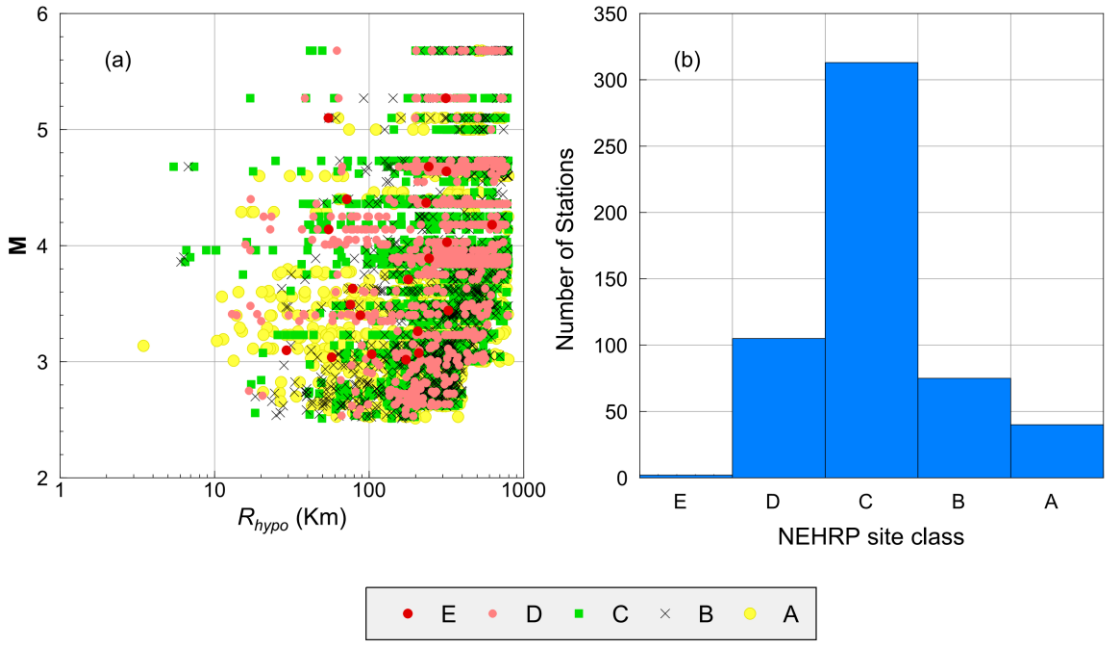

Figure 4.2: (a): Magnitude-distance distribution of the database, by NEHRP site class; (b): histogram of number of stations in each site class.

4.1.3 H/V Spectral ratio calculation

The conventional method for calculating the H/V spectral ratios is to use the Fourier amplitude spectra from S-wave windows. However, as discussed by Zhao et al. (2006a), smoothing the Fourier spectra is an essential part of the H/V calculation, in order to extract the spectral peaks corresponding to site response. An expedient alternative

method to calculate H/V spectral ratios is to use the 5% damped response spectra (PSA). An advantage of using response spectra is that the damping ratio (e.g. 5%) acts as a smoothing function for the input signal and the smoothing effect is the same for all records in the database. Moreover, PSA is more widely available. In this study we use the response spectra to calculate the H/V spectral ratios. We define the H/V spectral ratio as the geometric mean of the response spectra of the two horizontal components divided by the response spectrum of the corresponding vertical component:

$$\log(H/V)_{ij} = 0.5\big(\log(H_1)_{ij} + \log(H_2)_{ij}\big) - \log(V_{ij}), \tag{4.1}$$

where $(H/V)_{ij}$ is the H/V spectrum of event *i* recorded at station *j*, $(H_1)_{ij}$ and $(H_2)_{ij}$ are the response spectra of the two horizontal components, and $(V)_{ij}$ is the response spectrum of the corresponding vertical component. Note that we use base-10 log units throughout. The average H/V spectrum for station *j* is obtained as the geometric mean of the individual H/V spectra of the recorded events at station *j*:

$$\log(\overline{H/V})_{j,f} = \frac{\sum_{i=1}^{n_{j,f}} \log(H/V)_{ij}}{n_{j,f}}, \tag{4.2}$$

where $(\overline{H/V})_{j,f}$ is the average H/V spectrum and $n_{j,f}$ is the number of the recorded events at station *j* at frequency *f*. $(\overline{H/V})_{j,f}$ is calculated in the usable frequency bandwidth of station *j*. The usable frequency bandwidth is defined as a sequence of frequencies in which we have at least three recorded events at all of the data points. We note that the number of data points at each frequency ($n_{j,f}$) may vary. We retain those H/V spectra having usable frequency bandwidth of at least 10 consecutive points (out of 28 equally log-spaced frequencies from 0.1 to 50 Hz). This criterion ensures sufficient bandwidth to determine the site fundamental frequency (f_{peak}).

The procedure that we use to determine the site fundamental frequency in an objective and reproducible way is described in the Appendix. Among 1379 stations of the NGA-East database, only 535 recorded at least three events. For these 535 stations, 286 (54%) show a single significant peak (e.g. station 128A in Figure A.1), 29 (5%) show two

distinct significant peaks (e.g. station P26A), and 220 stations (41%) show no significant peak (e.g. station DMCQ). For stations with two significant peaks, we assume the significant peak with higher amplification is the primary site response peak. Recording stations with no significant peaks can be subclassified into two categories. The first category includes stations on hard rock, which have either a flat or rising H/V curve. The second category includes jagged-shape H/V curves with no clear peaks, usually the result of limited available bandwidth or a small number of recorded events.

4.1.4 Estimating V_{S30} at seismographic stations based on their fundamental frequencies

It has been shown that the frequency corresponding to the peak of the H/V spectral ratio is approximately equivalent to the site fundamental frequency (f_{peak}) (Nakamura, 1989; Kawase et al., 2011; Ghofrani et al., 2013). For a simple one- dimensional single-layer model over a half-space, if we have a soil site with average shear- wave velocity of V_L overlaying a much harder layer with average shear-wave velocity of V_R, the first dominant frequency of the site can be written as (Kramer, 1996):

$$f_{peak} = V_L/4d_L, \tag{4.3}$$

where d_L is the thickness of the soil layer. Assuming $d_L \leq 30m$, V_{S30} can be written as:

$$V_{S30} = 30/(d_L/V_L + d_R/V_R), \tag{4.4}$$

where d_R is the thickness of the hard rock layer (e.g. lying below the soil layer but < 30 m from the ground surface). By replacing d_L/V_L with $1/4f_{peak}$ using Equation (4.3) and replacing d_R with $30 - d_L$ we have:

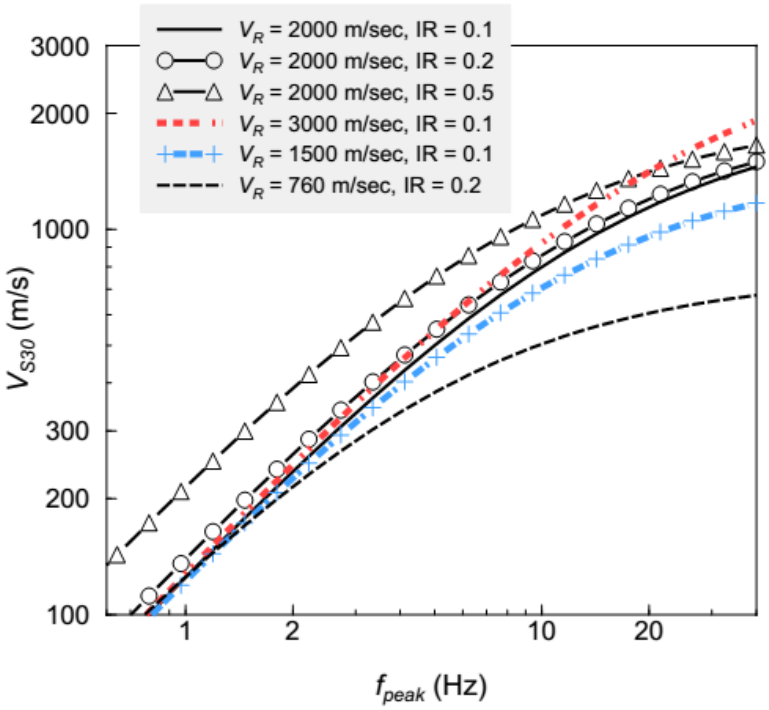

Figure 4.3: Expected relationship between V_{S30} and f_{peak} (Equation 4.5) for different sets of impedance ratio (IR) and V_R (bedrock velocity) values.

$$V_{S30} = \frac{30}{\frac{1}{4f_{peak}}\left(1 - \frac{V_L}{V_R}\right) + \frac{30}{V_R}} \tag{4.5}$$

, where V_L/V_R is approximately the impedance ratio (IR) of the sediment layer over the half-space (assuming the same density for the soil layer and the half-space). Equation (4.5) implies that for sediments shallower than 30 m, the relation between f_{peak} and V_{S30} depends on the impedance ratio and the shear-wave velocity of the half-space. If the impedance ratio is small enough (IR $\leq$ 0.2), it has little effect in Equation (4.5). Consequently, the relation between f_{peak} and V_{S30} is dominated by the shear-wave velocity of the half-space (V_R). Figure 4.3 shows the estimated V_{S30} values as a function of f_{peak} for different impedance ratios and V_R values, based on Equation (4.5). Note that V_{S30} increases with increasing f_{peak}, with shallow sites (high f_{peak}) having high V_{S30} due to the

influence of the underlying bedrock. For lower f_{peak} values ($\leq$ 2 Hz), corresponding to deeper sites, as long as the impedance ratio is small enough ($\leq$ 0.2), all of the different combinations of V_R and IR result in approximately the same V_{S30} estimate.

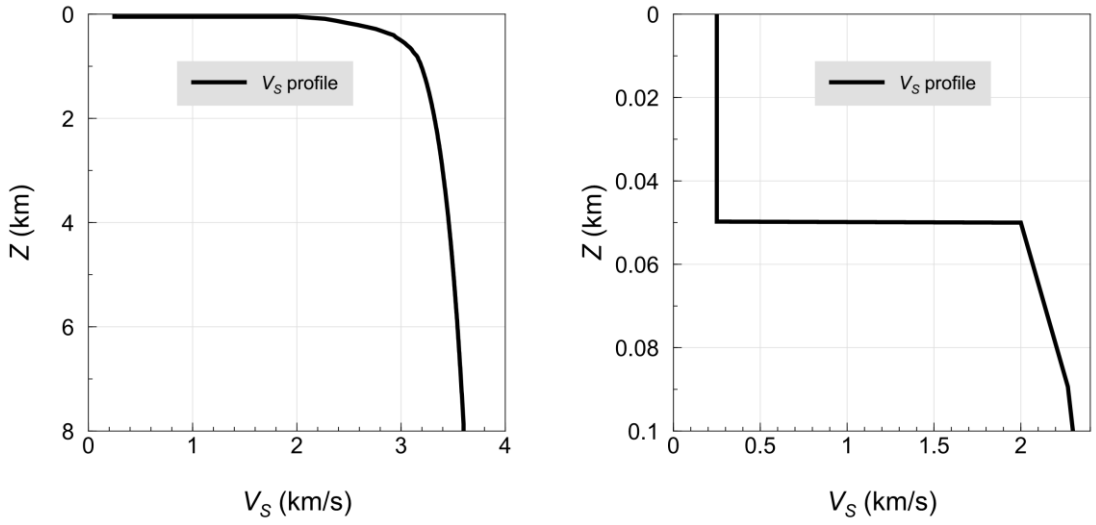

Figure 4.4: Adopted shear-wave velocity (V_S) profile as a function of depth (Z) for a single-layer model with constant velocity of V_L = 250 m/s, thickness of d_L = 50 m, and V_R = 2000 m/s.

In order to consider the relation between f_{peak} and V_{S30} in more detail, we implement the Joyner et al. (1981) square root impedance ratio method (SRI) to estimate the theoretical site amplifications for chosen shear-wave velocity profiles, and determine the corresponding V_{S30} and f_{peak} values. The SRI method is a rapid way to calculate a linear and smooth site amplification using an input shear-wave velocity profile. The assumptions of the method are that the site amplification is not sensitive to details of the shear-wave velocity profile, and that the amplification at a selected frequency is controlled by the shear-wave velocity structure up to a depth which represents $1/4$ of a wavelength (Boore and Joyner, 1997; Boore, 2003; 2013). The selected shear-wave velocity profile represents a soil layer with constant shear-wave velocity of V_L, thickness of d_L, and density of ρ_L, overlying a hard substratum. For the substratum we adopt the CENA shear-wave velocity profile of Frankel et al. (1996) for depths from d_L (with V_R) to 8 km (3600 m/s) and assume $\rho_L = 2.5\ gr/cm^3$. The selected shear-wave velocity profile

for d_L = 50 m, V_L = 250 m/s and V_R = 2000 m/s (the reference model) is shown in Figure 4.4.

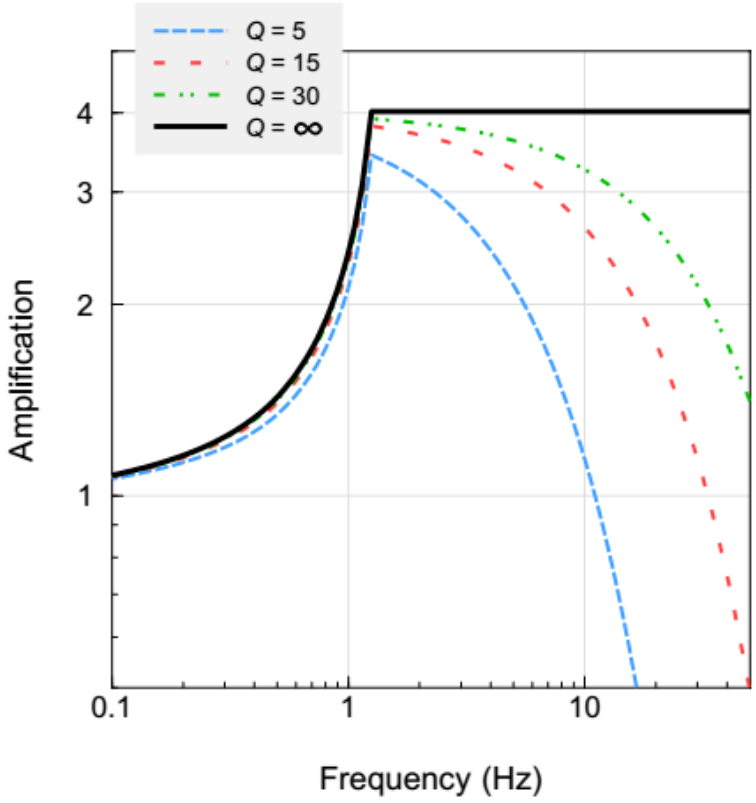

Figure 4.5: Site amplification as a function of frequency for different quality factor (Q) values for the reference shear-wave velocity profile (Figure 4).

The effect of the near surface attenuation can be considered as:

$$\exp(-\pi\kappa_0 f), \tag{4.6}$$

where κ_0 is the near surface diminution term (Anderson and Hough, 1984). Near-surface attenuation effects can also be considered using the surface layer quality factor (Q). The relation between Q and κ_0 can be written as:

$$\kappa_0 = d_L/(V_L\ Q), \tag{4.7}$$

where d_L/V_L corresponds to the one-way travel time of shear-wave in the sediment layer. Figure 4.5 shows the theoretical site amplifications multiplied by the near-surface attenuation effect for three different Q values of 5, 15 and 30, which correspond to κ_0 of 0.040, 0.013 and, 0.007, respectively. Here, we use the reference profile described above and shown in Figure 4.4. It can be seen that the site fundamental frequency is independent of the selected Q or κ_0 values. The same fundamental frequency value (1.25 Hz) can also be obtained using Equation (4.3).

Using the SRI method we are able to calculate the expected f_{peak} and V_{S30} for a selected shear-wave velocity profile, while by varying the V_L, d_L and V_R values we are able to define the relation between f_{peak} and V_{S30} for different profiles. Figure 4.6 shows V_{S30} as a function of f_{peak} for the reference shear-wave velocity profile, but varying V_L (150, 250 and 350 m/s) and d_L (from 2 m to 200 m). Here, V_R is fixed to 2000 m/s and Q = 15 (although Q is unimportant as shown in Figure 4.5). For all of the V_L values, the relation between f_{peak} and V_{S30} follows a bilinear trend with a hinge frequency (f_{hinge}) in the middle. The hinge frequency corresponds to a sediment layer with d_L = 30 m. For peak frequency smaller than f_{hinge} or sediments deeper than 30 m, V_{S30} remains constant, and is equal V_L. For peak frequencies higher than f_{hinge} or sediments shallower than 30 m, V_{S30} has an increasing trend with increasing f_{peak} values; all of the curves follow the same general trend.

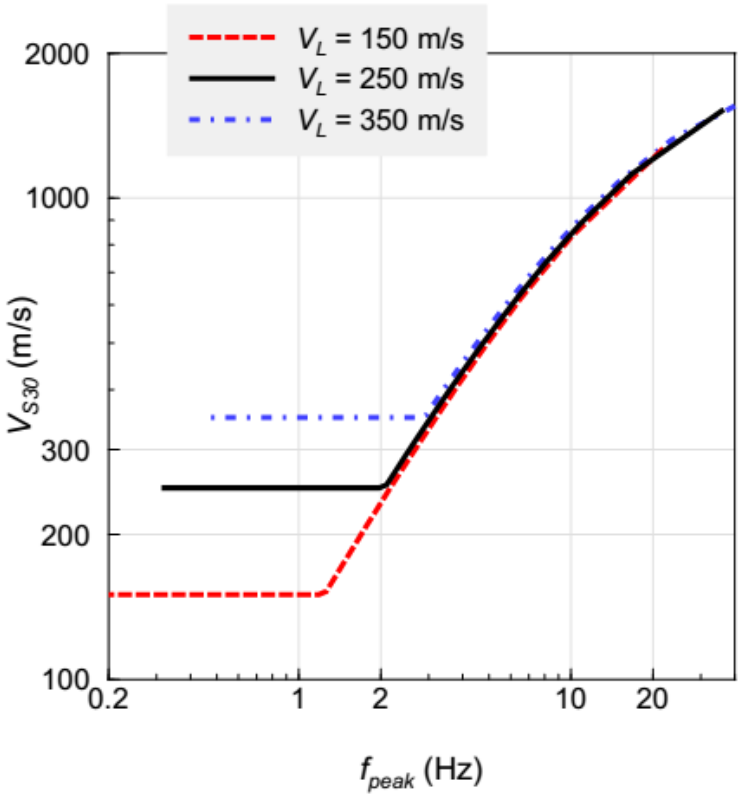

Figure 4.6: Expected relationship between V_{S30} and f_{peak} for three different layer velocity (V_L) values using the reference shear-wave velocity profile (Figure 4.4). For each of the curves the thickness of the layer (d_L) varies from 2 m to 200 m and Q = 15.

In Figure 4.7, we fix V_L to 250 m/s. For V_R values of 760, 1500, 2000, and 3000 m/s we define the relation between f_{peak} and V_{S30}. Here again, d_L varies from 2 m to 200 m, and Q = 15. As we can see here, f_{hinge} is the same (~ 2 Hz) for all of the V_R values. This is due to the fact that the V_L value is the same for all of the assumed shear-wave velocity profiles. Moreover, for frequencies higher than f_{hinge} (sediments shallower than 30 m), for higher V_R values, V_{S30} increases more rapidly with increasing f_{peak}.

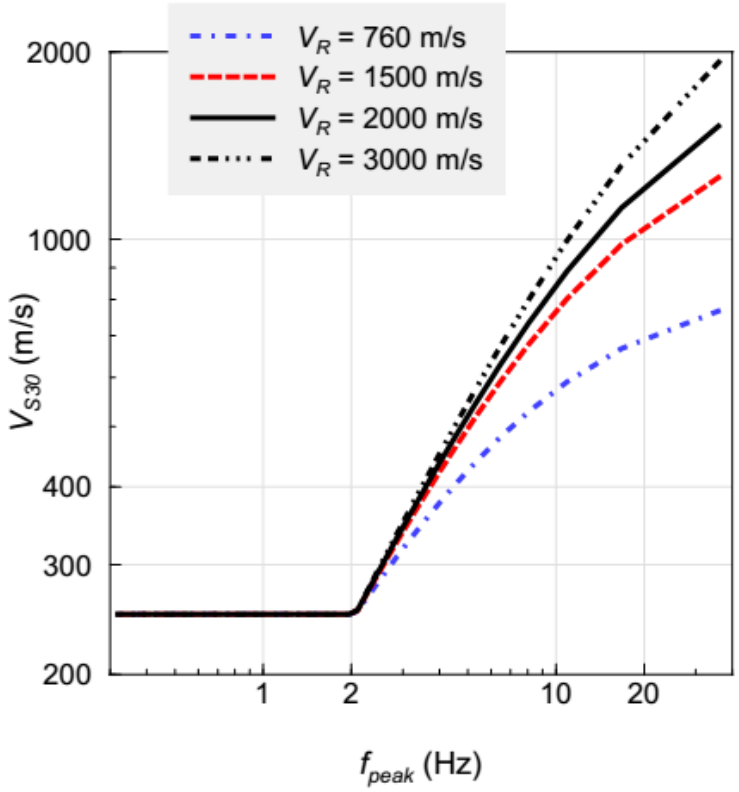

Figure 4.7: Expected relationship between V_{S30} and f_{peak} for four different bedrock velocity (V_R) values using the reference shear-wave velocity profile (Figure 4.4) For each of the curves, the layer thickness (d_L) varies from 2 m to 200 m and Q = 15.

Finally, we plot the measurement-based V_{S30} values as a function of their corresponding f_{peak} values in Figure 4.8. We also plot the expected V_{S30}-f_{peak} relation using Equation (4.5) for V_R = 2000 m/s and IR =0.1, and the corresponding expectations from the SRI method for the reference shear-wave velocity profile (different combination of V_L and V_R values). It can be seen that there is good agreement between the observed V_{S30}- f_{peak} pairs and the expected relationship based on Equation (4.5), for V_R = 2000 m/s and IR =0.1, for f_{peak} > 2 Hz. There is also a good match between the observed V_{S30}-f_{peak} pairs and the expectations of the SRI method (for V_L =250 m/s and V_R = 2000 m/s). This implies that for the plotted V_{S30} - f_{peak} pairs, bedrock shear-wave velocity (V_R) is close to 2000 m/s on average, assuming a simple single-layer model. The observed deviations of the datapoints in Figure 4.8 from the conceptual model may be related to different V_R values from that assumed, and also to complexity relative to the assumed single-layer model. For sites

with $f_{peak} \leq 2$ Hz, the average V_{S30} value is ~ 250 m/s. Thus a bilinear equation can be used to predict V_{S30} values using known f_{peak} values:

$$\log(V_{S30}) = \begin{cases} 2.2(\pm 0.04) + 0.63(\pm 0.06) log10\left(f_{peak}\right) & f > 2\ Hz \\ log10(250) & f \leq 2\ Hz \end{cases} \quad (4.8)$$

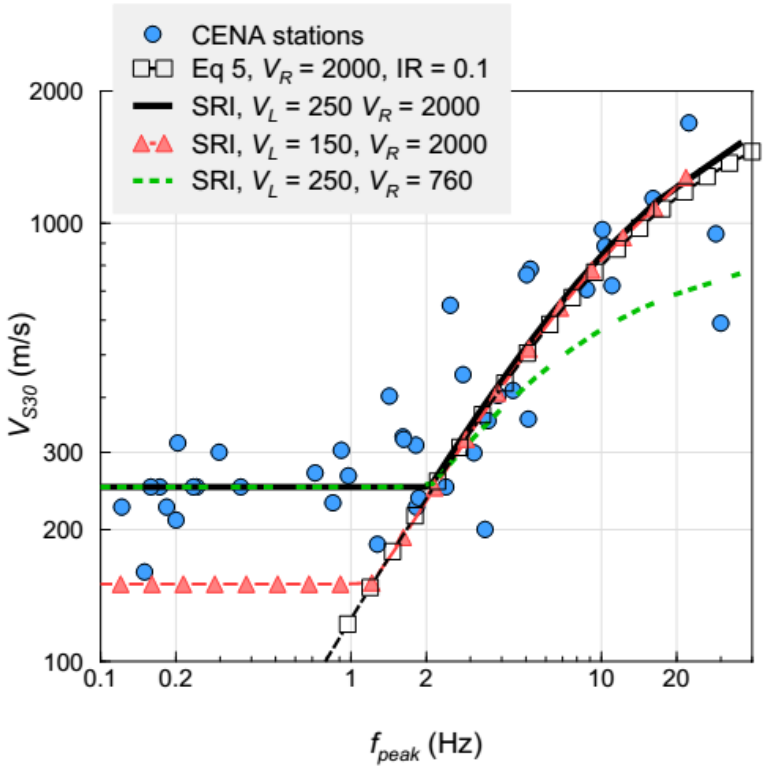

Figure 4.8: Measured V_{S30} values for CENA sites plotted versus their f_{peak} values (circles). The SRI method results for the reference shear-wave velocity profile, for different combinations of layer velocity (V_L) and bedrock velocity (V_R) are also shown. The output of Equation (4.5) for V_R = 2000 m/s and impedance ratio (IR) of 0.1 is also shown (squares).

. The standard deviation of Equation (4.8) is equal to 0.14 in $\log_{10}$ units. The uncertainty of the V_{S30} estimate using the f_{peak}-based model is much lower (0.14, $\log_{10}$ units) than that for the proxy-based methods used in the NGA-East database (0.25 $\log_{10}$ units). Figure 4.9 shows the proposed f_{peak}-based V_{S30} models for CENA (this study) compared to those for the NGA-West2 and Japan databases (Ghofrani and Atkinson, 2014). The observed

differences may be attributable to differences in the underlying shear-wave velocity (V_R) of the regions beneath the soil profiles. The CENA f_{peak}-based V_{S30} model implies the highest bedrock velocities amongst the models.

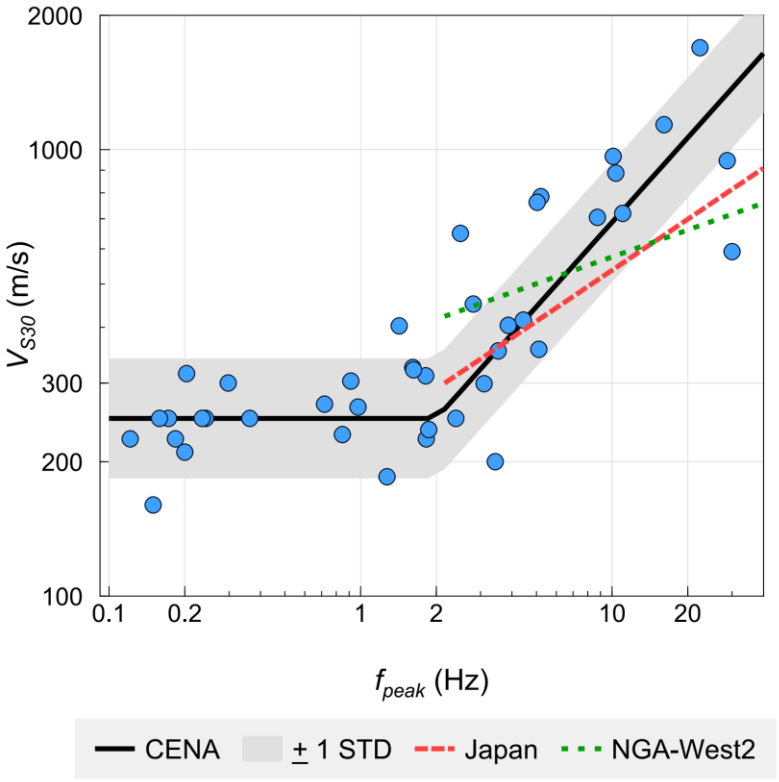

Figure 4.9: Measured V_{S30} values in CENA plotted versus their corresponding f_{peak} values (circles). Solid line shows the fitted model and its corresponding standard deviation (shaded area). Dotted line and dashed line show models for NGA-West2 and Japan recording stations, respectively (Ghofrani and Atkinson, 2014).

We note that the proposed f_{peak}-based V_{S30} proxy shown in Equation (4.8) is based on the limited number of sites with measured V_{S30} and determined f_{peak} values in the NGA-East database (only 41 sites). This relation can be improved in future by implementing more V_{S30} measurments and applying ambient noise studies for sites. By having more data, it is also possible to regionalize the model for sub-regions in CENA with different V_R and V_L values. Moreover, for sites with $f_{peak} \leq 2$ Hz we assumed that $V_{S30} \sim 250$ m/s based on the measured V_{S30} values for those stations. We note that for deep sediments (sediments deeper than 30 m) V_{S30} is not an ideal site indicator as it doesn't provide any information

from deeper sediment layers. On the other hand, f_{peak} is directly related to both sediment shear-wave velocity (V_L) and sediment depth (d_L), and it may not correlated with V_{S30} in the manner proposed here. For example, for a site with V_L = 500 m/s and d_L = 125, V_{S30} and f_{peak} would be equal to 500 m/s and 1 Hz respectively. Therefore, we caution the user to consider the geological condition of the area of interest before applying the proposed model for deeper sediments ($f_{peak} \leq 2$ Hz).

4.1.5 Variability of the NGA-East GMPE models using the f_{peak}-based V_{S30} model

As we showed earlier, using the proposed f_{peak}-based V_{S30} model (Equation 4.8) the standard deviation of the V_{S30} estimates can be reduced significantly relative to the NGA-East proxy-based V_{S30} estimate (~44% reduction in standard deviation). The new f_{peak}-based V_{S30} model can be used to update the V_{S30} estimates for the 315 sites (out of 1379 sites) for which f_{peak} can be determined. It is of interest to see how the new estimates of V_{S30} affect the overall variability of recently-proposed NGA-East GMPE models (Goulet et al., 2015). We consider the Yenier and Atkinson (2015) generic GMPE model (YA15) as an example. YA15 is a robust simulation-based generic GMPE, which was developed for B/C site conditions (V_{S30} = 760 m/s), after using the Boore et al. (2014) site effects model from NGA-West2 to subtract assumed site amplifications from the observed ground-motion amplitudes. We use a selected database to calculate the variability parameters. The selected database only includes stations with determined f_{peak} values, to enable evaluation of how the new estimates of V_{S30} affect the variability parameters. We perform a simple test to see if the variability of the residuals for this GMPE is reduced by replacing the V_{S30} values from the NGA-East database with the f_{peak}-based values derived in this study.

We calculate the residuals in both cases:

$$\log(re_{ij}) = \log(obs_{ij,\,B/C}) - \log(pre_{ij,\,B/C}), \tag{4.9}$$

where re_{ij} is the residual estimated for event i at station j, $obs_{ij,B/C}$ is the observed ground-motion parameter adjusted for B/C site condition using the Boore et al. (2014)

site amplification model (using V_{S30} from either the NGA-East database or the f_{peak}-based estimate), and $pre_{ij,B/C}$ is the YA15 predicted ground-motion parameter for B/C site condition for the corresponding record. We calculate the residuals for PSA at 0.5 Hz to 20 Hz in 17 equally log-spaced frequencies. The residuals from Equation (4.8) can be written as:

$$\log(re_{ij}) = C + \eta_i + \varepsilon_{ij}, \tag{4.10}$$

where C is the bias of the selected GMPE model, η_i is the random event term for event i, and ε_{ij} represents the within-event residual term for station j recorded at event i. We apply a mixed effect regression of residuals according to Abrahamson and Youngs (1992) to solve Equation (4.10) and perform an iterative regression to maximize the likelihood of the equation. The error terms (η_i and ε_{ij}) are normally distributed (in $\log_{10}$ units) and have standard deviations τ and φ, respectively. The total standard deviation (σ) is:

$$\sigma = \sqrt{\tau^2 + \varphi^2}, \tag{4.11}$$

Figure 4.10 shows the estimated between-event standard deviation (τ) and within-event standard deviation for both cases. We have converted these residuals to natural log units for the purposes of the plot, in order to facilitate comparisons with the NGA studies of these results (the NGA studies use natural log units). We note that the ground-motion variability parameters (τ and φ) at $1 \leq f \leq 10$ Hz are reduced using the proposed f_{peak}-based V_{S30} model. The variability reduction is mostly apparent in the within-event variability. This is expected as we only updated V_{S30} values, which are the site-term indicator in the selected GMPE model. Overall, we are able to reduce sigma (Equation 4.11) by 3% on average for PSA at 1 Hz to 10 Hz, just by improving the V_{S30} estimate for those sites having a determined value of f_{peak}. The reason that the reduction in error is not more significant may be due to the fact that we use the Boore et al. (2014) site effects model to remove the site amplification in CENA, which implicitly assumes that amplification is related to V_{S30} in the same way as for active tectonic regions. This is likely not an applicable model for many CENA sites, which are dominated by resonant

response of a layer over hard rock. Recently, Hassani and Atkinson (2016b) examined the applicability of the NGA-West2 site effects model (Boore et al., 2014), which is a V_{S30}-based model, to sites in CENA. They determined residual site terms by comparing the observed ground-motion amplitudes adjusted to B/C site condition using the (Boore et al., 2014) site effects model to the corresponding predicted amplitudes of a selected CENA ground-motion prediction equation for B/C site condition (Yenier and Atkinson, 2015; YA15). These authors found significant f_{peak}-dependent residual site terms at all frequencies for CENA sites, when western V_{S30}-based models are used. Average residual site terms can be as large as 0.45 in $\log_{10}$ units, which reveals significant limitations of such site effects models when applied to CENA ground motions. Therefore, a well-calibrated regional site effects model should be used in order to examine the efficiency of the proposed f_{peak}-based site characterization.

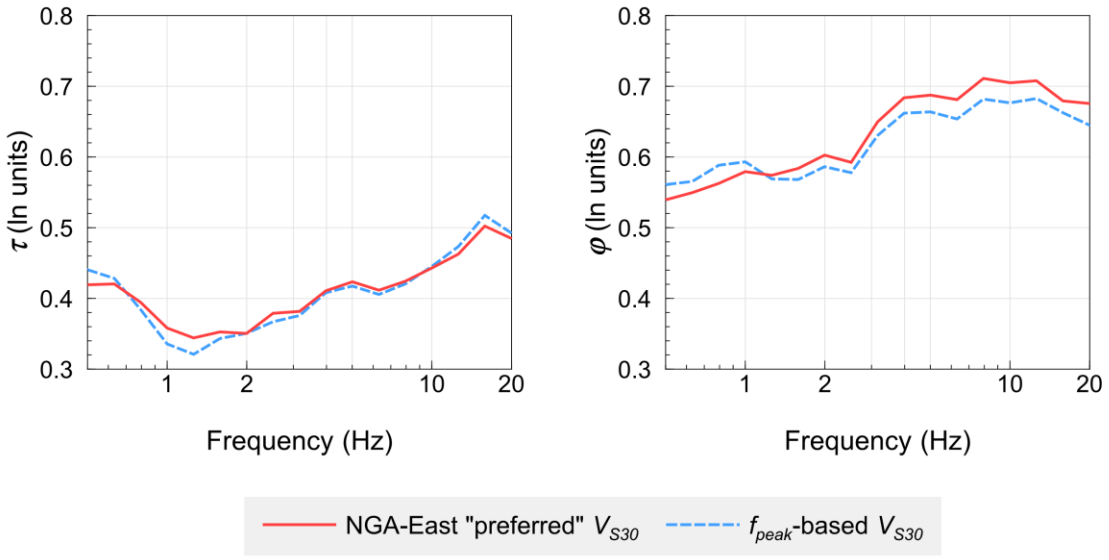

Figure 4.10: Between-event (τ, left plot) and within-event (φ, right plot) standard deviations using the NGA-East "preferred" V_{S30} values (solid line), and using the f_{peak}-based V_{S30} estimates (dashed line). Note that variability parameters are in natural log units (ln) to facilitate comparisons with other studies.

4.1.6 Conclusion

V_{S30} is the most commonly-used site effects parameter, and the error in V_{S30} estimates can directly affect the variability of GMPE models. In this study, we show that the site fundamental frequency, measured by the H/V ratio, is a particularly effective proxy for V_{S30} for many sites in CENA. Using f_{peak}, we are able to significantly reduce the error of V_{S30} compared to V_{S30} estimates based on topographic slope and surface geology proxies. However, the applicability of f_{peak} as a V_{S30} proxy is limited compared to topographic slope and surface geology proxies, which are universally available for the whole CENA region. Specifically, we were only able to determine f_{peak} for 23% of the recording stations in the NGA-East database (315 out of 1379 sites), due to limited available bandwidth or a small number of recorded events. However, the range of applicability would increase by implementing ambient noise studies and/or by recording additional ground-motion data at stations without a clear f_{peak}. The results of this study can be used to update V_{S30} estimates for sites with known f_{peak} values in CENA and improve GMPE models. The same approach can also be implemented for other regions to improve V_{S30} estimates. However, we emphasize that V_{S30} is not a good choice of site characterization variable for sites in which the response is dominated by the fundamental frequency of a soil layer overlying a much harder substratum. For such sites, f_{peak} is a more meaningful site descriptor. We recommend that site characterization include an estimate of the dominant frequency of a site, in addition to an estimate of its stiffness.

4.1.7 Data and Resources

The ground-motion database for calculating H/V spectral ratios was extracted from several sources. The processed ground-motion parameters (PGA, PGV and PSA) were obtained either from the early release of the NGA-East database as provided by Chris Cramer (https://umdrive.memphis.edu/ccramer/public/NGAeast/, last accessed December 2013), which includes both horizontal and vertical ground-motion parameters, or were extracted from the Engineering Seismology Toolbox website (www.seismotoolbox.ca, last accessed December 2013). Additional unprocessed data were extracted form Hassani and Atkinson (2015). For calculating the selected GMPE model variability, we used the latest version of the NGA-East database (Goulet et al., 2014). We used MATLAB

(www.mathworks.com, last contacted August 2015) for implementation of regressions and site fundamental frequency detection procedures, and we used CoPlot (www.cohort.com, last contacted August 2015) for making the figures.

4.1.8 Acknowledgments

This work was funded by the National Sciences and Engineering Research Council of Canada. We thank the NGA-East project for the excellent databases and ongoing discussions. We are grateful to Hiroshi Kawase and two anonymous reviewers for their constructive comments, which enabled us to improve the quality of the manuscript. We would also thank Chris Cramer for providing the early release of the NGA-East database.

4.2 Applicability of the NGA-West2 Site effects model for central and eastern North America[4]

4.2.1 Introduction

Ground-motion prediction equations (GMPEs) are a key component in seismic hazard analysis. GMPEs predict the expected median ground-motion amplitudes by using source, path and site terms to describe how ground-motion amplitudes scale with magnitude, distance and site conditions. In modern empirical GMPEs, site effects are usually characterized by a set of simplified parameters (often only one) that characterize the overall near-surface state. Common site parameters include site fundamental frequency (f_{peak}) (Zhao et al., 2006b) and V_{S30} (time-averaged shear-wave velocity in the upper 30 m) (e.g. Bozorgnia et al., 2014). V_{S30} is currently the most prevalent site parameter for development of GMPE models, especially in North America. For example, the well-known Next Generation Attenuation GMPEs (NGA-West1 and NGA-West2; Bozorgnia et al., 2014), developed for shallow crustal earthquakes in active tectonic regions, use V_{S30} as the site parameter. As part of the NGA-West2 project, Seyhan and Stewart (2014) (SS14) derived a semi-empirical V_{S30}-based site amplification model based on the NGA-West2 data and simulations. Their model was adopted as the site term in the Boore et al. (2014; BSSA14) NGA-West2 GMPE model. In the SS14 model, the amplitude and frequency-dependent site effects are defined as a function of V_{S30}, relative to a reference site condition. The reference condition is a site for which V_{S30} = 760 m/s; this is the B/C boundary between NEHRP site classes (National Earthquake Hazard Reduction Program) (NEHRP, 2000). The SS14 model includes both linear and nonlinear site effects. For the linear part of the model, site effects scale linearly with the logarithm of V_{S30} at all frequencies. For the rest of the NGA-West2 GMPE models (Abrahamson et al., 2014; Campbell and Bozorgnia, 2014; Chiou and Youngs, 2014; Idriss, 2014), V_{S30} was also chosen as the main input parameter for their selected site functional forms. The site functional forms may differ slightly from one to another; however in all of the western models the linear part of the site response scales linearly with the logarithm of

[4] A version of this section has been published. Hassani, B., and G.M. Atkinson (2016). Applicability of the NGA-West2 Site Effects Model for Central and Eastern North America, *Bull. Seismol. Soc. Am.* **106,** In press.

V_{S30} in a way that is very similar to the SS14 model. While the use of V_{S30} as an effective predictive variable for site effects has been well-documented for western North America (WNA), (e.g Abrahamson et al., 2014; Boore et al., 2014; Campbell and Bozorgnia, 2014; Chiou and Youngs, 2014; Idriss, 2014) it is not clear if such models apply to sites in central and eastern North America (CENA). The typical geological setting in many parts of CENA, where site response is often dominated by the fundamental frequency (f_{peak}) of a soil layer overlying a much harder substratum, is much different than that in WNA.

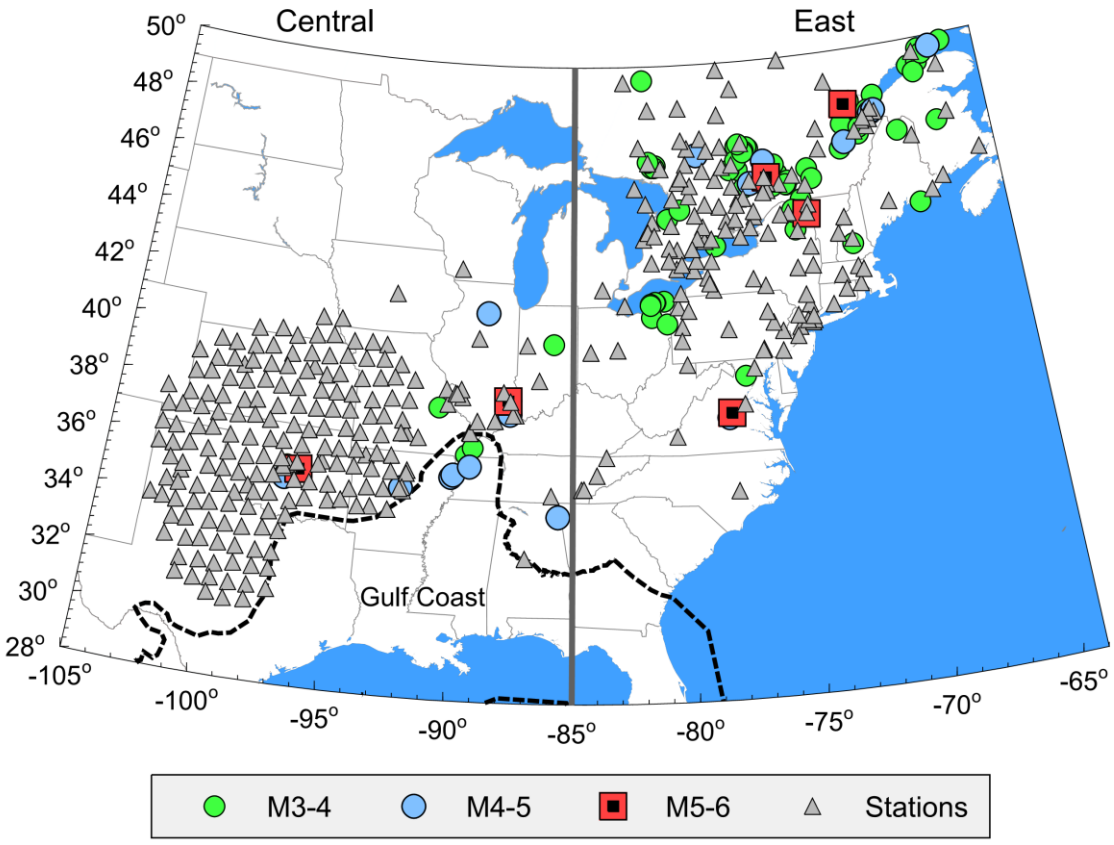

Figure 4.11: Epicenters of study events and locations of recording stations in central and eastern North America (CENA). Dashed line shows the assumed Gulf coast boundary (Dreiling et al., 2014), and solid line shows the boundary between East and Central regions.

Recently, the Pacific Earthquake Engineering Research–Next Generation Attenuation-East (NGA-East) project published a comprehensive set of GMPE models for CENA, intended to be applicable for shallow crustal earthquakes in stable tectonic regions (Goulet et al., 2015). For the NGA-East project, V_{S30} was also selected as the main site conditions indicator, to mirror its use in the NGA-West models and also its general use in North American building code applications. However, no regional model for how site amplification in CENA scales with V_{S30} has been proposed, due to a lack of empirical data to calibrate such a model. Therefore, many of the GMPE modelers used western-based site effects models to level the observed ground-motion amplitudes in CENA to a common reference condition (Hassani and Atkinson, 2015; Pezeshk et al., 2015; Shahjouei and Pezeshk, 2015; Yenier and Atkinson, 2015). Some modelers developed their own V_{S30}-based functional forms (Al-Noman and Cramer, 2015; Darragh et al., 2015; Graizer, 2015; Hollenback et al., 2015) using the reported V_{S30} values of the NGA-East database (Goulet et al., 2014), and some modelers did not apply any site adjustment, instead using a V_{S30}-limited dataset (e.g. such as sites with $V_{S30} \geq 760$ m/s or $V_{S30} \approx 2000$ m/s) to justify their models (Boore, 2015; Frankel, 2015).

In the NGA-East database only 6% of the recording stations have measured V_{S30} values (Goulet et al., 2014). Therefore, most of the reported V_{S30} values in the NGA-East database are derived from a weighted average of different proxy-based V_{S30} estimates; these proxies include topographic slope (Wald and Allen, 2007) and a set of surface-geology proxies (Kottke et al., 2012). The proxy-based V_{S30} estimates have large assigned uncertainties (0.20 to 0.25 $\log_{10}$ units). Therefore, even the GMPE modelers that developed a regional V_{S30}-based site functional form have large uncertainties in the site-effects component of their prediction models.

In CENA, V_{S30} may not be the best choice of site variable, as it may be a poor proxy for site response (Castellaro et al., 2008). It was originally developed based on empirical observations that show how the amplification of ground motion behaves in California (Borcherdt, 1994), where alluvial soils transition gradually to rock as depth increases, generally without any clear interface between soil and rock. CENA has been tectonically stable over the last several hundred million years, resulting in competent crustal

conditions that are generally characterized by high velocities and low attenuation. Much of CENA was glaciated about 10,000 to 13,000 years ago, resulting in many areas in which post-glacial soil profiles overlie much harder bedrock (e.g. Murphy and Eaton, 2005; Dreiling et al., 2014). Typical near-surface velocities for bedrock in CENA are in the range from 1800 to 3500 m/s, while post-glacial soils can have near-surface velocities <150 m/s (Motazedian et al., 2011). Thus there are many regions in which post-glacial soils, which may be shallow or deep, overlie a much harder glaciated bedrock surface, providing a sharp impedance contrast and setting up the conditions for strong amplification at the fundamental frequency of the site.

In this study we explore the applicability of empirical site effects models developed for WNA for sites in CENA. We adopt the SS14 site effects model (as representative of WNA site models). We use the SS14 site model to adjust the NGA-East observed ground-motion amplitudes to reference B/C site conditions, using the reported V_{S30} values of the NGA-East database (Goulet et al., 2014). Then, we use the Yenier and Atkinson (2015) (hereafter YA15) GMPE model, which was calibrated for the NGA-East database with the reference B/C site conditions, to find the residual between the observed and predicted ground-motion amplitudes. This measures the effectiveness of the SS14 site model, because the YA15 model also used SS14 to adjust the NGA-East amplitudes to the B/C reference condition, before model calibration. Specifically, their model calibration optimizes the fit of the YA15 GMPE to the site-corrected amplitudes of the NGA-East database. Therefore, the residuals of YA15 as a function of unexplored site variables, such as the peak frequency of the H/V ratio at a site, reveal trends not accounted-for in the V_{S30} -based site model from WNA that was used in its development.

By analyzing the residuals of the NGA-East ground motions with respect to the YA15 GMPE, we determine the residual site terms of the recording stations in CENA (i.e. after the SS14 model effects based on V_{S30} have been removed). We observe significant site term residuals that are centered around the site fundamental frequency (f_{peak}), where the site fundamental frequency is determined by the H/V ratios of the NGA-East 5% damped pseudoacceleration [PSA] data. This trend persists even if we consider only sites for which V_{S30} has been determined by direct measurement. Finally, we compare the site

terms for CENA recording stations with their corresponding horizontal to vertical spectral ratios (H/V). This comparison indicates that H/V provides a robust preliminary site effects model for CENA recording stations, which may be more applicable than the use of V_{S30} as it is able to reflect the observed f_{peak} -dependent site term trends.

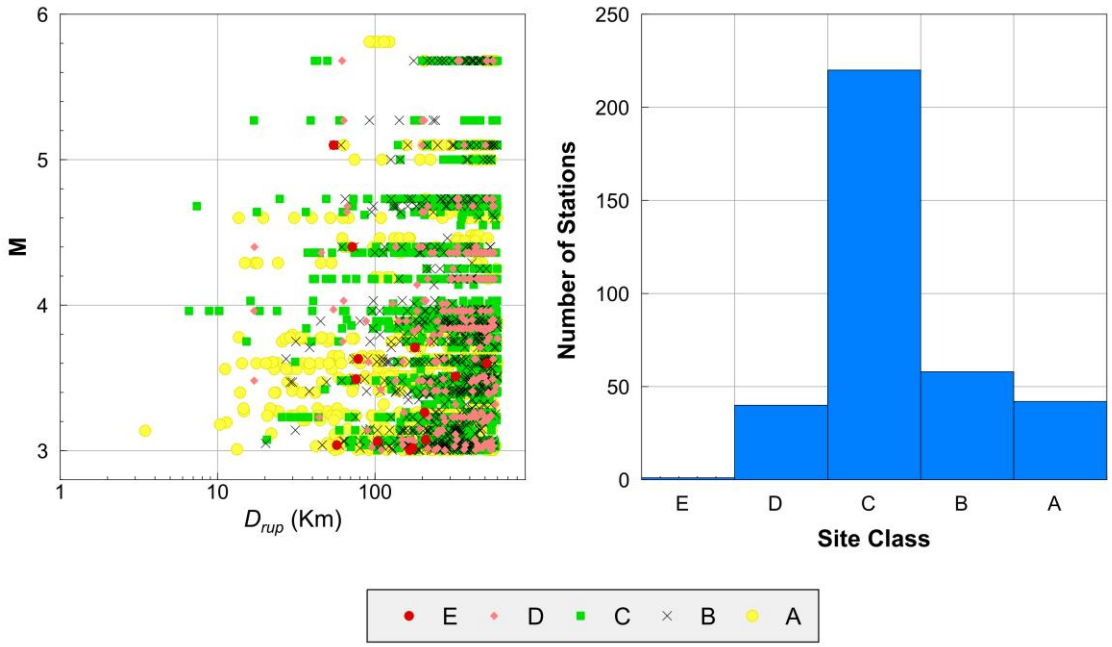

Figure 4.12: Left: Magnitude-distance distribution of study database; data points are shown with different symbols for NEHRP (National Earthquake Hazards Reduction Program) site classes (A: V_{S30} > 1500 m/s, B: 760 m/s < V_{S30} ≤ 1500 m/s, C: 360 m/s < V_{S30} ≤ 760 m/s, D: 180 m/s < V_{S30} ≤ 360 m/s and E: V_{S30} ≤ 180 m/s) (NEHRP, 2000). Right: Histogram of number of stations in each of the NEHRP site classes.

4.2.2 Database

We use the ground-motion data for the events and stations as shown in Figure 4.11. This is the same CENA ground-motion database as used by Hassani and Atkinson (2015), which was compiled from the NGA-East database (Goulet et al., 2014), supplemented by some additional data from Ontario (See Section 4.2.5). The database consists of horizontal-component peak ground-motion amplitudes (peak ground acceleration [PGA], peak ground velocity [PGV]) and response spectra (5% damped pseudo-spectral

acceleration [PSA]) sampled at 16 equally log-spaced frequencies from 0.5 to 15.8 Hz. We use events having moment magnitude (**M**) greater than 3 that were recorded on at least three stations with rupture distance $D_{rup} \leq 600$ km; we use only those stations that recorded at least three such events. We removed recorded ground motions in the Gulf Coast region (Figure 4.11) from our database, because of significantly deep sediments in this region which cause considerably different attenuation behavior (Electric Power Research Institute [EPRI], 2004; Dreiling et al., 2014).

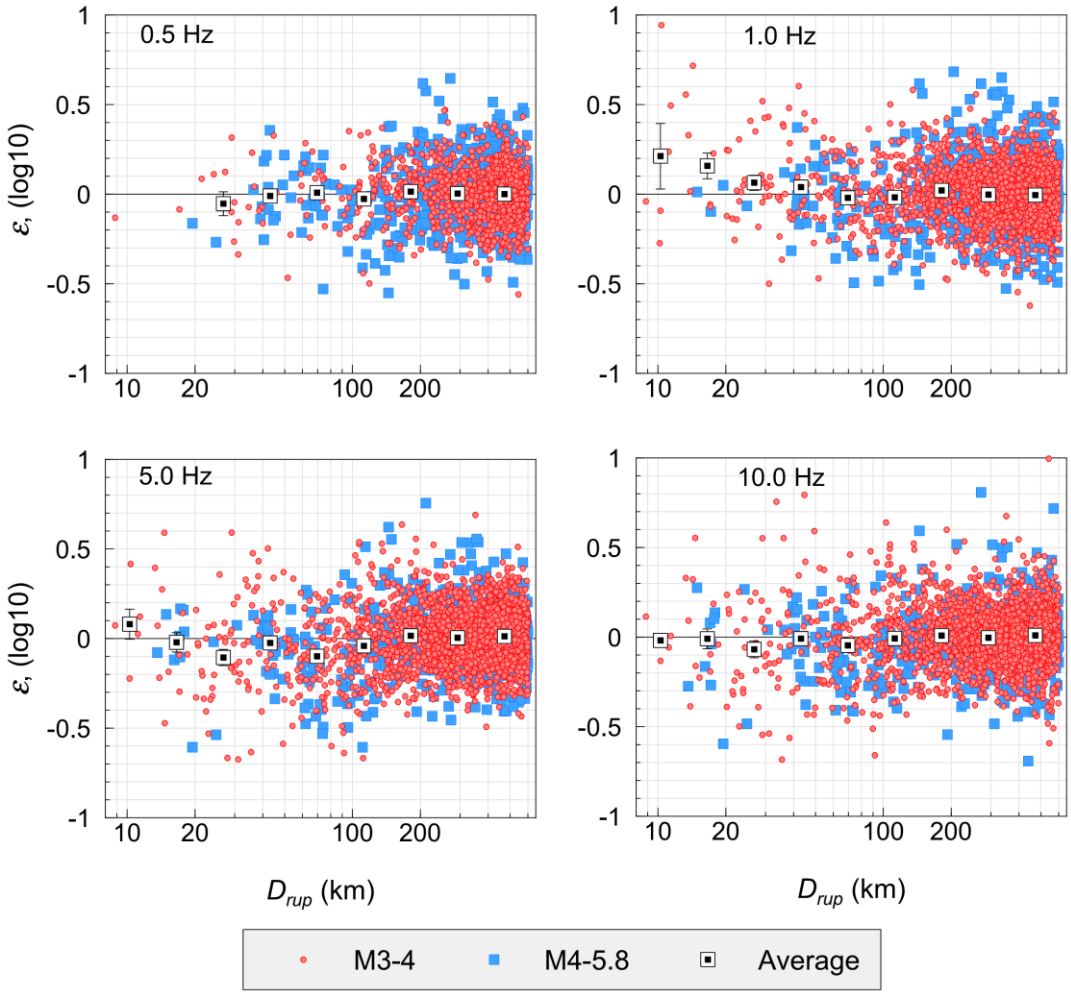

Figure 4.13: Within-event residuals (ε) as a function of rupture distance (D_{rup}), classified for different magnitude bins and shown for four frequencies (0.5, 1.0, 5.0, and 10 Hz). Squares show the average residuals at equally log-spaced distance bins and their standard errors.

The distribution of the database in magnitude, distance and site condition is shown in Figure 4.12. The selected database consists of 3274 horizontal-component ground-motion parameter sets (PGA, PGV and PSA) from 118 events and 361 stations. Note that the largest event in the CENA database has **M**5.8, and we have few observations at close distances (≤ 50 km). Therefore, we can assume that the rupture distance (D_{rup}) is equivalent to the hypocentral distance. We can also assume that site response effects are linear, as the number of records that might potentially include any nonlinear effects is negligible.

Site fundamental frequencies (f_{peak}) and horizontal to vertical spectral ratios (H/V) were extracted from Hassani and Atkinson (2016a), in which we used 5% damped PSA spectra of the NGA-East database to calculate H/V spectral ratios and determine the site fundamental frequencies (f_{peak}) for the recording stations in CENA. H/V spectral ratios are available for 353 of the stations (i.e. there are 353 stations that have the required minimum of three recordings), of which f_{peak} values are clearly observed for 192 stations.

4.2.3 Determination of residual site terms

We determine residual site terms by analysing the residuals calculated from the observed ground-motion amplitudes with respect to the corresponding predictions from a selected GMPE model. We first use the Seyhan and Stewart (2014) site effects model (SS14) to adjust all observed ground-motion amplitudes to the equivalent amplitudes for B/C site conditions (the reference condition), using the assigned V_{S30} value in the NGA-East database for each record (Goulet et al., 2014). The predicted ground-motion amplitudes for each record are calculated using the Yenier and Atkinson (2015) generic GMPE model (YA15) for the same reference B/C site conditions. The YA15 model is particularly suitable because it is a robust simulation-based generic GMPE that has been calibrated to match the NGA-East database, using the same SS14 site effects model. We already know that the YA15 model is free of residual trends in magnitude, distance and V_{S30} (Yenier and Atkinson, 2015). Thus we can use residuals with respect to this model to look for trends in other variables not included in the model. Specifically, we search for residual site effects that were not accommodated by the use of V_{S30} as a site effects predictive variable. We define the residuals as:

$$\log(re_{ij,B/C}) = \log(obs_{ij,\,B/C}) - \log(pre_{ij,\,B/C}), \tag{4.12}$$

where $re_{ij,B/C}$ is the residual estimated for event *i* at station *j*, $obs_{ij,B/C}$ is the observed ground-motion parameter adjusted for B/C site conditions using the SS14 site amplification model, and $pre_{ij,B/C}$ is the YA15 predicted ground-motion parameter for B/C site conditions for the corresponding record. We calculate the residuals for PSA at 0.5 Hz to 15.8 Hz in 16 equally log-spaced frequencies. The residuals obtained from Equation (4.12) can be written as:

$$\log(re_{ij,\,B/C}) = S_j + \eta_i + \varepsilon_{ij}, \tag{4.13}$$

where S_j is the site term for site *j* (relative to the reference B/C site conditions) after removing the site effects using the SS14 site amplification model, η_i is the random event term for event *i*, and ε_{ij} represents the within-event residual term for station *j* recorded at event *i*. We apply a mixed effect regression of residuals according to (Abrahamson and Youngs, 1992) to solve Equation (4.13) and perform an iterative regression to maximize the likelihood of the equation. The error terms (η_i and ε_{ij}) are normally distributed (in $\log_{10}$ units) and have standard deviations τ and φ, respectively. The total standard deviation (σ) is:

$$\sigma = \sqrt{\tau^2 + \varphi^2}, \tag{4.14}$$

Figure 4.13 shows the within-event residuals (ε) as function of distance (D_{rup}). The residuals are classified for different magnitude bins. The residuals do not show any apparent distance or magnitude dependency, and the average residual values attain a zero value at all distance bins, indicating good agreement between the model and the data. This is as we would expect because the YA15 model was calibrated to the NGA-East database. The only exception is at near distances (D_{rup} < 30 km) at low frequencies (f < 1 Hz), where the YA15 model underestimates the sparse amplitude data on average by ~ 0.1 $\log_{10}$ units (~ 25%).

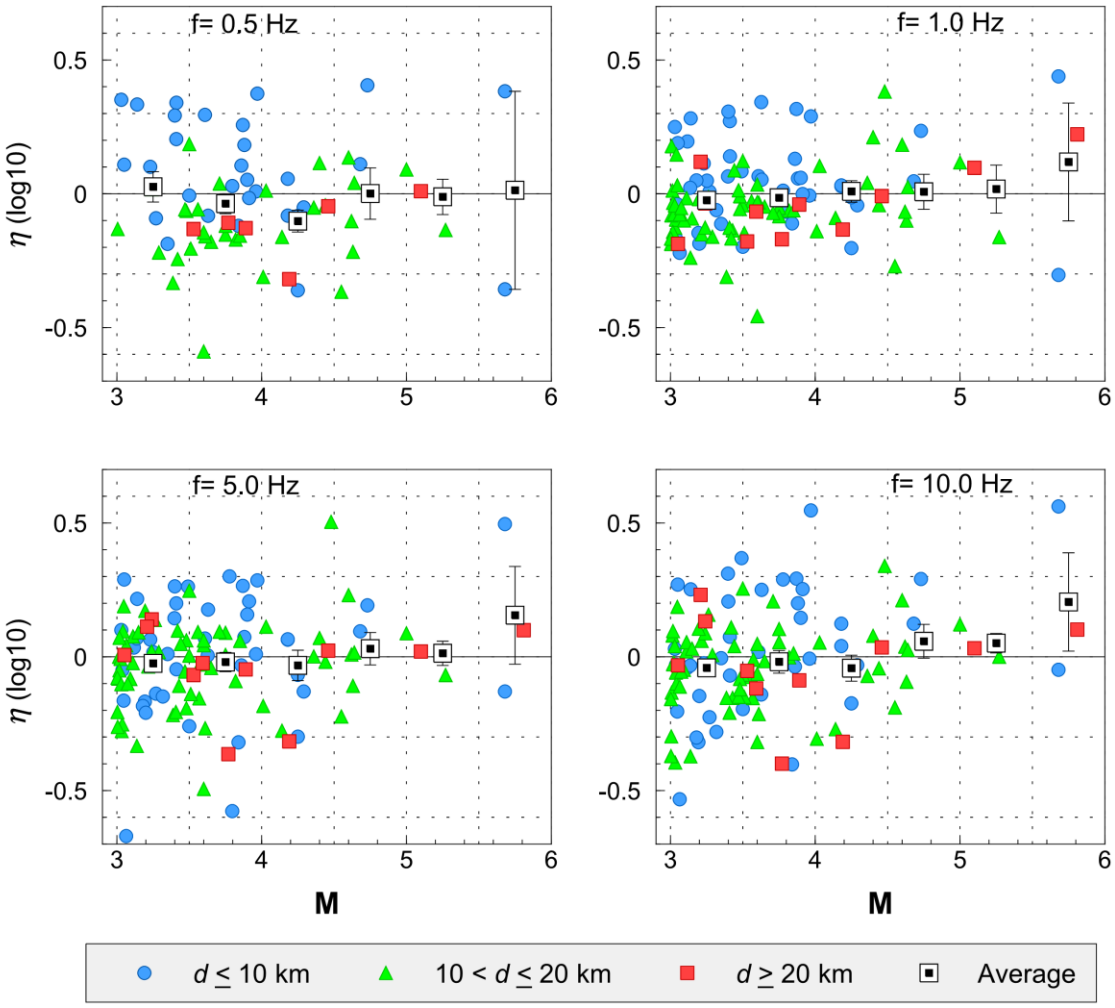

Figure 4.14: Between-event residuals (η) as a function of moment magnitude (M), classified for different depth (d) bins. Squares show the average residuals at equally-spaced magnitude bins and their standard errors.

In Figure 4.14, the between-event residuals η are plotted as a function of moment magnitude (**M**) and classified for different depth bins. The overall behavior of the residuals at all frequencies is again satisfactory, as we would expect. However we note that at 0.5 Hz for small magnitude events (**M** $\leq$ 3.5) there is a tendency to higher average residuals for shallow events (depth $\leq$ 10 km), though observations are sparse. From the foregoing, we conclude that the YA15 GMPE is predicting the database well with respect to the modeled parameters. However, it may also be noted that the variability is high. The value of σ is in the range of 0.34 to 0.39 $\log_{10}$ units for 0.5 Hz $\leq f \leq$ 15 Hz. Atkinson et al.

(2015) found smaller σ values (0.21 to 0.25 $\log_{10}$ units) when they used only data in southern Ontario and removed the regional site effects as obtained from inversion. Atkinson (2013) also found smaller σ values when using only the data in the Charlevoix seismic zone, recorded on hard rock sites. The large σ observed here can include the effects of a number of factors, such as use of a broader region like CENA instead of a confined database (e.g. southern Ontario or Charlevoix seismic zone).

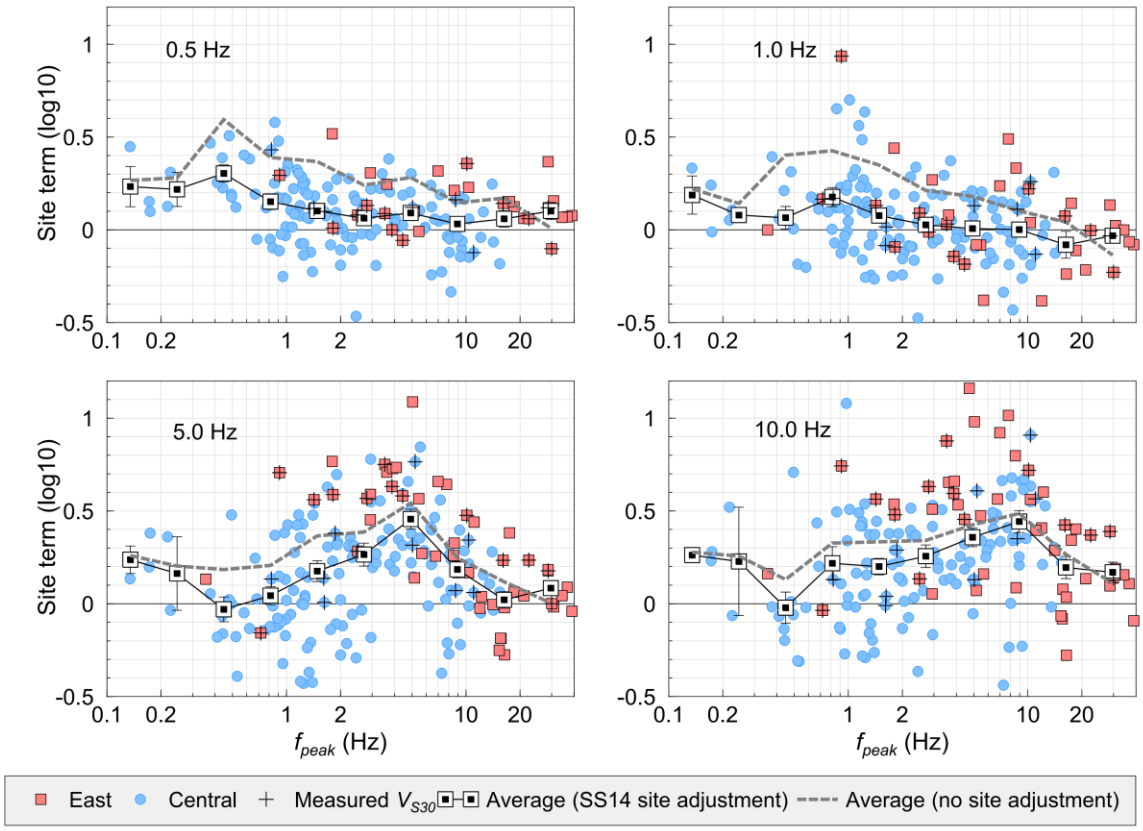

Figure 4.15: Residual site terms (*S*) plotted versus their corresponding fundamental frequencies (f_{peak}), and classified for Central and East regions (as shown in Figure 4.11). Plus signs shows the sites with measured V_{S30} values (Goulet et al., 2014). Squares show the residual site term averages in equally log-spaced f_{peak} bins and their standard errors. Dashed line shows average value of total site terms, as obtained when no site adjustment was applied to the observed data (no SS14 site adjustment).

Another important factor in the large variability is the way that we define site effects for the study sites. We hypothesize that much of the variability is attributable to site effects that are not well-modeled using the SS14 site model in V_{S30}. To explore this hypothesis, we use Equation (4.13) to calculate average residual site terms for each station in the database having at least three recordings; these site terms contain any site effects that were not already removed by the SS14 site effects model. Figure 4.15 plots these residual site terms as a function of site fundamental frequency (f_{peak}). The site fundamental frequencies were extracted from Hassani and Atkinson (2016a). We observe that there is a significant dependence of the residual site terms on f_{peak}, which represents an additional site effect not handled by the assumed SS14 model in V_{S30}. Sites in the East region (see Figure 4.11) mostly have high f_{peak} values (f_{peak} > 5 Hz), implying shallow sediments over a harder layer, while sites in the Central region mostly have low to intermediate f_{peak} values (0.1 Hz< f_{peak} < 5 Hz), implying deeper sediments. We observe the maximum residual site terms values near $f_{peak} \approx f$, implying that there is a dominant site fundamental frequency effect in the observed residual site terms. The maximum value of the residual site amplification is approximately 0.3 $\log_{10}$ units on average (a factor of two) for frequencies between 0.5 to 15.8 Hz. Thus the unmodeled site effects in CENA around the predominant frequency are very significant.

To see how the accuracy of V_{S30} estimates may affect the f_{peak}-dependent site terms, we also plot the residual site terms considering just those sites with measured V_{S30} values reported in the NGA-East database (Goulet et al., 2014). As shown on Figure 4.15, sites with measured V_{S30} values also show significant f_{peak}-dependent site terms at various frequencies; however, the number of sites with measured V_{S30} values is limited (41 stations).

It is also interesting to see the trend of the determined site terms versus f_{peak}, without applying any site effects adjustment to the observed data. In order to do that, we recalculate the residuals in Equation (4.12) without applying the SS14 (or any other) site correction factors [e.g. $\log(re_{ij}) = \log(obs_{ij}) - \log(pre_{ij,\,B/C})$], and use Equation (4.13) to determine the total site terms relative to the predictions for B/C. These total site terms are also shown in Figure 4.15. As we would expect, the total site terms are higher than the

residual site terms, indicating that using the western site effects model is better than no site adjustment at all. At lower frequencies (f < 1 Hz), the SS14 site effects model handles the CENA site effects relatively well, accounting for much of the observed total amplification relative to B/C. At higher frequencies the SS14 model accounts for very little of the observed amplification, leaving behind a large residual f_{peak} -dependent site term. The likely explanation is that site terms at low frequencies are controlled by deeper, more gradational soil profiles compared to site terms at high frequencies. The most important differences in soil profiles between WNA and CENA are that shallow-to-intermediate depth deposits are often underlain by a harder substratum, leading to significant amplification peaks that are particularly apparent at high frequencies.

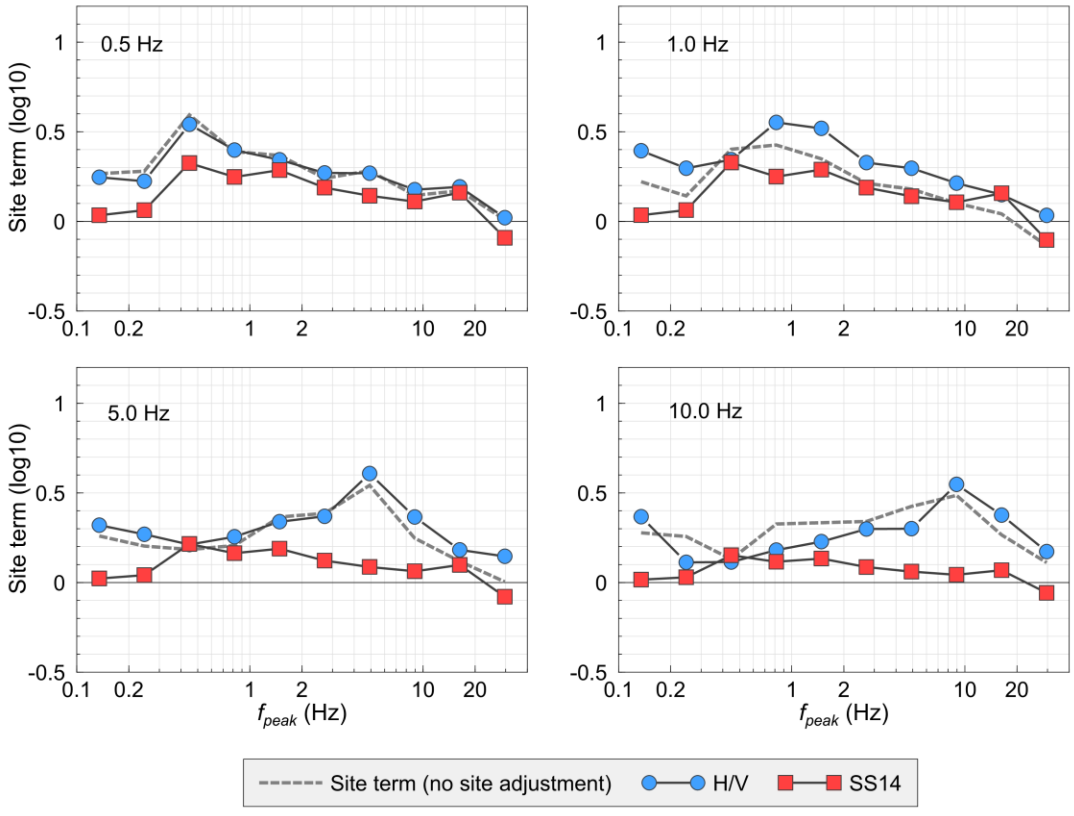

Figure 4.16: Average total site terms (no site adjustment) (solid lines), average H/V spectral ratios extracted from Hassani and Atkinson (2016b) (circles), and average SS14 site effects model calculated using the reported V_{S30} values reported from the NGA-East database (squares). Amplifications are plotted as a function of site fundamental frequency (f_{peak}) for the sites in the database.

From Figure 4.15, it can be noted that ground-motion variability increases at higher frequencies (≥ 5 Hz). This could be partly due to regional attenuation differences carried within the NGA-East database, which may map into the site terms and increase the data scatter. For instance, Atkinson et al. (2015) found lower regional anelastic attenuation when they only used the southern Ontario ground-motion database, in comparison to the corresponding attenuation obtained for the whole NGA-East database (Yenier and Atkinson, 2015). Moreover, there are many stations near the Gulf Coast boundary, which could be partly affected by the high attenuation of the Gulf Coast zone. These effects are more apparent at higher frequencies (≥ 5 Hz) and can result in negative residual site terms (e.g. some of the sites with 1 Hz ≤ f_{peak} ≤ 2 Hz have negative residuals at higher frequencies).

The obvious dependence of the site amplification terms on peak frequency motivates us to consider the use of the H/V ratio as a site variable. The main assumption of this method is that horizontal-component ground motions are amplified around the fundamental frequency of a site, while the vertical-component of ground motion experiences relatively little net amplification (Nakamura, 1989; Lermo and Chávez-García, 1993). Therefore, the H/V ratio provides a good estimate of the dominant frequency and corresponding amplification of the site. Hassani and Atkinson (2016b) calculated the H/V spectral ratios for the NGA-East recording stations using the PSA database. Here, we compare these H/V response spectral ratios with the total site terms relative to B/C, as determined from this study. Figure 4.16 shows the comparison between the average total site terms obtained from Equation (4.13) (no site corrections applied to data), the average H/V spectral ratios, and also the average of site terms predicted by the SS14 site effects model, based on the reported V_{S30} values from the NGA-East database. There is excellent agreement between the average total site terms from Equation (4.13) and the average H/V spectral ratios, indicating that H/V is a good predictor of the observed f_{peak}-dependent site term trends at all frequencies. At some frequencies the H/V method tends to slightly overpredict the amplitude of the observed site terms. This might be because the total site terms obtained from Equation (4.13) are relative to B/C site conditions, while the H/V spectral ratio is reflecting the total amplification from a firmer underlying basement condition. By contrast, we note that the

SS14 site correction terms tend to follow the observed f_{peak} dependent site terms trends at low frequencies (up to 1 Hz), although slightly underpredicting the site terms around $f \approx f_{peak.}$. At higher frequencies (e.g. near 5 Hz) the SS14 site effects model does not track the observed f_{peak} -dependent site term trends at all, and underpredicts the site terms by as much as 0.45 $\log_{10}$ units (e.g. by a factor of three) around $f \approx f_{peak}$.

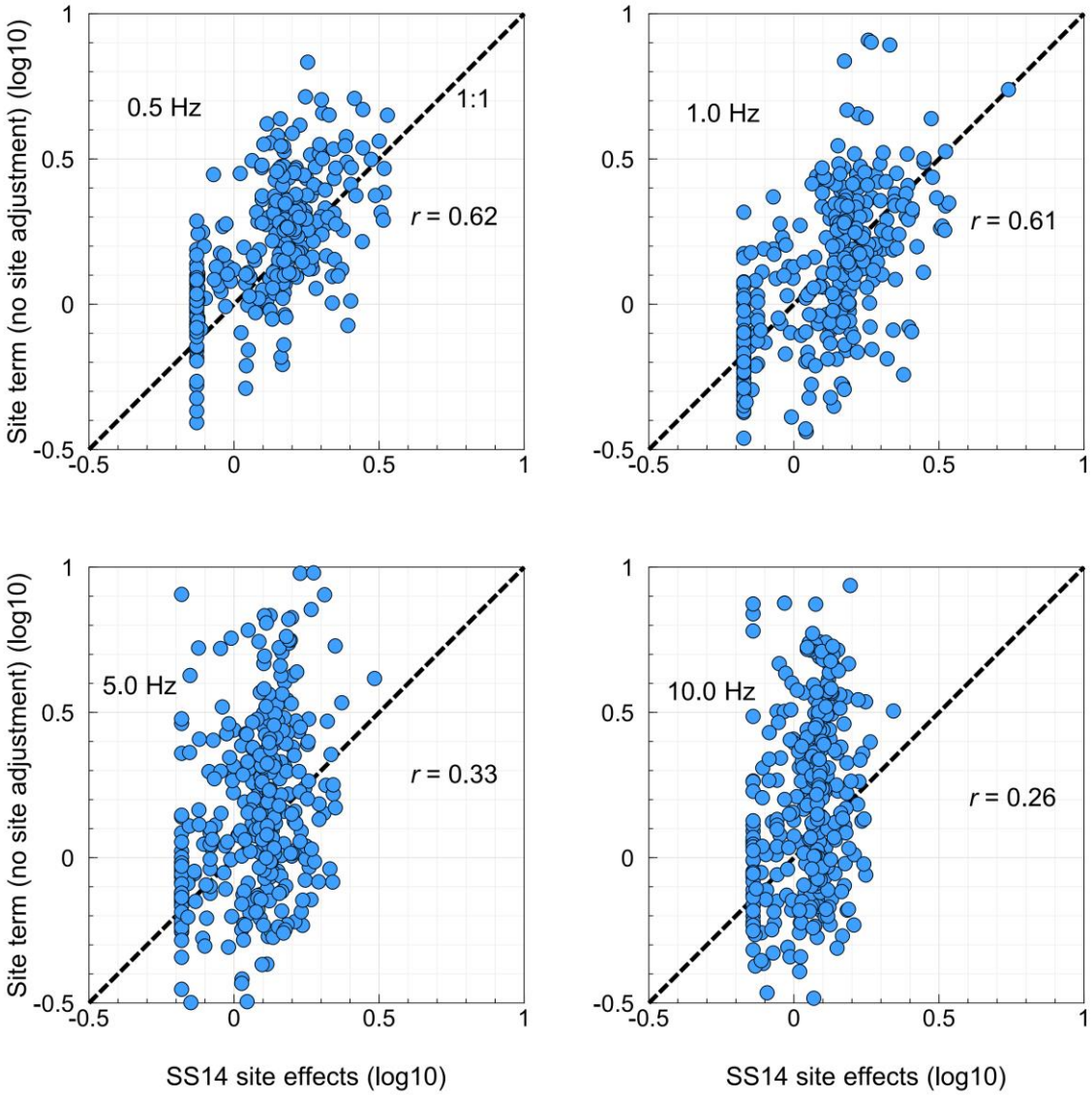

Figure 4.17: Total site terms (no site adjustment) are plotted versus SS14 site effect terms as obtained using the reported V_{S30} values from the NGA-East database (circles). Correlation coefficients are also shown for the selected frequencies.

To investigate the site terms in more detail, the correlation between the total site terms of Equation (4.13) (no site adjustment), and the estimates of the SS14 site effects model using the reported V_{S30} values of NGA-East database are plotted in Figure 4.17 for several frequencies; the corresponding correlation coefficients (r) are also shown. As we observe here, the correlation coefficient degrades as we move toward higher frequencies due to increased data scatter. At low frequencies ($f \leq 1$ Hz), site terms in CENA can be modelled fairly effectively by V_{S30} , though with significant scatter. At higher frequencies, site terms cannot be properly modelled using V_{S30} because of very large scatter, and the correlation coefficient (r) drops significantly. This implies that V_{S30} is not a good site indicator for CENA for frequencies $f > 1$ Hz, where the largest site terms will be observed at $f \approx f_{peak}$.

Figure 4.18 shows the correlation between the total site terms from Equation (4.13) (no site adjustment) and the corresponding H/V spectral ratios. It can be seen that there is a good correlation between the observed site terms and estimates of H/V spectral ratios. The data scatter still increases with increasing frequency; however, the scatter is significantly smaller than that obtained using the SS14 site amplification model (Figure 4.17). The increase in the data scatter at higher frequencies could be due to regional attenuation differences in the NGA-East database as discussed earlier.

Finally, in Figure 4.19 we compare the correlation coefficients obtained using the SS14 site effects model based on V_{S30} as a site predictor variable to those based on using the H/V spectral ratio as a site predictor variable. For the SS14 site effects model, the correlation coefficient starts to drop rapidly for frequencies greater than 1 Hz, becoming as low as ~ 0.2 at 10 Hz. For the H/V spectral ratio site effects model, the correlation coefficient is ~0.7 for frequencies up to 5 Hz, and starts to drop at higher frequencies as the scatter in the data increases. However, at all frequencies the correlation coefficients achieved using H/V spectral ratios to estimate site response are significantly better than the equivalent values obtained using the V_{S30}-based model. This indicates that in the absence of a well-calibrated regional site effects model for CENA based on V_{S30}, H/V spectral ratios can be used to provide a site effects model which is able to properly reflect the observed f_{peak}-dependent site terms for CENA recording stations. Such a model

renders the NGA-East database more useful, in that it enables site effects to be more effectively removed in GMPE modeling, thus allowing a reduction in aleatory variability.

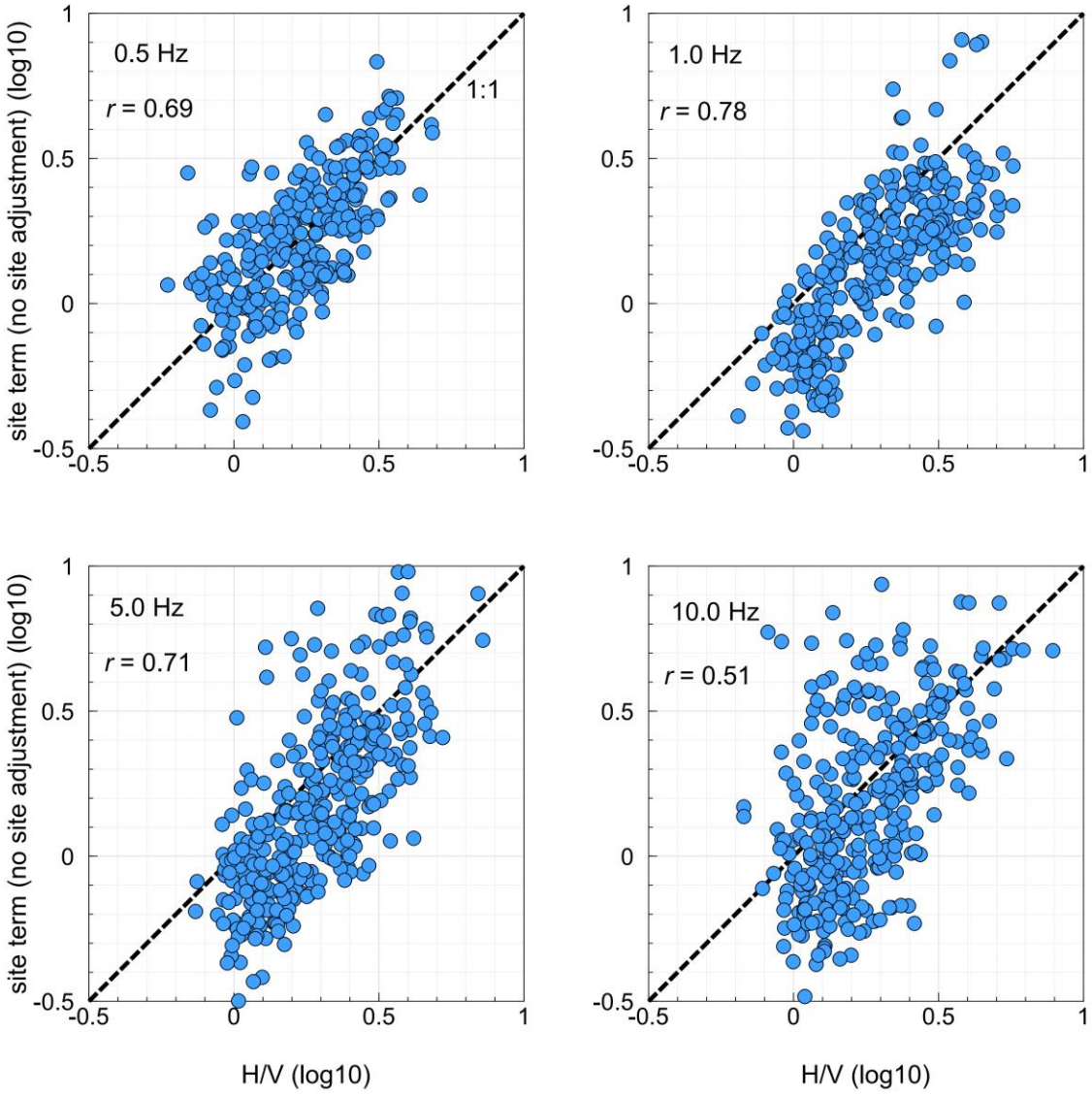

Figure 4.18: Total site terms (no site adjustment) are plotted versus the amplitude of the H/V spectral ratio, for four selected frequencies. Correlation coefficients are also shown.

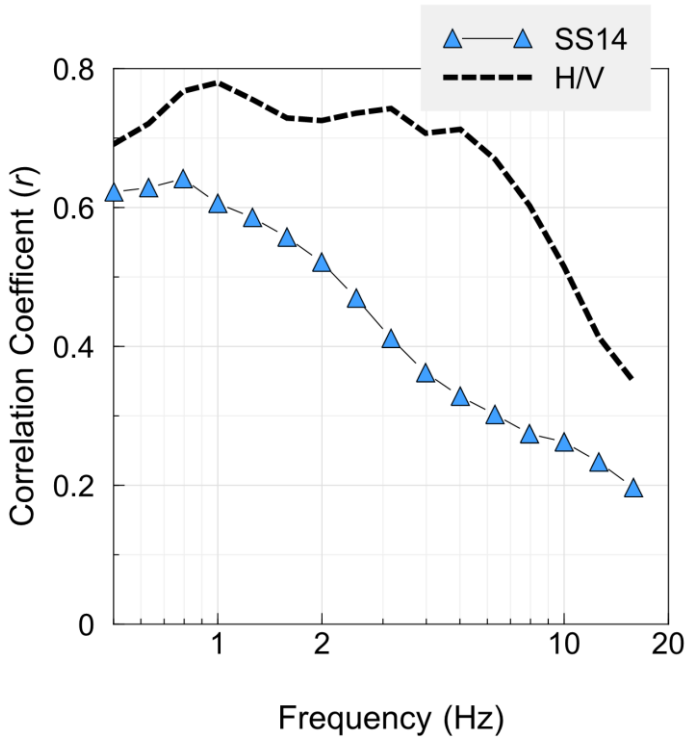

Figure 4.19: Correlation coefficients between the observed total site terms (no site adjustment) and a selected site effects model are plotted for two cases: 1) using the SS14 site effects model (triangles), and 2) using a site effects model based on the H/V spectral ratio (dashed line).

4.2.4 Conclusion

In the absence of a regional site effects model in V_{S30} developed specifically for CENA, GMPE developers tend to use generic site effect models from data-rich regions like WNA. However, the applicability of such V_{S30}–based models to sites in CENA appears to be marginal. In this study, we have shown that WNA V_{S30}-based models, such as those used in the NGA-West2 project, underpredict the observed site terms for CENA recording stations at frequencies around $f \approx f_{peak}$ by a factor of about two. We find that at low frequencies (f < 1 Hz), CENA site terms can be modeled by V_{S30}; however at higher frequencies the CENA site amplifications do not correlate with V_{S30}. By contrast, H/V spectral ratios are an effective site amplification predictive variable for CENA recording stations, properly matching the observed f_{peak}-dependant site terms. The results of this

study show the necessity of developing a well-calibrated regional site effects model for CENA, which should include an estimate of the dominant frequency of a site as well as an estimate of its stiffness.

4.2.5 Data and Resources

The ground-motion database of this study is the same as the database developed by Hassani and Atkinson (2015). In summary, most of the data in their database were extracted from the NGA-East database (Goulet et al., 2014) which were already processed and include PGA, PGV and PSA for the rotation-angle independent geometric average of horizontal ground-motion amplitudes (RotD50) (Boore, 2010). The rest of the processed data were obtained from the Engineering Seismology Toolbox website, which includes three-component processed ground-motion parameters (www.seismotoolbox.ca; last accessed December 2013). The unprocessed data were either obtained from the Automatic Data Request Manager Facility (AutoDRM) of the Geological Survey of Canada (autodrm@seismo.nrcan.gc.ca; last contacted December 2013) or the AutoDRM of the Incorporated Research Institutions for Seismology (breq_fast@iris.washington.edu, last contacted December 2013). The processing of the unprocessed data was as described by (Assatourians and Atkinson, 2010). For the unprocessed data and the data extracted from Engineering Seismology Toolbox website, the geometric mean of the horizontal components was used, which is approximately equivalent to RotD50. We used MATLAB for all of the regressions (www.mathworks.com, last contacted November 2015), and we used CoPlot for making the figures (www.cohort.com, last contacted November 2015).

4.2.6 Acknowledgments

This study was supported by the Natural Sciences and Engineering Research Council of Canada. We are grateful to the PEER NGA-East Project for their database compilation. We thank Chris Cramer and an anonymous reviewer for their helpful comments which improved the quality of the manuscript.

4.3 References

Abrahamson, N.A., and R.R. Youngs (1992). A stable Algorithm for regression analysis using the random effects model, *Bull. Seismol. Soc. Am.* **82,** 505-510.

Abrahamson, N.A., W.J. Silva, and R. Kamai (2014). Summary of the ASK14 ground motion relation for active crustal regions, *Earthq. Spectra.* **30,** 1025-1055.

Al-Noman, M., and C.H. Cramer (2015). Empirical Ground-Motion Prediction Equations for Eastern North America, in *NGA-East: Median Ground-Motion Models for the Central and Eastern North America Region*, Chap. 8, PEER Report No. 2015/04, Pacific Earthquake Engineering Research Center, Berkeley, CA, 193-212.

Anderson, J.G., and S.E. Hough (1984). A model for the shape of the Fourier amplitude spectrum of acceleration at high frequencies, *Bull. Seismol. Soc. Am.* **74,** 1969-1993.

Anderson, J.G., P. Bodin, J.N. Brune, J. Prince, S.K. Singh, R. Quaas, and M. Onate (1986). Strong ground motion from the Michoacan, Mexico, earthquake, *Science*. **233,** 1043-1049.

Andrews, D.J. (1986). Objective determination of source parameters and similarity of earthquakes of different size, in *Earthquake source mechanics*, S. Das (Editor), American Geophysical Union, Geophysical Monograph, Vol. 37, 259–267.

Assatourians, K., and G.M. Atkinson (2010). Database of Processed Time Series and Response Spectra Data for Canada: An Example Application to Study of 2005 MN 5.4 Riviere du Loup, Quebec, Earthquake, *Seism. Res. Lett.* **81,** 1013-1031.

Atkinson, G. (2013). Empirical evaluation of aleatory and epistemic uncertainty in eastern ground motions, *Seism. Res. Lett.* **84,** 130-138.

Atkinson, G.M., B. Hassani, A. Singh, E. Yenier, and K. Assatourians (2015). Estimation of Moment Magnitude and Stress Parameter from ShakeMap Ground-Motion Parameters, *Bull. Seismol. Soc. Am.* **105,** 2572-2588.

Bonilla, L.F., J.H. Steidl, G.T. Lindley, A.G. Tumarkin, and R.J. Archuleta (1997). Site amplification in the San Fernando Valley, California: variability of site-effect estimation using the S-wave, coda, and H/V methods, *Bull. Seismol. Soc. Am.* **87,** 710-730.

Boore, D.M. (2003). Simulation of ground motion using the stochastic method, *Pure and applied geophysics*. **160,** 635-676.

Boore, D.M. (2013). The uses and limitations of the square-root-impedance method for computing site amplification, *Bull. Seismol. Soc. Am.* **103,** 2356-2368.

Boore, D.M. (2015). Point-Source Stochastic-Method Simulations of Ground Motions for the PEER NGA-East Project in *NGA-East: Median Ground-Motion Models for the Central and Eastern North America Region*, Chap. 2, PEER Report No. 2015/04, Pacific Earthquake Engineering Research Center, Berkeley, CA, 11-49.

Boore, D.M., and W.B. Joyner (1997). Site amplifications for generic rock sites, *Bull. Seismol. Soc. Am.* **87,** 327-341.

Boore, D.M., J.P. Stewart, E. Seyhan, and G.M. Atkinson (2014). NGA-West2 equations for predicting PGA, PGV, and 5% damped PSA for shallow crustal earthquakes, *Earthq. Spectra.* **30,** 1057-1085.

Borcherdt, R.D. (1970). Effects of local geology on ground motion near San Francisco Bay, *Bull. Seismol. Soc. Am.* **60,** 29-61.

Borcherdt, R.D. (1994). Estimates of site-dependent response spectra for design (methodology and justification), *Earthq. Spectra.* **10,** 617-653.

Bozorgnia, Y., N.A. Abrahamson, L.A. Atik, T.D. Ancheta, G.M. Atkinson, J.W. Baker, A. Baltay, D.M. Boore, K.W. Campbell, B.S.-J. Chiou, R. Darragh, S. Day, J. Donahue, R.W. Graves, N. Gregor, T. Hanks, I.M. Idriss, R. Kamai, T. Kishida, A.R. Kottke, S.A. Mahin, S. Rezaeian, B. Rowshandel, E. Seyhan, S. Shahi, T. Shantz, W. Silva, P. Spudich, J.P. Stewart, J. Watson-Lampery, K. Wooddell, and R. Youngs (2014). NGA-West2 research project, *Earthq. Spectra.* **30,** 973-987.

Campbell, K.W., and Y. Bozorgnia (2014). NGA-West2 ground motion model for the average horizontal components of PGA, PGV, and 5% damped linear acceleration response spectra, *Earthq. Spectra.* **30,** 1087-1115.

Castellaro, S., F. Mulargia, and P.L. Rossi (2008). V_{S30}: Proxy for seismic amplification?, *Seism. Res. Lett.* **79,** 540-543.

Chiou, B.S.-J., and R.R. Youngs (2014). Update of the Chiou and Youngs NGA model for the average horizontal component of peak ground motion and response spectra, *Earthq. Spectra.* **30,** 1117-1153.

Darragh, R.B., N.A. Abrahamson, W.J. Silva, and N. Gregor (2015). Development of Hard Rock Ground-Motion Models for Region 2 of Central and Eastern North America in *NGA-East: Median Ground-Motion Models for the Central and Eastern North America Region*, Chap. 3, PEER Report No. 2015/04, Pacific Earthquake Engineering Research Center, Berkeley, CA, 51-84.

Dreiling, J., M.P. Isken, W.D. Mooney, M.C. Chapman, and R.W. Godbee (2014). NGA-East Regionalization Report: Comparison of Four Crustal Regions within Central and Eastern North America using Waveform Modeling and 5%-Damped Pseudo-Spectral Acceleration Response, *PEER Report 2014*. **15**.

EPRI, E.P.R.I. (2004). CEUS Ground Motion Project Final Report 1009684, EPRI, Palo Alto, California.

Field, E.H., and K.H. Jacob (1995). A comparison and test of various site-response estimation techniques, including three that are not reference-site dependent, *Bull. Seismol. Soc. Am.* **85,** 1127-1143.

Frankel, A., C. Mueller, T. Barnhard, D. Perkins, E. Leyendecker, N. Dickman, S. Hanson, and M. Hopper (1996). National seismic-hazard maps: documentation June 1996, *U.S. Geol. Surv. Open-File Rept. 96-532*.

Frankel, A.D. (2015). Ground-Motion Predictions for Eastern North American Earthquakes Using Hybrid Broadband Seismograms from Finite-Fault Simulations with Constant Stress-Drop Scaling in *NGA-East: Median Ground-*

Motion Models for the Central and Eastern North America Region, Chap. 6, PEER Report No. 2015/04, Pacific Earthquake Engineering Research Center, Berkeley, CA, 149-163.

Ghofrani, H., and G.M. Atkinson (2014). Site condition evaluation using horizontal-to-vertical response spectral ratios of earthquakes in the NGA-West 2 and Japanese databases, *Soil Dynam. Earthq. Eng.* **67,** 30-43.

Ghofrani, H., G.M. Atkinson, and K. Goda (2013). Implications of the 2011 M9. 0 Tohoku Japan earthquake for the treatment of site effects in large earthquakes, *Bulletin of Earthquake Engineering*. **11,** 171-203.

Goulet, C.A., Y. Bozorgnia, and N.A. Abrahamson (2015). Introduction, in *NGA-East: Median Ground-Motion Models for the Central and Eastern North America Region*, Chap. 1, PEER Report No. 2015/04, Pacific Earthquake Engineering Research Center, Berkeley, CA, 1-10.

Goulet, C.A., C.H. Cramer, R.B. Darragh, W.J. Silva, Y.M.A. Hashash, J. Harmon, J.P. Stewart, K.E. Wooddell, and R.R. Youngs (2014). *PEER NGA-East database*, PEER Report No. 2014/17, Pacific Earthquake Engineering Research Center, Berkeley, CA.

Graizer, V. (2015). Ground-Motion Prediction Equations for the Central and Eastern United States, in *NGA-East: Median Ground-Motion Models for the Central and Eastern North America Region*, Chap. 9, PEER Report No. 2015/04, Pacific Earthquake Engineering Research Center, Berkeley, CA, 213-249.

Hassani, B., and G.M. Atkinson (2015). Referenced Empirical Ground-Motion Model for Eastern North America, *Seism. Res. Lett.* **86,** 477-491.

Hassani, B., and G.M. Atkinson (2016a). Applicability of the site fundamental frequency as a V_{S30} proxy for Central and Eastern North America, *Bull. Seismol. Soc. Am.* **106,** In press.

Hassani, B., and G.M. Atkinson (2016b). Applicability of the NGA-West2 Site Effects Model for Central and Eastern North America, *Bull. Seismol. Soc. Am.* **103,** In press.

Hollenback, J., N. Kuehn, C.A. Goulet, and N.A. Abrahamson (2015). PEER NGA-East Median Ground-Motion Models, in *NGA-East: Median Ground-Motion Models for the Central and Eastern North America Region*, Chap. 11, PEER Report No. 2015/04, Pacific Earthquake Engineering Research Center, Berkeley, CA, 273-309.

Idriss, I. (2014). An NGA-West2 empirical model for estimating the horizontal spectral values generated by shallow crustal earthquakes, *Earthq. Spectra.* **30,** 1155-1177.

Joyner, W.B., R.E. Warrick, and T.E. Fumal (1981). The effect of Quaternary alluvium on strong ground motion in the Coyote Lake, California, earthquake of 1979, *Bull. Seismol. Soc. Am.* **71,** 1333-1349.

Kawase, H., F.J. Sánchez-Sesma, and S. Matsushima (2011). The optimal use of horizontal-to-vertical spectral ratios of earthquake motions for velocity inversions based on diffuse-field theory for plane waves, *Bull. Seismol. Soc. Am.* **101,** 2001-2014.

Kim, B., Y.M. Hashash, E.M. Rathje, J.P. Stewart, S. Ni, P.G. Somerville, A.R. Kottke, W.J. Silva, and K.W. Campbell (2015). Subsurface shear-wave velocity characterization using P-wave seismograms in Central and Eastern North America, *Earthq. Spectra.* in press, DOI: http://dx.doi.org/10.1193/123013EQS299M.

Konno, K., and T. Ohmachi (1998). Ground-motion characteristics estimated from spectral ratio between horizontal and vertical components of microtremor, *Bull. Seismol. Soc. Am.* **88,** 228-241.

Kottke, A.R., Y. Hashash, J.P. Stewart, C.J. Moss, S. Nikolaou, E.M. Rathje, W.J. Silva, and K.W. Campbell (2012). Development of geologic site classes for seismic site amplification for central and eastern North America, *Proc. 15th World Conf. on Earthquake Eng.*, Lisbon, Portugal, 24–28 September 2012, Paper Number 4557.

Kramer, S.L. (1996). *Geotechnical earthquake engineering*, Prentice-Hall International Series in Civil Engineering and Engineering Mechanics, Prentice-Hall, Upper Saddle River, NJ.

Lermo, J., and F.J. Chávez-García (1993). Site effect evaluation using spectral ratios with only one station, *Bull. Seismol. Soc. Am.* **83,** 1574-1594.

Motazedian, D., J. Hunter, A. Pugin, and H. Crow (2011). Development of a Vs30 (NEHRP) map for the city of Ottawa, Ontario, Canada, *Can. Geotech. J.* **48,** 458-472.

Murphy, C., and D. Eaton (2005). Empirical site response for POLARIS stations in southern Ontario, Canada, *Seism. Res. Lett.* **76,** 99-109.

Nakamura, Y. (1989). A method for dynamic characteristics estimation of subsurface using microtremor on the ground surface, *Q. Rep. Railway Tech. Res. Inst.* **30,** 25–30.

NEHRP (2000). NEHRP Recommended provisions for seismic regulations for new buildings and 550 other structures, Part 1, Provisions, FEMA 368, *Federal Emergency Management Agency, Washington, D.C*

Pezeshk, S., A. Zandieh, K.W. Campbell, and B. Tavakoli (2015). Ground motion prediction equations for CENA using the hybrid empirical method in conjunction with NGA-West2 empirical ground motion models, in *NGA-East: Median Ground-Motion Models for the Central and Eastern North America Region*, Chap. 5, PEER Report No. 2015/04, Pacific Earthquake Engineering Research Center, Berkeley, CA, 119-147.

Seyhan, E., and J.P. Stewart (2014). Semi-empirical nonlinear site amplification from NGA-West2 data and simulations, *Earthq. Spectra.* **30,** 1241-1256.

Seyhan, E., J.P. Stewart, T.D. Ancheta, R.B. Darragh, and G.R. W (2014). NGA-West2 Site Database, *Earthq. Spectra.* **30,** 1007-1024.

Shahjouei, A., and S. Pezeshk (2015). Hybrid Empirical Ground-Motion Model for Central and Eastern North America using Hybrid Broadband Simulations and NGAWest2 GMPEs, in *NGA-East: Median Ground-Motion Models for the Central and Eastern North America Region*, Chap. 7, PEER Report No. 2015/04, Pacific Earthquake Engineering Research Center, Berkeley, CA, 165-192.

Shearer, P.M., and J.A. Orcutt (1987). Surface and near-surface effects on seismic waves theory and borehole seismometer results, *Bull. Seismol. Soc. Am.* **77,** 1168-1196.

Thompson, E.M., and W.J. Silva (2013). Empirical assessment of site amplification and development of NEHRP factors for CEUS: collaborative research with Pacific Engineering and Tufts University, Report to USGS, *http://earthquake.usgs.gov/research/external/reports/G12AP20003.pdf*.

Wald, D.J., and T.I. Allen (2007). Topographic slope as a proxy for seismic site conditions and amplification, *Bull. Seismol. Soc. Am.* **97,** 1379-1395.

Yenier, E., and G.M. Atkinson (2015). Regionally adjustable generic ground-motion prediction equation based on equivalent point-source simulations: Application to central and eastern North America, *Bull. Seismol. Soc. Am.* **105,** 1989-2009.

Yong, A., S.E. Hough, J. Iwahashi, and A. Braverman (2012). A terrain-based site-conditions map of California with implications for the contiguous United States, *Bull. Seismol. Soc. Am.* **102,** 114-128.

Zhao, J.X., K. Irikura, J. Zhang, Y. Fukushima, P.G. Somerville, A. Asano, Y. Ohno, T. Oouchi, T. Takahashi, and H. Ogawa (2006a). An empirical site-classification method for strong-motion stations in Japan using H/V response spectral ratio, *Bull. Seismol. Soc. Am.* **96,** 914-925.

Zhao, J.X., J. Zhang, A. Asano, Y. Ohno, T. Oouchi, T. Takahashi, H. Ogawa, K. Irikura, H.K. Thio, P.G. Somerville, and others (2006b). Attenuation relations of strong ground motion in Japan using site classification based on predominant period, *Bull. Seismol. Soc. Am.* **96,** 898-913.

Chapter 5

5 Site effects model for central and eastern North America based on peak frequency[5]

In the last chapter we showed the inadequacy of the western site-effects models which are V_{S30}-based (time-averaged shear-wave velocity in the upper 30 m) when applied to sites in central and eastern North America (CENA). We also showed the importance of the site fundamental frequency (f_{peak}) as a site indicator for sites in CENA. In this chapter, we develop a regional site-effects model for CENA based on an analysis of the residuals of observed ground-motion parameters relative to two regional ground-motion prediction equations (GMPEs): one model has a hard-rock (site class A) reference site condition while the other is referenced to B/C boundary site condition (site classification of National Earthquake Hazard Reduction Program). We derive an f_{peak}-based site amplification model with respect to B/C and hard-rock reference site conditions. Implementing the f_{peak}-based model, we reduce random variability in amplitudes (sigma) by 10% on average, for a selected database from the Next Generation Attenuations-East (NGA-East) Project, relative to the value obtained when using a generic site effects model parameterized by V_{S30}.

5.1 Introduction

Ground-motion prediction equations (GMPEs) are a widely-used tool in seismic hazard analysis. GMPEs describe ground-motion amplitudes as a function of explanatory variables characterizing the effects of source, path and site. An important issue in GMPE development is the definition of a site effects model that will capture the salient effects of the surficial geology and topography, using very limited site-specific information. Common site parameters in modern empirical GMPE models include site fundamental frequency (f_{peak}) (e.g. Zhao et al., 2006b) and time-averaged shear-wave velocity in the upper 30 m (V_{S30}) (e.g. Boore et al., 2014). V_{S30} is currently the most prevalent site

[5] A version of this chapter has been submitted for publication. Hassani, B., and G.M. Atkinson (2016). Site Effects Model for Central and Eastern North America Based on Peak Frequency, *Bull. Seismol. Soc. Am.* Submitted.

parameter in GMPE models; it provides a good index of the site stiffness that can be obtained by a site-specific study or estimated using a proxy such as topographic slope (Wald and Allen, 2007). However, the uncertainty in the GMPE model is affected by the use of a single-index parameter to describe a range of geological conditions; that uncertainty is compounded when the value of the index parameter is estimated based on a proxy.

An example of recent empirical GMPEs which use V_{S30} as the site indicator is the set of Next Generation Attenuation-West (NGA-West2) models (e.g Abrahamson et al., 2014; Boore et al., 2014; Campbell and Bozorgnia, 2014; Chiou and Youngs, 2014; Idriss, 2014), developed for shallow crustal earthquakes in active tectonic regions (Bozorgnia et al., 2014). In all of the NGA-West2 models the linear component of the site response scales with the logarithm of V_{S30}. Another example of recent empirical GMPEs which use V_{S30} as the site indicator is the Next Generation Attenuation-East (NGA-East) project which produced a set of GMPE models applicable for shallow crustal earthquakes in stable tectonic regions, specifically central and eastern North America (CENA) (Goulet et al., 2015). In the absence of a well-calibrated regional site effects model for CENA, many of the NGA-East GMPE modelers used a western-based site effects model based on V_{S30}, such as that of Seyhan and Stewart (2014), to level the observed ground-motion amplitudes in CENA to a common reference site condition (e.g.(Hassani and Atkinson, 2015; Pezeshk et al., 2015; Shahjouei and Pezeshk, 2015; Yenier and Atkinson, 2015). However, it is not clear if the assumed site response model is applicable to CENA. V_{S30}-based site amplification models were originally developed based on empirical observations that show how the amplification of ground motion behaves in California (Borcherdt, 1994), where the crust has been recently shaped by active tectonism, and where alluvial soils transition gradually to rock as depth increases, often without any sharp interface between soil and rock.

There are numerous studies which have questioned the applicability of V_{S30} as an appropriate site condition indicator (e.g. Castellaro et al., 2008; Kokusho and Sato, 2008), especially for: (i) sediments deeper than 30 m; (ii) shallow sediments overlying a much harder layer, which results in resonant response in the intermediate-to-high frequency

band; and (iii) sites with complex geology or topography. The most-commonly proposed alternative site variables are those that take account of sediment thickness, either directly or through the site fundamental frequency (f_{peak}; inversely related to the sediment thickness) (e.g Rodriguez-Marek et al., 2001; Cadet et al., 2010). Zhao et al. (2006a) used horizontal-to-vertical spectral ratios to classify sites in Japan. Fukushima et al. (2007) used the same scheme for a database composed mainly form European earthquakes. In another study, Di Alessandro et al. (2012) modified the site classification of Zhao et al. (2006a) to characterize sites in Italy. A more detailed classification scheme was recently proposed by Pitilakis et al., (2012, 2013) which uses geotechnical parameters such as standard penetration test blow count, plasticity index and undrained shear strength, in combination with site fundamental frequency, sediment thickness and average shear-wave velocity, in deriving normalized response spectra for different site classes.

CENA has been tectonically stable over the last several hundred million years, resulting in competent crustal conditions that are generally characterized by high velocities and low attenuation. There are many regions in which post-glacial soils, which may be shallow or deep, overlie a much harder glaciated bedrock surface, providing a sharp impedance contrast and setting up the conditions for strong amplification at the fundamental frequency of the site. Moreover, in the NGA-East database only 6% of the recording stations have measured V_{S30} values (Goulet et al., 2014). Over 90% of the reported V_{S30} values are derived from proxy-based estimates such as topographic slope (Wald and Allen, 2007) and surface-geology (Kottke et al., 2012), carrying with them large estimation uncertainties (0.20 to 0.25 $\log_{10}$ units) (Goulet et al., 2014). Thus even an appropriate regional V_{S30}-based model would potentially transfer the large measurement uncertainties in V_{S30} into GMPE uncertainties.

Hassani and Atkinson (2016b) explored this issue by using the NGA-East database to plot residual site terms, relative to a CENA GMPE as given for B/C site condition, as a function of the site fundamental frequencies (f_{peak}). (Note: B/C is a NEHRP [National Earthquake Hazard Reduction Program, 2000] site condition given by V_{S30} = 760 m/s). They observed significant residual trends in f_{peak} at all frequencies. The residual site terms can be as large as 0.45 in $\log_{10}$ units of amplitude (nearly a factor of 3) around $f \approx f_{peak}$.

This demonstrates the importance of f_{peak} as a site indicator for recording stations in CENA, and provided the motivation for the current study.

In this study, we develop f_{peak}-based site amplification models for CENA based on the analysis of residuals obtained relative to two CENA GMPE models. The first GMPE model is the Yenier and Atkinson (2015) (YA15) model developed for B/C site condition in CENA. YA15 is a simulation-based generic GMPE that has been calibrated to match the NGA-East database, after first using the Seyhan and Stewart (2014) (SS14) site effects model to level all amplitudes to B/C site condition (and thus implicitly assuming that the SS14 model is applicable to CENA). The second model is the Atkinson et al. (2015) GMPE model developed for hard-rock site condition (NEHRP site class A, with $V_{S30} > 1500$ m/s) in the region covered by the southern Ontario seismographic network (SOSN). The Atkinson et al. (2015) (SOSN) model is likewise a simulation-based GMPE model, and has the same magnitude scaling and geometrical spreading terms as the YA15 model.

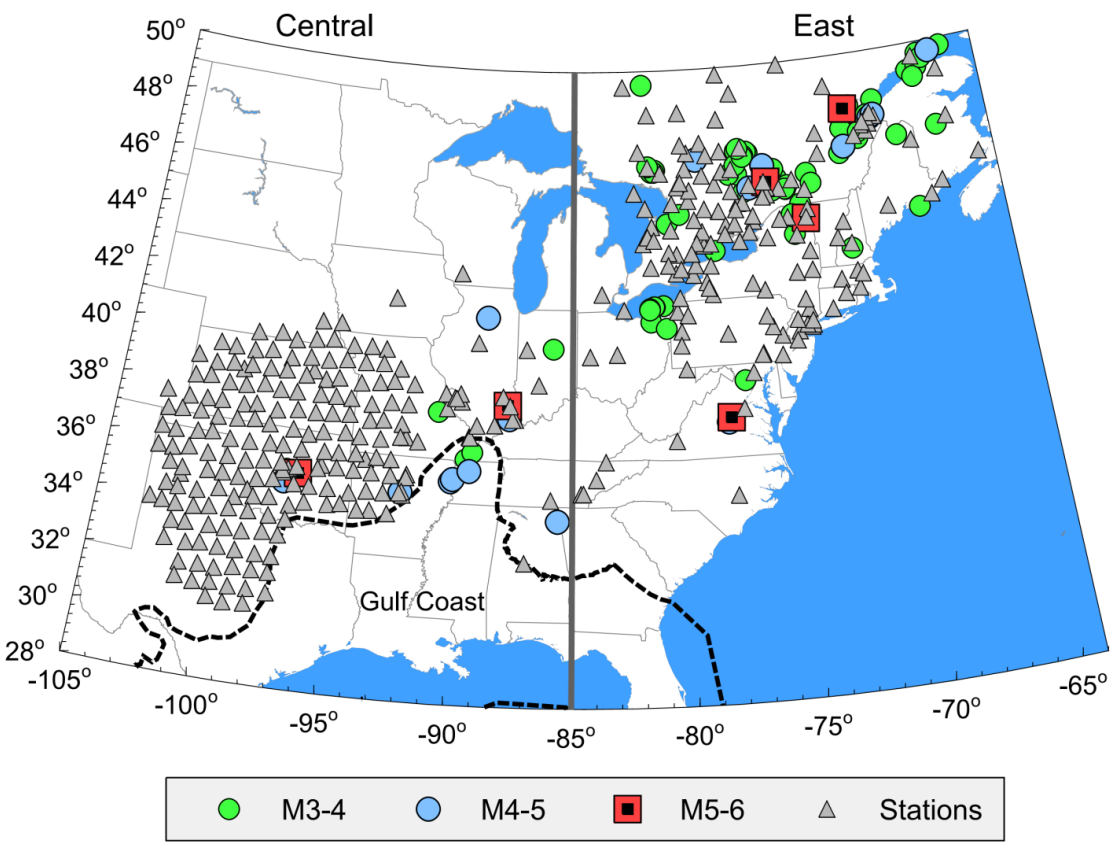

Figure 5.1: Epicenters of study events and locations of recording stations in the region. Dashed line represents the assumed Gulf coast boundary (Dreiling et al., 2014), and solid line shows the boundary between East and Central regions.

The key difference is that in the SOSN model, to adjust the observed amplitudes to the reference hard-rock site conditions that are typical of seismograph sites in eastern Canada, the site terms for non-rock sites were determined empirically, using the generalized inversion scheme proposed by Andrews (1986) (Atkinson et al., 2015). We know from these previous studies that both models are calibrated to match the empirical data, and will therefore have no significant residual trends in magnitude and distance (Atkinson et al., 2015; Yenier and Atkinson, 2015). The substantive difference between the two models is the different reference site condition (B/C versus hard-rock) (Atkinson et al., 2015; Yenier and Atkinson, 2015). What we wish to explore are the behavior of the residuals with respect to site effect variables not included in the models, specifically f_{peak} . Therefore, we analyze the residuals obtained relative to the two GMPE models (SOSN

and YA15) as a function of f_{peak}. For the SOSN GMPE, the identified residual trends represent unmodeled site amplification effects with respect to the reference hard-rock site condition. For the YA15 model the residual trends are referenced to B/C site conditions.

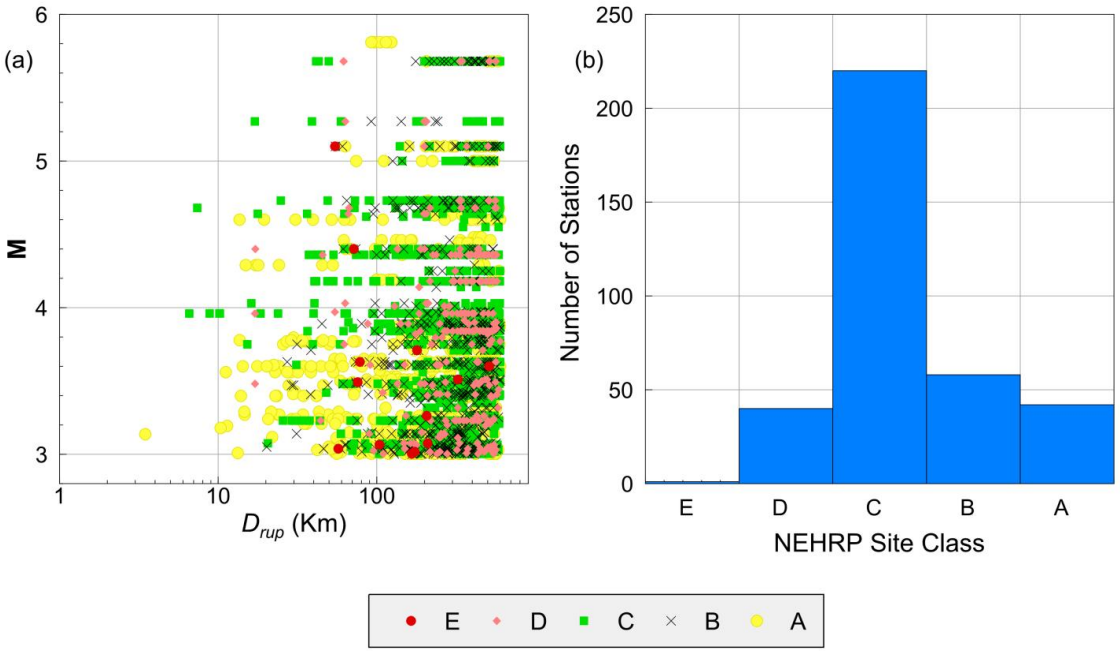

Figure 5.2: (a): Magnitude-distance distribution of study database; data points are shown with different symbols for NEHRP (National Earthquake Hazards Reduction Program) site classes (A: V_{S30} > 1500 m/s, B: 760 m/s < V_{S30} ≤ 1500 m/s, C: 360 m/s < V_{S30} ≤ 760 m/s, D: 180 m/s < V_{S30} ≤ 360 m/s and E: V_{S30} ≤ 180 m/s) (NEHRP, 2000): Histogram of number of stations in each of the NEHRP site classes.

5.2 Database

The ground-motion database of this study is the same as that used by Hassani and Atkinson (2015). In summary, most of the data comes from the NGA-East database (Goulet et al., 2014), which is supplemented by additional data from southern Ontario (See Section 5.5). The database includes horizontal-component peak ground-motion amplitudes (peak ground acceleration [PGA], peak ground velocity [PGV]) and response spectra (5% damped pseudoacceleration [PSA]) sampled at 16 equally log-spaced frequencies from 0.5 to 15.8 Hz. We use events having moment magnitude (**M**) greater

than 3 that were recorded on at least three stations with rupture distance $D_{rup} \leq 600$ km; we use only those stations that recorded at least three such events. Figure 5.1 is a map showing the locations of the events and stations in CENA. We excluded the Gulf Coast region (Figure 5.1) because of known deep sediments in this region which cause considerably different attenuation behavior (Electric Power Research Institute [EPRI], 2004; Dreiling et al., 2014). The database includes 3274 horizontal-component ground-motion parameter sets (PGA, PGV and PSA) from 118 events and 361 stations. Figure 5.2 shows the distribution of the database in magnitude-distance space, and by site class. The largest events in the CENA database have **M** < 6, and there are few observations at close distances (≤ 50 km). Therefore, we can assume that the rupture distance (D_{rup}) is equivalent to the hypocentral distance. We can also assume that site response effects are linear, as the number of records that might potentially include significant nonlinear effects is negligible.

Site fundamental frequencies (f_{peak}) and horizontal to vertical spectral ratios (H/V) were extracted from Hassani and Atkinson (2016a), who calculated these parameters from the same CENA response spectra database used in this study; thus the H/V ratios are for response spectra (not Fourier spectra). H/V spectral ratios are available for 353 of the stations (i.e. there are 353 stations that have the required minimum of three recordings), of which f_{peak} values are clearly observed for 192 stations.

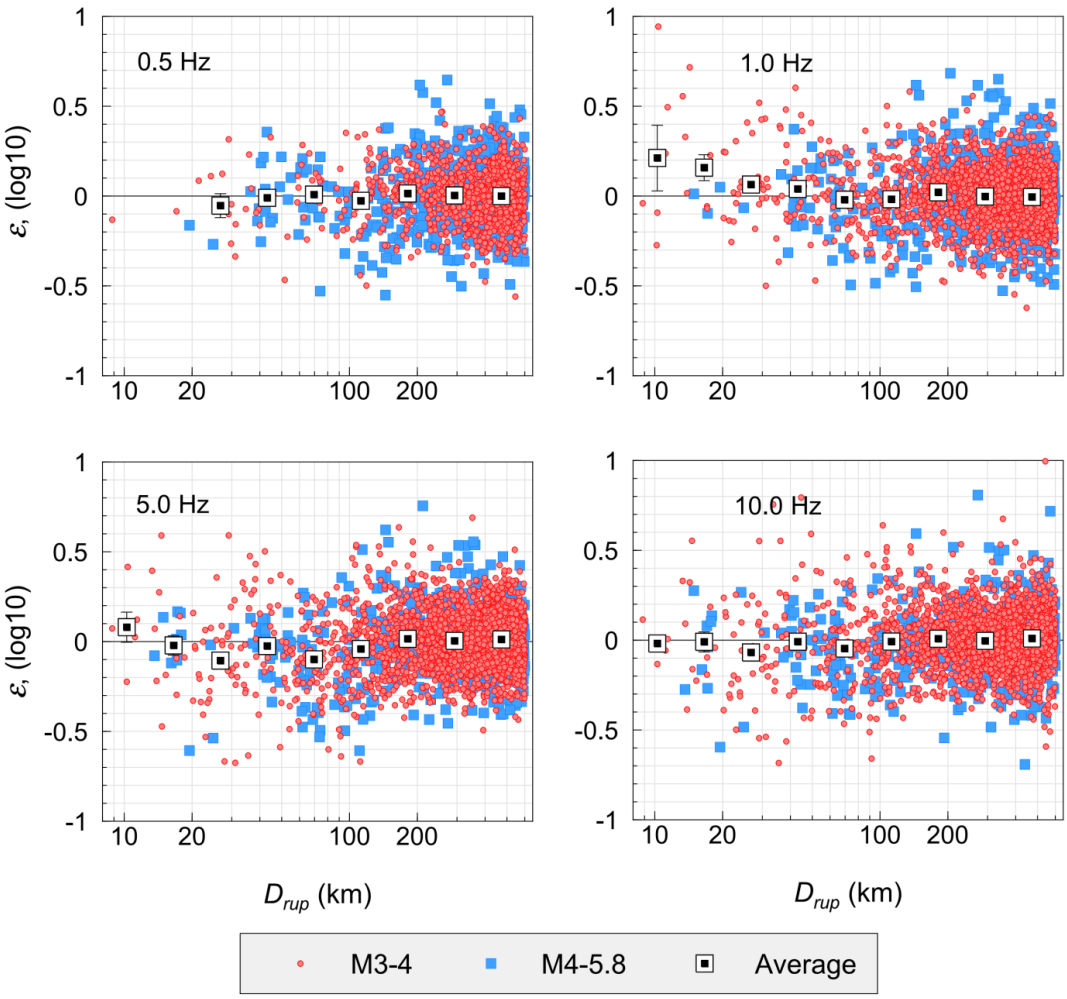

Figure 5.3: Within-event residuals (ε) as a function of rupture distance (D_{rup}) determined using the YA15 GMPE model (Yenier and Atkinson, 2015), classified for different magnitude bins and shown for four frequencies (0.5, 1.0, 5.0, and 10 Hz). Squares show the average residuals at equally log-spaced distance bins and their standard errors.

5.3 Determination of site terms

Site terms are determined for each station by analysing the residuals calculated from the observed ground-motion amplitudes with respect to the corresponding predictions from the two GMPE models. The predicted ground-motion amplitudes are obtained using the

Yenier and Atkinson (2015) GMPE model (YA15) for B/C reference site condition, and using the Atkinson et al. (2015) GMPE model (SOSN) for hard-rock site conditions (~ site class A). We define the residuals as:

$$\log(re_{ij}) = \log(obs_{ij}) - \log(pre_{ij}), \tag{5.1}$$

where re_{ij} is the residual estimated for event *i* at station *j* relative to either the YA15 or SOSN GMPE model, obs_{ij} is the observed ground-motion parameter, and pre_{ij} is the predicted ground-motion amplitude (by either YA15 or SOSN) for the corresponding record. We calculate the residuals for each of the ground-motion parameters (PGA, PGV, and PSA at different frequencies). The residuals obtained from Equation (5.1) can be written as:

$$\log(re_{ij}) = S_j + \eta_i + \varepsilon_{ij}, \tag{5.2}$$

where S_j is the site term for site *j* with respect to the reference site condition of the YA15 GMPE model (B/C site condition) or SOSN GMPE model (~ site class A), η_i is the random event term for event *i*, and ε_{ij} represents the within-event residual term for station *j* recorded at event *i*. To solve Equation (5.2), we apply a mixed effect regression of residuals according to Abrahamson and Youngs (1992) to find the variability parameters and the site terms for each of the GMPE models.

Figure 5.3 shows the within-event residuals (ε) as function of distance (D_{rup}) for the residuals calculated relative to YA15 GMPE model. The residuals are classified for different magnitude bins. The residuals do not show any apparent distance or magnitude dependency, and the average residual values attain a zero value at all distance bins, indicating good agreement between the model and the data. This is as we would expect because the YA15 model was calibrated to the observed data. The only exception is at near distances (D_{rup} < 30 km) at low frequencies (f < 1 Hz), where the YA15 model underestimates the sparse amplitude data on average by ~ 0.1 $\log_{10}$ units (~ 25%).

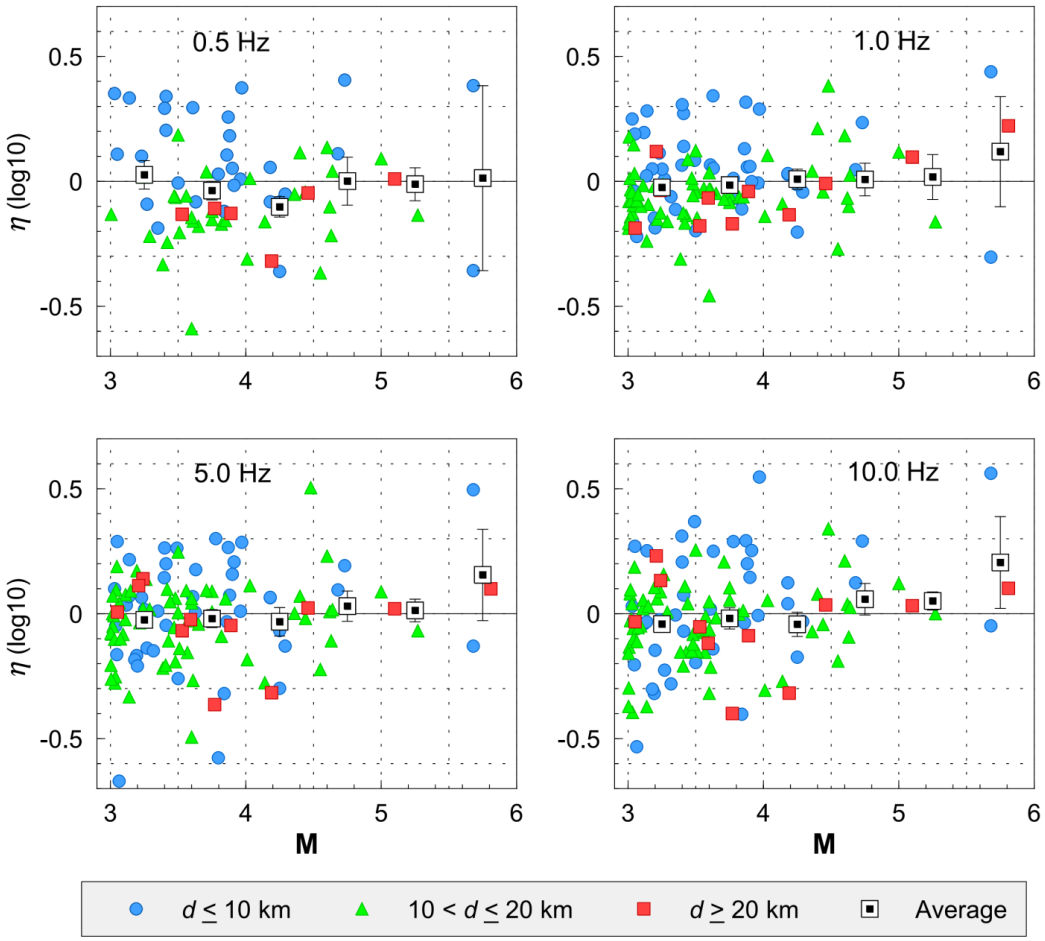

Figure 5.4: Between-event residuals (η) as a function of moment magnitude (M) determined using the YA15 GMPE model (Yenier and Atkinson, 2015), classified for different depth (d) bins. Squares show the average residuals at equally-spaced magnitude bins and their standard errors.

Figure 5.4 shows the between-event residuals η plotted as a function of moment magnitude (**M**) and classified for different depth bins for the YA15 GMPE model. The overall behavior of the residuals at all frequencies is satisfactory. However, we note that at 0.5 Hz for small magnitude events (**M** ≤ 3.5) there is a tendency to higher average residuals for shallow events (depth ≤ 10 km), though observations are sparse. For the SOSN GMPE model we also observe no apparent magnitude and distance dependency in

the within-event (ε) and between-event (η) residual terms, and the residual trends are well-behaved (not shown here; see Atkinson et al., 2015). As expected, the residuals suggest that the YA15 and SOSN GMPE models are well-calibrated, in that the assumed magnitude-scaling and attenuation functions are consistent with the observed ground-motion data in CENA.

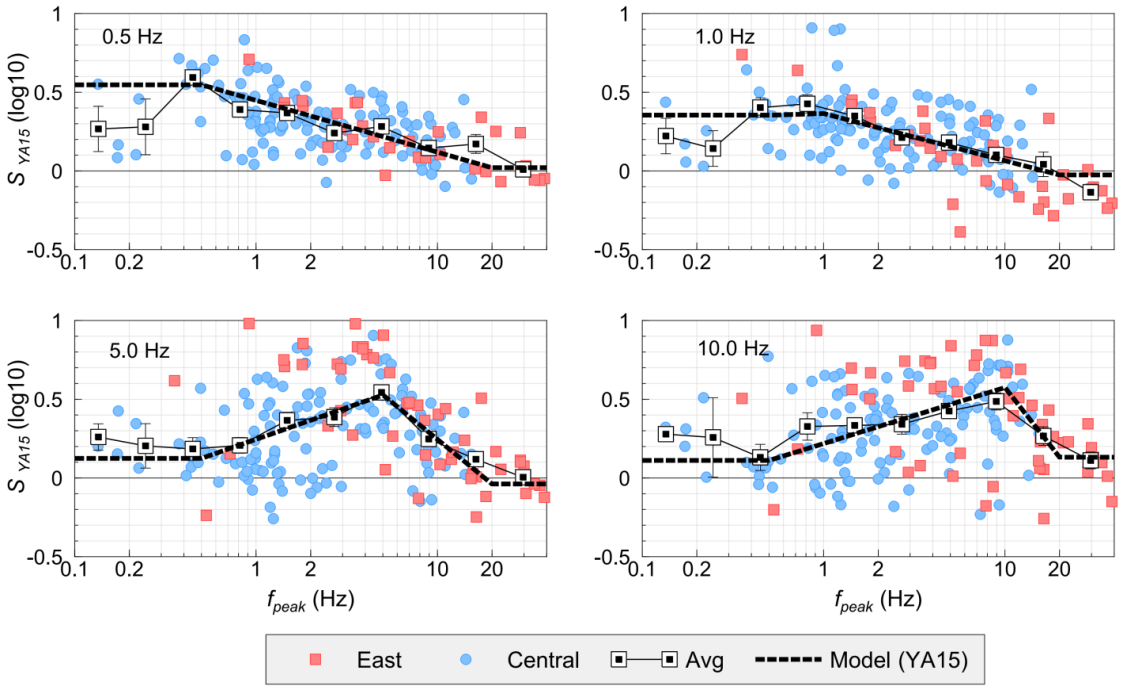

Figure 5.5: Site terms with respect to B/C reference site condition determined using the YA15 GMPE model (Yenier and Atkinson, 2015) (S_{YA15}) plotted versus their corresponding fundamental frequencies (f_{peak}), and classified for Central and East regions (as shown in Figure 5.1). Squares show the site term averages in equally log-spaced f_{peak} bins and their standard errors. Dashed lines show the f_{peak} -dependent site term model as given by Equation (5.3).

Figure 5.5 shows the site terms with respect to the B/C reference site condition that are obtained by plotting the residuals of the YA15 GMPE model (S_{YA15}, Equation 5.2) as a function of site fundamental frequency (f_{peak}); the site term model developed in the following section is also shown. The site terms have been averaged in equally log-spaced f_{peak} bins. Site terms are plotted with different symbols for East and Central regions

(Figure 5.1) to investigate any regional dependency. Sites in the Central region mostly have low to intermediate f_{peak} values (0.1 Hz< f_{peak} < 5 Hz), representing deep sediments, while sites in the East region mostly have intermediate to high f_{peak} values (f_{peak} > 5 Hz), representing shallow sediments. However, the overall f_{peak}-dependent trends are the same for both regions. As seen in the figure, the average of the site terms is almost constant for sites with $f_{peak} \leq 0.5$ Hz (very deep sediments), except at $f = 0.5$ Hz, for which the data are sparse. Site terms increase with increasing f_{peak} values, reaching the maximum value at $f_{peak} \approx f$; the peak amplification is approximately 0.5 in $\log_{10}$ units. Site terms decrease as we move away from $f_{peak} \approx f$, levelling off for sites with $f_{peak} \geq 20$ Hz (very shallow sediments). The observed trend implies that there is a dominant site fundamental frequency effect in the observed site terms at all frequencies, which was not captured by levelling the observations to B/C reference site conditions. It can also be noted that the scatter in the site terms increases at higher frequencies. This may reflect regional attenuation differences in the NGA-East database which have been mapped into the site terms. For instance, ground motions recorded in southern Ontario exhibit slightly lower anelastic attenuation compared to the rest of the NGA-East database (Atkinson et al., 2015), which is more apparent at higher frequencies (≥ 5 Hz). Moreover, there are many stations near the Gulf Coast boundary which may be partly affected by the high attenuation of the Gulf Coast region, and this effect could be mapped into the corresponding site terms at higher frequencies (≥ 5 Hz). Another explanantion for the observed scatter at higher frequeines could be that the wavefield is significantly affected by small-scale heterogeneities within the crust. Thus overall the scatter of the observed ground-motion amplitudes at higher frequencies tends to be relatively large.

Figure 5.6 shows the site terms with respect to hard-rock site condition (~site class A) as obtained by analyzing the residuals relative to the SOSN GMPE model (S_{SOSN}, Equation 5.2) as a function of site fundamental frequency (f_{peak}). The f_{peak} dependent trend of the site terms follows that observed for the YA15 GMPE model (Figure 5.5). However, the amplitudes of the site terms are different, because the reference site condition of the two GMPE models are different (hard-rock vs. B/C reference site condition). Relative to the

hard-rock SOSN model, site terms are almost constant for sites with $f_{peak} \leq 0.5$ Hz, they increase to their maximum value at $f_{peak} \approx f$, then they decrease at higher f_{peak} values, levelling off for sites with $f_{peak} \geq 20$ Hz.

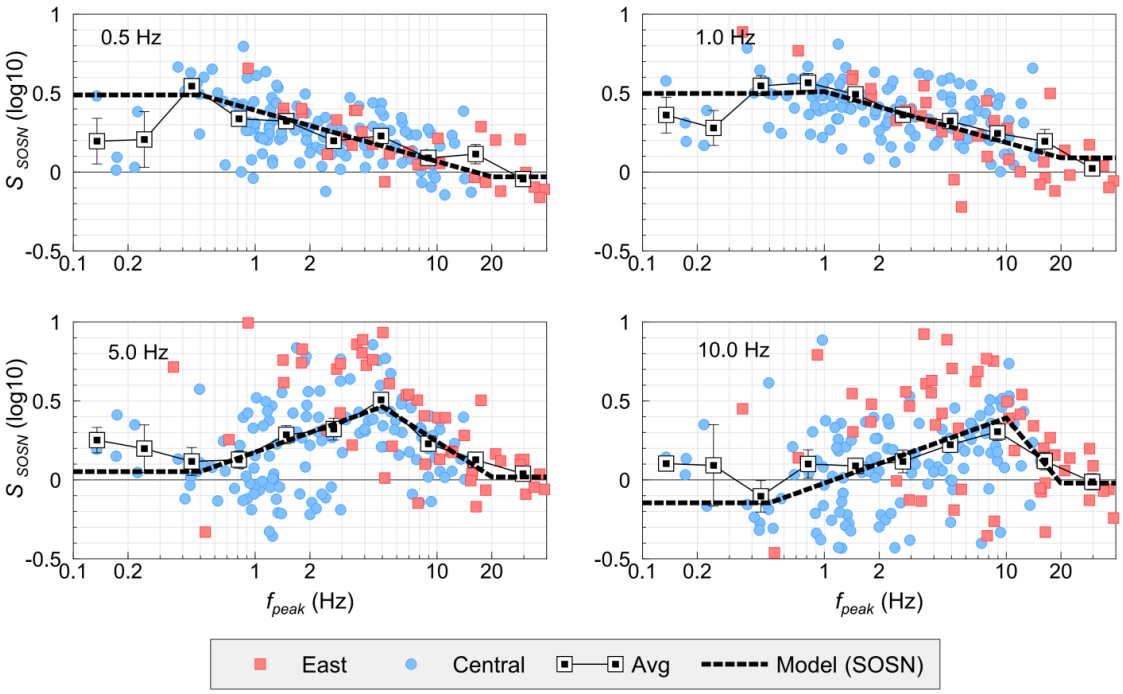

Figure 5.6: Site terms with respect to hard-rock reference site condition (~site class A) determined using the SOSN GMPE model (Atkinson et al., 2015) (S_{SOSN}) plotted versus their corresponding fundamental frequencies (f_{peak}), and classified for Central and East regions (as shown in Figure 5.1). Squares show the site term averages in equally log-spaced f_{peak} bins and their standard errors. Dashed lines show the f_{peak}-dependent site term model as given by Equation (5.3).

To shed more light on the site terms, we calculate the difference between the individual site terms with respect to hard-rock (site class A) as obtained using the SOSN GMPE model from Equation (5.2), and the corresponding individual site terms with respect to B/C reference site condition as obtained using the YA15 GMPE model (S_{SOSN} - S_{YA15}). This difference is equivalent to the ratio of the YA15 predicted ground-motion amplitude for B/C reference site conditions to the corresponding SOSN predicted ground-motion amplitude for hard-rock site conditions [e.g. $log10\ (pre_{YA15}/pre_{SOSN})$] and thus is a

measure of the average amplification of B/C sites in CENA relative to hard-rock sites. The individual site term differences, as well as their frequency-binned averages and the smoothed averages (using a weighted 5-point moving average function), are shown in Figure 5.7. We also show the conversion factors proposed by Boore (2015) for adjusting the ground-motion amplitudes for different reference site conditions in CENA. Boore (2015) (B15) calculated the expected value of the adjustment factors needed to convert ground-motion amplitudes at sites with V_{S30} = 760 m/s and V_{S30} = 2000 to equivalent values for sites with V_{S30} = 3000 m/s (very hard rock), using the ratios of the simulated ground-motion amplitudes for the selected reference site condition; the simulations included the amplification through a typical shear-wave velocity profile specified for each reference condition. There is good overall consistency between the conversion factors obtained here ($C_{SOSN/YA15}$) and their expected values based on Boore's simulations assuming near-surface attenuation of κ_0= 0.03 s (using the Atkinson (2004) attenuation model). We note that the κ_0 for the reference site condition of the SOSN GMPE (hard-rock) is close to the value assumed by Boore (2015) ($\kappa_0 = 0.006$)for hard-rock, while the assumed κ_0 for the YA15 GMPE model is 0.025 s. Therefore the comparison with Boore's simulations for κ_0= 0.03 s is appropriate. The observed discrepancies may reflect differences in the shear wave velocity profiles assumed in the simulations and those assumed for the selected GMPE models of this study (SOSN and YA15).

The apparently-strong influence of f_{peak} on the site terms motivates us to use the horizontal-to-vertical component response spectral ratio (H/V) as a site term index variable. The implicit assumption of this method is that the horizontal components of ground motions are amplified around the fundamental frequency of a site, while the vertical-component of ground motion experiences much less amplification (Nakamura, 1989; Lermo and Chávez-García, 1993). Therefore, the H/V ratio provides a good estimate of the dominant frequency and expected amplification of the site. We focus on the H/V from response spectra for simplicity and expediency, because our ultimate goal involves modeling ground motion in the response spectral domain. We use f_{peak} as calculated from the H/V spectral ratios by Hassani and Atkinson (2016b) for the NGA-East recording stations as a predictive variable for site response; these values are shown

in Figure 5.8. As we can see in the figure, the average of the H/V spectral ratios follows the same trends observed in the site terms obtained from the residual analysis of the YA15 and SOSN GMPE models, although with different amplitudes. We also observe that the scatter of the site terms obtained from H/V spectral ratios is significantly reduced at higher frequencies (≥ 5 Hz) compared to the site terms obtained from the GMPE models. This is probably because the propagation mechanism is similar for both components, and is effectively removed by taking the H/V ratio.

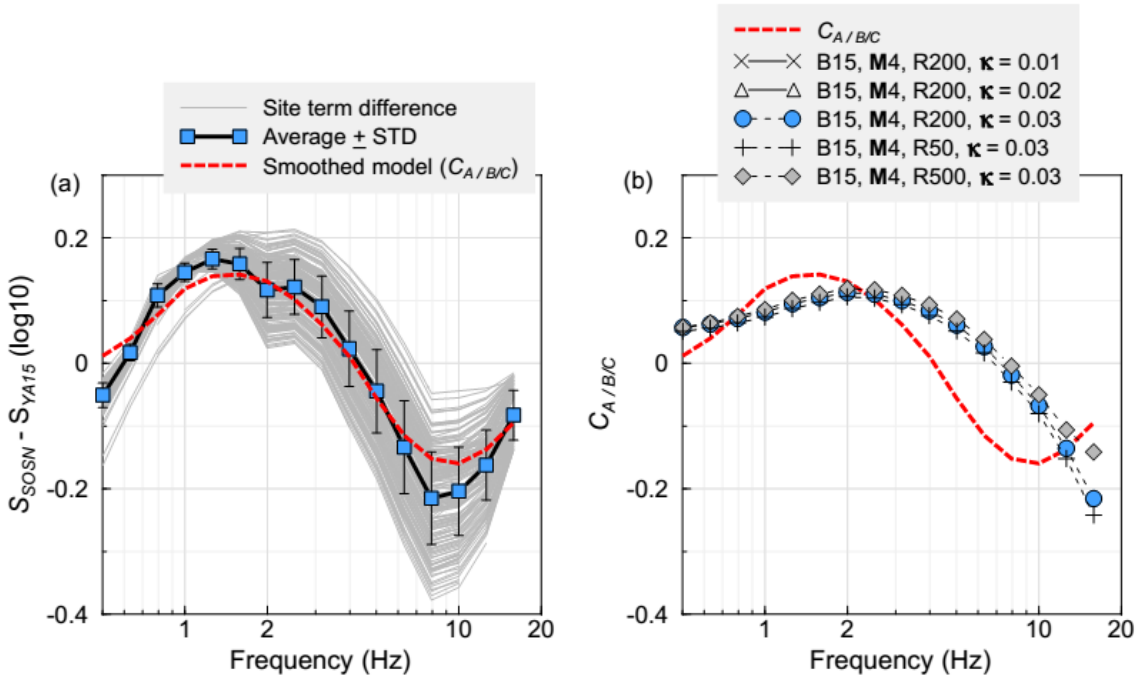

Figure 5.7: (a): Difference of the estimated site terms with respect to hard-rock site conditions (site class A) obtained using the SOSN GMPE model (Equation 5.2) and the site terms obtained with respect to B/C reference site condition obtained using the YA15 GMPE model (S_{SOSN} - S_{YA15}). The average values in equally log-spaced frequency bins and their corresponding standard deviations are also shown, as well as the smoothed model ($C_{A/B/C}$); (b): comparison between the empirical conversion ratio ($C_{A/B/C}$) and the simulation-based conversion ratio of Boore (2015) for M4 distances of 50, 200 and 500 km and kappa (κ_0) values of 0.01, 0.02 and 0.03 s (for sites with V_{S30} = 760 m/s relative to sites with V_{S30} = 2000 m/s, using the Atkinson (2004) attenuation model).

We define a f_{peak} -based site effects model $(C_s(f, f_{peak}))$ using a simple function to match the observed trends. As shown in Figure 5.9 we define:

$$C_s(f, f_{peak}) \tag{5.3}$$

$$= \begin{cases} C_1 & f_{peak} < 0.5\ Hz \\ C_1 + \left[\frac{C_2 - C_1}{log(f/0.5)}\right] \times \log(f_{peak}/0.5) & 0.5\ Hz \leq f_{peak} < f \\ C_2 + \left[\frac{C_3 - C_2}{\log(20/f)}\right] \times [\log(f_{peak}/f)] & f \leq f_{peak} < 20\ Hz \\ C_3 & 20\ Hz \leq f_{peak} \end{cases}$$

, where C_1 is the constant site term value for sites with f_{peak} < 0.5 Hz (very deep sediments), C_2 is the maximum site term value at $f_{peak} \approx f$, and C_3 is the constant site term value for sites with $f_{peak} \geq$ 20 Hz (very shallow sediments) (as shown in Figure 5.5, 5.6 and 5.8). We use L1-norm regression to find the coefficients for the site terms with respect to each of the GMPE models (SOSN and YA15), and also the site terms implied by the H/V spectral ratios. Figure 5.10, 5.11 and 5.12 show the frequency-dependent coefficients (C_1, C_2, and C_3), which are listed in Table 5.1. The coefficients are smoothed in the frequency domain by applying a weighted 5-point moving average smoothing function. The f_{peak} -based site term models for PGA and PGV are also shown. For PGV, the site terms are maximized for sites with $f_{peak} \approx$ 2 Hz, while for PGA the site terms are maximized for sites with $f_{peak} \approx$ 5 Hz. It may be noted that the PGA site terms and the 5 Hz site terms are quite similar (i.e. compare to Figures 5.5 and 5.6).

Using the defined site term model (Equation 5.3), we can determine the corresponding site amplifications for selected f_{peak} values. Figure 5.13 shows the site amplifications for various f_{peak} values relative to the SOSN and YA15 GMPE models for the applicable reference site conditions (Equation 5.3 and Table 5.1). Note that the amplifications are in non-log units. The site amplifications with respect to the SOSN model should be closer to the absolute site amplifications, in comparison to those with respect to the YA15 model, because of the difference in reference site conditions (A vs. B/C).

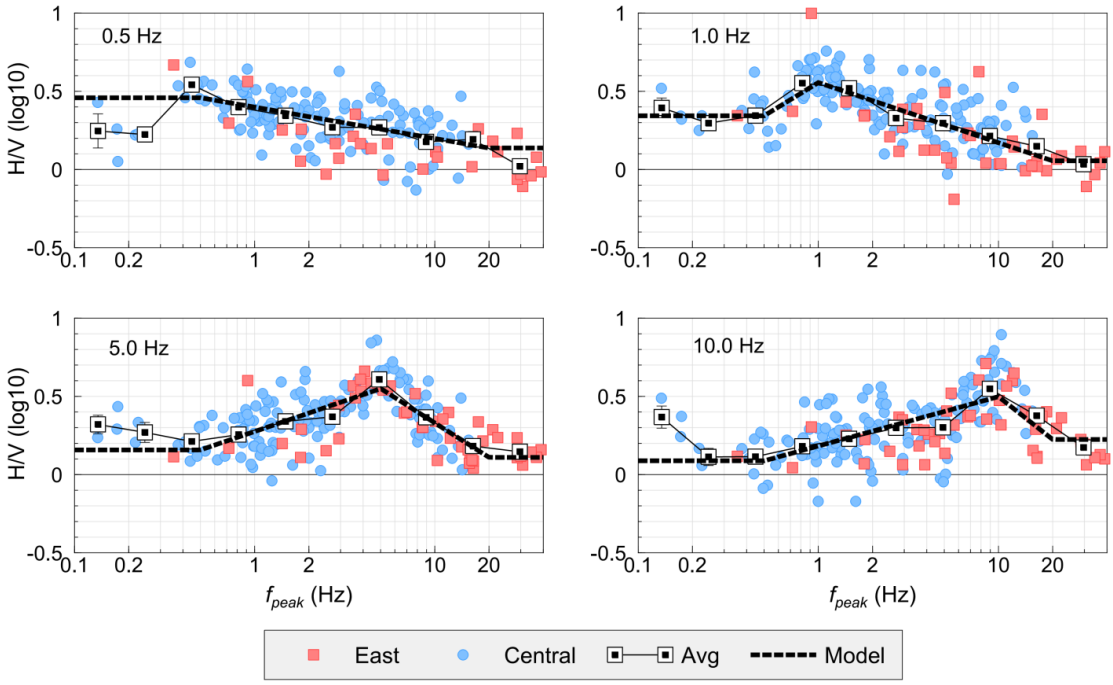

Figure 5.8: H/V spectral ratios extracted from Hassani and Atkinson (2016b) plotted versus their corresponding fundamental frequencies (f_{peak}), and classified for Central and East regions (as shown in Figure 5. 1). Squares show the H/V ratios averages in equally log-spaced f_{peak} bins and their standard errors. Dashed lines show the f_{peak} -dependent H/V model as given by Equation (5.3).

Based on the site term model (Equation 5.3) and its coefficients (Table 5.1), we can calculate the expected value of the H/V ratio at sites with known f_{peak} values, which is shown in Figure 5.14. We can also examine the degree of consistency between the site amplification estimated directly from H/V and that obtained using the GMPE-based models (Equation 5.2). We find the difference of the individual site terms with respect to site class A site condition as determined using the SOSN GMPE model (Equation 5.2) and the corresponding individual H/V spectral ratios (S_{SOSN}– H/V). We also find the difference of the individual site terms with respect to B/C site conditions as determined using the YA15 GMPE model (Equation 5.2) and the corresponding individual H/V spectral ratios (S_{YA15}– H/V). The average values of these differences, for each of the

reference site conditions, are also shown in Figure 5.14 ($C_{A/H/V}$ and $C_{B/C/H/V}$) and presented in Table 5.1. This quantity shows how good a job the H/V ratio does as a measure of the actual site amplification, and tells us something about how much amplification may exist on the vertical component. For the SOSN GMPE model (site terms relative to site class A reference site condition) ($C_{A/H/V}$), there is good agreement between the average site terms and H/V spectral ratios up to 4 Hz. At higher frequencies H/V spectral ratios tend to overestimate the site amplification term (with respect to hard-rock site condition), which may be due to relative difference in κ_0 effects on the horizontal and vertical components. For the corresponding comparison with the site amplification relative to theYA15 GMPE model ($C_{B/C/H/V}$), it is inferred that the H/V spectral ratios may overestimate the site terms at frequencies lower than 6 Hz. At higher frequencies there is good agreement between the two models, perhaps because κ_0 effects for B/C site conditions counterbalance the amplification on the vertical components.

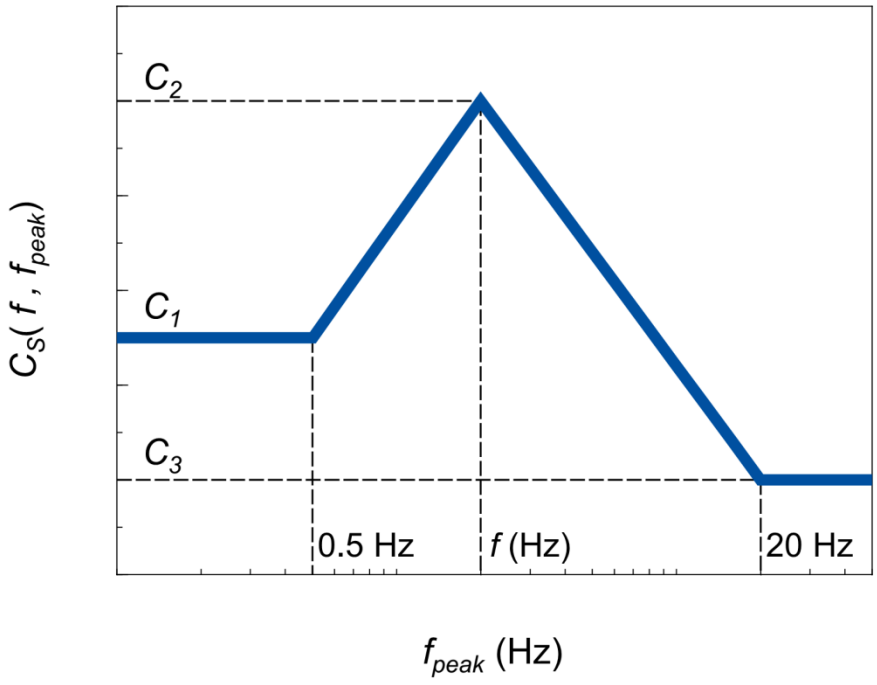

Figure 5.9: The proposed f_{peak}-based site term model (Equation 5.3).

Table 5.1: f_{peak} -based site term model coefficients (Equation 5.3) obtained with respect to B/C and site class A reference site conditions using the selected GMPE models (YA15 and SOSN). The corresponding coeffecients for f_{peak}-based H/V spectral ratio model are presented here too. The conversion factor between different reference site conditions are also shown here.

Frequency (Hz)	B/C ($\log_{10}$)			A ($\log_{10}$)			H/V ($\log_{10}$)			$C_{A/B/C}$ ($\log_{10}$)	$C_{A/HV}$ ($\log_{10}$)	$C_{B/C/HV}$ ($\log_{10}$)
	C_1	C_2	C_3	C_1	C_2	C_3	C_1	C_2	C_3			
PGV* (2 Hz)	0.19	0.45	-0.01	0.29	0.51	0.10	0.30	0.48	0.20	0.08	-0.02	-0.10
PGA* (5 Hz)	0.13	0.50	0.26	-0.02	0.34	0.19	0.21	0.44	0.32	-0.12	-0.12	0.00
0.50	0.50	0.50	0.04	0.51	0.51	0.04	0.40	0.40	0.11	0.01	-0.02	0.00
0.63	0.48	0.47	0.01	0.51	0.52	0.04	0.40	0.48	0.09	0.04	-0.01	-0.03
0.79	0.44	0.43	-0.02	0.51	0.52	0.05	0.39	0.52	0.08	0.08	0.02	-0.07
1.00	0.37	0.40	-0.06	0.49	0.52	0.06	0.36	0.56	0.06	0.12	0.02	-0.12
1.26	0.29	0.38	-0.09	0.43	0.52	0.06	0.31	0.57	0.06	0.14	0.01	-0.14
1.58	0.21	0.38	-0.13	0.34	0.52	0.04	0.27	0.59	0.06	0.14	-0.01	-0.16
2.00	0.16	0.40	-0.15	0.27	0.53	0.03	0.24	0.59	0.06	0.13	-0.02	-0.15
2.51	0.11	0.43	-0.14	0.19	0.52	0.02	0.22	0.59	0.07	0.10	-0.03	-0.14
3.16	0.10	0.46	-0.12	0.13	0.51	0.02	0.19	0.58	0.08	0.06	-0.04	-0.12
3.98	0.09	0.51	-0.09	0.07	0.51	0.00	0.16	0.57	0.10	0.01	-0.06	-0.08
5.01	0.09	0.55	-0.04	0.02	0.48	-0.01	0.15	0.55	0.11	-0.06	-0.10	-0.05
6.31	0.09	0.57	0.01	-0.04	0.44	-0.02	0.14	0.54	0.14	-0.11	-0.15	-0.01
7.94	0.09	0.57	0.06	-0.07	0.41	0.00	0.13	0.52	0.17	-0.15	-0.17	0.02
10.00	0.09	0.55	0.12	-0.07	0.38	0.04	0.12	0.49	0.22	-0.16	-0.16	0.03
12.59	0.09	0.48	0.17	-0.07	0.34	0.10	0.12	0.46	0.27	-0.14	-0.13	0.02
15.85	0.09	0.40	0.23	-0.07	0.31	0.19	0.12	0.42	0.33	-0.09	-0.03	0.05

* For PGV, the site terms are maximized at f_{peak} = 2 Hz and for PGA the site terms are maximized at f_{peak} = 5 Hz.

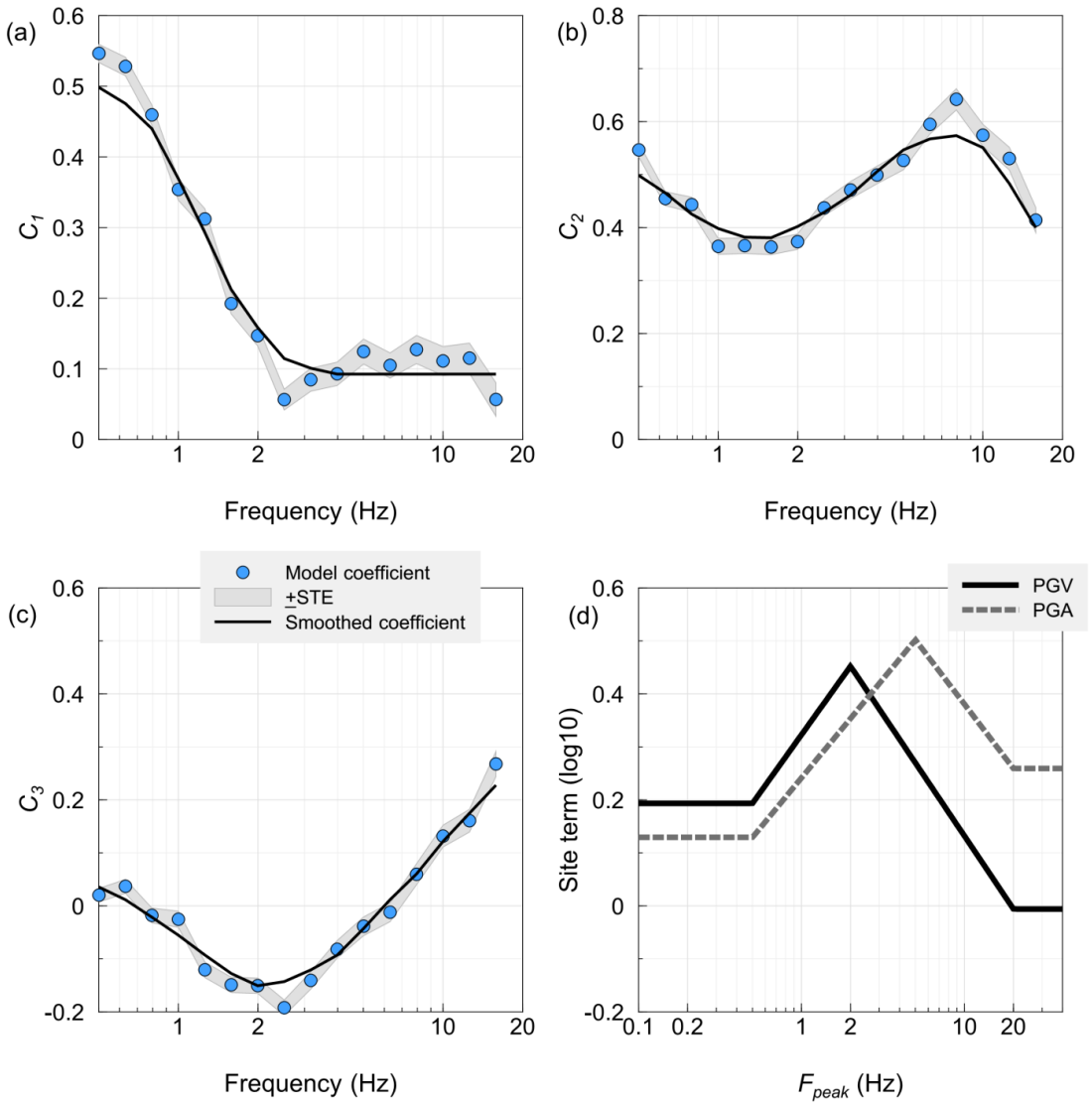

Figure 5.10: (a), (b) and (c): f_{peak} -based site term model coefficients with respect to B/C reference site conditions as determined for YA15 GMPE model, with their corresponding standard errors and smoothed coefficients; (d) residual model for PGV and PGA as a function of f_{peak} with respect to B/C reference site condition.

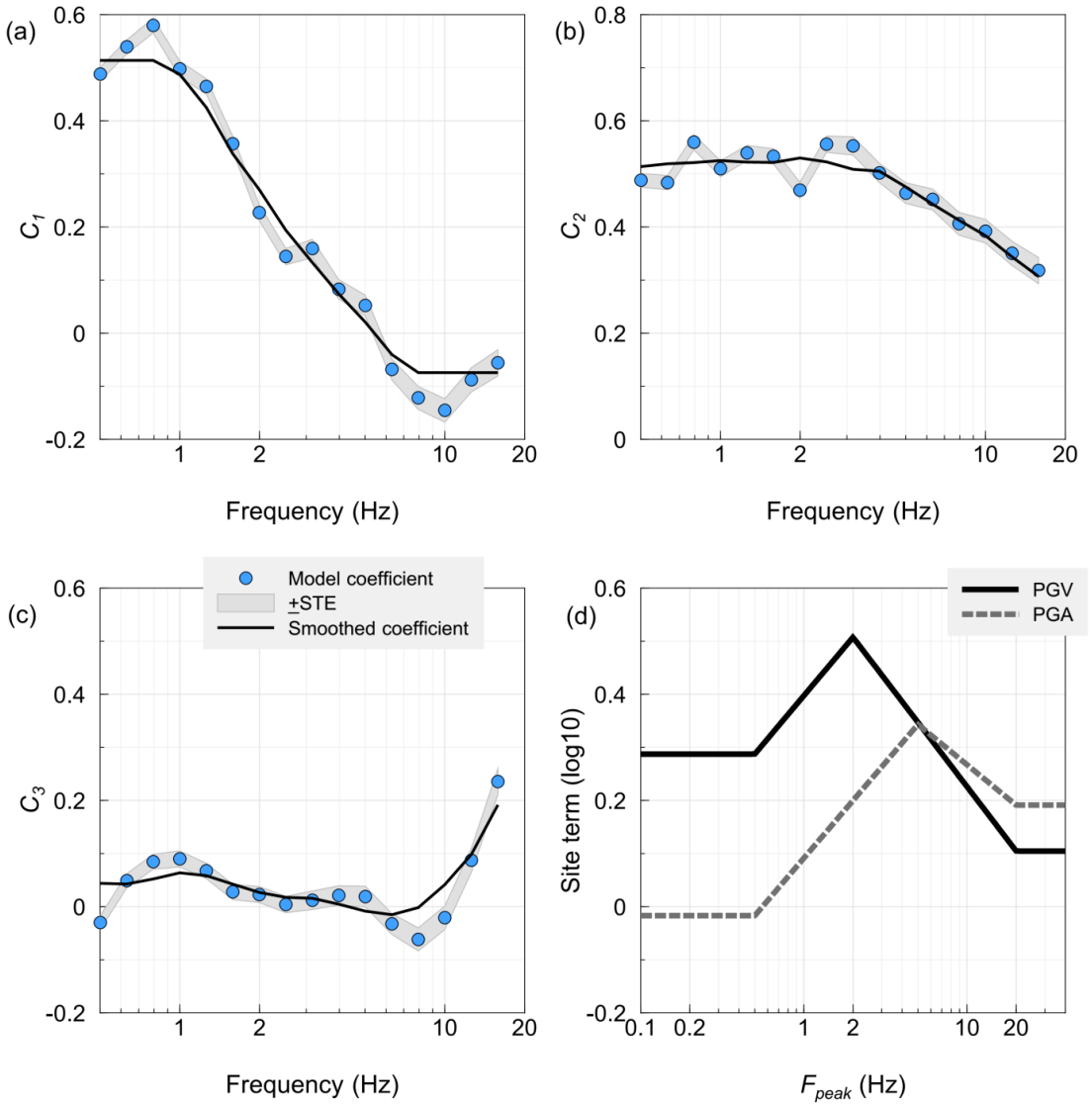

Figure 5.11: (a), (b) and (c): f_{peak} -based site term model coefficients with respect to hard-rock reference site conditions as determined for SOSN GMPE model, with their corresponding standard errors and smoothed coefficients; (d) residual model for PGV and PGA as a function of f_{peak} with respect to hard-rock reference site condition.

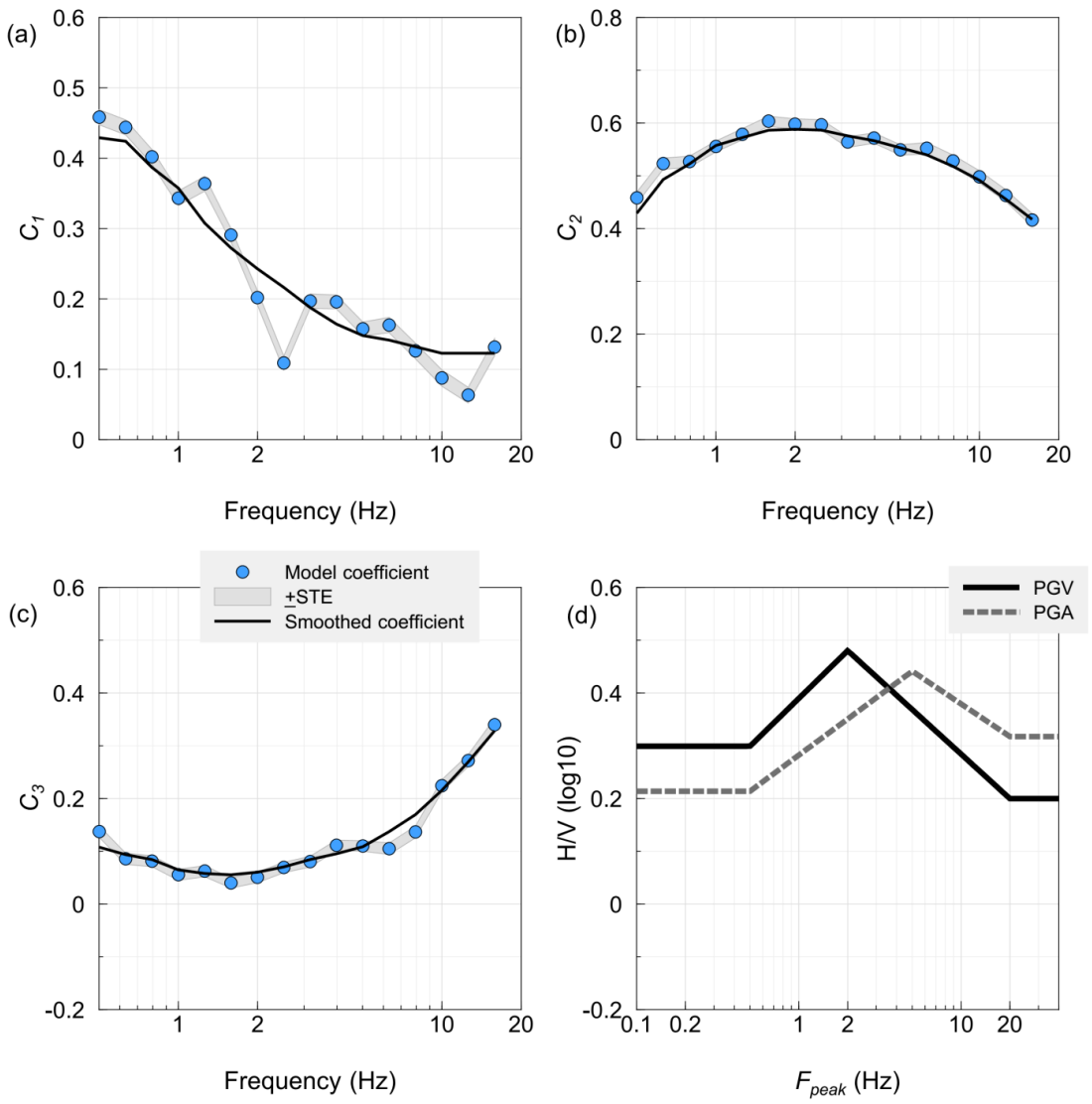

Figure 5.12: (a), (b) and (c): f_{peak} -based H/V model coefficients with their corresponding standard errors and smoothed coefficients; (d) H/V model for PGV and PGA as a function of f_{peak}.

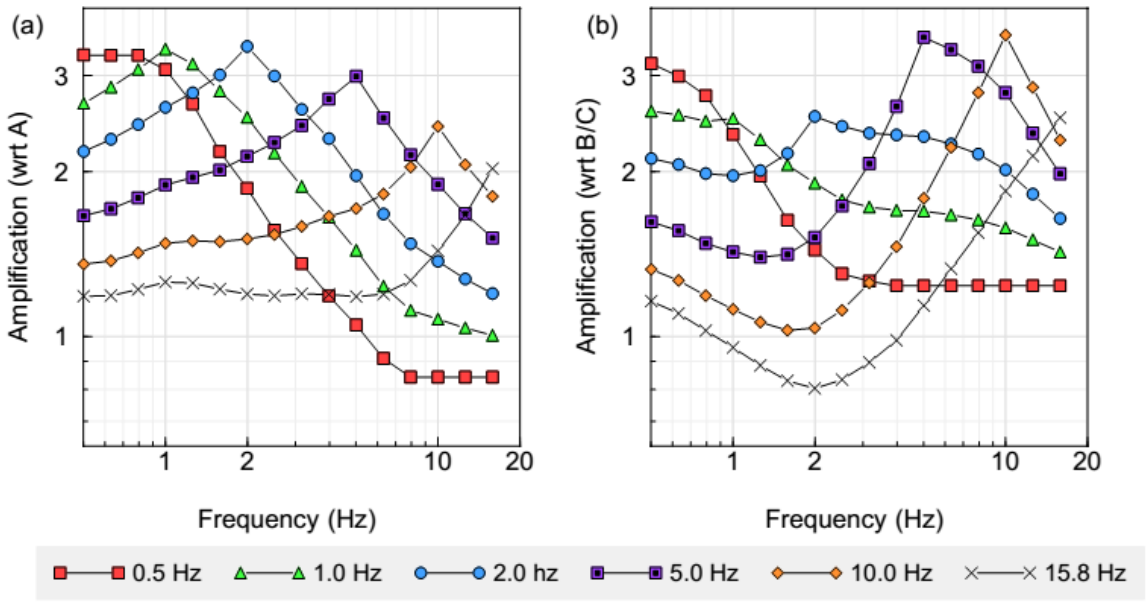

Figure 5.13: (a): f_{peak} -based site amplification with respect to site class A plotted for different f_{peak} values; (b): f_{peak}-based site amplification model with respect to B/C plotted for the same f_{peak} values. Note that the amplifications are in non-log units.

In Figure 5.15, we compare our f_{peak}-dependent site amplification model with that derived by Zhao et al. (2006b) using Japanese strong ground-motion data. Zhao et al. (2006b) regressed response spectral data to obtain a site amplification model using a classification proposed by Molas and Yamazaki (1995). Based on their classification, hard rock sites have no f_{peak} and V_{S30} > 1100 m/s; site class I (SC I) is the rock site condition including sites with f_{peak} > 5 Hz and V_{S30} > 600 m/s; site class II (SC II) is the hard soil site condition including sites with 2.5 Hz < f_{peak} ≤ 5 Hz and 300 < V_{S30} ≤ 600 m/s; site class III is the medium soil condition, including sites with 1.67 Hz < f_{peak} ≤ 5 Hz, and site class IV is the soft soil condition including sites with f_{peak} ≤ 1.67 Hz and V_{S30} ≤ 200 m/s. Zhao et al. (2006b) site amplifications are plotted with respect to SC I. We plotted our site amplification model with respect to site class A using the coefficients presented in Table 5.1 and Equation (5.3) for the same f_{peak} values reported by Zhao et al. (2006b) for each of the site classes, which are 1.1 Hz for SC IV, 2 Hz for SC III, 4 Hz for SC II, and 12 Hz for SC I. In order to derive a smooth amplification model, for each of the assumed f_{peak} values we implemented a Monte Carlo simulation assuming a log-normal distribution for

f_{peak} with arbitrary standard deviation of 0.1. We took the average of 1000 simulations and smoothed the final spectrum using a weighted 5-point moving average function. Comparing the two amplification models shows very similar shape for all of the site classes for frequencies lower than 10 Hz. Interestingly, the CENA sites show lower amplifications near 1 Hz, and higher amplifications near 4 Hz, relative to similar sites in Japan, pointing to the importance of regional factors in controlling site amplification. For frequencies higher than 10 Hz, Japanese sites have larger amplification than those in CENA. This may reflect the lower kappa values for rock in CENA (Silva, 1995) relative to Japan (Van Houtte et al., 2011).

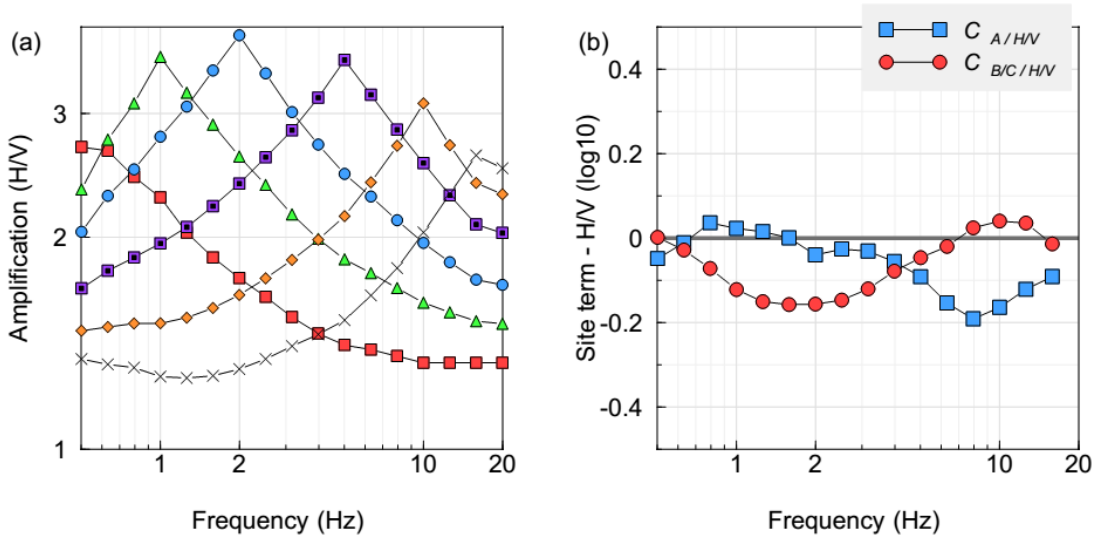

Figure 5.14: f_{peak} -based H/V spectral ratio model plotted for different f_{peak} values. Note that the amplifications are in non-log units. (b) Average difference of the estimated site terms with respect to site class A reference site condition (hard-rock) determined using the SOSN GMPE model (Equation 5.2) and the corresponding H/V spectral ratios ($C_{A\,/\,H/V}$) for individual stations; average difference of the estimated site terms with respect to B/C reference site condition determined using the YA15 GMPE model (Equation 5.2) and the corresponding H/V spectral ratios ($C_{B/C\,/\,H/V}$) for individual stations.

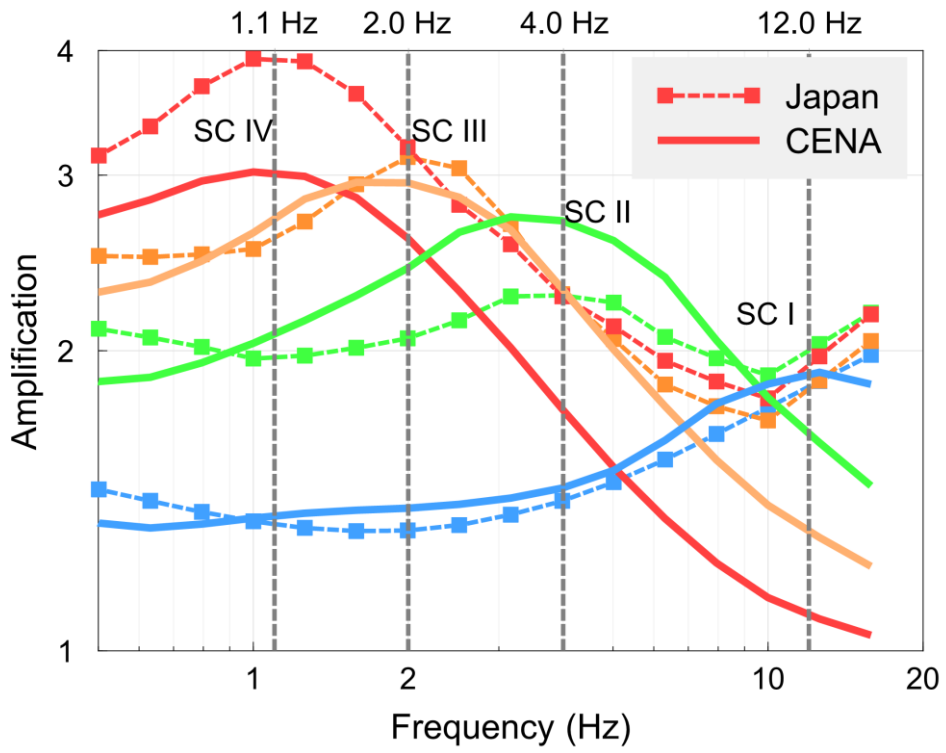

Figure 5.15: Comparison between the proposed f_{peak}-based amplification model of this study with respect to site class A and the amplification values derived by Zhao et al. (2006b) for four site classes in Japan (SC I, II, III, and IV) (with respect to SC I), based on the Molas and Yamazaki (1995) classification. Selected f_{peak} values for each of the site classes are shown with vertical dashed lines.

Finally, we compare the predicted response spectra for four NEHRP site classes (site class E assuming V_{S30} = 150 m/s, site class D assuming V_{S30} = 300 m/s, site class C assuming V_{S30} = 500 m/s, and site class B assuming V_{S30} = 900 m/s) for a typical weak-motion scenario, an event of **M**5 at 100 km, using two site amplification models. The first amplification model is the f_{peak}-based amplification model of this study with respect to B/C reference site conditions using the coefficients presented in of Table 5.1 and Equation (5.3). In order to obtain a smooth amplification model we perform a Monte Carlo simulation as discussed earlier and find the average of 1000 simulations. The second amplification model is the SS14 V_{S30}-based amplification function. To facilitate the comparisons we assume a simple soil profile, consisting of a single soil layer, less than 30 m thick, having layer velocity of V_L = 150, 250, 350, or 550 m/s overlying a hard

substratum with shear-wave velocity of V_R = 2000 m/s. Since $f_{peak} = V_L/ 4d_L$ (Kramer, 1996) for a single layer model, and $V_{S30} = 30/(d_L/V_L + d_R/V_R)$, in which d_L and d_R are the travel distances in the layer and rock, respectively, we can find combinations of f_{peak}, d_L and d_R such that we obtain V_{S30} = 150 m/s for site class E, V_{S30} = 300 m/s for site class D, V_{S30} = 500 m/s for site class C, and V_{S30} = 900 m/s for site class B. Figure 5.16 shows the response spectra for the four site classes using the YA15 GMPE model for an event with **M**5, depth of 10 km at *Drup* = 100 km, applying the SS14 V_{S30}-based amplification model for the assumed V_{S30} values (150, 300, 500 and 900 m/s), in comparison to the corresponding response spectra applying the f_{peak}-based amplification model of this study. For some of the site classes only a few V_L values provide combinations that obtain the target V_{S30} values. For example, for site class E with assumed V_{S30} = 150 m/s, the only applicable model is V_L = 150 m/s, d_L = 30 m , and d_R = 0 m. Therefore, in this case we only have one f_{peak} value for site class E (f_{peak} = 1.25 Hz). For most sites classes, alternative parameter combinations are possible for the target V_{s30}. The variation of f_{peak} values within each of the site classes for different parameter combinations is not significant. It is interesting to note that for site class E, the SS14 V_{S30}-based amplification model results in higher response spectral amplitudes in comparison with the response spectrum obtained using the f_{peak}-based model. For other site classes we observe similar response spectral amplitudes for frequencies lower than 2 Hz. However, for frequencies higher than 2 Hz, the SS14 amplification model underestimates the response spectral amplitudes relative to those suggested by the f_{peak}-based amplification model. Overall, we can clearly see how the site fundamental frequency can affect the shape and the amplitude of the response spectrum and amplify it around $f \approx f_{peak}$, an important feature of site response that is difficult to capture using a V_{S30}-based model.

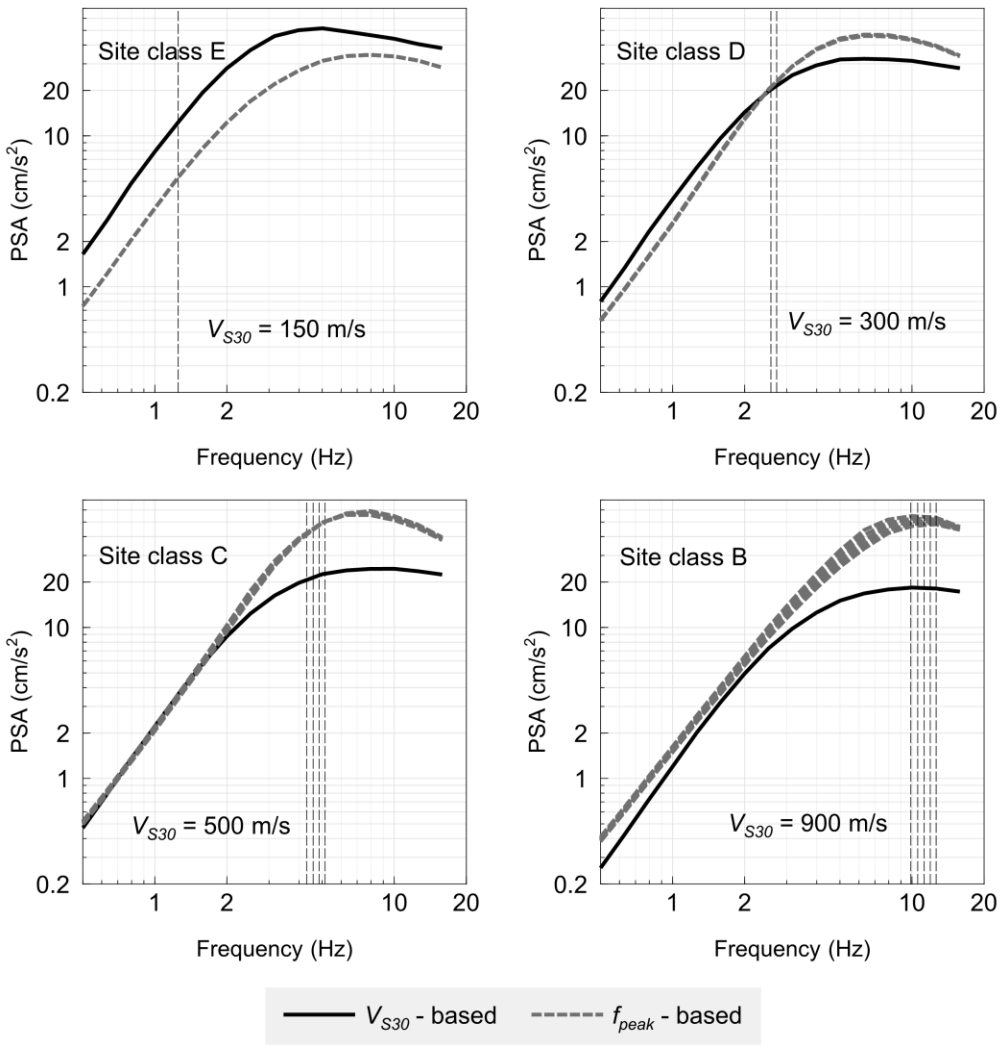

Figure 5.16: Comparison between the response spectra obtained from YA15 GMPE model for an event with M**5 and depth of 10 km at *Drup* = 100 km using two different site amplification models: f_{peak}-based amplification model of this study with respect to B/C site condition, and the SS14 V_{S30}-based amplification model. Comparison are made for four NEHRP site classes: E with V_{S30} = 150 m/s, D with V_{S30} = 300 m/s, C with V_{S30} = 500 m/s, and B with V_{S30} = 900 m/s. Vertical dashed lines shows the derived f_{peak} values assuming different sediment shear-wave velocities (V_L).**

5.3.1 Variability analysis

It is of interest to see how the f_{peak} -based site amplification model affects the sigma value (σ) of the selected GMPE models in comparison with V_{S30}- based site amplification models. In order to investigate that, we use the YA15 GMPE model, which is already adjusted for B/C site conditions using the SS14 (Seyhan and Stewart, 2014) NGA-West2 amplification model. We consider the variability for the subset of data comprised of stations with determined f_{peak} values.

We calculate the residuals in both cases:

$$\log(re_{ij,B/C}) = \log(obs_{ij,\,B/C}) - \log(pre_{ij,\,B/C}), \tag{5.4}$$

where $re_{ij,B/C}$ is the residual estimated for event *i* at station *j*, $obs_{ij,B/C}$ is the observed ground-motion parameter adjusted for B/C site condition using either the SS14 site amplification model or the f_{peak} -based site amplification model obtained for the YA15 GMPE (Equation 5.3 and Table 5.1), and $pre_{ij,B/C}$ is the predicted ground-motion parameter for B/C site condition for the corresponding record, according to YA15. The residuals can be written as:

$$\log(re_{ij,B/C}) = C + \eta_i + \varepsilon_{ij}, \tag{5.5}$$

where *C* is the bias of the selected GMPE model, η_i is the random event term for event *i*, and ε_{ij} represents the within-event residual term for station *j* recorded at event *i*. We apply a mixed effect regression of residuals according to Abrahamson and Youngs (1992) to solve Equation (5.5) and perform an iterative regression to maximize the likelihood of the equation. The error terms (η_i and ε_{ij}) are normally distributed (in $\log_{10}$ units) and have standard deviations τ and φ, respectively. The total standard deviation (σ) is:

$$\sigma = \sqrt{\tau^2 + \varphi^2}, \tag{5.6}$$

Figure 5.17 shows the sigma values in ln units (to be comparable with other GMPE developers models) for both of the amplification models. Using the proposed f_{peak} -based

site amplification model, we are able to reduce sigma by 10% on average for frequencies larger than 1 Hz in comparison to the sigma value we determined using the SS14 V_{S30}-based model. For frequencies lower than 1 Hz the reduction in sigma is not significant. This can be explained by the fact that western V_{S30}-based site amplification models correlate well with the estimated site terms in CENA at frequencies lower than 1 Hz, as pointed out by Hassani and Atkinson (2016a). The likely explanation is that site terms at low frequencies are controlled by deeper, more gradational soil profiles compared to site terms at high frequencies. The most important differences in soil profiles between WNA and CENA are that shallow-to-intermediate depth deposits are often underlain by a harder substratum in CENA, leading to significant amplification peaks that are particularly apparent at high frequencies.

To further investigate the variability reduction from the proposed f_{peak} -based site amplification model, we break down the within-event variability terms as follows (Al Atik et al., 2010):

$$\varepsilon_{ij} = \delta S2S_j + SWS_{ij}, \tag{5.7}$$

where $\delta S2S_j$ is the average site-to-site variability for station j, and SWS_{ij} is the within-site residual for event i at station j. The standard deviation of the site-to-site term is denoted as φ_{S2S}, and the standard deviation of within-site residuals (single-station sigma) is denoted as φ_{SS}. We perform another mixed-effect regression of residuals (Abrahamson and Youngs, 1992) to solve Equation (5.7). The variability terms obtained from Equation 5.6 (τ and φ) as well as the within-event variability terms obtained from Equation (5.7) (φ_{S2S} and φ_{SS}) are shown in Figure 5.15. As we observe here, the reduction in φ plays the main role in the reduction of sigma, because we have improved only the site amplification model. Moreover, by further breaking down the within-event terms it can be see that the almost all of the reduction in φ comes from the reduction in site-to-site variability (φ_{S2S}) and not the within-site variability. We are able to reduce φ_{S2S} on average by 20% for frequencies between 1 and 10 Hz.

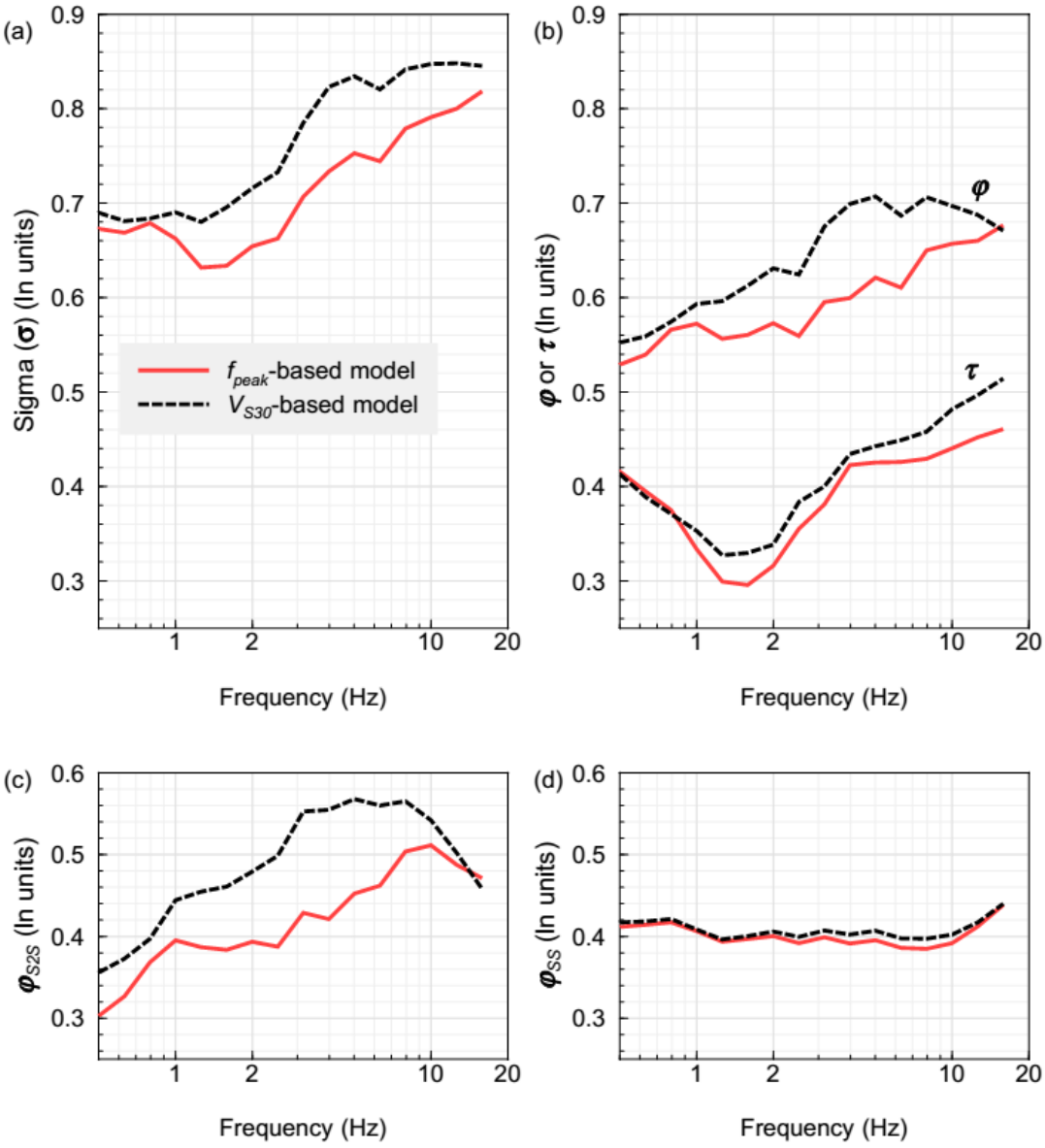

Figure 5.17: Comparison of variability parameters for the YA15 GMPE model for two different site amplification models; the f_{peak} -based model (Equation 5.3), and the SS14 site amplification model (Seyhan and Stewart, 2014).

5.4 Conclusion

Site amplification models based on V_{S30} are common in modern GMPE models, but their applicability in CENA is marginal, as the site terms for many of the sites reflect a strong effect of the site fundamental frequency. In this study, we developed an f_{peak} -based site

effects model for CENA by analyzing the residuals for two regional GMPE models (YA15 and SOSN), referenced to B/C site condition (V_{S30} = 760 m/s) and hard-rock site condition (V_{S30} ≈ 2000 m/s, ~ site class A), respectively. We showed that sigma (σ) can be reduced by 10% using the f_{peak} -based model instead of a V_{S30}-based model. This reduction is largely attributeable to a 20% reduction in the site-to-site variability terms (φ_{S2S}). We note that the derived amplification model is only applicable for linear site effects. In cases where nonlinearity effects could be significant (e.g. large magnitude events at nearby distances), a nonlinear amplification model from other studies should be implemented to adjust the amplification level. An important factor that was ignored in our site term parameterization was the effect of the sediment stiffness (e.g. average shear-wave velocity of the sediment layer) on the observed site terms. Although site fundamental frequency inherently carries some corresponding sediment stiffness information (e.g. $f_{peak} = V_L/4d_L$), for a fixed f_{peak} value there is a trade-off between the sediment layer shear-wave velocity (V_L) and it's corresponding depth (d_L). Sites with similar f_{peak} values can have different amplification levels due to stiffness variations. Some portion of the variability that we observed in our model might be due to this effect. Hence, more reduction in GMPE variability might be possible using a more refined amplification model (considering both f_{peak} and V_{S30}). However, considering the limited available information on V_{S30} values for sites in the NGA-East database, it is not currently feasible to derive a reliable model that directly incorporates stiffness, in our view. Moreover, there are other important factors that can significantly affect the amplification at a selected site such as topography and geologic complexity. For the derived amplification model, these effects are averaged out over the study sites. For any specific site, the actual site amplification may differ significantly from the average function.

5.5 Data and Resources

The ground-motion database of this study is that developed by Hassani and Atkinson (2015). Most of the data were extracted from the NGA-East database (Goulet et al., 2014) which were already processed and include PGA, PGV and PSA for the rotation-angle independent geometric average of horizontal ground-motion amplitudes (RotD50) (Boore, 2010). The rest of the processed data were obtained from the Engineering

Seismology Toolbox website, which includes three-component processed ground-motion parameters (www.seismotoolbox.ca; last accessed December 2013). The unprocessed data were either obtained from the Automatic Data Request Manager Facility (AutoDRM) of the Geological Survey of Canada (autodrm@seismo.nrcan.gc.ca; last contacted December 2013) or the AutoDRM of the Incorporated Research Institutions for Seismology (breq_fast@iris.washington.edu, last contacted December 2013). The processing of the unprocessed data was as described by (Assatourians and Atkinson, 2010). For the unprocessed data and the data extracted from Engineering Seismology Toolbox website, the geomean of the horizontal components was used, which is approximately equivalent to RotD50. We used MATLAB for all of the regressions (www.mathworks.com, last contacted January 2015), and we used CoPlot for making the figures (www.cohort.com, last contacted January 2015).

5.6 Acknowledgments

This work was funded by the National Sciences and Engineering Research Council of Canada. We thank the NGA-East project for the excellent databases and ongoing discussions. We are grateful to Valerio Poggi and an anonymous reviewer for their constructive comments, which enabled us to improve the quality of the manuscript.

5.7 References

Abrahamson, N.A., and R.R. Youngs (1992). A stable Algorithm for regression analysis using the random effects model, *Bull. Seismol. Soc. Am.* **82,** 505-510.

Abrahamson, N.A., W.J. Silva, and R. Kamai (2014). Summary of the ASK14 ground motion relation for active crustal regions, *Earthq. Spectra.* **30,** 1025-1055.

Al Atik, L., N. Abrahamson, J.J. Bommer, F. Scherbaum, F. Cotton, and N. Kuehn (2010). The variability of ground-motion prediction models and its components, *Seism. Res. Lett.* **81,** 794-801.

Andrews, D.J. (1986). Objective determination of source parameters and similarity of earthquakes of different size, in *Earthquake source mechanics,* S. Das (Editor), American Geophysical Union, Geophysical Monograph, Vol. 37, 259–267.

Assatourians, K., and G.M. Atkinson (2010). Database of Processed Time Series and Response Spectra Data for Canada: An Example Application to Study of 2005 MN 5.4 Riviere du Loup, Quebec, Earthquake, *Seism. Res. Lett.* **81,** 1013-1031.

Atkinson, G.M. (2004). Empirical attenuation of ground-motion spectral amplitudes in southeastern Canada and the northeastern United States, *Bull. Seismol. Soc. Am.* **94,** 1079-1095.

Atkinson, G.M., B. Hassani, A. Singh, E. Yenier, and K. Assatourians (2015). Estimation of Moment Magnitude and Stress Parameter from ShakeMap Ground-Motion Parameters, *Bull. Seismol. Soc. Am.* **105,** 2572-2588.

Boore, D.M. (2010). Orientation-independent, nongeometric-mean measures of seismic intensity from two horizontal components of motion, *Bull. Seismol. Soc. Am.* **100,** 1830-1835.

Boore, D.M. (2015). *Adjusting Ground-Motion Intensity Measures to a Reference Site for which V_{S30} = 3000 m/sec*, PEER Report No. 2015/06, Pacific Earthquake Engineering Research Center, Berkeley, CA.

Boore, D.M., J.P. Stewart, E. Seyhan, and G.M. Atkinson (2014). NGA-West2 equations for predicting PGA, PGV, and 5% damped PSA for shallow crustal earthquakes, *Earthq. Spectra.* **30,** 1057-1085.

Borcherdt, R.D. (1994). Estimates of site-dependent response spectra for design (methodology and justification), *Earthq. Spectra.* **10,** 617-653.

Bozorgnia, Y., N.A. Abrahamson, L.A. Atik, T.D. Ancheta, G.M. Atkinson, J.W. Baker, A. Baltay, D.M. Boore, K.W. Campbell, B.S.-J. Chiou, R. Darragh, S. Day, J. Donahue, R.W. Graves, N. Gregor, T. Hanks, I.M. Idriss, R. Kamai, T. Kishida, A.R. Kottke, S.A. Mahin, S. Rezaeian, B. Rowshandel, E. Seyhan, S. Shahi, T. Shantz, W. Silva, P. Spudich, J.P. Stewart, J. Watson-Lampery, K. Wooddell, and R. Youngs (2014). NGA-West2 research project, *Earthq. Spectra.* **30,** 973-987.

Cadet, H., P.-Y. Bard, and A. Rodriguez-Marek (2010). Defining a standard rock site: Propositions based on the KiK-net database, *Bull. Seismol. Soc. Am.* **100,** 172-195.

Campbell, K.W., and Y. Bozorgnia (2014). NGA-West2 ground motion model for the average horizontal components of PGA, PGV, and 5% damped linear acceleration response spectra, *Earthq. Spectra.* **30,** 1087-1115.

Castellaro, S., F. Mulargia, and P.L. Rossi (2008). V_{S30}: Proxy for seismic amplification?, *Seism. Res. Lett.* **79,** 540-543.

Chiou, B.S.-J., and R.R. Youngs (2014). Update of the Chiou and Youngs NGA model for the average horizontal component of peak ground motion and response spectra, *Earthq. Spectra.* **30,** 1117-1153.

Di Alessandro, C., L.F. Bonilla, D.M. Boore, A. Rovelli, and O. Scotti (2012). Predominant-period site classification for response spectra prediction equations in Italy, *Bull. Seismol. Soc. Am.* **102,** 680-695.

Dreiling, J., M.P. Isken, W.D. Mooney, M.C. Chapman, and R.W. Godbee (2014). NGA-East Regionalization Report: Comparison of Four Crustal Regions within Central and Eastern North America using Waveform Modeling and 5%-Damped Pseudo-Spectral Acceleration Response, *PEER Report 2014*. **15**.

Fukushima, Y., L.F. Bonilla, O. Scotti, and J. Douglas (2007). Site classification using horizontal-to-vertical response spectral ratios and its impact when deriving empirical ground-motion prediction equations, *Journal of Earthquake Engineering*. **11,** 712-724.

Goulet, C.A., Y. Bozorgnia, and N.A. Abrahamson (2015). Introduction, in *NGA-East: Median Ground-Motion Models for the Central and Eastern North America Region*, Chap. 1, PEER Report No. 2015/04, Pacific Earthquake Engineering Research Center, Berkeley, CA, 1-10.

Goulet, C.A., C.H. Cramer, R.B. Darragh, W.J. Silva, Y.M.A. Hashash, J. Harmon, J.P. Stewart, K.E. Wooddell, and R.R. Youngs (2014). *PEER NGA-East database*, PEER Report No. 2014/17, Pacific Earthquake Engineering Research Center, Berkeley, CA.

Hassani, B., and G.M. Atkinson (2015). Referenced Empirical Ground-Motion Model for Eastern North America, *Seism. Res. Lett.* **86,** 477-491.

Hassani, B., and G.M. Atkinson (2016a). Applicability of the site fundamental frequency as a V_{S30} proxy for Central and Eastern North America, *Bull. Seismol. Soc. Am.* **106,** 653-664.

Hassani, B., and G.M. Atkinson (2016b). Applicability of the NGA-West2 Site Effects Model for Central and Eastern North America, *Bull. Seismol. Soc. Am.* **106,** In press.

Idriss, I. (2014). An NGA-West2 empirical model for estimating the horizontal spectral values generated by shallow crustal earthquakes, *Earthq. Spectra.* **30,** 1155-1177.

Kokusho, T., and K. Sato (2008). Surface-to-base amplification evaluated from KiK-net vertical array strong motion records, *Soil Dynam. Earthq. Eng.* **28,** 707-716.

Kottke, A.R., Y. Hashash, J.P. Stewart, C.J. Moss, S. Nikolaou, E.M. Rathje, W.J. Silva, and K.W. Campbell (2012). Development of geologic site classes for seismic site amplification for central and eastern North America, *Proc. 15th World Conf. on Earthquake Eng.*, Lisbon, Portugal, 24–28 September 2012, Paper Number 4557.

Kramer, S.L. (1996). *Geotechnical earthquake engineering*, Prentice-Hall International Series in Civil Engineering and Engineering Mechanics, Prentice-Hall, Upper Saddle River, NJ.

Lermo, J., and F.J. Chávez-García (1993). Site effect evaluation using spectral ratios with only one station, *Bull. Seismol. Soc. Am.* **83,** 1574-1594.

Molas, G.L., and F. Yamazaki (1995). Attenuation of earthquake ground motion in Japan including deep focus events, *Bull. Seismol. Soc. Am.* **85,** 1343-1358.

Nakamura, Y. (1989). A method for dynamic characteristics estimation of subsurface using microtremor on the ground surface, *Q. Rep. Railway Tech. Res. Inst.* **30,** 25–30.

NEHRP (2000). NEHRP Recommended provisions for seismic regulations for new buildings and 550 other structures, Part 1, Provisions, FEMA 368, *Federal Emergency Management Agency, Washington, D.C*

Pezeshk, S., A. Zandieh, K.W. Campbell, and B. Tavakoli (2015). Ground motion prediction equations for CENA using the hybrid empirical method in conjunction with NGA-West2 empirical ground motion models, in *NGA-East: Median Ground-Motion Models for the Central and Eastern North America Region*, Chap. 5, PEER Report No. 2015/04, Pacific Earthquake Engineering Research Center, Berkeley, CA, 119-147.

Pitilakis, K., E. Riga, and A. Anastasiadis (2012). Design spectra and amplification factors for Eurocode 8, *Bulletin of Earthquake Engineering*. **10,** 1377-1400.

Pitilakis, K., E. Riga, and A. Anastasiadis (2013). New code site classification, amplification factors and normalized response spectra based on a worldwide ground-motion database, *Bulletin of Earthquake Engineering*. **11,** 925-966.

Rodriguez-Marek, A., J.D. Bray, and N.A. Abrahamson (2001). An empirical geotechnical seismic site response procedure, *Earthq. Spectra.* **17,** 65-87.

Seyhan, E., and J.P. Stewart (2014). Semi-empirical nonlinear site amplification from NGA-West2 data and simulations, *Earthq. Spectra.* **30,** 1241-1256.

Shahjouei, A., and S. Pezeshk (2015). Hybrid Empirical Ground-Motion Model for Central and Eastern North America using Hybrid Broadband Simulations and NGAWest2 GMPEs, in *NGA-East: Median Ground-Motion Models for the Central and Eastern North America Region*, Chap. 7, PEER Report No. 2015/04, Pacific Earthquake Engineering Research Center, Berkeley, CA, 165-192.

Silva, W. (1995). Engineering characterization of strong ground motion recorded at rock sites, Electric Power Research Institute.

Van Houtte, C., S. Drouet, and F. Cotton (2011). Analysis of the origins of κ (kappa) to compute hard rock to rock adjustment factors for GMPEs, *Bull. Seismol. Soc. Am.* **101,** 2926-2941.

Wald, D.J., and T.I. Allen (2007). Topographic slope as a proxy for seismic site conditions and amplification, *Bull. Seismol. Soc. Am.* **97,** 1379-1395.

Yenier, E., and G.M. Atkinson (2015). Regionally adjustable generic ground-motion prediction equation based on equivalent point-source simulations: Application to central and eastern North America, *Bull. Seismol. Soc. Am.* **105,** 1989-2009.

Zhao, J.X., K. Irikura, J. Zhang, Y. Fukushima, P.G. Somerville, A. Asano, Y. Ohno, T. Oouchi, T. Takahashi, and H. Ogawa (2006a). An empirical site-classification method for strong-motion stations in Japan using H/V response spectral ratio, *Bull. Seismol. Soc. Am.* **96,** 914-925.

Zhao, J.X., J. Zhang, A. Asano, Y. Ohno, T. Oouchi, T. Takahashi, H. Ogawa, K. Irikura, H.K. Thio, P.G. Somerville, and others (2006b). Attenuation relations of strong ground motion in Japan using site classification based on predominant period, *Bull. Seismol. Soc. Am.* **96,** 898-913.

Chapter 6

6 Summary, Conclusions and Future Studies

6.1 Summary

In Chapter 2, we updated the referenced empirical GMPE model for CENA. The proposed model is in agreement with regional ground-motion data to a distance of 400 km, while being constrained to follow the overall scaling behavior of ground motion that is observed for larger events in active tectonic regions. The predicted ground-motion amplitudes of the CENA referenced empirical model are very similar to the equivalent California values of BSSA14 model at close distances (R ≤50 km), at low to moderate frequencies ($f \leq 5$ Hz). At regional distances (R > 50 km) and at high frequencies ($f >5$ Hz), the CENA data suggest higher ground-motion amplitudes than the BSSA14 reference model, presumably due to lower attenuation and higher stress for CENA events relative to those in active tectonic regions. We also showed that the referenced empirical approach predicts ground motions that are consistent with those that would be produced by the hybrid empirical approach, considering recent equivalent point-source models that match both CENA and California ground-motion databases.

In Chapter 3, we proposed an algorithm for determining moment magnitude (**M**) and stress parameter ($\Delta\sigma$) in near-real-time in the immediate aftermath of a small to moderate earthquake (**M** ~3 to 6), from ShakeMap ground motion parameters (PSA at 1 Hz, 0.33 Hz, 10 Hz and/or PGA). These two source parameters are the essential input to an equivalent point-source stochastic model that can be optimized for the attenuation and site response attributes of a region of interest, allowing rapid event-specific GMPEs to be defined. To show the application of the approach, we used southern Ontario ground motions to derive a regionally-adjusted generic GMPE model, determining regional stress parameter, anelastic attenuation, calibration factor, and site amplification models from the observed data. Then, using the estimated regional models, we showed how to invert ShakeMaps parameters to estimate moment magnitude and stress parameter in near-real-time, in order to define an event-specific GMPE for an event that just happened. This

same approach could readily be used for other seismic networks in different seismotectonic regions. It is particularly useful for applications where ShakeMaps are desired for small-to-moderate events in sparsely-instrumented regions.

In chapter 4, we established the utility of f_{peak} as a site response indicator, and its use as a proxy measure for V_{S30} for sites in CENA. f_{peak} is measured from the horizontal–to-vertical spectral ratios (H/V) of recorded ground motion (or ambient noise). In this study, H/V spectral ratios were obtained from 5%-damped pseudo spectral acceleration (PSA) from seismograph stations in CENA using the NGA-East database. We correlated the measured V_{S30} values at recording stations with the corresponding f_{peak} values to obtain a predictive relationship for V_{S30}. The uncertainty of the V_{S30} estimate using the f_{peak}-based model is small (0.14 $\log_{10}$ units) in comparison to that for the proxy-based methods (e.g. topographic slope and surface geology proxies) used in the NGA-East database (0.25 $\log_{10}$ units). We also examined the applicability of the NGA-West2 site effects model (Seyhan and Stewart, 2014), which is a V_{S30}-based model, to sites in CENA, using the NGA-East ground-motion database. We determined residual site terms by comparing the observed CENA ground-motion amplitudes, adjusted to B/C reference site conditions using the western site-effects model, to the corresponding predicted amplitudes of a CENA ground-motion prediction equation for B/C site conditions (Yenier and Atkinson, 2015; YA15). The CENA prediction model used the same western site model to level the database before model development. Thus residual trends reveal inadequacies of the western site effects model when applied to CENA ground motions. Plotting the residual site terms versus their corresponding f_{peak} values reveals significant f_{peak}-dependent trends at all frequencies. Average residual site terms for CENA sites, after the western site amplifications have been removed, can be as large as 0.45 in $\log_{10}$ units (2.8 in non-log units) around $f \approx f_{peak}$. Correlating the site terms with western site effects predictions reveals that at $f < 1$ Hz, site terms in CENA scale with V_{S30} in a manner that is similar to the way they behave in the NGA-West2 database. However, at higher frequencies the correlation of site amplification with V_{S30} decreases markedly in CENA. By contrast, the H/V spectral ratio (as obtained from the NGA-East ground-motion data) is a good predictor of the observed f_{peak}-dependent site terms, suggesting that H/V is a more

reliable predictor of site amplification for the recording stations of the NGA-East database.

Finally in chapter 5, we derived an f_{peak}-based site effects model for sites in CENA by finding the site terms (no site correction) relative to two of the regional GMPE models with different reference site conditions. Site terms were determined with respect to the a reference GMPE model for B/C reference site conditions, and a reference GMPE model for hard rock site conditions (~ site class A) as discussed in Chapter 3. Using the derived f_{peak}-based model and a selected database, we are able to reduce sigma (σ) by 10% on average comparing to the one we determined from the V_{S30}- site effects model. By further analyzing the variability parameters, we show that the main reduction in sigma comes from the reduction in the site correction variability (φ_{S2S}) and not the random site term variability (φ_{SS}). The results of this study emphasises the importance of f_{peak} and inadequacy of V_{S30} as the appropriate site effects indicator for sites in CENA.

6.2 Conclusions

The main conclusions of this study are as follows:

- The referenced empirical model suggests that ground-motion amplitudes in CENA are similar to those predicted by the BSSA14 reference model for California at distances smaller than 50 km at frequencies ≤5 Hz.
- At higher frequencies and larger distances, CENA ground-motion amplitudes are significantly higher than predicted by the BSSA14 model, reflecting higher stress parameter and lesser attenuation in ENA relative to active tectonic regions.
- The trend lines obtained from the referenced empirical approach follow the predictions of the hybrid empirical method well overall, at least for small to moderate magnitude events (e.g. M4). This shows that the approach is in demonstrable agreement with predictions that would be made using the hybrid empirical approach for CENA.
- The updated referenced empirical GMPE model of this study can replace the former referenced empirical GMPE model for probabilistic seismic hazard analysis of sites in CENA.

- Reliable near-real-time estimates of **M** and $\Delta\sigma$ can be computed using commonly-available ShakeMap parameters. The methodology is based on relating ShakeMap parameters to source and attenuation parameters within the context of a generic stochastic point-source model, which allows rapid event-specific GMPEs to be defined. **M** can be estimated from low frequency ShakeMap ground-motion parameters (0.33 and 1 Hz PSA), while $\Delta\sigma$ can be estimated form high frequency ShakeMap parameters (10 Hz PSA and PGA).
- A regionally adjusted GMPE model is developed for southern Ontario for hard-rock reference site condition using the generic GMPE approach of Yenier and Atkinson (2015). The model parameters are derived based on the observed ground-motion amplitudes in southern Ontario.
- Slightly slower anelastic attenuation is observed in southern Ontario compared to CENA as a whole.
- We show that f_{peak} values derived from H/V of ground motion or ambient noise can be used as a reliable proxy measure for V_{S30} for sites in CENA. The uncertainty of the V_{S30} estimate using the f_{peak}-based model is small (0.14 $\log_{10}$ units) in comparison to that for the proxy-based methods (e.g. topographic slope and surface geology proxies) used in the NGA-East database (0.25 $\log_{10}$ units).
- In CENA, V_{S30} may not be the best choice of site variable, as it may be a poor proxy for site response. Western site-effects models (e.g. SS14) do not work well in CENA, leaving residual site terms as large as 0.45 in $\log_{10}$ units (2.8 in non-log units) around $f \approx f_{peak}$.
- For frequencies less than 1 Hz, site terms in CENA scale with V_{S30} in a manner that is similar to the way they behave in active tectonic regions. However, at higher frequencies the correlation of site amplification with V_{S30} decreases markedly in CENA.
- H/V is a more reliable predictor of site amplification than V_{S30} for sites in CENA.
- A regional amplification model is developed for sites in CENA based on empirical observations. The proposed model is f_{peak}-dependent to mirror the strong observed amplification at the fundamental frequency of the sites in CENA.

- Using the f_{peak}-dependent amplification model we are able to reduce variability in ground motions (σ) by 10% relative to that obtained with a V_{S30}-based model. The reduction in σ is mainly apparent in within-event standard deviation (φ); most of this reduction comes from the variability reduction in the site-to-site correction terms (φ_{S2S}) (20% reduction) and not the random variability of the single-station terms (φ_{SS}).

6.3 Suggestions and Future Studies

In Chapter 2, we updated the referenced empirical GMPE model for CENA. This model can be implemented in probabilistic seismic hazard analysis of sites in CENA and, along with other models, can update hazard maps used in building codes. In Chapter 3, we showed that how we can develop a regionally adjusted GMPE model for regions with sparse seismicity. The approach developed here can be easily implemented for other seismic networks to drive near real-time estimations of moment magnitude and stress parameter. This approach is particularly useful for applications where ShakeMaps are desired for small-to-moderate events in sparsely-instrumented regions.

In order to have a better assessment of the near-real time estimates of moment magnitude and stress parameter and their corresponding variabilities, we can implement the proposed approach in a real-time seismic network for future events. Event-specific GMPE models can be developed for an event that just happened knowing the near-real time estimates of moment magnitude and stress parameter and also using the regionally adjusted GMPE model. These models can later be used along with the observed data in seismographic stations and also an amplification map for a region of interest to derive ShakeMaps or interactive ground-motion maps for the ground surface which are fully compatible with the observed data, the regionally adjusted GMPE model, as well as the regional amplification model. Future work includes the continued calibration and testing of this approach.

The f_{peak}-based V_{S30} proxy proposed in Chapter 4 was obtained from a limited number of measurement-based V_{S30} values (only 41 stations), and a limited number of sites with determined f_{peak} values (only 23% of the NGA-East recording stations). This relation can

be improved significantly in future by conducting site specific studies to gather more detailed information from which to develop correlations between V_{S30} and f_{peak} values. It would also be possible to regionalize the model for sub-regions in CENA having different velocity structures.

In order to define the f_{peak} values for all of the seismographic stations in CENA, one practical approach is to use H/V spectral ratios determined from the selected noise windows of the stations. This can be done by retrieving pre-event and post-event noise data from IRIS for all of the stations in CENA.

This thesis demonstrated that western V_{S30}-based site effects models are not able to capture the observed f_{peak}-dependent site term trends in CENA. The proposed f_{peak}-based site amplification model of this study can be used as the site effects indicator for future regional GMPE models of CENA.

In order to develop this model further, it would be useful to conduct ambient noise studies at all of the NGA-East recording stations. An improvement to the f_{peak}-based site effects model would be adding a stiffness indicator (e.g. V_{S30}) to the site effects functional form, which would require more V_{S30} measurements in CENA. Alternatively, other parameters that would address stiffness in site response modeling could be explored.

Appendices

Appendix A.Generic GMPE model coefficients for ShakeMap ground-motion parameters

Table A.1: Model coefficients of the magnitude scaling term (F_M) and the geometrical spreading function (F_Z) in the generic GMPE (from Yenier and Atkinson, 2015b). PGV is in cm/s, PGA and PSA are in g.

Frequency (Hz)	M_h	e_0	e_1	e_2	e_3	b_3	b_4
PGV	5.90	5.96	1.03	-0.17	1.08	-0.58	0.057
PGA	5.85	2.22	0.69	-0.14	0.77	-0.62	0.060
0.33	6.65	0.52	1.91	-0.09	1.42	-0.51	0.068
1.00	6.45	1.99	1.34	-0.25	0.98	-0.30	0.028
3.33	5.85	2.63	0.85	-0.36	0.88	-0.21	0.005
10.00	5.45	2.78	0.71	-0.26	0.79	-0.38	0.025

Table A.2: Model coefficients of the stress adjustment factor ($F_{\Delta\sigma}$) in the generic GMPE (from Yenier and Atkinson, 2015b). PGV is in cm/s, PGA and PSA are in g.

Frequency (Hz)	s_0	s_1	s_2	s_3	s_4
PGV	-2.25	1.95	-0.52	0.061	-0.0027
PGA	-2.13	1.94	-0.50	0.058	-0.0025
0.33	-7.98	6.64	-1.92	0.237	-0.0104
1.00	1.07	-0.46	0.04	0.010	-0.0011
3.33	-0.32	-0.14	0.17	-0.029	0.0014
10.00	-4.05	3.10	-0.76	0.083	-0.0034

Table A.2: (cont'd)

Frequency (Hz)	s_5	s_6	s_7	s_8	s_9
PGV	-1.76	1.38	-0.33	0.035	-0.0014
PGA	-1.44	1.24	-0.29	0.030	-0.0012
0.33	-4.18	3.32	-0.89	0.099	-0.0039
1.00	-4.47	4.05	-1.27	0.171	-0.0081
3.33	2.25	-2.00	0.63	-0.077	0.0033
10.00	-2.45	1.57	-0.29	0.023	-0.0007

Table A.3: Anelastic attenuation coefficients to adjust the generic GMPE for CENA. The corresponding values for California are also shown.

Frequency (Hz)	γ_{CENA}	$\gamma_{California}$
PGV	-0.0028	-0.0063
PGA	-0.0047	-0.0098
0.33	-0.0011	-0.0027
1.00	-0.0013	-0.0051
3.33	-0.0031	-0.0094
10.00	-0.0056	-0.0125

Appendix B. Site fundamental frequency (f_{peak}) determination procedure

In the following we describe the procedure used to determine the site fundamental frequencies (f_{peak}) for the recording stations of this study.

We calculate the average of $(\overline{H/V})_{j,f}$ (Equation 4.2) over the usable frequency bandwidth of station j as:

$$\log(\overline{H/V})_j = \frac{\sum_{f_1}^{f_2} \log(\overline{H/V})_{j,f}}{n_j} \tag{B.1}$$

, where $(\overline{H/V})_j$ is the average of $(\overline{H/V})_{j,f}$ over the usable frequency bandwidth of station j, f_1 and f_2 are the first and the last usable frequencies of station j respectively, and n_j is the number of frequencies in the bandwidth of station j (from f_1 to f_2).

In order to determine f_{peak}, we first find the local maxima points of the H/V spectral ratios. Figure B.1 shows the selected local maxima points for four of the stations. As we observe here, not all of the selected local maxima points represent the site fundamental frequency. Some of the selected points show amplifications smaller than $(\overline{H/V})_j$, some of them are close to each other without any significant trough between them, and some of them are due to peak-to-peak variability of the H/V spectra. Therefore, we need to define a set of criteria which enable us to determine the significant peaks and consequently the main site fundamental frequency. First, we define significant peaks as local maxima points with amplifications larger than $(\overline{H/V})_j$ and having a value of >0.3 (minimum amplification of 2 in non-log units). For each of these selected local maxima points we calculate the difference between their corresponding amplification values (A_{peak}) and $\overline{H/V}$ (H/V frequency bandwidth average, Equation B.1) ($A_{peak} - \overline{H/V}$) as shown in Figure B.1. In Figure B.2 we plot this difference for the first two local maxima points (those with the highest $A_{peak} - \overline{H/V}$ values) as a function of their corresponding peak frequencies for all of the stations. The average $A_{peak} - \overline{H/V}$ value attains a value of ~0.17, and does not show any apparent frequency dependency. Figure B.2 also shows the

histogram of the number of local maxima points as a function of their $A_{peak} - \overline{H/V}$ values. We only consider local maxima with amplifications larger than $\overline{H/V} + 0.17$, and value > 0.3, as points which could represent the significant peaks in site response. We then fit a Gaussian function to the neighborhood of the selected local maxima points, and using the fitted curve we estimate the value at which the function peaks. This provides a more stable f_{peak} determination as the number of frequency points are limited (28 points in the frequency range of 0.1 to 50 Hz) and the H/V spectra are not entirely smooth. The neighboring points are defined as the points that are above $\overline{H/V}$ in vicinity of the selected significant peaks. We define the Gaussian function as (Ghofrani and Atkinson, 2014):

$$Y = a \times \exp\left(-(X/w)^2\right) + c, \tag{B.2}$$

where *a*, *w* and *c* are the coefficients of the Gaussian function and *X* is:

$$X = \log(f/f_{peak}). \tag{B.3}$$

For each of the selected significant peaks, we use the simplex search method of Lagarias et al. (1998) to estimate the coefficients of Equation (B.2) and f_{peak} in Equation (B.3) These fitted Gaussian curves are also shown on Figure B.1, along with the determined significant peaks.

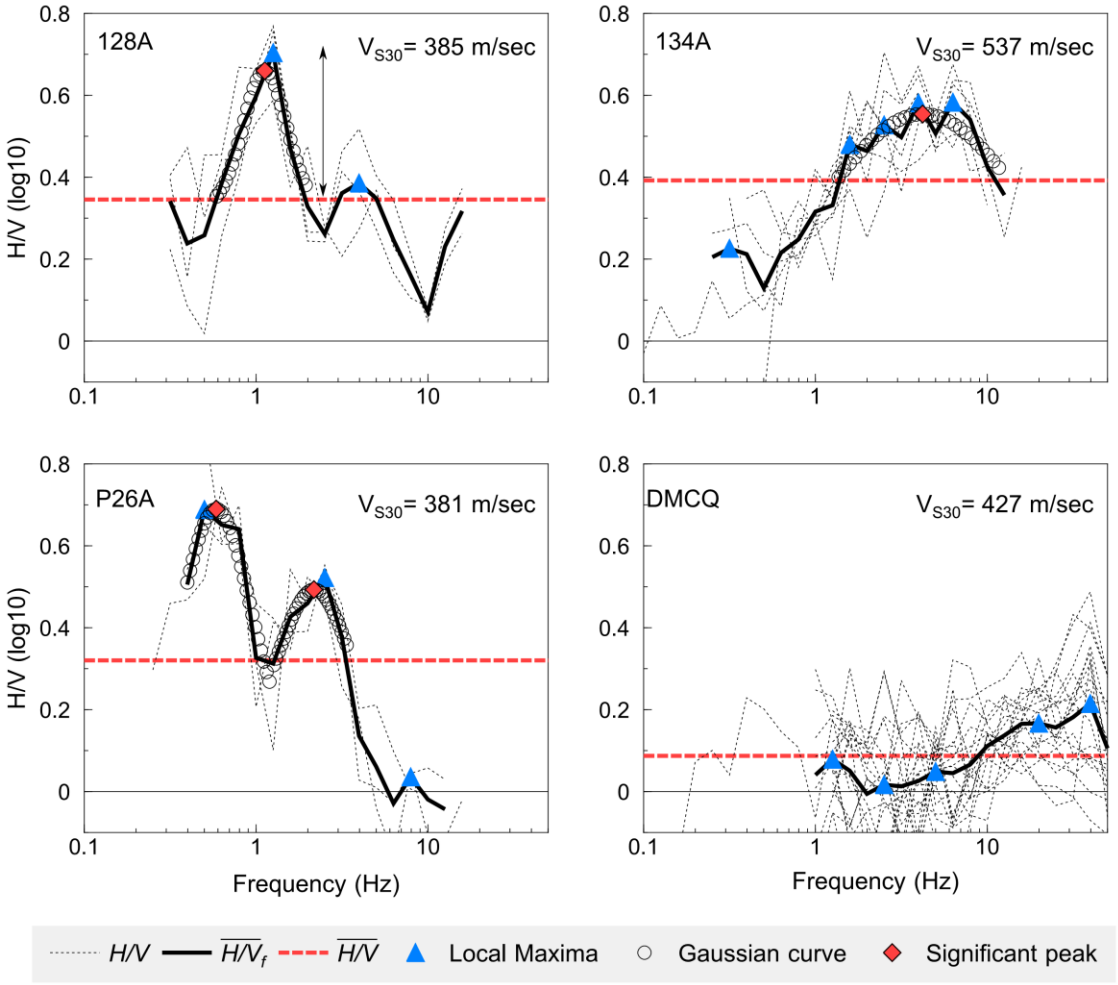

Figure B.1: Individual H/V spectra for four example stations (dotted lines), with average H/V spectra ($\overline{H/V_f}$) (solid line). Dashed lines show average H/V spectra ($\overline{H/V}$, Equation B.1) over all frequencies, while triangles show local maxima points. Double headed arrow shows the difference between the selected local maxima amplification (A_{peak}) and the bandwidth average of H/V spectra (A_{peak}- $\overline{H/V}$). Circles show the fitted Gaussian curves, and diamonds show the selected significant peaks. V_{S30} values are the reported NGA-East "preferred" V_{S30} values.

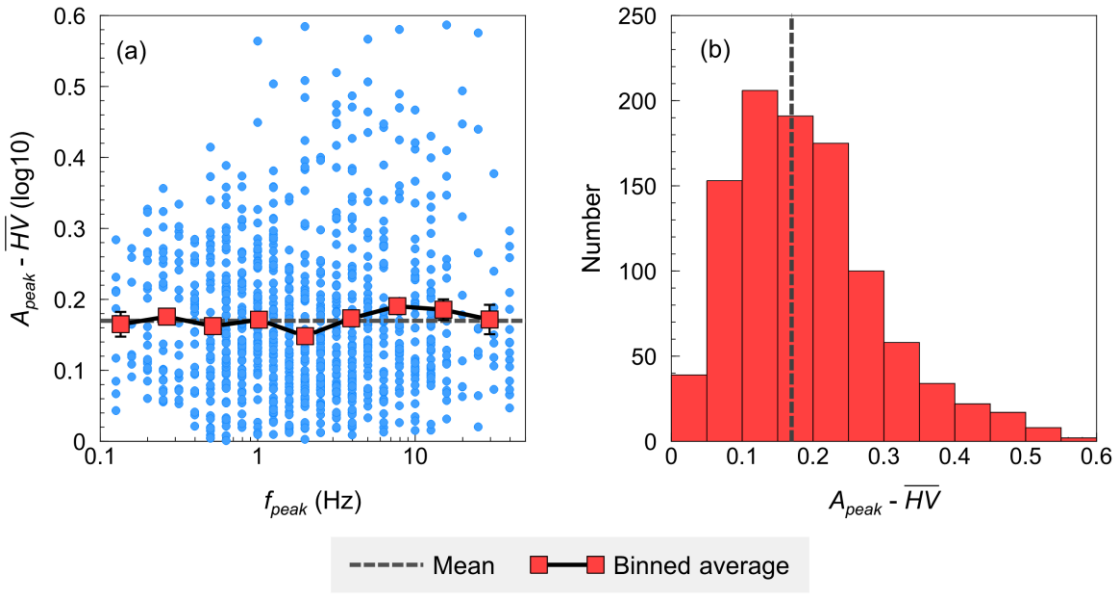

Figure B.2: (a): Difference between the amplification of the local maxima points (A_{peak}) and the H/V bandwidth average (A_{peak}- $\overline{H/V}$), shown for the highest two local maxima points. Squares show the average of A_{peak}- $\overline{H/V}$ values in equally log-spaced frequency bins, and their corresponding standard error bars. Dashed line shows the average of A_{peak}- $\overline{H/V}$ obtained from all data points, and (b): histogram of A_{peak}- $\overline{H/V}$; average A_{peak}- $\overline{H/V}$ is shown by dashed line.

Curriculum Vitae

Name:	Behzad Hassani
Post-secondary Education and Degrees:	University of Tabriz Tabriz, Iran 2003-2007 B.Sc. In Civil Engineering (structural engineering) University of Tehran Tehran, Iran 2007-2010 M.Sc. In Earthquake Engineering Western University London, Ontario, Canada 2012-2016 . Ph.D. In Geophysics
Honours and Awards:	Chevron Canada Outstanding Student Paper in Seismology, CGU and AGU joint assembly, 2015 KEGS (The Canadian Exploration Geophysical Society) student scholarship, 2013 Geophysics Travel Scholarship, 2014, 2015 Western Graduate Research Scholarships (WGRS), 2012-2016
Related Work Experience	Teaching Assistant/Research Assistant Western University London, Ontario, Canada 2012-2016 Research Assistant International Institute of Earthquake Engineering and Seismology (IIEES), Tehran, Iran 2010-2012

Publications:

Hassani, B., and G.M. Atkinson (2016). Applicability of the site fundamental frequency as a V_{S30} proxy for Central and Eastern North America, *Bull. Seismol. Soc. Am.* **106,** 653-664.

Hassani, B., and G.M. Atkinson (2016). Applicability of the NGA-West2 Site Effects Model for Central and Eastern North America, *Bull. Seismol. Soc. Am.* **106,** In press.

Hassani, B., and G.M. Atkinson (2016). Site Effects Model for Central and Eastern North America Based on Peak Frequency, *Bull. Seismol. Soc. Am.* Accepted.

Braganza, S., G.M. Atkinson, H. Ghofrani, B. Hassani, L. Chouinard, P. Rosse, D. Motazedian, and J. Hunter (2016). Modeling Site Amplification in Eastern Canada on a Regional Scale, *Seism. Res. Lett.* Accepted.

Hassani, B., and G.M. Atkinson (2015). Referenced Empirical Ground-Motion Model for Eastern North America, *Seism. Res. Lett.* **86,** 477-491.

Atkinson, G.M., B. Hassani, A. Singh, E. Yenier, and K. Assatourians (2015). Estimation of Moment Magnitude and Stress Parameter from ShakeMap Ground-Motion Parameters, *Bull. Seismol. Soc. Am.* **105,** 2572-2588.

Zafarani, H., M. Rahimi, A. Noorzad, B. Hassani, and B. Khazaei (2015). Stochastic Simulation of Strong-Motion Records from the 2012 Ahar–Varzaghan Dual Earthquakes, Northwest of Iran, *Bull. Seismol. Soc. Am.* **105,** 1419-1434.

Zafarani, H., and B. Hassani (2013). Site response and source spectra of S waves in the Zagros region, Iran, *Journal of seismology*. **17,** 645-666.

Zafarani, H., B. Hassani, and A. Ansari (2012). Estimation of earthquake parameters in the Alborz seismic zone, Iran using generalized inversion method, *Soil Dynam. Earthq. Eng.* **42,** 197-218.

Hassani, B., H. Zafarani, J. Farjoodi, and A. Ansari (2011). Estimation of site amplification, attenuation and source spectra of S-waves in the East-Central Iran, *Soil Dynam. Earthq. Eng.* **31,** 1397-1413.